Université de Montréal

IMPACT OF THE PULVINAR ON THE VENTRAL PATHWAY OF THE CAT VISUAL CORTEX

par Bruno Oliveira Ferreira de Souza

École d'Optométrie

Thèse présentée
en vue de l'obtention du grade de PhD
en Sciences de la Vision
option neurosciences de la vision et psychophysique

Février, 2019

Résumé

Les signaux provenant de la rétine sont relayés dans le corps géniculé latéral où ils sont envoyés au cortex visuel primaire. L'information passe ensuite à travers plusieurs aires visuelles où la complexité du traitement augmente progressivement. Des données tant anatomiques que fonctionnelles ont démontré l'existence de deux voies principales qui traitent différentes propriétés de l'information visuelle : les voies dorsale et ventrale. Les aires corticales composant la voie dorsale sont impliquées principalement dans le traitement du mouvement tandis que les aires de la voie ventrale sont impliquées dans le traitement de la forme et de la couleur. Cette vision classique de l'organisation fonctionnelle du cortex est toutefois remise en question par l'existence de connections réciproques entre les aires corticales visuelles et le pulvinar, un noyau thalamique. En effet, ces connections permettent la création d'une voie trans-thalamique parallèle aux connections cortico-corticales à travers la hiérarchie visuelle.

Le but principal de la présente thèse consiste en deux volets : le premier est d'obtenir une meilleure compréhension du traitement des incréments et décréments de la lumière dans une aire de la voie ventrale du chat (aire 21a); le second est de caractériser la nature des inputs thalamo-corticaux du noyau latéral postérieur (LP) à l'aire 21a chez le chat.

Dans l'étude #1, nous avons investigué le profil spatiotemporel des réponses des neurones de l'aire 21a aux incréments (blancs) et décréments (noirs) de lumière en utilisant l'analyse de corrélation inverse d'un stimulus de bruit épars. Les neurones de l'aire 21a ont répondu plus fortement aux stimuli noirs, en montrant des champs récepteurs avec des sous-champs noirs plus larges. Cependant, aucune différence n'a été trouvée en ce qui concerne les dynamiques temporelles des réponses aux blancs et aux noirs. En comparaison avec le cortex visuel primaire, la préférence aux stimuli noirs dans l'aire 21a s'est avérée fortement augmentée. Ces données indiquent que les asymétries entre les réponses aux blancs et aux noirs sont transmises et amplifiées à travers la voie ventrale.

Dans l'étude #2, nous avons investigué l'impact de l'inactivation pharmacologique réversible du noyau LP sur la fonction de réponse au contraste (CRF) des neurones de l'aire 21a et du cortex visuel primaire (aire 17). L'inactivation a eu différents effets dans les deux aires

corticales. Alors que, dans l'aire 17, l'inactivation du LP a causé une légère réduction du gain de la réponse, une forte augmentation a été observée dans l'aire 21a. Ainsi, nos résultats suggèrent que le LP exerce une influence modulatrice dans le traitement cortical à travers la voie ventrale avec un impact plus important dans des aires extrastriées de plus haut niveau.

Nos résultats ont permis d'avoir une meilleure compréhension des propriétés fonctionnelles de la voie ventrale du chat et de contribuer à enrichir les connaissances actuelles sur le rôle du pulvinar dans le traitement cortico-thalamo-cortical de l'information visuelle.

Mots-clés : aire 21a, cortex visuel primaire, corrélation reverse, noyau latéral postérieur, réponse au contraste, électrophysiologie, inactivation thalamique.

Abstract

Signals from the retina are relayed to the lateral geniculate nucleus from which they are sent to the primary visual cortex. At the cortical level, the information is transferred across several visual areas in which the complexity of the processing increases progressively. Anatomical and functional evidence demonstrate the existence of two main pathways in visual cortex processing distinct features of the visual information: the dorsal and ventral streams. Cortical areas composing the dorsal stream are implicated mostly in motion processing while those comprising the ventral stream are involved in the processing of form and colour. This classic view of the cortical functional organization is challenged by the existence of reciprocal connections of visual cortical areas with the thalamic nucleus named pulvinar. These connections allow the creation of a trans-thalamic pathway that parallels the cortico-cortical communications across the visual hierarchy.

The main goal of the present thesis is twofold: first, to obtain a better comprehension of the processing of light increments and decrements in an area of the cat ventral stream (area 21a); second, to characterize the nature of the thalamo-cortical inputs from the cat lateral posterior nucleus (LP) to area 21a.

In study #1, we investigated the spatiotemporal response profile of neurons from area 21a to light increments (brights) and decrements (darks) using a reverse correlation analysis of a sparse noise stimulus. Our findings showed that 21a neurons exhibited stronger responses to darks with receptive fields exhibiting larger dark subfields. However, no differences were found between the temporal dynamics of brights and darks. In comparison with the primary visual cortex, the dark preference in area 21a was found to be strongly enhanced, supporting the notion that the asymmetries between brights and darks are transmitted and amplified along the ventral stream.

In study #2, we investigated the impact of the reversible pharmacological inactivation of the LP nucleus on the contrast response function (CRF) of neurons from area 21a and the primary visual cortex (area 17). The thalamic inactivation yielded distinct effects on both cortical areas. While in area 17 the LP inactivation caused a slight decrease in the response gain, in area 21a a strong increase was observed. Thus, our findings suggest that the LP exerts a modulatory influence on

the cortical processing along the ventral stream with stronger impact on higher order extrastriate areas.

Taken together, our findings allowed a better comprehension of the functional properties of the cat ventral stream and contributed to the current knowledge on the role of the pulvinar on the cortico-thalamo-cortical processing of visual information.

Keywords: area 21a, primary visual cortex, reverse correlation, lateral posterior nucleus, contrast response, electrophysiology, thalamic inactivation.

Table of contents

List of Tables

List of Figures

INTRODUCTION

ARTICLE #1

Abbreviations

1D, 2D, 3D: One, two, three dimensions

AchE: Acethylcholinesterase

AEV: Anterior ectosylvian area

ALLS: Anterior lateral suprasylvian cortex

AMPA: α-amino-3-hydroxy-5-methyl-4-isoxazolepropionic acid

BA: Bright subfield area

BARS: Bayesian adaptive regression splines

Cb: Center of mass of bright subfield

Cd: Center of mass of dark subfield

CI: Confidence interval

Cm: Magnocellular layers

Cp: Parvocellular layers.

CRF: Contrast response function

Ctr: Control

DA: Dark subfield area

DC: Direct current

dLGN: Dorsal part of the lateral geniculate nucleus

ECG: Electrocardiogram

EPSP: Excitatory postsynaptic potential

FFN: Feedforward network

FS: Fast spiking

GABA: Gamma-Aminobutyric Acid

GABAa: Ionotropic GABA receptor

GABAb: Metabotropic GABA receptor

GUI: Graphical user interface

Inj: Injection

LGN: Lateral geniculate nucleus

LP: Lateral posterior nucleus

LPl: Lateral part of LP

LPm: Medial part of LP

MT: Middle temporal area

NMDA: N-Methyl-D-aspartic acid

OA: Overlapped area

PCA: Principal component analysis

PI: Inferior pulvinar

PIp, PIm, PIcm, PIcl: Posterior, medial, central medial and central lateral parts of PI.

PLLS: Posterior lateral suprasylvian cortex

PLvl: Ventrolateral part of the lateral pulvinar

PMLS: Posteromedial lateral suprasylvian cortex

PSTH: Peri-stimulus time histogram

RDK: Random dots kinematogram

Rec: Recovery

RF: Receptive field

RS: Regular spiking

SEM: Standard error of the mean

SNR: Signal to noise ratio

SOI: Subfield overlap index

SSI: subfield size index.

TEO: Posterior part of the inferotemporal cortex

TMS: Transcranial magnetic stimulation

UN: Unclassified

V1, V2, …: cortical visual areas (primary, secondary...)

VLS: Ventral lateral suprasylvian area

Ao meu mentor, compadre e amigo,
Professor Dr Fabrício Bezerra de Sá

Acknowledgements

First, I would like to express my gratitude to my supervisor, Dr Christian Casanova, who, despite his heavy schedule, found the time to discuss and to give me valuable guidance in my research endeavours. I would like to thank my co-supervisor, Dr Frédéric Lesage for his support and availability which was of great help, mainly in the first years of my PhD.

I would like to present my special thanks to my PPPPPG partner #1, M Thomas, who always participated actively in my research projects, motivated me to push my limits and to see through the BS factor. It was an honor to work with you, my friend. A special thanks to my friend and PPPPPG partner #2, Samuel. You always encouraged me and taught me to see the bright side in every dark moment during my research. Thank you both, my PPPPPG partners. I am still confident that we are in the right track regarding our *Cervidae* brain-debugging project.

Thank you, Geneviève, for your valuable support. Without your help, it would be impossible to carry out all the projects that I worked on.

Thanks to my friend, Jimmy, for having my back during the long hours of cat experiments and virtual battles.

I extend my sincere thanks to Reza, Azadeh, Alexandre Castonguay and Marianne Groleau for being so kind and always generous with their time to help me during my first moments in the lab.

My special thanks to Fred. Unfortunately, we did not work together, but I enjoyed having another Arduino enthusiast to talk to. Your dedication to science greatly inspired me.

Thanks to all my friends from the other labs: Bruno, Mira, Jun, Rafael and Jesse. A special thanks to Robyn and Thomas, that always took the lead to organize our extra-curricular activities. Nothing would have happened without you.

My sincere thanks to Jeroen and Julie for the great moments that we spent together in and outside the lab.

I also extend my sincere gratitude to the following former and present members of the school staff: Mme Guitouni, Mme Bélanger, Mme Oriol, M Fethy, Mme Ginette Parent, Sabine

Demosthènes, Mme Chantal, Mme Nicole and François for their support and assistance during my PhD.

A special thanks to my friend Umit. You always applied the same scientific rigor in the analysis of the most mundane subjects. It was great to work with you.

Thanks to my lab colleagues Nelson, Olivia and Visou. My special thanks to Nelson. Thank you for the significant help with my project and for the several interesting discussions. Thanks to Olivia for the huge help with the corrections of my thesis. Thanks to Visou for the help with my cat experiments. It was a valuable experience to work with you guys.

My sincere thanks to my Sabine who had the patience and wisdom to deal with the several nervous breakdowns from a PhD student at his final years. Thanks to Mme Laurie and M Pierre for the encouragement.

And finally, but not least, I am deeply grateful to my mother, Edna, for the emotional and moral support given to me my whole life.

Introduction

The visible light constitutes a small fraction of the electromagnetic spectrum. The survival of most life forms on earth depends directly or indirectly on their interactions with light. For instance, plants use light to generate energy through photosynthesis, while animals use vision, along with other sensorial systems, to probe their surroundings.

The eye is the sensory organ of the visual system. The eye's anatomy and function intrigued scientists for centuries. Since then, several aspects of the eye's development, anatomy and functions were unraveled (Gehring, 2014). Nonetheless, a perfect understanding of how the eye works is not sufficient to explain how vision works. Indeed, the eye presents only the first steps in order to understand the phenomenon of vision. The visual information generated in the back of the eye (i.e. the retina) is carried across the optic nerve to the brain. In the brain, networks of neurons are responsible for the transformation of the visual signal originated in the eye to create the visual perception in order to guide behaviour (Kandel et al., 2000). To date, several aspects of the structure and function of these neuronal networks remain unknown. Nonetheless, the study of the visual system allowed not only a better comprehension of the several mechanisms underlying visual perception, but also contributed to the understanding of neuronal mechanisms involved in distinct processes of brain function.

In this thesis, I will present the results from our research which focuses on different aspects of the cortical processing of visual information in cats. More specifically, one study explores the functional properties of an extrastriate cortical area (area 21a). In a second study, we investigated the implications of the inactivation of the Pulvinar (a thalamic nucleus involved in visual processing) on the activity of area 21a and the primary visual cortex (area 17).

1 The organization of the visual system

In this section, I will explore the current knowledge on the structure and function of the visual system in mammals. I will briefly address the organization of subcortical key structures that compose the retino-geniculo-cortical pathway, before focusing on the structure and function of the visual cortex. Since the cat constituted the animal model used in my research, several aspects of the visual system of this species will be addressed in more detail. However, the visual system of other species will be addressed for comparison purposes.

The retina lies on the fundus of the ocular globe and represents the first stage of the visual system where the information is transformed from light (photons) to electro-chemical signals that are conveyed to the cortex via the thalamus. Often regarded as an extension of the central nervous system, the retina is organized in *strata* consisting of different neuronal types and glial cells. In the outermost layer of the retina are located the light-sensitive cells (photoreceptors) responsible for transforming the light in electric impulses. In the absence of light, the photoreceptors are maintained in a depolarized state and once the light reaches its outer segments, the photoreceptor hyperpolarizes initiating the transmission of the visual information. The signal is then modulated throughout the synapses with different neuronal types and finally reaches the ganglion cell layers from which the information is sent to the thalamus through the optic nerve (Kandel et al., 2000).

Signals originating from the retina are heterogenous in nature. Based on electrophysiological recordings of ganglion cells, optic nerve fibres and thalamic neurons, three distinct types of functional routes were identified: X, Y and W pathways. These pathways are classified based on their physiological properties that are linked to different morphological types of ganglion cells, the beta, alpha and gamma cells, respectively. Neurons from the X pathway are characterized by exhibiting a burst response followed by a tonic response to high spatial frequencies at low temporal frequencies. In contrast, the Y cells exhibit mainly a burst response to stimuli with low spatial frequencies at high temporal frequencies (Enroth-Cugell and Robson, 1966; Ferster, 1990). The X and Y pathways process fairly distinct features of the visual scene. X cells are responsible for the processing of fine details, such as shape and colour while Y cells are good movement detectors. Furthermore, recordings of the optical nerve showed that the

temporal dynamics of X and Y cells differ, in which Y fibres transmit the action potentials faster than X fibers (Ferster, 1990). In other words, the Y pathway provides the cortex with a fast information about sudden changes in the visual scene (i.e. if something moved), while later the X pathway informs the visual cortex about the details of the visual scene (i.e. what moved). The less investigated W pathway is characterized by cells whose responses are frequently described as "sluggish" and exhibiting features that are in between the X and Y (Payne and Peters 2002).

The signals from the retina are conveyed to the cortex via the thalamus. Axons from the optic nerve make synapses with two main subcortical structures, the superior colliculus and the dorsal part of the lateral geniculate nucleus (dLGN). The superior colliculus, located in the mesencephalon, is largely connected with subcortical structures and is associated with oculomotor control, while the dLGN represents the main thalamic relay transmitting the visual information to the primary visual cortex (Laties and Sprague, 1966; Matteau et al., 2003; Meikle and Sprague, 1964; Niimi and Sprague, 1970).

The cat dLGN is located dorso-laterally in the thalamus and has a sigmoid shape antero posteriorly. The nucleus is organized in layers divided in two main regions based on the size of the cell bodies: magnocellular and parvocellular. The magnocellular region covers the dorsal part of the dLGN and is constituted of three distinct layers: A, A1 and Cm. The parvocellular region is located ventrally to the Cm layer and is also comprised of three layers: C1, C2 and C3. These are more compact and their boundaries less distinguishable than the magnocellular layers and are often considered as one layer (Cp). The retinal input to each layer is alternated between the nasal part of the contralateral and the temporal part of the ipsilateral retina. This anatomical segmentation parallels the functional segregation of the distinct pathways originated at the retina. The layers A and A1 receive X and Y signals while layer Cm receives Y signals only. The W pathway makes synapses mostly with the parvocellular layers. A similar organization pattern is observed in the macaque monkey where the Magno, Parvo and Koniocellular fibres from the retina arrive at their respective layers in dLGN (Payne and Peters 2002, Figure 1).

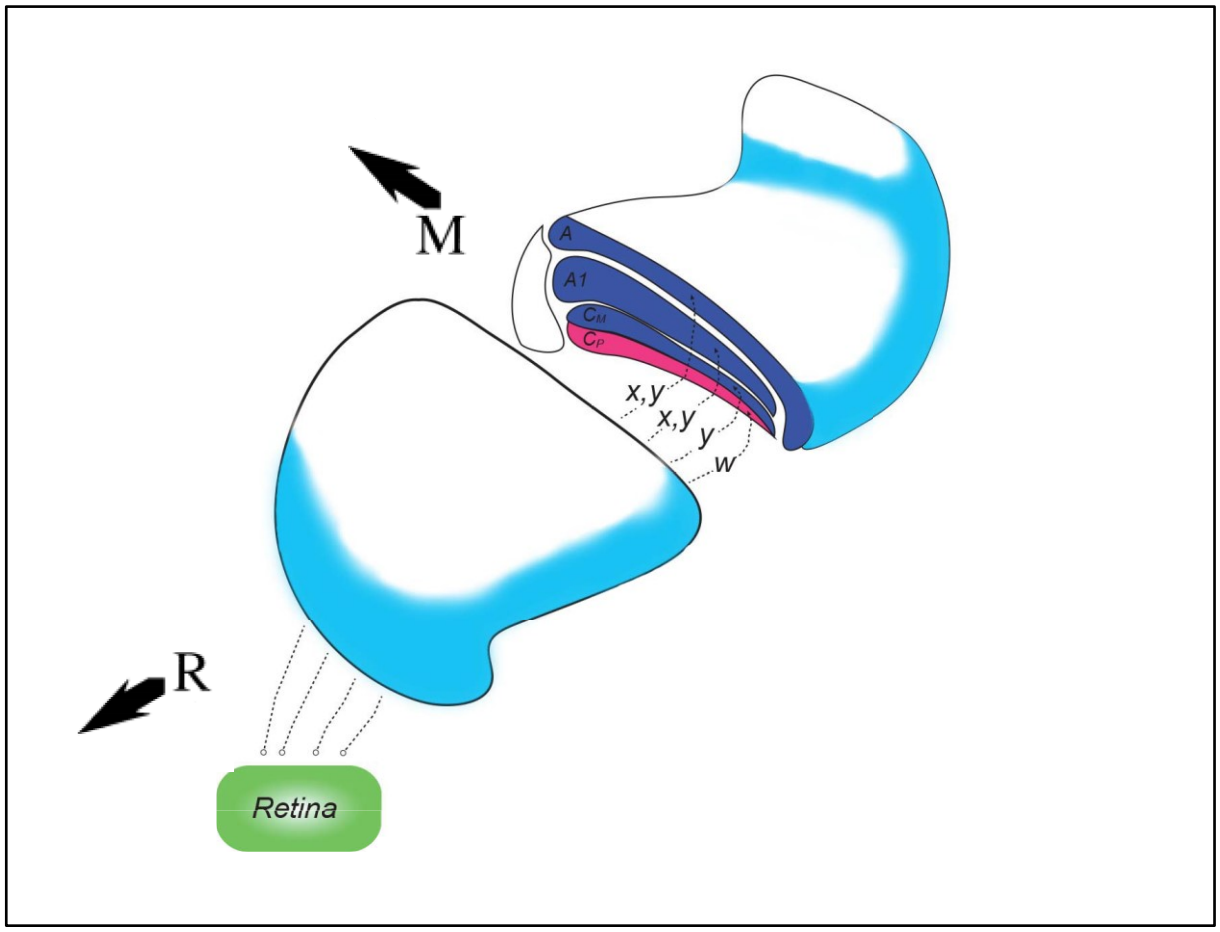

Figure 1. Representation of the cat LGN and the main retinal inputs (X,Y and W) projecting to the magnocellular (A, A1 and Cm) and parvocellular layers (Cp). Adapted from Payne and Peters (2002). R: rostral; M: medial.

Another level of organization found in the dLGN is its retinotopy. In brief, a retinotopic organization is achieved when neighbouring ganglion cells in the retina project to neighbouring neurons in the dLGN creating a topographic map of the visual space. Indeed, the two-dimension representation of the visual space from each retina is distributed in the 3D volume of both dLGN where the elevation is represented in the antero-posterior axis and the azimuth is represented in the latero-lateral axis (Naito, 1986; Sanderson, 1971).

The dLGN consists of two main cellular types: relay neurons and interneurons. Differences between these neurons lie mainly on their connectivity pattern and on the nature of these connections (e.g., neurotransmitters and receptor types). Regarding the connectivity of dLGN neuronal types, the relay neurons are the only ones establishing synapses with the visual cortex, and therefore, are responsible for conveying the message to the cortex. The interneurons are

mostly connected with the relay neurons and with themselves. The relay neurons are excitatory in nature using glutamate as a neurotransmitter. On the other hand, the interneurons are inhibitory and use the neurotransmitter GABA. Although, the dLGN is often seen as a simple relay of the retinal signals to the cortex, the activity of relay neurons is modulated by the local circuitry of interneurons as well as by feedback cortical projections. Therefore, this view remains an oversimplification of the dLGN function. It is noteworthy to mention that other thalamic nuclei are equally directly or indirectly involved in the processing of the visual information. For instance, the pulvinar represents an important thalamic nucleus involved in the cortical visual processing (Sherman, 2017). The main structural and functional characteristics of this nucleus will be addressed in section 4.3.

Although the information originating from the retina is modulated at the dLGN, the output remains segregated (i.e. X and Y pathways) until it reaches the primary visual cortex. This underlies a common feature of the sensorial system in which distinct signals are conveyed to the brain in a parallel fashion. Then, at the cortical level, the signals are extensively converged and passed to higher levels of processing in order to construct the full perceptual visual experience (Nassi and Callaway, 2009).

In the next section, I will explore the organization and function of the visual cortex with an emphasis on the different neuronal properties that arise at the primary visual cortex as well as the main features of extrastriate areas and their connectivity.

2 Visual cortex

The neocortex is the latest structure to be developed in brain evolution. For most vertebrates, the cortex is composed of distinct functional areas in which different neuronal types are organized in layers. In addition, the visual cortex is classically viewed as organized in an hierarchical manner, where the complexity of information increases from one area to another, culminating with the perceptual visual experience. The primary visual cortex represents the first level of processing of visual signals coming from the thalamus, and its basic structure and neuronal properties will be addressed.

2.1 The primary visual cortex

The primary visual cortex of the cat is composed of two areas: areas 17 and 18 (Payne and Peters 2002). At a first glance, it seems odd that two distinct areas share the first stage of cortical processing of visual information instead of one single area, as the primate V1. That is mainly due to the fact that both areas are targeted by the main afferents originating from the dLGN. The thalamic input into those areas differ significantly. Area 17 receives mostly signals from the X and Y pathways, while area 18 is mostly innervated by Y fibres (Humphrey et al., 1985; Stone and Dreher, 1973). All dLGN fibres arrive to layer 4 of the primary visual cortex (Freund et al., 1985). The local neuronal circuitry, along with long-range synapses from other cortical areas, transforms the signal originating from thalamus, which is passed along the cortical hierarchy and also to subcortical visual structures (Hubel and Wiesel 1962; Updyke 1977).

The convergence of thalamic inputs into neurons in the primary visual cortex gives rise to new properties that are absent in the lower levels of the visual system. Classical experiments performed in cats and monkeys by Hubel and Wiesel in the 1960's demonstrated that neurons from the primary visual cortex fire when a bar is presented only at specific orientations, while neurons from the dLGN do not express selectivity for any orientation of the stimulus (Hubel and Wiesel 1962; Hubel and Wiesel 1968). These studies demonstrated that the signals from the dLGN are integrated at cortical level conferring a new feature (orientation selectivity) that lacks at precedent stages of the visual processing (Figure 2). The study of these neuronal properties, in addition to the knowledge of the cortical connectivity, allowed scientists to better comprehend the mechanisms underlying the cortical processing of visual information.

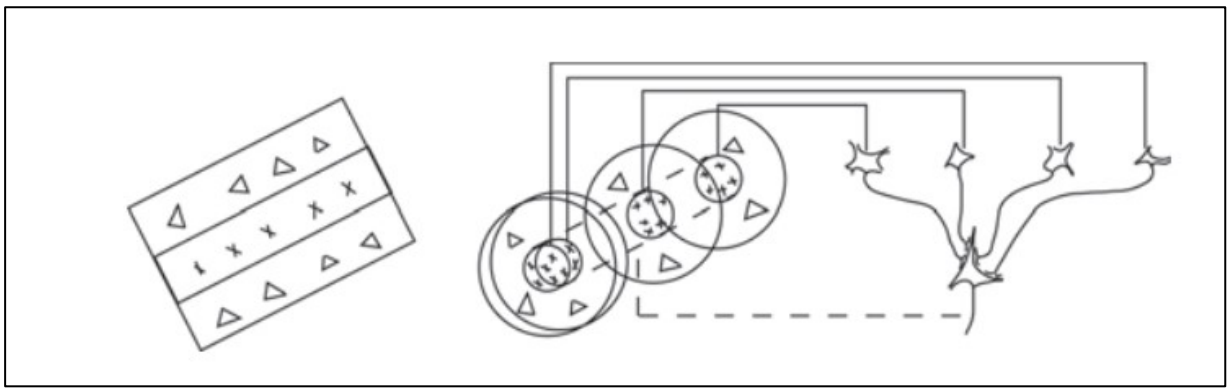

Figure 2. Hubel and Wiesel's view of the receptive field of a V1 simple cell. On the left, the representation of the spatial profile of the neuron's receptive field showing a ON region (crosses) flanked by two OFF regions (triangles). On the right, diagram showing the origin of the simple cell's receptive field by the integration of signals from different dLGN neurons. Adapted from Hubel and Wiesel (1962).

2.2 The neuron receptive field

The concept of receptive field (RF) was first used in vision in the late 1930s by Hartline (1938) to describe the area in the retinal surface that, when illuminated, elicits a neuronal response. Since then, the concept was applied to all areas of the visual system and it has been updated in order to cope with the increasing complexities of neurons across cortical areas (David et al., 2006; DeAngelis et al., 1993a; Jones et al., 1987; Livingstone et al., 2001).

Receptive fields of retinal ganglion cells and dLGN neurons are organized in two concentric regions responding to opposite stimuli. For example, some ganglion cells respond to a light spot directed at the centre of its RF (ON-center), but when the light is positioned at the surround region, the neuron's firing rate is significantly reduced. On the other hand, OFF-center neurons are inhibited by a light spot on its centre and stimulated when the light is positioned at the surround area (Figure 3). This type of RF organization is known as the centre surround (Kuffler, 1953) and this spatial organization represents the building blocks for the construction of more complex RFs found in the visual cortex (Hubel and Wiesel, 1968).

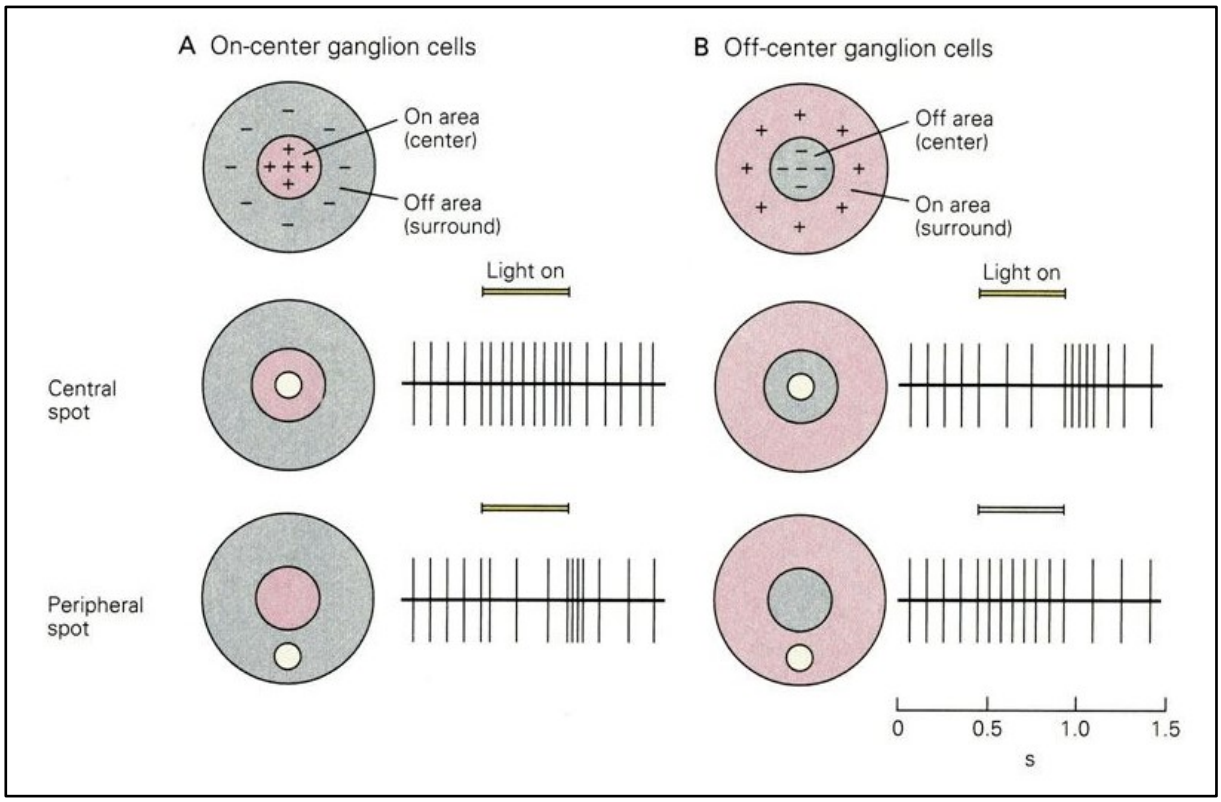

Figure 3. Representation of the centre surround organization of the receptive fields of ON-center (A) and OFF-center (B) ganglion cells showing the modulation of the neuronal activity (vertical traces) depending on the position of the visual stimulus (light spot). From Kandel, Schwartz, and Jessell (2000).

As in the X/Y pathways introduced in section 1, light increments (ON) and decrements (OFF) are equally processed in parallel throughout the early visual system (Hartline, 1938; Kuffler, 1953). In addition, an asymmetry in the processing of ON and OFF channels is observed early in the visual system. For instance, in the retina, neurons encode OFF signals faster than ON (Burkhardt, 2011; Burkhardt et al., 1998; Copenhagen et al., 1983; Nichols et al., 2013). Those differences are preserved in the LGN and in neurons from layer IV of the primary visual cortex (Jin et al., 2011, 2008; Komban et al., 2014). Additionally, evidence suggests that the differences between ON and OFF pathways are preserved throughout the visual cortex (Chubb and Nam, 2000; Komban et al., 2011, 2014; Motoyoshi et al., 2007).

In the primary visual cortex, neurons respond differently to ON and OFF signals. Two main cell types can be identified based on the spatial arrangement of ON/OFF responses: simple and complex cells. Simple cells are characterized by having RFs with ON and OFF subregions located next to the other. For instance, when a light bar was positioned over a ON region, the

neurons discharged, but when the bar was extended to the adjacent OFF region the response was reduced, showing that the concomitant stimulation of opposite regions cancel each other. On the other hand, complex cells exhibit a distinct RF organization in which ON and OFF subregions are superimposed. In this case, once a light bar is drifted across the RF, the neuron exhibits a sustained response independent of the position of the stimulus (Hubel and Wiesel 1962).

The RF structure from neurons of the primary visual cortex is directly linked with basic properties of those neurons. For instance, simple cell RFs are elongated and oriented at a particular angle. Interestingly, when a light bar is drifted across the RF, the neuron maximal discharge is obtained when the bar is positioned at the RF's orientation, giving rise to an orientation selectivity tuning (Figure 4). Furthermore, the size and the number of ON and OFF RFs' subregions is associated with the neuron's spatial frequency selectivity (Jones and Palmer, 1987). Since the early work from Hubel and Wiesel (1962), different approaches were used to study the neuronal properties of the primary visual cortex. For instance, drifting sinusoidal gratings were extensively used to characterize the RF properties from cells of the primary visual cortex. Due to the nature of the stimulation, the response to the gratings can be easily assessed by Fourier transformation. Indeed, previous studies showed that neurons from the cat primary visual cortex can be classified based on the linearity of the response to drifting gratings (De Valois et al., 1982; Movshon et al., 1978a; Skottun et al., 1991). For instance, linear responses correspond to neurons that are highly modulated by the stimulus, whereas neurons with non-linear profiles are poorly modulated. These response profiles are associated with the RF structure-based classification in simple (high modulation) and complex (low modulation) cells previously proposed by Hubel and Wiesel (Skottun et al., 1991) and are used in the classification of neurons from the primary visual cortex. In addition, the Fourier decomposition of the responses to gratings were previously used to create a 2D spectral structure of simple cells receptive fields (Jones et al., 1987). The method used in the study allowed the researchers to investigate the assumption that the spatial frequency and orientation selectivity were the result of two separate processes. Interestingly, they have found that was not the case, suggesting that the spatial frequency and orientation are interdependent.

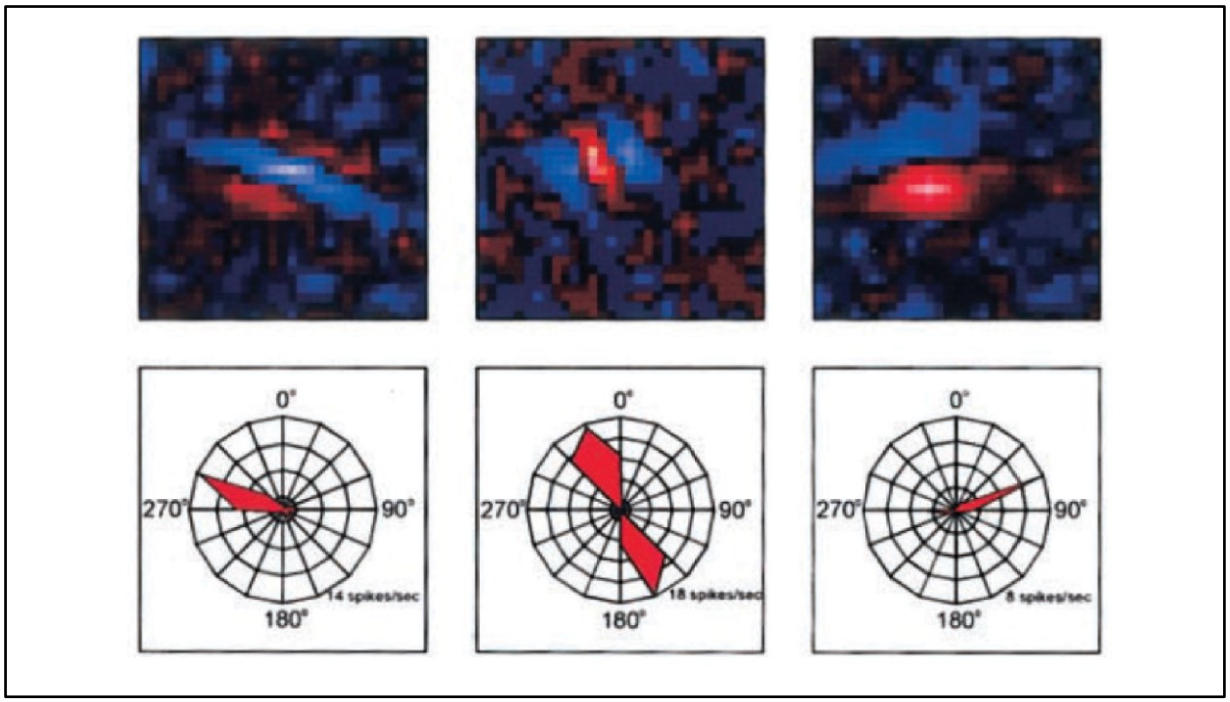

Figure 4. Examples of receptive fields (top) and orientation tuning curves (bottom) from simple cells of the ferret primary visual cortex. From Usrey, Sceniak, and Chapman (2003).

2.2.1 The reverse correlation method

As introduced above, several properties of visual neurons were characterized by the analysis of the average neuronal response to distinct visual stimuli, such as drifting light bars or sinusoidal gratings. Despite this, most of these approaches do not fully take into account the 3D structure of the receptive field: the 2D spatial domain and the time domain (DeAngelis, Ohzawa, and Freeman 1995). In order to address this issue, different methods have been used to provide a more comprehensive description of the receptive field features of neurons in the visual cortex. For instance, the sparse noise reverse correlation technique has been successfully used in the characterization of neurons from the primary visual cortex (J. P. Jones and Palmer 1987, Figure 5). This method was used in a set of experiments for this thesis in order to characterize the RF profile of neurons from a higher cortical area of the cat (study #1).

The reverse correlation method consists in the cross correlation of a neuron's action potentials (spikes) with stimuli previously presented in a predetermined time window (Jones and Palmer, 1987). In this method, the correlation of the spikes with the preceding visual stimuli gives an approximation of a neuron's RF (Eggermont et al., 1983). This procedure is undertaken as a

function of time, which creates an estimate of the spatiotemporal (3D) RF structure (DeAngelis, Ohzawa, and Freeman 1993a).

A variety of visual stimuli has been used to assess the RF structure using the reverse correlation method (Borghuis et al., 2003; DeAngelis et al., 1993a; Nishimoto et al., 2006; Pack et al., 2006; Ringach et al., 1997). For instance, in our study #1, the spatiotemporal RF of 21a neurons was obtained using a sparse noise stimulus. The stimulus consisted on a pseudo-random sequence of small white and black squares briefly presented over a gray screen (Figure 5). This visual stimulus tends to have a small effective energy (Reid et al., 1997). Thus, there is a minimum stimulus size and duration of presentation in order to reliably elicit a spike (DeAngelis et al., 1993a; Reid et al., 1997). Another aspect of the sparse noise reverse correlation that should be taken into consideration is the number of stimuli presented. This method is sensitive to the absolute number of spikes generated by the dark and bright stimuli and a considerable number of repetitions (20 to 50 presentations) is necessary to generate reliable spatiotemporal RF maps (DeAngelis et al., 1993a; Jones and Palmer, 1987; Reid et al., 1997).

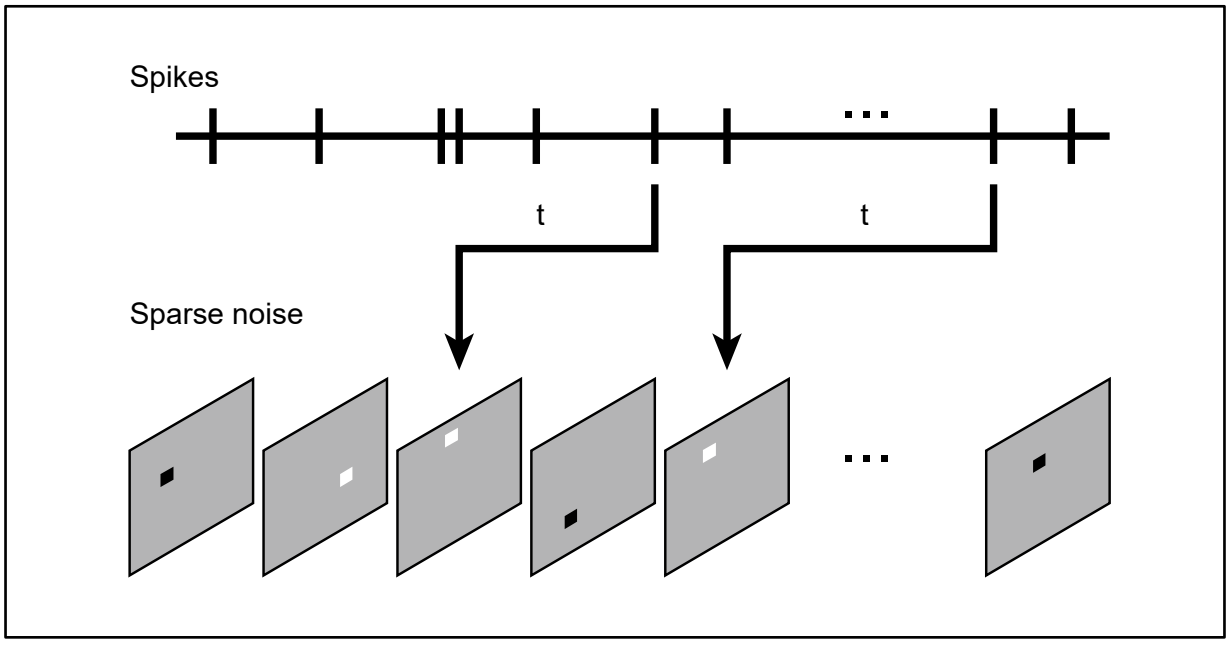

Figure 5. Diagram representing the reverse correlation algorithm. The spikes are correlated with the preceding visual stimulus (sparse noise) at different time delays (t). Inspired by (Yeh et al., 2009a).

Simple cells from the cat primary visual cortex were extensively studied using the method of reverse correlation. Jones and Palmer described several types of simple cells with subfields

exhibiting different sizes, shapes, relative position and strength (Jones and Palmer, 1987). Due to limitations on their equipment, the RF's temporal profile was not characterized at the time. About five years later, DeAngelis, Ohzawa and Freeman were able to overcome this technical barrier as they conducted a thorough investigation of the RF properties from simple cells in the spatiotemporal dimensions (DeAngelis et al., 1993a, 1993b). The RFs of simple cells from the cat primary visual cortex were analysed in the space-time joint domain by creating X-T plots where one dimension represents the axis perpendicular to the RF orientation and the other represents time. For simplicity, the spatial dimension corresponding to the RF orientation was not considered. The analysis of the X-T plots revealed two main types of simple cells: space-time separable and inseparable. Space-time separable receptive fields suggest that spatial and temporal features are processed independently. In other words, the 2D spatiotemporal profile (X-T profile) can be estimated as the product of two 1D profiles (i.e., spatial and temporal functions). In contrary, RFs that are space-time inseparable exhibit X-T profiles with oblique subfields showing that the spatial location of these regions changes over time. This indicates that the spatiotemporal profile cannot be explained by the product of two 1D independent functions (DeAngelis, Ohzawa, and Freeman 1993a).

Previous studies have demonstrated that simple cells integrate their inputs linearly both in space (DeAngelis et al., 1993b; DeValois et al., 1979; Movshon et al., 1978a) and time (DeAngelis et al., 1993a, 1993b). Given that, several response properties of simple cells, such as spatial, temporal and velocity tunings, can be estimated from the Fourier decomposition of their first-order spatiotemporal RF structure (DeAngelis et al., 1993a, 1993b). In contrast, complex cells are known to integrate the input signals in a nonlinear fashion (Movshon et al., 1978b). Thus, one cannot accurately predict the neuronal properties of complex cells based on the Fourier decomposition of their first-order RF structure, as performed in simple cells (DeAngelis et al., 1993b; Szulborski and Palmer, 1990). Instead, higher-order responses are used to investigate the RF of complex cells (Ohzawa et al., 1990; Szulborski and Palmer, 1990). For instance, Szulborski and Palmer (1990) characterized the spatial profile of complex cells from the cat area 17 using a modified method of sparse noise reverse correlation where two stimuli were presented at a time. In this case, the second-order spatial RF structure was created by assessing the

responses of complex cells as a function of the relative position and polarity of the light bars on the screen (Szulborski and Palmer, 1990).

Different visual stimuli were used with reverse correlation and other similar approaches have been used in order to investigate different properties from RFs of neurons across the visual system (Borghuis et al., 2003; Churan et al., 2012; Pack et al., 2006). For instance, a common stimulus used in the reverse correlation is the dense noise (i.e., white noise). The stimulus consists of a sequence of images formed by pixels with opposite polarities randomly distributed in space and time and it is mainly used to assess linear RFs (Reid et al., 1997; Ringach and Shapley, 2004; Sakai et al., 1988) but it is also applied to non-linear systems under specific circumstances (Chichilnisky, 2001). More recently, Nishimoto et al. (2006) developed a different reverse correlation method using the white noise stimulus in which a spectral analysis of the cross correlation is performed with sections of the visual stimulus (local spectra reverse correlation). The main advantage of this method is that the spatial frequency tunings and orientation can be obtained from both simple and complex cells and the fact that the spectral analysis is performed in small regions of the stimulus spatial heterogeneity can be identified in and between the RF subfields (Nishimoto et al., 2006). Sinusoidal gratings are equally used with the reverse correlation technique in which a random sequence of gratings at different orientations and spatial frequencies is presented. This method is useful to assess the neurons' optimal responses to those parameters and, when the linearity assumption is respected, the neuron's spatial frequency tuning can be obtained from the Fourier decomposition of the RF spatial profile (Nishimoto et al., 2005; Ringach and Shapley, 2004; Ringach et al., 1997).

Recent studies have explored the usage of more sophisticated visual stimuli in the investigation of the RF structure (Livingstone et al., 2001; Pack et al., 2006; Talebi and Baker, 2012). For instance, Richert et al. (2013) created a reverse correlation method in order to investigate the RFs of neurons from the primate extrastriate area MT, a higher order cortical area associated with motion processing. Their stimulus consisted of a grid in which small dots drift independently of each other. The reverse correlation reveals a high resolution receptive field map that provides information about the direction selectivity of each subregion. Interestingly, the method revealed MT neurons with heterogenous preferred directions providing insight on the complexity of the neuronal processing of these higher order cortical areas. Naturalistic visual

stimuli have been increasingly used in vision research (Sekuler and Bennett, 2001; Simoncelli and Olshausen, 2001). David et al. (2006) used natural images to assess the RF of the primate area V4, an extrastriate area specialized in processing shape and colour. They were able to characterize the spatial and orientation tuning of neurons from area V4 based on the Fourier analysis of RFs. Furthermore, based on the spectral structure of the responses to natural images, the researchers could predict the neuronal tunings for classical stimuli such as sinusoidal gratings. Similarly, reverse correlation analysis of neuronal responses from cat area 18 to natural images, dense and sparse noise revealed that the former, along with sparse noise, had the most predictive power regarding the neuronal frequency tunings (Talebi and Baker, 2012). More recently, the same group used natural images to characterize the spatiotemporal structure of RFs of neurons from the cat area 18 (Talebi and Baker, 2016). Interestingly, they identified different RF types based on their responses to the naturalistic visual stimuli that challenges the classical classification of simple and complex cells in the early visual cortex.

Thus, the concept of receptive field initially proposed by Hartline (1938) was greatly expanded throughout the last decades. The advances in the technology and the development of sophisticated analytical methods contributed to the understanding that the receptive field is a dynamic structure that is modulated by the visual input in both the spatial and temporal domains. Furthermore, the comprehension of the spatiotemporal structure of the receptive field is important in order to understand the mechanisms underlying the cortical processing of visual information.

2.3 The response to contrast

In the natural environment, the level of luminance of the visual scene is highly variable, with areas with low (shadows) and high (highlights) luminance, rapidly changing as the eye scans the surroundings. Even though individual photoreceptors in the retina are primarily sensitive to variations in luminance levels, this does not provide much useful information about the environment. Instead, the differences of luminance across the visual scene relative to the average luminance level (i.e. contrast) is found to be more relevant in the visual system. Indeed, the contrast coding arises early in the retina where bipolar (Burkhardt, 2011) and ganglion cells RFs (Kuffler, 1953) are sensitive to local differences in luminance levels.

In general, visual neurons in the cortex increase their firing rate monotonically with increasing contrast. However, neurons respond weakly to lower contrasts while it reaches a plateau at high contrast levels giving the neuron's response a sigmoidal profile. This nonlinear response pattern is named the contrast response function (CRF) and it was observed across several visual areas in different species such as cats, primates and humans (Albrecht and Hamilton, 1982; Gardner et al., 2005; Ohzawa et al., 1982; Sclar et al., 1990). The shape of the CRF is better characterized by a hyperbolic function first used by Naka and Rushton (1966) in retinal recordings (Albrecht and Hamilton, 1982). The Naka-Rushton equation is shown in Figure 6A and described in detail in the methods section in article #2 of the thesis.

To date, it is widely accepted that visual neurons from different cortical areas respond similarly to contrast. This seemingly ubiquitous response profile across the visual hierarchy makes the CRF a useful tool to investigate the visual function. Indeed, several studies used the CRF in a plethora of methodological approaches from single-unit recordings to psychophysical measurements (Albrecht and Hamilton, 1982; Boynton, 2005; Duong and Freeman, 2008; Gardner et al., 2005; May and Solomon, 2015; Soma et al., 2013). Furthermore, since the response to contrast arises early in the retina and is preserved throughout the visual hierarchy (Burkhardt et al., 1998; Ohzawa et al., 1982; Tardif et al., 1996; Zhao et al., 2001), one could say that the CRF represents a "raw" measurement of the mechanisms underlying a neuron's processing of visual information. Additionally, changes in the shape and position of a neuron's CRF gives us clues on how the information is transformed throughout the cortical circuitry (Soma et al., 2013). For instance, a change in a neuron's sensitivity to contrast can be translated into a left or rightwards shift of the CRF (contrast gain control, Figure 6 C), changes in the spontaneous activity is translated as a baseline control (Figure 6B), while a change of a neuron's

firing rate in function of the contrast level would be identified as a change on the CRF shape (response gain control, Figure 6 D).

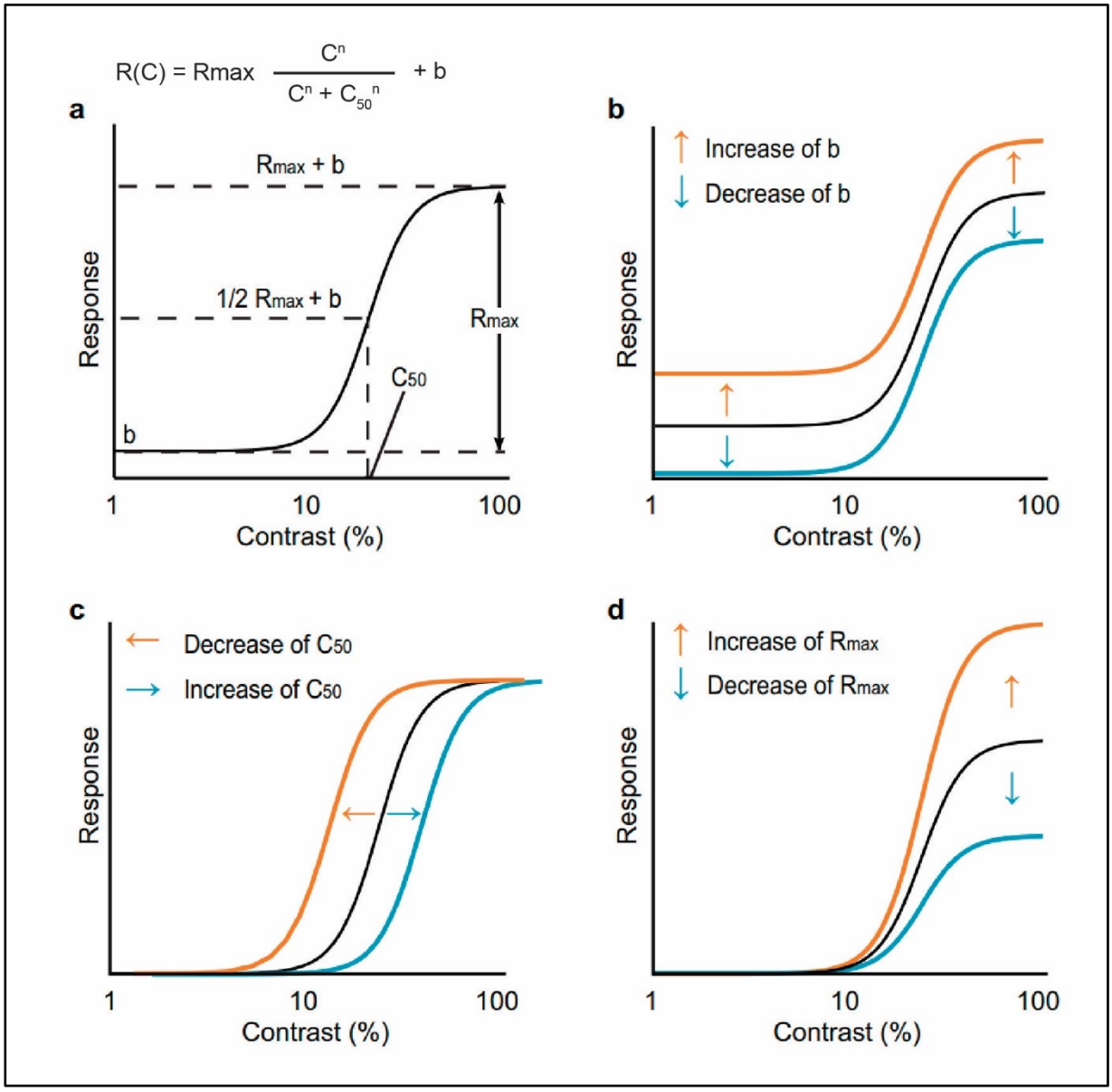

Figure 6. The Naka-Rushton function and three examples of changes in the contrast response profile. A) Naka-Rushton function and graphical representation of its variables (the factor "n" representing the curve slope is not depicted in the graph), B-D) Examples of changes in the contrast response function characterized by changes in the Naka-Rushton variables. B) Baseline control (b). C) Contrast gain control (C50). D) Response gain control (Rmax). From Soma et al. (2013).

3 The cortical hierarchy

As briefly introduced in the previous section, the visual cortex is known to be organized in a hierarchical manner, in which the processing of visual information becomes progressively complex when the signal passes from lower to higher levels in the cortical hierarchy. For decades, this concept was investigated by several research groups and a body of evidence shows that the visual cortex exhibits a hierarchical organization based on anatomical as well as on functional properties (Felleman and Van Essen, 1991; Jay Hegdé and Daniel J. Felleman, 2007; Kaas and Collins, 2001).

From an anatomical standpoint, the visual hierarchy is defined by the connectivity patterns between cortical areas. These patterns are characterized by the laminar position of feedforward and feedback connections between cortical areas. In general, feedforward connections originate from the supragranular layers from a lower level area reaching the granular layer (layer IV) of the next area. Then, feedback projections from the infragranular layers of the higher-level area attain the supragranular layers of the lower level area. For instance, V1, the first level of the cortical hierarchy, receives inputs from the dLGN at the granular layer IV. Supragranular layers of V1 send feedforward inputs to V2 (higher cortical area) while the infragranular layers receive feedback inputs from V2 supragranular layers. Based on these parameters, Felleman and Van Essen (1991) mapped the hierarchical structure of the primate visual cortex with 32 cortical areas placed in 10 hierarchical levels. Later, Scannel et al. (1995) applied the methods used by Felleman and Van Essen (1991) to trace the hierarchical structure of the cat visual cortex. They have identified 22 visual cortical areas occupying 14 levels in the cat visual hierarchy (Figure 7).

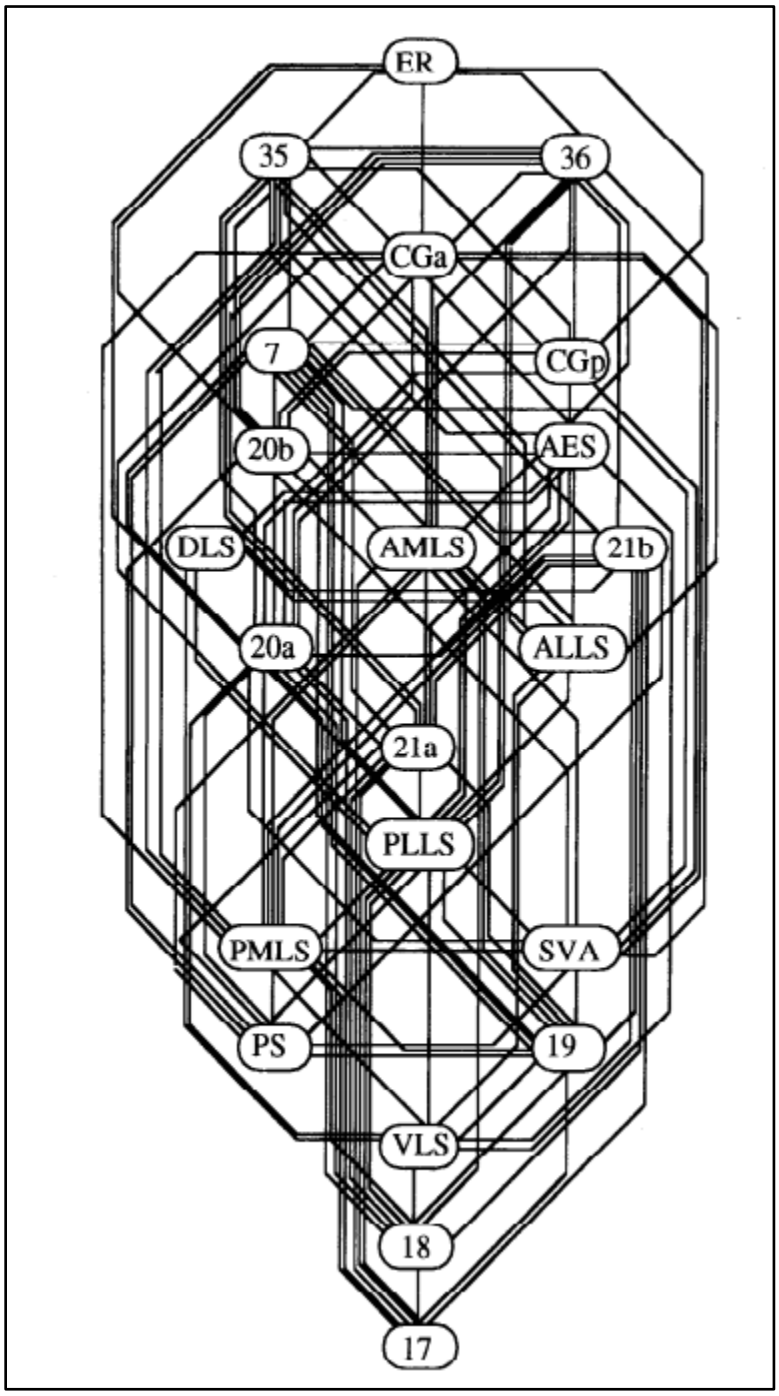

Figure 7. Hierarchy of the cat visual system. (Scannell et al., 1995).

Although there is a consensus on the anatomical hierarchical organization of the visual cortex, there is no evidence that the visual processing follows strictly the same anatomical hierarchy. Indeed, previous studies have demonstrated that the cortical processing of visual information, although exhibiting some degree of hierarchy, is not undertaken in an orderly hierarchical sequence (Jay Hegdé and Daniel J. Felleman, 2007). Instead, a body of evidence indicates that distinct aspects of the visual scene (e.g., colour, form and motion) are processed in parallel pathways involving different cortical areas at different hierarchical levels (Grill-Spector and Malach, 2004). The studies of Mishkin et al (1983) were of most importance for the establishment of the functional organizational framework of the visual cortex. In their lesion studies in monkeys, they observed that focal lesions on the parietal cortex caused significant impairment during a spatial task, while lesions on the temporal cortex compromised the recognition of objects. They proposed that the visual processing is divided into two main parallel pathways: the dorsal and ventral streams (Mishkin, Ungerleider, and Macko 1983; Goodale and Milner 1992, Figure 8). The dorsal stream, also known as the "where" pathway, is implicated in spatial location, while the ventral stream, associated with object recognition, is known as the "what" pathway (Grill-Spector and Malach, 2004; Mishkin et al., 1983).

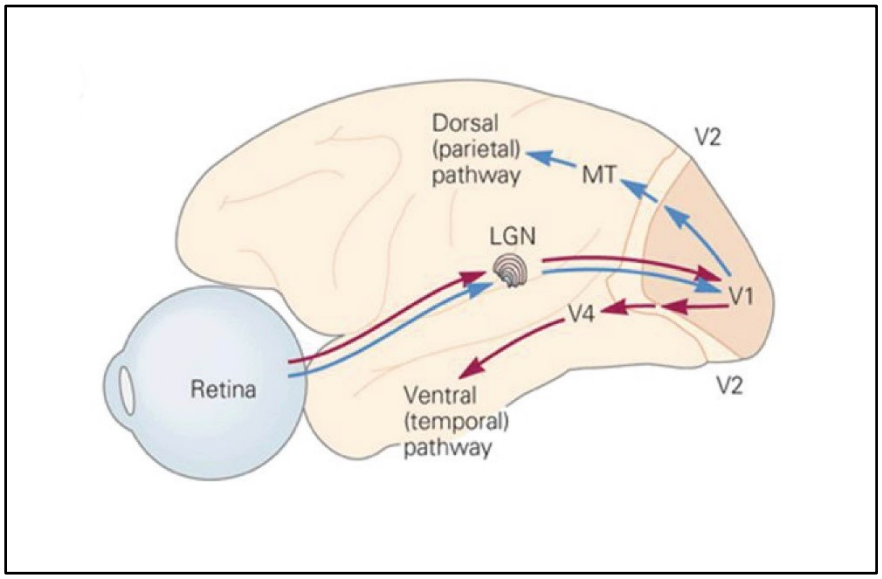

Figure 8. Diagram of the visual streams of the primate visual cortex. The gateway higher order areas from the dorsal (MT) and ventral (V4) pathways are depicted. From Kandel, Schwartz, and Jessell (2000).

3.1 The dorsal visual stream

The dorsal stream is composed of visual areas located at the occipital-parietal cortex. As mentioned above, studies in primates revealed that lesions in the dorsal stream cause specific impairments related to visuospatial behaviour (Mishkin et al., 1983; Ungerleider and Haxby, 1994). In addition, several reports of lesions in visual areas in the human brain described impairments in different visually guided behaviours such as object reaching and spatial localization (de Haan and Cowey, 2011; Kravitz et al., 2011).

One particular feature of the visual processing that the dorsal stream is known to be implicated in motion perception. In the primate brain, the area MT represents the gateway of the dorsal stream and previous studies indicated that it is directly implicated in movement perception. For instance, lesions to this area causes akinetopsia, the inability to perceive motion, in humans and non-human primates (Blanke et al., 2002). Neurons from area MT receive inputs from the primary visual cortex through areas V2 and V3. MT neurons have large RFs and are highly selective to stimulus direction, which may be explained by the fact that this area receives inputs from V1 direction selective neurons. However, the similarities between MT and V1 ends there. In contrast with the primary visual cortex, MT neurons are capable of processing more complex visual stimuli such as pattern and global motions (Ajina et al., 2015; Pack et al., 2001; Smith et al., 2005; Wang and Movshon, 2015).

In cats, a body of evidence based on anatomical and functional properties indicate that the extrastriate visual cortex is equally organized in dorsal and ventral streams (Lomber, 2001; Lomber et al., 1996; Payne, 1993). Among the areas composing the dorsal stream, the area PMLS is the most studied. Previous studies identified this area as a homolog of the primate area MT and it is considered to be the gateway area of the cat dorsal stream (Burke et al., 1998; Lomber, 2001; Payne, 1993). PMLS receives its main input from supragranular layers of cortical areas 17 and 18 as well as from area 19 (Symonds and Rosenquist, 1984b, 1984a) and PMLS neurons exhibit similar properties with their primate counterpart. For instance, PMLS neurons are highly direction selective and exhibit large RFs (Piché, Thomas, and Casanova 2013; Toyama et al. 1994; Vajda, Lankheet, and van de Grind 2005; Y. Wang et al. 1995). Additionally, previous studies have demonstrated that PMLS neurons respond to complex

stimuli such as global motion and moving texture patterns (Brosseau-Lachaine et al., 2001; Li et al., 2000a; Merabet et al., 2000; Villeneuve et al., 2006).

3.2 The ventral visual stream

The ventral stream is located along the occipito-temporal cortex. In the primate visual hierarchy, it begins with the area V4 and extends to higher order areas such as area TE. The processing of visual information increases in complexity across the ventral stream hierarchy. The ventral stream is implicated in the processing of different visual features, from the physical properties of objects (e.g. colour, shape, size, orientation and texture) to the more complex computing such as face and body recognition (Kravitz et al., 2011; Mishkin et al., 1983; Taylor and Downing, 2011). In addition, the ventral stream establishes connections with the hippocampus and amygdala which are implicated in visual memory (e.g. recalling a familiar visual object) and perception of emotions (de Haan and Cowey, 2011).

In the primate visual cortex, the area V4 represents the first step on the ventral stream processing. It receives its main input from V1 and V2 and it is in the area V4 that several visual features associated with physical properties of objects are encoded. For instance, evidence has clarified the role of area V4 in the processing of complex shapes (Kobatake and Tanaka, 1994; Orban, 2008; Pasupathy and Connor, 1999). The group of Van Essen assessed the responsiveness of V4 neurons to a type of complex stimuli named non-cartesian gratings, consisting of hyperbolic and polar sinusoidal gratings. They observed that V4 neurons are more responsive to hyperbolic and polar gratings compared to classic cartesian gratings (Gallant et al., 1993). Later, they have identified subgroups of neurons that are selective to specific types of non-cartesian gratings and that cells with similar preferences are anatomically clustered (Gallant et al., 1996). These results show that the processing of the visual information in area V4 is more complex than what was previously described in earlier areas of the cortical hierarchy. The area V4 was also found to be involved in texture perception. Arcizet et al. (2008) used a database of different natural images in which several texture patterns at different illumination conditions were presented to awake monkeys. In their study, most of V4 neurons recorded were selective to natural texture patterns and the texture preference was not influenced by the

illumination angle. This “illumination invariance” of texture perception is important in object recognition where the illumination conditions of the visual scene are constantly changing.

Previous studies conducted by Connor and colleagues investigated the responses of V4 neurons to contours (e.g. angles and curvatures), which are considered as a primitive type of shape (Pasupathy and Connor, 1999, 2001, 2002; Yau et al., 2013). They have demonstrated that most V4 neurons responded preferentially to the contour stimuli compared to bars and gratings. In addition, many V4 neurons were selective to a specific contour position and orientation. When combining different curves into more complex shapes, Pasupathy and Connor (2001) demonstrated that V4 neurons are selective to specific curves in relation to the centre of the shape. Later, they calculated that V4 could encode complex shapes at a populational level based on the neuronal processing of individual contours and boundaries (Pasupathy and Connor, 2002).

3.2.1 The cat area 21a

Among the different extrastriate areas of the cat visual cortex encompassed in the ventral stream, the area 21a was the most explored. The area 21a is considered as the gateway of the ventral stream in this species and it is known to be a homolog of the primate area V4 (Payne, 1993). The area 21a is located at the posterior bank of the lateral suprasylvian cortex and it makes boundaries medially and caudally with area 19 and laterally with areas PMLS, VLS and 21b (Shipp and Grant, 1991; Tusa and Palmer, 1980). The area 21a receives cortical input from the primary visual cortex (areas 17 and 18) and to a lesser extent from area 19 (Conway et al., 2000; Grant and Hilgetag, 2005; Shipp and Grant, 1991; Symonds and Rosenquist, 1984b, 1984a). Nevertheless, evidence suggests that the main cortical driver input comes from area 17. For instance, a previous study demonstrated that the inactivation of area 17 by reversible cooling caused a significant decrease of neuronal activity in area 21a (Michalski et al., 1993). Moreover, the area 21a receives its main thalamic input from the cortico-recipient region of the lateral posterior nucleus and the pulvinar (Symonds et al. 1981; Raczkowski and Rosenquist 1983).

The area 21a exhibits a retinotopic representation of part of the central visual space covering around 20 degrees of visual axis (Michalski et al., 1993; Tusa and Palmer, 1980). Most of 21a neurons are complex-like and exhibit a wide range of RF sizes (average of 5 degrees) that

increase in function of the eccentricity (Dreher et al., 1993; Wimborne and Henry, 1992). Previous studies have characterized several properties of 21a neurons using classical visual stimuli such as bars and sinusoidal gratings (Wimborne and Henry 1992; Mizobe et al. 1988; Toyama et al. 1994; Tardif et al. 1996; Morley and Vickery 1997; Dreher et al. 1993). For instance, most neurons are selective to orientation while exhibiting poor direction selectivity (Mizobe et al., 1988; Toyama et al., 1994; Wimborne and Henry, 1992). More recently, Villeneuve et al. (2009) used the technique of optical imaging of intrinsic signals to characterize the modular organization of area 21a. They observed that, while 21a exhibits a clear modular pattern for orientation selectivity, this cortical area lacks a direction selectivity map (Figure 9). In addition, most of 21a neurons are sharply tuned to low spatial frequencies and exhibit poor selectivity to temporal frequencies (Tardif et al. 1996; Wimborne and Henry 1992; Morley and Vickery 1997). In a more recent study, the analysis of local field potentials in area 21a revealed that the neuronal activity is poorly correlated with the stimulus motion and lacks temporal selectivity tuning (Kayser and Konig, 2006). Taken together, these studies demonstrate that area 21a displays unique functional properties compatible with the processing of spatial features of the visual scene that is characteristic of the ventral stream. Moreover, previous studies demonstrated that most of 21a neurons are optimally activated by binocular stimulation and are sensitive to binocular disparity, indicating that the area 21a may also play a role in depth perception (Vickery and Morley 1999; Morley and Vickery 1999).

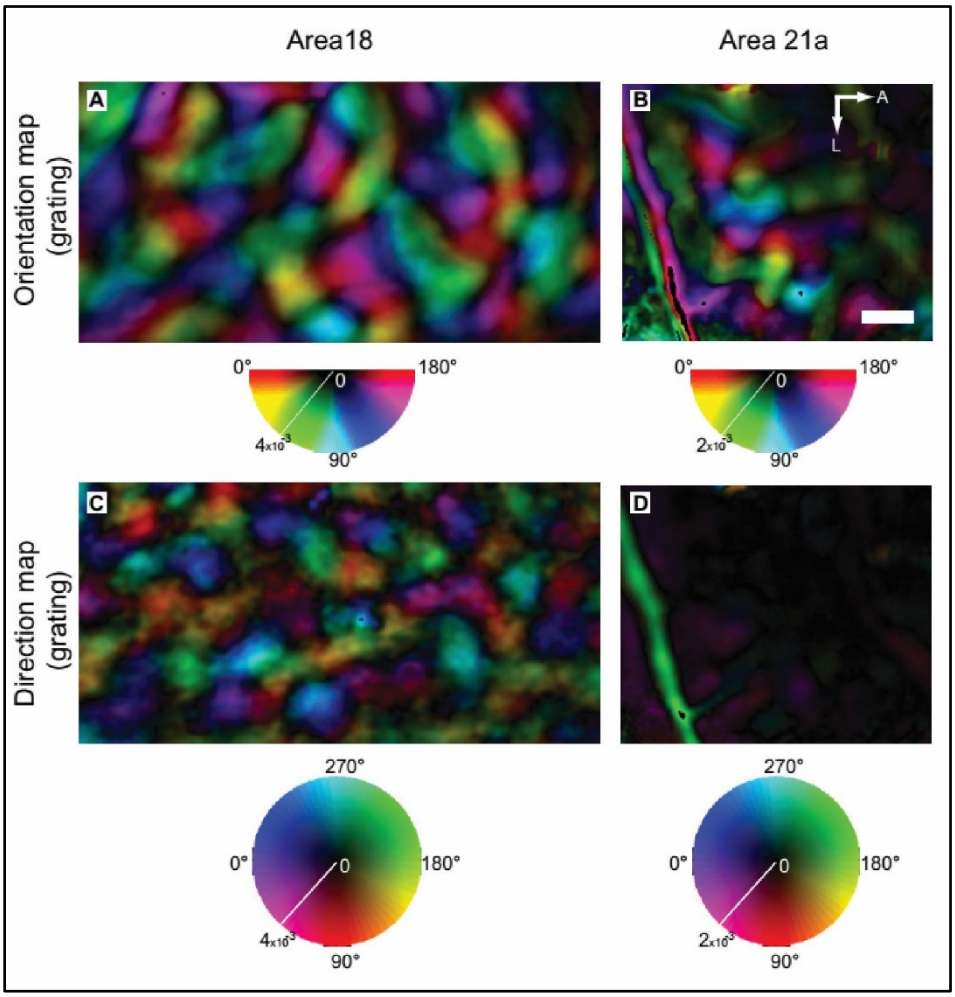

Figure 9. Organization of orientation (top) and direction (bottom) of areas 18 and 21a revealed by optical imaging of intrinsic signals. Contrary to area 18, area 21a exhibits an orientation map but lacks a modular organization for direction. From Villeneuve, Vanni, and Casanova (2009).

3.3 Perception and action

In parallel with the neurophysiological experiments performed in non-human primates and cats, several psychophysical studies in humans addressed the same questions about the cortical hierarchy and its functional organization in dorsal and ventral streams. In a particular set of experiments performed in a patient with visual agnosia (patient DF), Goodale and Milner (1992) provided a reinterpretation of the "what" and "where" pathways first proposed by Mishkin and Ungerleider (1982). In their interpretation, instead of having two systems dedicated to process object recognition and visuospatial perception, both dorsal and ventral streams would

use both types of information to achieve two distinct outputs: visually guided behaviour and visual perception respectively (Ganel and Goodale, 2017).

It is worth noting that the findings in the field of neuropsychology do not necessarily invalidate the body of evidence on the anatomical and neurophysiological data. Indeed, the question of how the processing of the different visual features is divided across the distinct cortical areas remains a topic under debate (Ganel and Goodale, 2017; Milner, 2017; Rauschecker, 2017). In the next section, I will introduce another piece of this puzzle by explaining the role of the thalamus on the cortical processing of visual information.

4 The visual thalamus

In the previous section, we reviewed the main aspects of the cortical hierarchical organization and how the visual information flows across the different cortical areas in order to create visual perception. In the classical view of the visual system, the retinal signals are relayed through the thalamus to the visual cortex where information processing is mainly undertaken (Kandel et al., 2000). Under this perspective, the thalamic structures involved in visual processing are regarded as simple relays placed between the retina and the primary visual cortex (Sherman and Guillery 1996). The idea of the thalamic structures as a relay was present in the minds of neuroscientists for a long time and is still portrayed in basic neuroscience textbooks. As it will be addressed below, a large body of evidence indicates that the role of the thalamus in visual processing lies beyond the function of a simple relay.

The lateral geniculate nucleus, in particular its dorsal part (dLGN), is the most studied thalamic structure involved in visual processing. For decades, a growing number of studies described the complex structure and connectivity of the dLGN (Laties and Sprague, 1966; Naito, 1986; Niimi and Sprague, 1970; Sanderson, 1971; Stone and Dreher, 1973; Van Horn et al., 2000). Despite this, its role in visual function was frequently associated with a simple machinelike relay (Sherman and Guillery 1996). Instead, the thalamus was previously believed to be mostly involved with changes in the arousal states of the brain as well as in sleep and wakefulness cycles, with little impact on the processing of visual signals *per se* (Sherman and Guillery, 1996). In fact, this is not the case, as the visual thalamus is actively implicated in different levels of the cortical processing. For instance, the dLGN not only sends the information from the retina

to the cortex, but also receives a large number of cortico-thalamic inputs from different visual cortical areas that makes possible to dynamically modulate the dLGN's output to the primary visual cortex (Kawamura et al., 1974; Updyke, 1977). This is only one example from a large body of evidence that underscores the notion that the visual thalamus supersedes its classical view as a simple relay of retinal signals (Sherman 2007).

Among several research groups, the influential work of Sherman and Guillery made an important contribution for the current knowledge of the role of the thalamus on sensory information processing. They have provided a framework of the thalamic circuitry organization that largely instigated further studies helping to advance the knowledge on the thalamic function. The main aspects of their work, and others that followed, will be addressed below.

4.1 Drivers and modulators

The organizational framework proposed by Sherman and Guillery is based on the properties of the inputs received by the thalamic neurons that are connected to the cortex. The authors have identified two main types of inputs: drivers and modulators (Sherman and Guillery 1998). Driver inputs transmit the main message that is relayed to the cortex. On the other hand, modulator inputs influence the transmission of the driver without causing any substantial changes in the main message (Sherman and Guillery 1998; Reichova and Sherman 2004).

The presence of both inputs, drivers and modulators, was reported in several thalamic nuclei involved in sensory processing. In particular, the cat dLGN was extensively studied and is frequently referred to as a typical example to illustrate the driver/modulator concept (Sherman and Guillery 1998; Sherman and Guillery 1996). The driver input to the dLGN comes from the retina, while descending projections from the cortex represent the main modulatory inputs to the relay neurons. Previous studies estimated that only a minority of the synapses made with a relay neuron (5-10%) is of driver type while corticothalamic modulatory projections comprise 30 to 40% of inputs (Figure 10A) (Sherman 2017). The remaining arise from the local inhibitory GABAergic neurons, the thalamic reticular nucleus and projections from the brainstem (Sherman 2007; Van Horn, Erişir, and Sherman 2000).

The main aspects that differentiate drivers and modulators are associated with the morphology of input axons, their relationship with the thalamic relay neuron, as well as with the structure and functional properties of synapses (Sherman and Guillery 2013). Drivers are characterized by thick axons with large terminals (Figure 10C). Those terminals make synapses at the proximal regions of the relay neuron's dendrites. In contrast, modulators exhibit thin axons with small terminals that are mostly located at the distal parts of the dendrites (Van horn and Sherman 2004; Liu, Honda, and Jones 1995). Another criterion that differentiates drivers from modulators is the degree of convergence of the axons onto the target relay neuron. Driver inputs converge less into a relay neuron while modulators are highly converged (Reichova and Sherman, 2004). This assumption is supported by morphological and physiological evidence (Sherman and Koch 1986; Usrey, Reppas, and Reid 1999). For instance, as stated above, previous studies have demonstrated that dLGN relay neurons are connected to a small number of retinal axons (low convergence of drivers) while a larger number of synapses with corticothalamic projections (high convergence of modulators) is present (Hamos et al., 1987; Van Horn et al., 2000). Furthermore, the degree of convergence can be estimated by assessing the responses of a relay neuron in function of the electrical stimulation of its inputs (Reichova and Sherman, 2004). The rationale behind it is that an increasing stimulation of highly converged inputs create a monotonic increase of the neuron's response. However, the increasing electric stimulation of inputs with low convergence induces an all-or-none step response by the relay neuron (Lee and Sherman, 2008). Previous studies successfully used this functional approach to corroborate the nature of thalamic inputs based on morphological criteria (Lee and Sherman, 2008; Reichova and Sherman, 2004; Viaene et al., 2011).

At the synaptic level, drivers and modulators differ mainly on the type of glutamatergic postsynaptic receptor. Drivers activate only ionotropic receptors (i.e. AMPA and NMDA) while modulators activate both types, but mostly metabotropic receptors (Figure 10A) (Sherman 2017). The differences in the synaptic composition of drivers and modulators cause distinct effects on the excitatory postsynaptic potentials (EPSPs) at the relay neuron. For instance, electrophysiological recordings of thalamic relay neurons revealed that the stimulation of driver inputs induces large EPSPs whereas the activation of modulatory synapses creates EPSPs with small amplitudes (Reichova and Sherman, 2004). In addition, the repetitive stimulation of driver

synapses causes a progressive decrease of EPSPs (paired-pulse depression, Figure 10B) (Lee and Sherman, 2008; Reichova and Sherman, 2004). This is due to both the depletion of synaptic vesicles and to the desensitization of postsynaptic receptors. This phenomenon indicates that driver synapses have a high probability of neurotransmitter release. On the other hand, the activation of modulatory synapses causes paired-pulse facilitation, indicating a low probability of neurotransmitter release (Sherman and Guillery 2013). In summary, the functional properties of ionotropic and postsynaptic metabotropic glutamatergic receptors are strictly associated with the concept of drivers and modulators, respectively. Ionotropic receptors have a fast temporal resolution and, as stated above, are reliably activated creating large EPSPs. Those characteristics are compatible with the transmission of the driver signal. Instead, postsynaptic metabotropic receptors have a slower temporal dynamic and higher firing rates from the presynaptic neurons are required in order to be activated. These properties are compatible with modulatory inputs allowing a longer-lasting change of the neuron's state to modulate its response to the driver input (Reichova and Sherman 2004; Sherman and Guillery 2013).

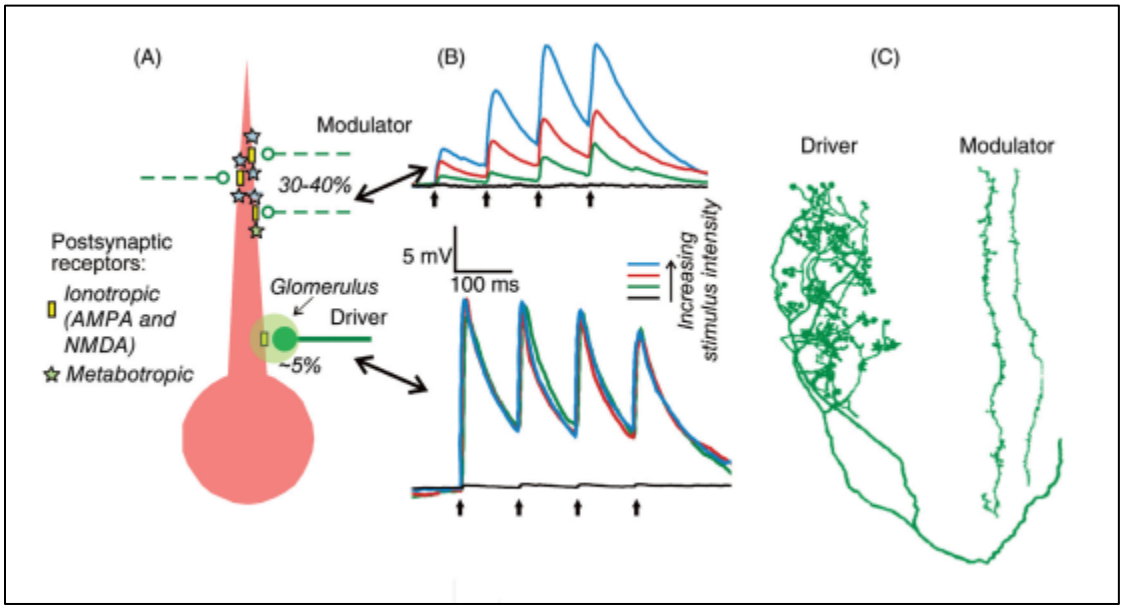

Figure 10. Functional and morphological features of drivers and modulator thalamic inputs (Sherman 2017).

Until now, evidence suggests that driver signals are only transmitted by excitatory neurotransmitters such as glutamate (Sherman and Guillery 2013). On the other hand, it is worth noting that different neuromodulators, such as acetylcholine and dopamine, area also implicated in the thalamocortical circuitry (Govindaiah and Cox, 2006; Soma et al., 2013). Nevertheless, evidence suggests that these inputs are more sparsely distributed in the thalamus and may exhibit different anatomo-functional properties from the glutamatergic postsynaptic modulators (Sherman and Guillery 2013).

Although the classification of inputs into two categories allowed a better understanding of the role of thalamic structures on the cortical processing of information, this classification system was not meant to be exhaustive and recent efforts on the expansion of this framework have been made. For instance, recent studies suggested the existence of more than two types of projections (Bickford, 2016; Viaene et al., 2011). In a recent review, Bickford extended the classification of drivers and modulators by acknowledging the existence of a third type of projection named "driver-like" that exhibits morphological and functional features that are "in between" drivers and modulators and are mostly present in tectorecipient thalamic nuclei (Bickford, 2016). In a different approach, Abbot and Chance (2005) proposed a classification of driver and modulator based on the net output of a neuron. They have considered driver the inputs that provoke linear transformations of a neuron's membrane potentials while modulator inputs would cause a non-linear multiplicative net effect on the membrane voltage.

4.2 First and higher order thalamic nuclei

The concept of drivers and modulators gave rise to another organizational framework that categorizes thalamic nuclei in function of the nature of their driving inputs. Sherman and Guillery (1998) identified two types of thalamic nuclei: first and higher order. First order nuclei receive their driving input from the periphery (e.g., retinal input to the dLGN). Therefore, first order nuclei are responsible for relaying the information from the world to the cortex. Higher order nuclei, on the other hand, have no or little driving input from subcortical areas, receiving most of its driving inputs from the cortex, specifically from layer 5 (Sherman and Guillery 1998; Rovó, Ulbert, and Acsády 2012; Jones 2001). The best-known example of a higher order nucleus

is the pulvinar, which is involved in visual processing and it will be addressed in more detail further below.

Apart from the origin of the main driving input, previous studies have demonstrated that there are other differences between first and higher order nuclei. For instance, the proportion of driving inputs in higher order nuclei is smaller than in first order nuclei (2% and 5%, respectively), suggesting that modulatory inputs are relatively more abundant in the former (Van Horn et al., 2000; Wang et al., 2002). Indeed, previous studies have demonstrated that higher order nuclei receive a greater number of GABAergic projections from several subcortical regions compared to first order nuclei (Bokor et al., 2005; Gulcebi et al., 2012).

4.2.1 Higher order nuclei and the transthalamic pathway

The classical hierarchical view of sensory processing simply does not take into account the existence of higher order thalamic nuclei. Instead, one could say that the classical view is somewhat "corticocentric" in which the information is transferred to the cortex via first order relays and is processed sequentially at cortical level before producing an output. Nevertheless, in a context where the brain machinery is regarded as a circuit in which it receives inputs from the external world (e.g., visual signals), interprets it and subsequently plans and executes an output (e.g., visually guided behaviour), the presence of higher order thalamic nuclei is justified (Sherman 2016).

The connectivity pattern of higher order nuclei shows that these thalamic structures are intimately related to the cortex. Indeed, higher order nuclei are reciprocally connected with several cortical areas allowing the thalamus to participate actively in the transmission of the sensorial information across the cortex. In other words, higher order nuclei participate in a transthalamic or cortico-thalamo-cortical pathway that, in some extent, parallels the cortico-cortical transmission of information (Guillery and Sherman 2002; Sherman and Guillery 2002; Petrof, Viaene, and Sherman 2012; Casanova 2004).

In this alternative view, where higher order thalamic nuclei are implicated in a parallel transthalamic pathway, one important question stands out: why would a transthalamic parallel pathway linking different cortical areas exist when corticocortical connections are present? In fact, a body of evidence on morphological and functional properties of higher order nuclei and

their connections with the cortex provided important insights into this question (Sherman and Guillery 2013; Casanova 2004). For instance, neurons involved in corticocortical connections do not project branches to subcortical structures, while neurons that project to higher order thalamic nuclei, exhibit axon branches targeting subcortical areas, mostly motor centres (Petrof et al., 2012). This supports the idea that the corticocortical and the transthalamic pathways carry distinct information across cortical areas. In addition, the idea that corticothalamic axons project to lower motor areas implies that higher order nuclei function as a router of efference copies (Sherman 2016). The information sent to a subcortical motor region from a particular cortical area is equally received by the higher order thalamic nucleus which informs the next cortical area in the hierarchy about the message from the previous one (Sherman 2016).

Another interesting hypothesis is that higher order nuclei act as a gating mechanism that controls the information flow across cortical areas (Purushothaman et al. 2012; Sherman and Guillery 2013). Sherman and Guillery (2013) argue that the strong GABAergic input in higher order nuclei makes them a suitable structure for gating control, which is unlikely to occur by the direct corticocortical pathway. This gating control would be pertinent in routine situations (e.g., resting or walking through a familiar path) in which the cortex is not actively engaged, and the gate would be shut and no transthalamic information would flow towards higher cortical areas. In the opposite condition, an opened thalamic gate would allow a concomitant flow of information through both corticocortial and transthalamic pathways. This would allow a significant increase of the input strength at a particular cortical area receiving both thalamocortical and corticocortical inputs by means of nonlinear summation inducing strong activation of the cortical area (Sherman and Guillery 2013). Based on the knowledge of the anatomical hierarchy of cortical connections, Crick and Koch (1998) hypothesized that the nature of the connections (i.e., drivers or modulators) between the cortical areas and the thalamus should obey certain rules. In the so-called “no-strong-loop” hypothesis, it was postulated that reciprocally connected areas cannot drive each other. The rationale is that the existence of such hypothetical loops would be impossible because areas driving each other would invariably end up in an uncontrolled oscillatory state (Crick and Koch, 1998).

It is noteworthy that due to the complexity of the connectivity patterns and their nature, a complete understanding of the role of higher order thalamic nuclei in the cortical processing of

sensorial information has yet to be achieved and further studies are necessary (Sherman 2017; Bickford 2016; Casanova 2004). For instance, in the present thesis we approached this question by studying the role of the pulvinar nucleus in cortical visual processing.

4.3 The pulvinar

As stated in the previous section, the pulvinar is the higher order thalamic nucleus involved in visual processing. In fact, the pulvinar is the largest thalamic structure in the primate brain (Zhou et al. 2017). In comparison with rodents, the primate pulvinar occupies a proportionally larger volume of the thalamus, indicating a correlation with the pulvinar size and the higher order cortical functions performed by these animals (Chalfin et al., 2007). Previous studies suggested that additional cellular migratory pathways present during human brain development, but absent in other primate species, contribute to an increased connectivity between the pulvinar and the neocortex, and could be associated with the high cognitive functions characteristic of our species (Letinic and Rakic, 2001).

For decades, the role of the pulvinar nucleus intrigued researchers and, still today, it is often referred to as a "mysterious" or "enigmatic" thalamic structure (Baldwin et al., 2017; Bridge et al., 2015; Grieve et al., 2000). The main reason for this is that the pulvinar is connected to a large number of higher order cortical regions as well as to subcortical areas that are involved in different sensorial processes. A body of evidence suggests that the pulvinar is implicated in distinct high level visual processes such as complex motion integration, visual recognition of emotions, fear, visual salience and attention (Maior et al. 2010; Liddell et al. 2005; Arend et al. 2008; Robinson and Petersen 1992; White et al. 2017; Villeneuve et al. 2005). This is illustrated by several reports of partial and total lesions in the human pulvinar creating a plethora of visual impairments often associated with responses to visual threats, feature binding, emotional recognition of facial expressions, visual attention and oculomotor control, among others (Snow et al., 2009; Van der Stigchel et al., 2010; Ward et al., 2002, 2005, 2007). More recently, a number of functional brain imaging studies indicated that the pulvinar is implicated in several visual impairments associated with the pathophysiology of neuropsychiatric diseases such as Dementia, Alzheimer, ADHD and Schizophrenia (Delli Pizzi et al. 2014; Byne et al. 2007; Xia et al. 2012; Li et al. 2012; Green et al. 2009; Silverstein and Keane 2011).

Studies in humans provided insightful information on the role of the pulvinar on several higher order brain functions, including vision (Arcaro et al., 2018; Arend et al., 2008; Snow et al., 2009; Ward et al., 2002). However, variations in the extent of pulvinar lesions as well as the broad impact of some neuropsychiatric diseases prevent the characterization of the specific roles of the pulvinar in visual processing. Thus, the use of animal models is necessary to study the pulvinar function and its relationship with the cortex in a more controlled way. To date, different species including rodents, carnivores and primates are extensively used in pulvinar research (Zhou et al. 2017; Yu et al. 2015; Casanova 1993; Baldwin, Balaram, and Kaas 2017; Petry and Bickford 2018). In the next sections, I will provide an overview of the main findings on the structure, connectivity and function of the pulvinar of primates and cats.

4.3.1 The primate pulvinar

The studies of the primate pulvinar allowed a better comprehension of the complexity of the structure, connectivity and function of this thalamic structure (Baldwin et al., 2017; Grieve et al., 2000). In fact, naming the pulvinar a "nucleus" is an understatement while it should be rather regarded as a "complex" formed by distinct nuclei that differ in their neurochemical composition as well as in their connectivity with the cortex and ultimately their function (Baldwin et al., 2017).

4.3.1.1 Structure and connectivity

Based on anatomical criteria, early studies have subdivided the pulvinar in four regions: anterior or oral, medial, inferior and lateral (Kaas and Lyon, 2007; Olszewski, 1952). Since then, the pulvinar parcellation was revised and expanded by the inclusion of histochemical markers and the connectivity of each subdivision. This contributed for a better understanding of the structure of the pulvinar complex and consequently of its function (Grieve et al., 2000; Kaas and Lyon, 2007).

The anterior pulvinar has connections with somatosensory cortical areas and is often disregarded in studies concerning the visual system (Kaas and Lyon 2007; Baldwin, Balaram, and Kaas 2017). The medial pulvinar is subdivided in lateral and medial parts. The medial pulvinar has connections with different associative cortical areas at the prefrontal inferior parietal cortex.

Similarly, the dorsomedial part of the lateral pulvinar establishes connections with associative non-sensorial cortical areas (Gutierrez et al., 2000) (Figure 11). On the other hand, the ventrolateral part of the lateral pulvinar (PLvl) and subdivisions of the inferior pulvinar (PI) are both connected with the visual cortical areas. Furthermore, each region exhibits a retinotopic representation of the contralateral visual hemifield (Gattass et al. 2013; Ungerleider et al. 2014; Ungerleider et al. 1984). Thalamocortical projections from the PLvl target mainly the early visual areas V1, V2 but also the higher order areas from the ventral stream. Indeed, previous studies have demonstrated that area V4 as well as other cortical areas from the inferior temporal cortex, such as the area TEO, receive projections from the PLvl, indicating that this subdivision of the pulvinar is closely implicated in the "what" pathway in cortical visual processing (Adams et al., 2000; Shipp, 2003). The primate inferior pulvinar is composed of four regions: posterior (PIp), middle (PIm), central medial (PIcm) and central lateral (PIcl) (Kaas and Lyon 2007). Like the PLvl, the PIcl has connections with early visual areas V1 and V2 as well as the ventral stream area V4 (Adams et al., 2000). On the other hand, PIp, PIm and PIcm have connections with cortical areas from the dorsal stream. For instance, the major pulvinar projections to area MT is from PIm with sparse inputs from PIp and PIcm (Adams et al., 2000; Cusick et al., 1993; Lin and Kaas, 1980; Stepniewska, 2003).

Even though the pulvinar complex is a higher order thalamic structure, it also receives inputs from subcortical visual areas. For instance, PIp, PIcm and PIcl receive projections from the superior colliculus (Lin and Kaas, 1979). Given the cortical connections of these regions with cortical areas from the dorsal stream, the input from the superior colliculus provides an alternative pathway for the visual information from the retina to reach higher order cortical areas bypassing the primary visual cortex (Berman and Wurtz, 2011; Lyon et al., 2010). In addition, previous studies demonstrated the existence of direct retinal input to the inferior pulvinar that would also convey the visual information to higher order cortical processing (Campos-Ortega et al., 1970; Cowey et al., 1994; Itaya and Vanhoesen, 1983; Wamer et al., 2010).

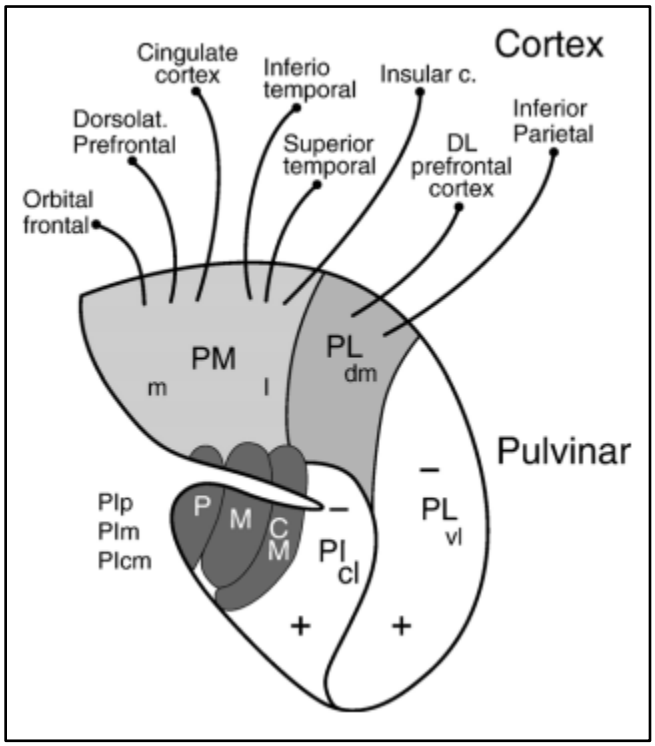

Figure 11. Representation of the primate pulvinar with its main subdivisions. The cortical targets of PM and PLdm are indicated (Kaas and Lyon 2007).

4.3.1.2 Functional properties and role in vision

The above-mentioned anatomical studies of the primate pulvinar provided an insight into the complexity of this thalamic structure and its connectivity with different cortical areas. Based on this knowledge, important questions are raised about the functional properties of the pulvinar subdivision and, more importantly, their role in visual processing.

In a first attempt to unravel the function of the pulvinar, early studies have investigated the RF properties of visual neurons from pulvinar subdivisions (Bender 1981, 1982). For instance, Bender (1982) described the response of neurons from the inferior pulvinar in anaesthetized macaques using simple visual stimuli such as drifting bars. Most of neurons in the inferior pulvinar exhibited large RFs that increased in size as a function of their visual field eccentricity. In addition, the majority of neurons were either selective to orientation or direction. This is not surprising, given the fact that the main driving input to the visual pulvinar comes from the primary visual cortex where neurons exhibit similar selectivity (Casanova 2004). On the other

hand, the responses to pulvinar neurons were found to be highly modulated by the brain arousal state (Bender 1982). Similar results were observed in another study performed in awake Rhesus monkeys in which the responses of neurons from the lateral and inferior pulvinar were profoundly modulated by eye movements and attention (Petersen et al., 1985). Later, the implication of the pulvinar in visual attention was confirmed behaviourally when the performance of monkeys during a visual attentional task was affected by the injection of GABA agonists in a region of the lateral pulvinar (Petersen et al., 1987).

Recent studies have further elucidated the role of the pulvinar in selective visual attention (Olshausen et al., 1993; Saalmann and Kastner, 2009, 2011; Shipp, 2004). For instance, a previous study suggested that the pulvinar controls the synchronicity between two cortical areas from the ventral stream (areas V4 and TEO) which is also highly modulated by attention (Saalmann et al., 2012). Similar results were reported in a later study in which the attentional modulation in the activity of area V4 was drastically reduced during pulvinar inactivation (Zhou, Schafer, and Desimone 2016). In addition, the authors observed that the pulvinar inactivation caused a reduction of the sensory-evoked activity of the recorded cortical area independently of the attention, suggesting that the pulvinar is also implicated in the basic processing of visual information in higher order cortical areas.

In the mechanism of selective attention, emotion-driven detection of visual stimuli is particularly important. For instance, the rapid detection of potential threats in the visual environment, such as predators, is imperative for the individual survival and, thus, confers a relevant evolutionary advantage to the perpetuation of the species. Indeed, previous studies have demonstrated that fearful images (e.g., snakes or spiders) are detected more rapidly than neutral images (e.g., flowers or mushrooms) in both humans and monkeys (Öhman et al., 2001; Shibasaki and Kawai, 2009). More specifically, a number of studies indicate a bias towards a faster detection of snakes in primates (Isbell, 2006; Le et al., 2013, 2014). The “snake detection theory” postulates that our highly developed pulvinar is a result of the pressure caused by the constant presence of those predators throughout the evolution of primate species (Isbell, 2006). In a previous study, the responses of neurons from the medial and dorsolateral part of the lateral pulvinar of monkeys were recorded during the presentation of images of snakes and other visual stimuli (e.g., faces, hands and geometrical shapes) (Le et al., 2013). Interestingly, for most of

the neurons recorded, images of snakes elicited the highest and fastest responses compared to the other image categories indicating that pulvinar neurons are preferentially responsive to snakes. In a later study, the same group observed that images of snakes in striking position elicited stronger responses compared to non-threatening postures, thus, supporting the concept that the evolution of the pulvinar in primates may be associated to the fast detection of snakes in primates (Le et al., 2014).

The amount of evidence on the involvement of the pulvinar on processes modulating visual perception (e.g., attention) is vast. Nevertheless, few studies have investigated the role of this thalamic structure on the hierarchical cortical processing of visual information. For instance, Soares et al. (2004) have investigated the impact of the inactivation of the lateral pulvinar on the activity of area V2 of a new world primate. Most neurons from area V2 exhibited an increased firing rate during the pulvinar inactivation by GABA injection. In addition, the pulvinar inactivation impacted the orientation and direction selectivity of V2 neurons, indicating that the input from the pulvinar acts as a modulator of the activity of this cortical area. In a more recent study, Purushothaman et al. (2012) have used a similar methodological approach by recording the activity of neurons from V1 layers 2/3 while injecting muscimol, a GABA agonist, in the lateral pulvinar of a prosimian primate. Interestingly, the pulvinar inactivation caused a drastic reduction of the neuronal responses to visual stimuli in V1, indicating that the pulvinar exerts a control in gating the corticocortical transmission of visual information already at the very first stage of the visual hierarchy.

4.3.2 The cat pulvinar

Along with primates, cats have been an animal model of choice to investigate the visual system. Across the decades, several studies in visual neuroscience were performed in cats, such as the seminal work of Hubel and Wiesel (1962) on the RF structure of V1 neurons, making important contributions to the comprehension of the mechanisms underpinning visual function. As a result, the visual system of the cat became very well known and, therefore, well suited to be used in pulvinar research.

4.3.2.1 Structure and connectivity

Like in primates, the cat pulvinar is described as an ensemble of thalamic nuclei. Two main regions form the cat pulvinar complex: the lateral posterior (LP) and the pulvinar (Casanova 2004). In addition, as observed in the primate pulvinar complex, early studies have parcelled the LP-pulvinar based on cyto and chemoarchitectonics as well as by its connectivity pattern (Berson and Graybiel 1978; Updyke 1977, 1981; Berson and Graybiel 1980). In a seminal anatomical study, Graybiel and Berson (1980) described the existence of two subdivisions of the LP based on the acethylcholinesterase (AchE) content in this thalamic region: a medial (LPm) and a lateral (LPl) part. The parcellation of the LP-pulvinar based on its chemoarchitecture was further corroborated by the distinct connectivity patterns described by other studies using tracing techniques (Raczkowski and Rosenquist, 1983; Updyke, 1981).

Previous studies have demonstrated that all three subdivisions of the cat LP-pulvinar are reciprocally connected with several cortical visual areas (Berson and Graybiel 1978, 1980, 1983; Abramson and Chalupa 1985; Updyke 1983; Raczkowski and Rosenquist 1983). For instance, the LPl receives projections from early visual cortical regions (e.g., areas 17, 18 and 19) as well as from areas from the dorsal (e.g., PMLS, AMLS) and ventral streams (e.g., area 21a) (Raczkowski and Rosenquist 1983). It is worth noting that the LPl is the only region in the LP-pulvinar complex that receives projections from the primary visual cortex (areas 17 and 18) and is, therefore, named the striate recipient zone (Berson and Graybiel 1983; Casanova 1993; Chalupa and Abramson 1989). The LPm also receives projections from several extrastriate areas from both dorsal and ventral streams (Updyke 1983; Raczkowski and Rosenquist 1983). Interestingly, the LPm receives subcortical inputs from the superior colliculus and is often referred to as the tectorecipient zone of the LP-pulvinar complex (Chalupa, Williams, and Hughes 1983; Casanova 2004). Finally, projections from several extrastriate areas of the suprasylvian cortex (e.g., 19, 21a, PLLS and ALLS) also targets the pulvinar subdivision of the LP-pulvinar complex (Raczkowski and Rosenquist 1983; Updyke 1981; Abramson and Chalupa 1988; Huppé-Gourgues et al. 2006). Similar to primates, direct retinal projections are also found to target all subdivisions of the cat LP-pulvinar complex (Boire et al., 2004; Matteau et al., 2003).

4.3.2.2 Functional properties and role in vision

One can assume that the parcellation of the LP-pulvinar into three subdivisions based on histochemical markers and connectivity patterns should be equally apparent at a functional level. Indeed, previous studies have demonstrated that each LP-pulvinar subdivision exhibits a retinotopic representation of the contralateral visual field (Raczkowski and Rosenquist 1981; Hutchins and Updyke 1989). Another distinction between the LP-pulvinar subdivisions can be made regarding the respective RF properties and neuronal responses to different visual stimuli.

The RF organization of most LPl neurons resembles those of complex cells from the primary visual cortex with overlapped ON and OFF subfields. In addition, surround suppression is present in most of LPl neurons (Chalupa and Abramson, 1989). Using basic visual stimuli such as drifting bars and gratings, previous studies characterized different response properties of LPl neurons (Casanova et al., 1989; Mason, 1981). For instance, LPl neurons were found to be mostly selective to orientation and direction. In addition, most of LPl neurons exhibited response facilitation when visual stimuli were presented binocularly and, in some cases, responding strictly to binocular stimulation (Casanova et al., 1989). When drifting gratings were used, LPl neurons preferred gratings at low spatial frequencies drifting at high temporal frequencies (Casanova et al., 1989).

In the tectorecipient zone of the LP (LPm), neurons exhibit RF properties that resemble those from LPl (Mason, 1981). Most neurons are selective to orientation and direction, exhibit binocular facilitation and surround suppression (Chalupa et al., 1983). On the other hand, RFs of LPm neurons are significantly larger than those from LPl and exhibit relatively simpler organization with most neurons exhibiting only ON or OFF responses (Chalupa, Williams, and Hughes 1983; Piché, Thomas, and Casanova 2015). In comparison with the LP subdivisions, there is less information on the functional properties of the pulvinar nucleus. Nevertheless, previous studies indicate that pulvinar neurons share several RF properties with those from the LP nucleus but seem to be less selective to orientation (Mason 1981; Casanova 2004).

Even though inputs from the primary visual cortex and the superior colliculus contribute to the RF structure of LP neurons, the extensive connectivity with several extrastriate visual areas plays a central role on the establishment of response properties (Casanova, Savard, and Darveau

1997, 17; Casanova and Savard 1996). Indeed, a body of evidence suggests that LP-pulvinar neurons are involved in several higher order visual processes (Casanova, 2004). More precisely, previous studies demonstrated that LP-pulvinar neurons are sensitive to higher order motion processing, which is characteristic of higher order visual areas of the dorsal stream such as the PMLS and AEV (Villeneuve, Ptito, and Casanova 2006; Zabouri, Ptito, and Casanova 2008). For instance, LP-pulvinar neurons were found to be selective to pattern motion. This was observed when neurons (mainly in LPm) were sensitive to the resultant motion vector of two overlapped gratings drifting at different directions (i.e. plaid patterns) (Merabet et al. 1998). Similar higher order motion processing was observed in a subset of neurons from the LP-pulvinar selective to the direction of random dots kinematograms (RDKs) in which local cues of direction or orientation are absent (Dumbrava et al., 2001).

As for primates, efforts have been made to unravel the role of the cat LP-pulvinar in the hierarchical cortical processing of visual information (Minville and Casanova, 1998; Shumikhina and Molotchnikoff, 1999). For instance, Minville and Casanova (1998) investigated the impact of the reversible inactivation of LPl on the responses of PMLS neurons. The LPl inactivation induced a decrease in the overall responsiveness of PMLS neurons with no impact on the neurons' selectivity to direction or spatial frequency suggesting that the LP-pulvinar exerts a modulatory role in this cortical area. Despite the existing evidence on the impact of LP-pulvinar disruption on neuronal activity of the visual cortex, the number of studies remains scarce and, therefore, the potential roles of this thalamic structure on several levels of the cortical visual hierarchy has yet to be discovered.

5 Objectives and hypotheses

In the previous sections, several key structures of the visual system and their functions were explored. Despite the amount of knowledge available, several questions about the properties of higher order visual areas, either cortical or thalamic (i.e., extrastriate areas and the pulvinar), remain open. In the context of our research, we contributed to answer these questions by conducting electrophysiological recordings in the anaesthetized cat. Our objectives were two-fold: first, to contribute to a better understanding of the functional properties of an extrastriate area from the ventral stream that receives a robust input from the pulvinar; secondly, to investigate the role of the pulvinar on the cortical processing of visual information, particularly among the ventral stream.

5.1 Article 1: Spatiotemporal processing of brights and darks in cat area 21a

Although several neuronal properties of the area 21a are known, different aspects of its RFs remain elusive. Therefore, the main objective of this study was to use the sparse noise reverse correlation technique to characterize the spatial and temporal features of the RFs of 21a neurons in processing bright and dark stimuli. In addition, the findings in this study can be compared with the ones from previous publications from our group, in which the same reverse correlation technique was used to investigate the RF properties of PMLS and LP-pulvinar neurons (Piché, Thomas, and Casanova 2013; Christian Casanova, Piché, and Ouellette 2008). Our hypothesis is that 21a neurons exhibit RFs with distinct properties from other extrastriate areas such as the PMLS, which would underscore the role of this cortical area in the processing of form.

5.2 Article 2: The impact of the pulvinar inactivation on the contrast response function of cat areas 17 and 21a.

In this study, the role of the LP-pulvinar on the cortical processing of visual information was investigated by assessing the impact of its pharmacological inactivation on the response to contrast of neurons in the primary visual area 17 and area 21a. The objective of this study was

to compare the effects of the LP-pulvinar inactivation on the activity at a lower (area 17) and higher (area 21a) level of the cortical hierarchy using a visual stimulus (contrast) eliciting reliable responses in both areas. Ultimately, our goal is to characterize the nature of the LP-pulvinar inputs (driver/modulators) in those cortical areas (figure 12).

Our hypothesis is that the thalamocortical inputs of the LP-pulvinar exhibit a modulatory nature at the primary visual cortex (area 17) and the thalamic inactivation will induce a response gain in the neuronal CRF. On the other hand, we hypothesize that the LP-pulvinar inputs to area 21a will exhibit a stronger driver component that will be revealed mostly by changes in the CRF contrast gain during thalamic inactivation.

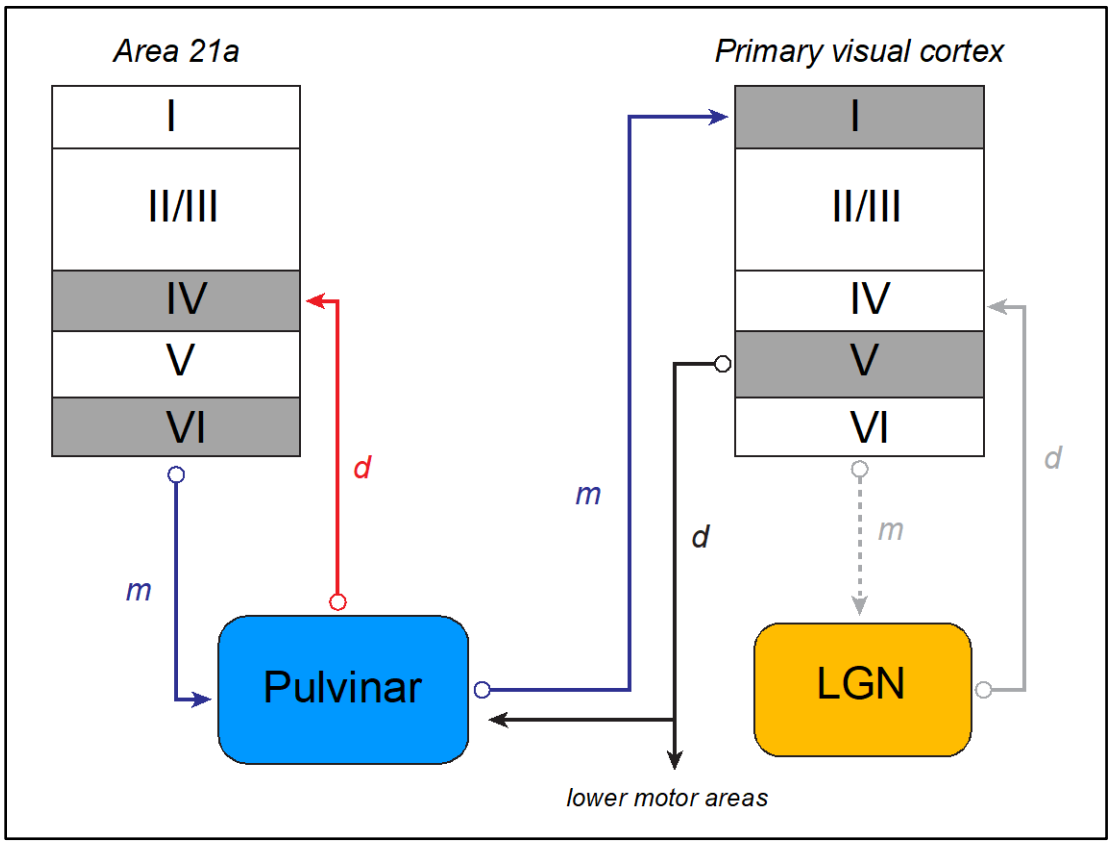

Figure 12. Hypothetical scheme of the nature of cortico-thalamo-cortical connections (d: drivers; m: modulators) involving the LP-pulvinar and the cortical areas 17 and 21a.

6 Article # 1

Manuscript published in *European Journal of Neuroscience*

Stronger Responses to Darks Along the Ventral Pathway of the Cat Visual Cortex

Bruno Oliveira Ferreira de Souza and Christian Casanova*

[1]School of Optometry, Université de Montréal, CP 6128 succursale centre-ville, Montreal, Quebec, Canada

Work completed at: School of Optometry, Université de Montréal, CP 6128 succursale centre-ville, Montreal, Quebec, Canada.

* Corresponding author:

Christian Casanova

E-mail: christian.casanova@umontreal.ca

School of Optometry

Université de Montréal

CP 6128, Succ Centre-Ville

Montréal, Québec

Canada, H3C-3J7

Tel: (514)-343-6948

Fax: (514)-343-2382

Running title: Enhanced dark dominance in area 21a

Total number of pages: 34

Total number of figures: 7

Total number of equations: 3

Total number of words (whole manuscript): 8337

Total number of words (Abstract): 195

Keywords: area 21a, receptive fields, reverse correlation, visual system, OFF responses

ABSTRACT

Light increments (brights) and decrements (darks) are differently processed throughout the early visual system. It is well known that a bias towards faster and stronger responses to darks is present in the retina, lateral geniculate nucleus and primary visual cortex. In humans, psychophysical and neurophysiological data indicate that darks are better detected than brights, suggesting that the dark bias found in early visual areas is transmitted across the cortical hierarchy. Here, we tested this assumption by investigating the spatiotemporal features of responses to brights and darks in area 21a, a gateway area of the cat ventral stream, using reverse correlation analysis of a sparse noise stimulus. The receptive field of most 21a neurons exhibited larger dark subfields. Additionally, the amplitude of the responses to darks was considerably greater than those evoked by brights. In the temporal domain, no differences were found between the response peak latency. Thus, the present study supports the notion that bright/dark asymmetries are transmitted throughout the cortical hierarchy and further, that the luminance processing varies as a function of the position in the cortical hierarchy, dark preference being strongly enhanced (in the spatial domain and response amplitude) along the ventral pathway.

INTRODUCTION

Early in visual processing, retinal signals carrying specific information about the environment are processed in parallel before being converged and integrated in the cortex to create a coherent visual perception (for a review see Nassi & Callaway, 2009). For instance, in cats, cells from the X and Y pathways encode distinct spatiotemporal aspects of the visual information associated with the processing of form and motion, respectively (Enroth-Cugell & Robson, 1966; Sherman & Spear, 1982; Ferster, 1990; Demb et al., 2001). In addition to theses pathways, increments (brights) and decrements (darks) in luminance are processed by distinct channels known as the ON and OFF pathways, respectively (Hartline, 1938; Kuffler, 1953). The profile of the ON and OFF responses differs across the visual system. For instance, previous studies have shown that, in the retina of various species, neurons process darks faster than brights (Copenhagen et al., 1983; Burkhardt et al., 1998; Burkhardt, 2011; Nichols et al., 2013). This temporal difference was also revealed for cells in the lateral geniculate nucleus (LGN) and for neurons in the thalamorecipient layer IV of the cat primary visual cortex (Jin et al., 2008, 2011; Komban et al., 2014). Despite the differences in the processing speed, the magnitude of the ON and OFF responses was equivalent in the retina and LGN (Krüger & Fischer, 1975; Kremers et al., 1993; Benardete & Kaplan, 1999) [but see Chichilnisky and Kalmar 2002) but not in the primary visual cortex where neurons in layers II/III respond more strongly to darks (Yeh, Xing, & Shapley, 2009).

Recent evidence indicates that the bias towards faster and stronger responses to darks in cortical neurons may arise from the convergence of thalamic signals and from local inhibition in primary visual cortex (Yeh, Xing, & Shapley, 2009; Jin et al., 2011; Komban et al., 2014; Taylor et al., 2018). In humans, studies using fMRI and visual evoked potentials showed a bias towards larger dark responses (Zemon et al., 1995; Olman et al., 2008). Further, psychophysical studies showed that bright/dark asymmetries influence visual perception, suggesting that the imbalanced luminance processing is preserved across the cortical hierarchy (Chubb & Nam, 2000; Motoyoshi et al., 2007; Komban et al., 2011, 2014). In a previous study, our group revealed that neurons in the posteromedial lateral suprasylvian cortex (PMLS), an area of the cat dorsal stream, (Piché et al., 2013, 2015) exhibited some degree of bias towards darks but with a variety

of spatiotemporal profiles that suggests that bright/dark asymmetries may vary across the cortical hierarchy and that preference to darks may not be maintained in higher-order areas.

In the present study, we used the reverse correlation analysis of sparse noise stimulus to investigate the responses to brights and darks of neurons from area 21a, an area of the cat ventral pathway considered as the homolog of the primate area V4 (Payne, 1993). The spatial and temporal profile of the neurons' responses were assessed. Here, we show that most 21a neurons exhibited spatially imbalanced receptive fields with larger dark subfields. In addition, responses to darks was considerably stronger than bright ones. These results suggest that the preference to darks is preserved and even enhanced in higher-order areas involved in form processing.

MATERIAL AND METHODS

Animal Preparation and Surgery

Experiments were carried out on normal adult cats weighing between 2 and 3.5 Kg. All surgical and experimental procedures were undertaken according to the guidelines of the Canadian Council on Animal Care and were approved by the Ethics Committee of the University of Montreal. Before the surgical procedure, atropine (0.1mg/kg) and acepromazine (Atravet®, 1mg/kg) were administered subcutaneously to reduce the parasympathetic effects of anesthesia and to provoke sedation, respectively. Subsequently, anesthesia was induced with 4% isofluorane in a 50:50 (vol/vol) gas mixture of O2 and N2O. A catheter was placed in the cephalic vein to provide intravenous access. A local anesthetic (lidocaine hydrochloride 2%) was used in all incisions and pressure points. Lubricant eye gel (Systane Gel drops®, ALCON) was used during surgical procedures to avoid corneal dehydration. Following anesthetic induction, isofluorane concentration was maintained at 1.5% during surgical procedures. Oxygen saturation was monitored using a pulse oximeter, cardiac activity was monitored throughout the experiment with ECG and the animal's temperature was maintained at 37°C by means of a heated blanket controlled by a rectal thermometer probe. A tracheotomy was performed prior to the transfer of the animal to the stereotaxic apparatus. A bolus intravenous injection of 2% gallamine triethiodide was administered to induce muscular relaxation and, subsequently, the animal was placed under artificial ventilation. A 1:1 (vol/vol) solution of 2%

gallamine triethiodide (10 mg/kg/h) in 5% of dextrose in lactated ringer was continuously administered intravenously to maintain relaxation and to provide nutrition and electrolytes. Expired levels of CO2 were maintained between 35 and 40 mmHg by adjusting the tidal volume and respiratory rate. The animal`s heart rate was maintained at 180 bpm ± 10 by adjusting the anesthesia level. Pupils were dilated using atropine (Mydriacyl®) and nictitating membranes were retracted using phenylephrine (Midfrin®). Rigid contact lenses with the appropriate power were applied to the corneas. The lubricant eye gel was replaced by a liquid one (Blink®, ABBOTT) during recordings and was used when needed.

A craniotomy window was performed at Horsley-Clarke coordinates 2-6P; 7-11L over the posterior portion of the suprasylvian gyrus exposing area 21a. Small durectomies were performed for each electrode penetration to preserve as much dura as possible in order to reduce cortical movements. In addition, a 2% solution of agar in saline was applied over the exposed cortex to further improve stability during recordings.

Visual Stimuli

Visual stimuli were generated using VPixx software (VPixx Technologies Inc., St-Bruno, Qc, Canada) and images were projected onto an isoluminant screen covering 104 by 84 degrees of visual angle positioned at a viewing distance of 57 cm. A sparse noise stimulus consisting in the presentation of a pseudo-random sequence of dark and bright squares over a gray background was used. The stimulus luminance was adjusted so that light increments and decrements were equal (bright: 50 cd/m2, dark: ≈ 0 cd/m2, gray: 25 cd/m2). Bright and dark squares measuring 4 by 4 degrees were presented in a grid of 26 columns by 21 rows. The duration of presentation for each square was 35 ms without any delay between presentations. Each stimulus was repeated in a set of 40 to 50 randomized trials. In a subset of experiments, the duration of the square presentation was increased to 200 ms in order to assess the temporal profile of 21a neurons to the dark and bright stimuli.

Electrophysiological Recordings and Data Acquisition

Electrophysiological recordings were undertaken using varnished tungsten electrodes (impedance of 1-2MΩ). Signals were amplified and digitalized using AlphaLab®. Signals were bandpass filtered at 300-6000 kHz and a threshold was applied to extract spikes waveforms.

Single-unit signals were obtained by means of a wavelet-based clustering algorithm using a custom script in MATLAB (Mathworks, Natick, MA, USA).

Spike Waveform Analysis

Putative inhibitory and excitatory neurons were classified as fast (FS) and regular (RS) spiking neurons respectively, based on the spike waveform profile (Sirota et al., 2008; Sakata & Harris, 2009). FS neurons were characterized by narrower waveforms while RS neurons exhibited wider spike waveforms. The classification was undertaken by extracting the average spike waveform from each unit. The temporal resolution was increased by spline interpolation. Two parameters were calculated: the half-width of the spike negative deflection and the delay between the negative and the positive peaks (trough-to-peak, see inset 1 in Figure 6). Cells were classified into two groups using K-means clustering. The clustering method was validated using the *silhouette* MATLAB function, which calculates an index (silhouette value) ranging from -1 to 1 where values indicate how similar a data point is from its respective group, with negative values indicating potentially misclassified data points. A threshold was arbitrarily applied and units with silhouette values below 0.5 were considered as unclassified and were excluded from further analysis.

Receptive Field Mapping

Receptive field maps were created using the reverse correlation technique (Jones & Palmer, 1987; DeAngelis et al., 1993) applied to the 35 ms sparse noise visual stimulus. In brief, receptive field maps were characterized as a series of 2D histograms obtained from the spike-triggered averaging to the bright and dark stimuli. The reverse correlation analysis was constrained to a pre-spike temporal window of 200 ms with a 1 ms resolution.

In order to quantify the responses to bright and dark stimuli, we used the signal to noise ratio (SNR) based on the spatial variance of the receptive field maps (Yeh, Xing, & Shapley, 2009). First, the peak latency was identified as the time of the maximum spatial variance. The SNR was calculated as the spatial variance averaged across a time window (40 ms) around the peak latency divided by the spatial variance of the first frame, considered here as noise. Receptive fields were considered as “mappable” when the SNR value of either bright or dark maps was greater than two.

Receptive Field Spatial Profile

Bright and dark receptive field maps were obtained by averaging the spatial variance across the same time window applied to the calculation of the SNR. The averaged bright and dark maps were spatially interpolated using a 2D adaptive pixelwise linear Wiener filter (MATLAB Image Processing Toolbox, Mathworks, Natick, MA, USA) which consisted in a low-pass filter using a 3 by 3-pixel area applied to the non-interpolated data. In order to detect the bright and dark subfields, the interpolated receptive field maps were transformed in Z score maps. For each map, the subfield was identified as the largest set of significant connected pixels (Z score > 2.3).

The RF spatial properties were assessed by calculating the subfields size and position in the visual field. The subfield sizes were compared using a subfield size index (SSI) which was calculated as the differential ratio between the bright subfield area (BA) and the dark one (DA) as defined by

$$SSI = \frac{BA - DA}{BA + DA}$$

Here, SSI < 0 indicates that dark subfields are larger than the bright ones, while SSI > 0 represents the opposite.

The relative position of bright and dark subfields was assessed by means of two measurements. First, the proportion of overlap between the subfields was calculated. The subfield overlap index (SOI) was obtained by computing the ratio of the overlapped area (OA) over the total RF area defined by

$$SOI = \frac{OA}{BA + DA - OA}$$

SOI values range between zero and one, with SOI = 0 representing a complete spatial dissociation of subfields while SOI = 1 a perfect overlap between subfields. Next, each subfield was fitted with an ellipse using the MATLAB function regionprops from which the center of mass of bright (Cb) and dark (Cd) subfields were calculated. Following the study of Mata and Ringach (Mata & Ringach, 2005), we computed the RF normalized distance (δ) which

represents the ratio of the distance between the subfields' center of mass and the mean square root of their respective areas. The normalized distance was defined as

$$\delta = \frac{|| Cb - Cd ||}{\frac{1}{2}\left(\sqrt{BA} + \sqrt{DA}\right)}$$

In case of perfectly overlapped subfields, $\delta = 0$, while distant subfields would exhibit increased normalized distance values ($\delta >> 0$).

Relative Subfield Strength

The SNR values were used to assess the relative response amplitudes to bright and dark stimuli. As previously described (Yeh, Xing, & Shapley, 2009), the relative response strength was determined by the ON/OFF ratio, which was calculated as the logarithm of the ratio between the bright and dark SNRs. Positive values characterize receptive fields with stronger responses to bright stimuli (bright dominant) while neurons with negative ON/OFF ratio values exhibit stronger responses to dark stimuli (dark dominant).

Temporal Profile Analysis

Temporal features of the responses to bright and dark stimuli were assessed by the analysis of sparse noise stimulus in which squares were presented for 200 ms. In contrast to the shorter stimulus duration (35 ms), the longer presentation time allows the unambiguous distinction and isolation of neuronal responses to the stimulus onset and offset.

In brief, a peri-stimulus time histogram (PSTH) was generated for each stimulus position in the visual field resulting in two PSTH grids corresponding to each polarity. For each grid, the PSTH with the highest mean firing rate during the stimulus presentation (200 ms) was selected. Subsequently, the PSTHs were smoothed using a Bayesian adaptive regression splines (BARS) fit (Kass et al., 2003) from which the peak responses to bright and dark stimuli were calculated.

Statistics

Bright and dark response comparisons were undertaken using a paired two-sided Wilcoxon signed rank test. For independent datasets, statistical comparisons were performed using a two-sided Wilcoxon rank sum test. Categorical data were compared using the Fisher's exact test. For some parameters, correlation analysis was performed, and the Pearson's

correlation coefficient was reported. Statistical analysis was performed in MATLAB. All data are expressed as mean ± SEM, unless otherwise stated.

Laminar Cortical Position

After each successful electrode penetration, electrolytic lesions (5μA for 5s) were performed at different cortical depths to identify the laminar position of each neuron recorded. At the end of the experiment, the animals were euthanized by intravenous injection of sodium pentobarbital (Euthanyl ®: 240 mg/ml) and subsequently perfused through the left ventricle with phosphate buffer saline and 4% paraformaldehyde. After overnight post-fixation, the brains were immersed in a 30% sucrose solution and subsequently frozen. Then, coronal sections of the visual cortex were undertaken. Cortical layers were identified using Nissl staining, and area 21a location was confirmed by the expression pattern of nonphosphorylated neurofilament proteins (Van Der Gucht et al., 2001). For statistical comparisons, layers I-IV and V-VI were grouped as superficial and deep layers respectively.

RESULTS

In the present study, the responses of 138 neurons to light increments and decrements (brights and darks) were assessed using sparse noise stimulus and a reverse correlation algorithm. A total of 74 neurons responded reliably to the visual stimulation exhibiting "mappable" RFs (see methods) and were included in the analysis. From those, the response strength and the spatial profile of 43 units were analyzed. A subset of 31 cells was used in the analysis of the temporal profile of RFs.

Panels A and B of Figure 1 show a representative example of a spatiotemporal RF profile in response to brights and darks. The response time course was represented as the normalized spatial variance. The peak latency was determined as the time delay at which the spatial variance reaches its peak (60.51 ± 2.29 ms). For each neuron, a 40 ms time window around the peak latency was used to calculate the spatial RF maps and SNR values of bright and dark subfields (panel B). Clearly, this neuron RF exhibits a stronger response to darks (see the additional examples in panel C).

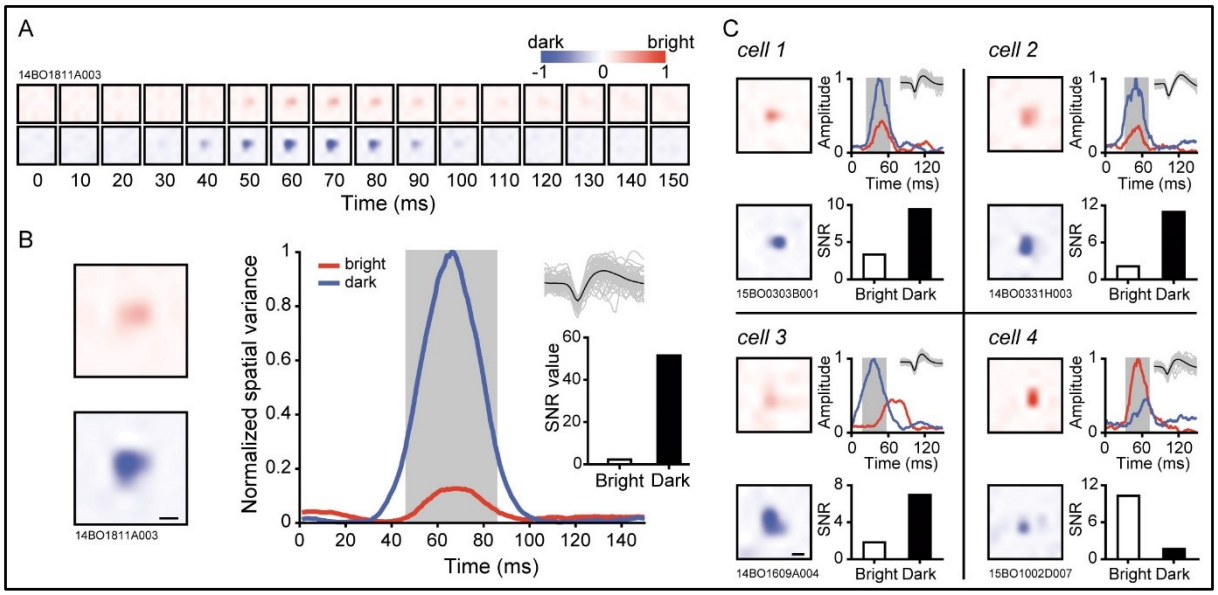

Figure 1. Spatiotemporal profile of responses to bright (red) and dark (blue) stimuli. (A) Time series of spatial variance maps of a representative neuron's responses to bright and dark squares generated by reverse correlation analysis. (B) Left: bright (top) and dark (bottom) RF spatial maps from the neuron depicted in (A). Right: temporal response profile shown as the normalized spatial variance and SNR values of bright and dark responses (inset). The spatial maps were obtained by calculating the average spatial variance in a time window (40 ms) around the response peak (shaded area in the plot). The bright and dark SNR values were calculated as the ratio between the averaged variance in the time window and the variance in the first frame (zero-time delay). (C) Four examples of 21a neurons' bright and dark responses of showing their respective spatial maps, temporal response profile and SNR values. In B and C, scale bars = 5 degrees.

Relative Response Strength

The responses strength to bright and dark stimuli were evaluated by calculating the ratio between their respective SNR values (ON/OFF ratio). Figure 2 shows the distribution of these values. Almost all 21a neurons (~88%) exhibited negative ON/OFF ratios (mean of = -0.59 ± 0.10) indicating a very strong preference for darks (dark-dominants) with only five units displaying bright-dominant receptive fields (see also Figure 1C, cell 4). On average, responses to darks were approximately five times larger than those to brights.

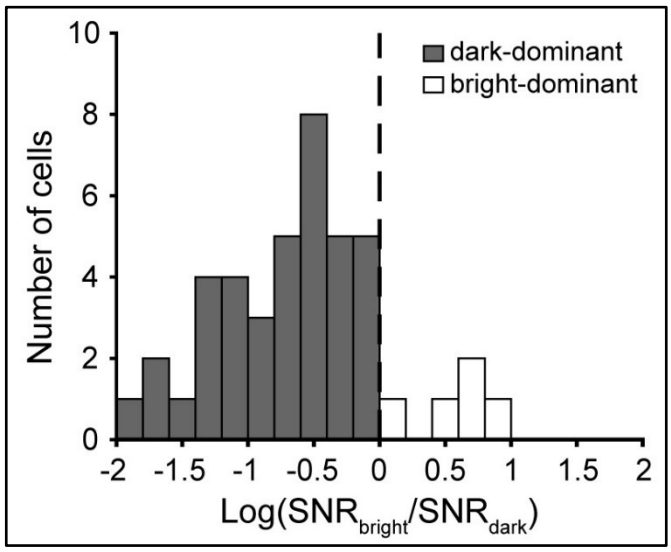

Figure 2. Histogram of ON/OFF ratio (log(SNRbright/SNRdark)). The ON/OFF ratio represents the neurons relative response strength in which positive and negative values indicate a preference to brights (bright dominant) and darks (dark dominant) respectively. Most cells preferred dark stimuli.

Spatial profile

The spatial profile of RFs was assessed by analyzing the relative size and position in visual space of bright and dark subfields (see Methods). The comparison of the subfield areas revealed an asymmetry in which the dark subfields were significantly larger than the bright ones (Z = -5.08, P = 3.7e-7, Wilcoxon signed rank test). The average dark subfield was 55% larger than its counterpart (means of 91.41 ± 7.47° vs 58.98 ± 5.44°). This is illustrated in the panel A of Figure 3, where most of the data points are located above the unity line. In addition, the distribution of subfield size index values (panel B) shows that most neurons exhibit negative SSI values (mean of -0.24 ± 0.03) with only six cells exhibiting larger bright subfields, further highlighting the existence of a strong bias towards larger dark subfields.

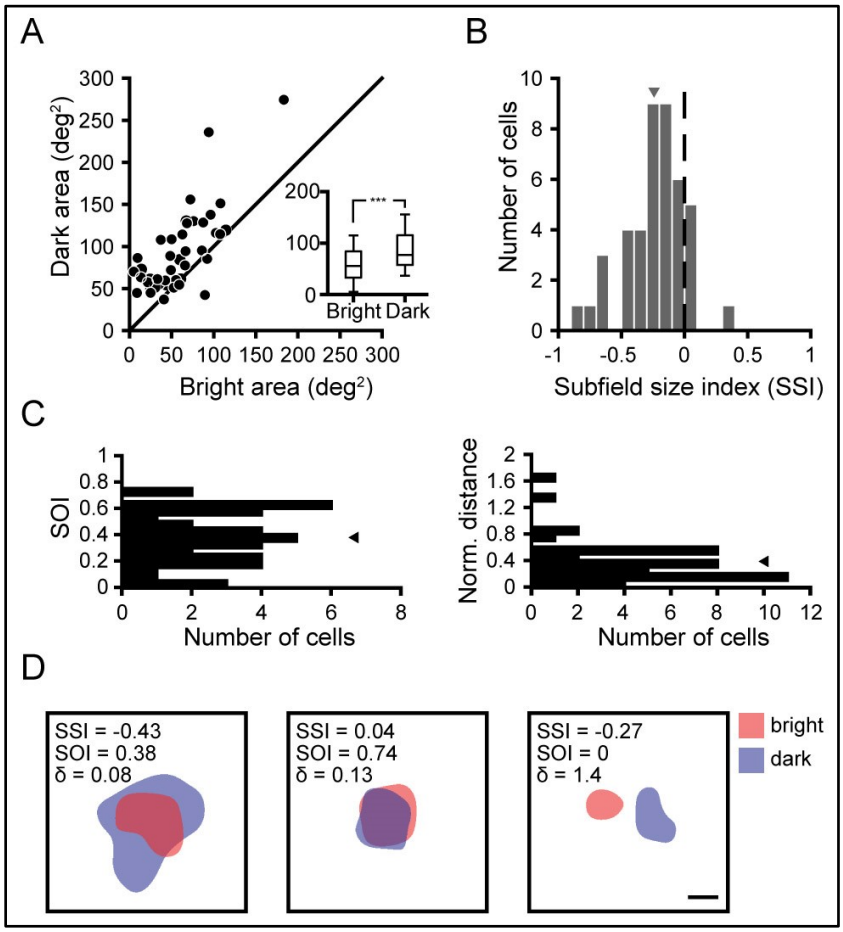

Figure 3. Analysis of spatial parameters extracted from RF maps. (A) Scatter plot of bright and dark subfield areas. Most units exhibited dark subfields significantly larger than brights (inset). (B) Histogram of the subfield size index (SSI). Positive and negative SSI values indicate neurons with larger bright and dark subfields respectively. (C) Histograms of spatial overlap index (SOI) and normalized distance (δ). (D) Three examples of the spatial arrangement of bright (red) and dark (blue) subfields. The respective spatial parameters are shown. In B and C, triangles represent the parameters' mean values. Scale bar = 5 degrees; *** P = 3.7e-7.

The relative position of bright and dark subfields in the visual space was assessed by calculating their respective spatial overlap (SOI) and normalized distance (δ). Panel C shows the distribution of both indices (SOI = 0.38 ± 0.03; δ = 0.39 ± 0.05). Based on the SOI, the RF of most neurons (~93%) exhibited a complex-like spatial organization (Henry, 1977) as shown by the extensive amount of overlap between dark and light with only ~7% (3/43) of cells showing simple-like RFs (see representative examples in panel D). It is worth noting that, since the SOI is a measure of the ratio between the overlapped area and the total RF area, this index is influenced by the significant differences in subfield size (i.e., larger dark subfields). However,

the normalized distance was less affected by the increased unbalance between subfield sizes. This is illustrated in panel D where the RF with larger subfield size asymmetry (left) exhibits a lower SOI than the one with a more balanced spatial profile (center) while the normalized distance values remain similar. In order to assess the reliability of the SOI as an overlap measure, we performed a correlation analysis with the normalized distance (Figure 4). Interestingly, both indices were strongly correlated (r_{41} = -0.81, P = 3.96e-11), suggesting that the subfield size asymmetry exerted a minor impact on the SOI. In addition, both parameters were significantly correlated with the SSI (SOI vs SSI: r41 = 0.53, P = 0.00023; δ vs SSI: r41 = -0.39, P = 0.01) indicating that the asymmetry in the subfield size is associated with their relative position in visual space. No significant correlation was observed between the above-mentioned parameters and the ON/OFF ratio. Taken together, the analysis of the RF spatial profile shows an imbalance of the subfield sizes and strength between responses to brights and darks with a strong preference for the latter.

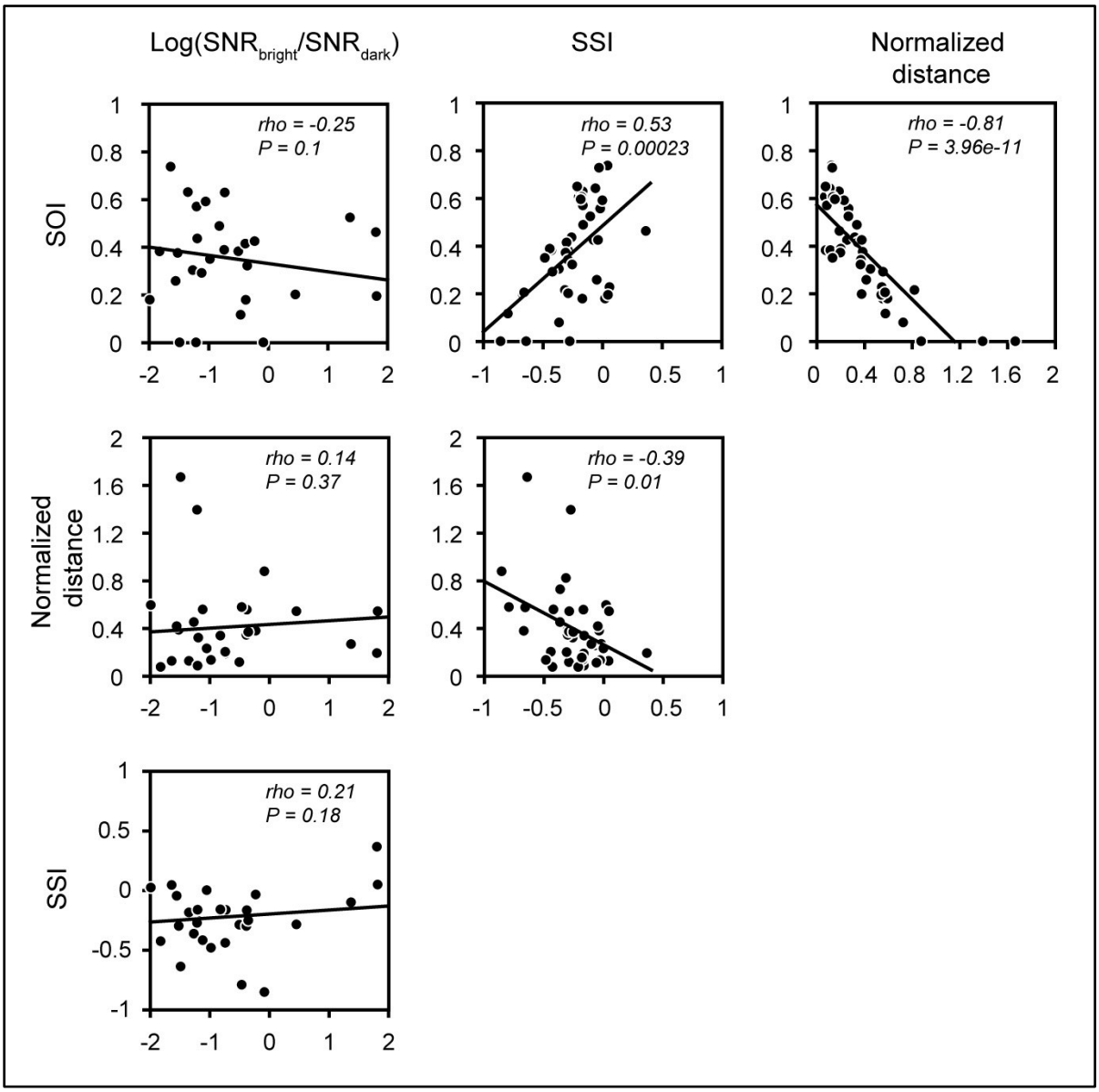

Figure 4. Correlation matrix between spatial parameters (SOI, normalized distance, and SSI) and ON/OFF ratio (log(SNRbright/SNRdark)). At the inset of each plot, Pearson's correlation coefficient (rho) and significance level (P) are indicated along with its respective linear regression line.

Temporal Profile

For a subset of neurons (n = 31), the duration of the stimulus presentation was increased to 200 ms in order to determine the responses' delay to brights and darks. The use of a longer stimulus presentation time allowed the unambiguous dissociation of the neurons' responses to the onset of brights and darks from their respective offsets (see offset peaks in Figure 5B). The response delay to bright and dark stimuli was measured at the respective onset peaks. Panel A of Figure 5 shows the distribution of the onset peak times for brights (mean of 112 ± 5.89 ms) and darks (mean of 106 ± 6.00 ms). Comparison between the onset peak times of brights and darks showed no significant differences (Z = 1.92, P = 0.0548, Wilcoxon signed rank test, inset in panel A) with an average difference of 5.97 (± 4.98) ms (panel C). Interestingly though, the dataset was characterized by the presence of two cell groups revealed by a k-means clustering method (clusters one and two in panel A). The first group (cluster one) was composed of neurons with shorter onset peak times (brights = 83.88 ± 3.25 ms; darks = 76.74 ± 3.09 ms, see cell 1 in panel B) while the second one (cluster two) exhibited longer response latencies (brights = 135.15 ± 4 ms, darks = 130.14 ± 3.98 ms, see cell 2 in panel B).

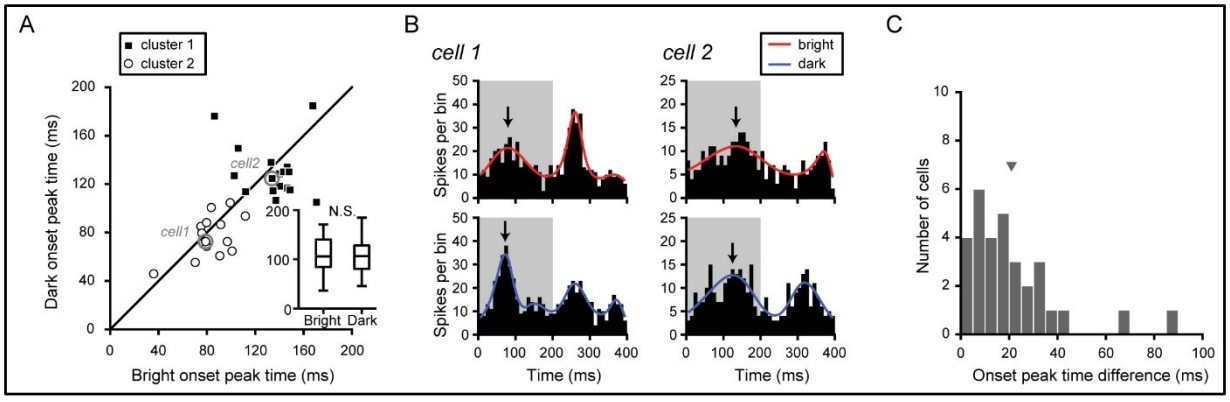

Figure 5. Temporal analysis of 21a neurons' responses to brights and darks. (A) Scatter plot and boxplot (inset) of bright and dark onset peak times. The dataset is classified into two clusters (k-means clustering analysis). (B) PSTH of responses of two neurons included in each cluster (identified in A). The smoothed PSTH of bright (red) and dark (blue) responses are shown. In each plot, arrows indicate the respective onset peak time during the stimulus presentation (shaded area). (C) Histogram of the difference between bright and dark onset peak times. Triangle represents the mean. N.S. = not significant.

Additionally, out of the 34 neurons analysed, 23 exhibited a response to the stimulus offset. The comparison of the offset peak times of brights and darks revealed no significant differences ($Z = 1.08$, $P = 0.28$, Wilcoxon signed rank test).

Cortical Laminar Position and Cell Class

The spatiotemporal RF features of 21a neurons were compared as a function of their laminar position and their spike waveform (i.e. cell class). The cortical laminar position of 68 neurons was assessed with 31 units located in the superficial layers and 37 units in the deep layers (see Methods). The parameters extracted from the spatial and temporal analyses were compared as a function of the laminar position. There were no significant differences between neurons in superficial and deep layers for all spatial (SOI: $Z = 1.12$, $P = 0.26$; δ: $Z = -0.78$, $P = 0.44$; SSI: $Z = 0.20$, $P = 0.84$; ON/OFF ratio: $Z = 0.57$, $P = 0.57$, Wilcoxon rank sum test, $N = 37$) and temporal parameters studied (bright onset peak time: $Z = -1.18$, $P = 0.24$; dark onset peak time: $Z = -0.38$, $P = 0.70$, Wilcoxon rank sum test, $N = 31$). In addition, there were no relationships between the neurons' clusters revealed by the temporal analysis (Figure 5A) and the laminar position ($P = 0.44$, Fisher exact test).

The same comparisons were performed with regards to the cell types. Neurons were classified as regular (RS) or fast spiking (FS) based on the width of their spike waveform (Figure 6). Previous studies have indicated that FS and RS cells correspond mainly to putative inhibitory and excitatory neurons, respectively (Sirota et al., 2008; Sakata & Harris, 2009). As for the laminar analysis, no significant differences were observed between RS and FS neurons when considering all spatial (SOI: $Z = -0.98$, $P = 0.33$; δ: $Z = 0.89$, $P = 0.37$; SSI: $Z = -0.08$, $P = 0.93$; ON/OFF ratio: $Z = -0.39$, $P = 0.70$, Wilcoxon rank sum test, $N = 35$) and temporal parameters (bright onset peak time: $Z = 0.89$, $P = 0.37$; dark onset peak time: $Z = 1.68$, $P = 0.09$, Wilcoxon rank sum test, $N = 27$). Further, there was no difference in cell types between the two temporal-defined clusters ($P = 0.13$, Fisher exact test). Taken together, these analyses indicate that the spatiotemporal profile of bright and dark responses of 21a neurons are independent from their laminar position and spiking characteristics.

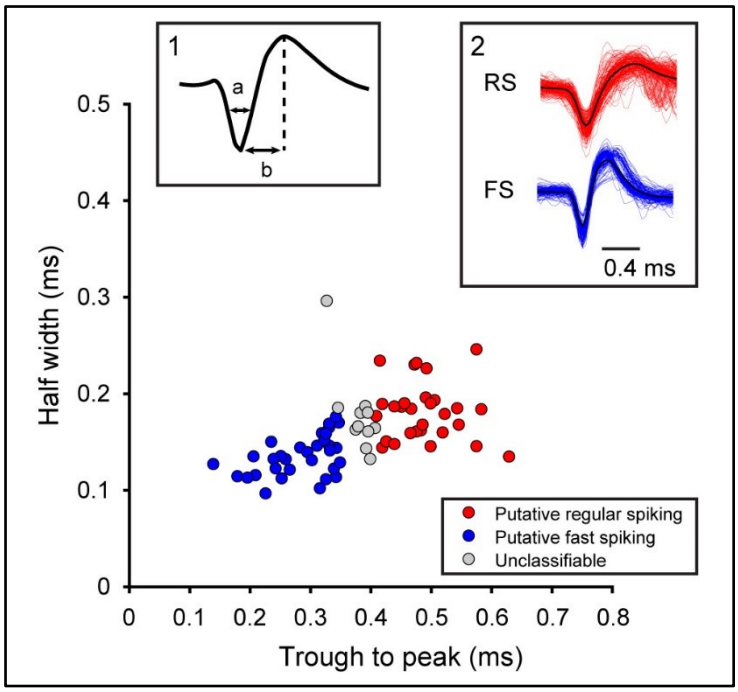

Figure 6. Spike waveform classification. Neurons were classified in two categories, putative regular (RS, N = 30) and fast-spiking (FS, N = 32) based on the half width and trough to peak (a and b in inset 1). Inset 2 shows example of RS and FS waveform of recorded spikes.

DISCUSSION

In this study, we investigated the processing of brights and darks in a higher-order cortical area involved in form processing using reverse correlation analysis of a sparse noise stimulus. Our results are the first to undoubtedly demonstrate that the bias towards responses to darks reported in the primary visual cortex is preserved along the ventral pathway. This preference was observed only in the spatial domain with dark subfields being larger and more responsive than bright subfields.

Spatial Domain

The RF of most of 21a neurons (~93%) exhibited extensive overlap between bright and dark subfields indicating that these neurons were complex-like (Henry, 1977). These findings are in accordance with previous studies reporting ~80 to ~93% of 21a neurons exhibiting complex-like features (Dreher et al., 1993; Tardif et al., 1996). Area 21a receives its main excitatory inputs from complex cells located in the supragranular layers of area 17 (Sherk, 1989; Dreher et al., 1993; Michalski et al., 1993; Morley et al., 1997; Conway et al., 2000; Grant & Hilgetag, 2005) which could explain the large proportion of spatially overlapped RFs. The small number of spatially dissociated neurons in area 21a could be attributed to projections originating

from the LGN (Raczkowski & Rosenquist, 1980). Nonetheless, one cannot rule out the possibility that the large proportion of neurons with overlapped subfields may have been slightly overestimated given the significant subfield size asymmetry (i.e., larger dark subfields) observed in our dataset.

Previous studies have characterized different aspects of the spatiotemporal RF of complex cells in area 17 (Szulborski & Palmer, 1990; DeAngelis et al., 1995; Liu et al., 2007). For instance, Liu et al. (2007) demonstrated that area 17 complex cells exhibit dark subfields that were 30% larger than brights. Our findings are in accordance with these data since the spatial RF profile of 21a neurons is biased towards broader dark subfields (55% larger).

In previous studies, our group used the same visual stimulation used here to assess the responses to brights and darks in the striate-recipient zone of the cat lateral posterior nucleus (LPl; Piché et al. 2015) and in the PMLS cortex, an area of the dorsal stream (Piché et al., 2013). Neurons in the striate-recipient zone of the cat lateral posterior nucleus (LPl) exhibit a similar spatial profile as in 21a with ~88% of neurons with larger dark subfields. On the other hand, in area PMLS, a smaller proportion of neurons (~51%) exhibited larger dark subfields. Since all the three areas receive their main excitatory inputs from area 17 (Dreher, Wang, et al., 1996; Casanova et al., 1997), this strengthened the assumption that complex cells in area 17 predominantly contribute to the spatial RF profile of neurons in area 21a. However, the observed difference between the PMLS cortex and area 21a data, suggests that this contribution is heterogeneous across visual areas with a larger impact on area 21a.

Temporal Domain

A large body of evidence has revealed that OFF responses are faster than ON responses in the retina and LGN (Burkhardt et al., 1998; Gollisch & Meister, 2008; Jin et al., 2008, 2011; Burkhardt, 2011). More recently, a similar temporal profile was observed in the primary visual cortex (Komban et al., 2014) in which dark-dominant neurons from layer IV of the cat area 17 exhibit faster responses than their bright-dominant counterparts. In addition to the neurophysiological data, psychophysical studies performed by the same group revealed that darks are detected faster than brights suggesting that the temporal profile of ON/OFF channels are maintained throughout the visual hierarchy (Komban et al., 2011, 2014). Our study is at odds

with this assumption since no significant differences were observed between bright and dark response delays. Instead, our results suggest that asymmetries in the spatial features and in response amplitudes (larger and more responsive dark subfields) could be more relevant in the ventral stream visual processing. Still, ON/OFF temporal differences could be relevant in other higher order visual areas processing motion (e.g., PMLS). Indeed, recent evidence demonstrated that differences in the temporal dynamic of thalamic inputs are crucial for the emergence of direction selectivity in primary visual cortex (Lien & Scanziani, 2018). For instance, while most neurons in area PMLS area are highly direction selective (Wang et al., 1995; Merabet et al., 2000; Villeneuve et al., 2006), the majority of area 21a cells are orientation selective and lack direction selectivity (Mizobe et al., 1988; Toyama et al., 1994; Tardif et al., 1996; Vickery & Morley, 1997), indicating that temporal differences between bright and dark responses may be more relevant in motion rather than form processing. Indeed, in comparison with our previous study (Piché et al., 2013), PMLS neurons tended to exhibit larger differences in response peak delays than in area 21a (mean of 10.3 ms vs 6 ms), even though they were not significant in any of the cases. Still, in both cases, dark responses tended to be faster than bright ones.

Response Strength

In addition to the differences in subfield size, the dark dominance observed in 21a neurons was mostly expressed by the increased response magnitude to darks. As for the spatial asymmetries observed between brights and darks, we believe that the bias towards stronger responses to darks in area 21a is mostly due to the inputs from area 17. Previous studies failed to identify significant differences between ON and OFF responses in early subcortical areas as the retina and LGN (Krüger and Fischer, 1975; Kremers et al., 1993; Benardete and Kaplan, 1999; Jin et al., 2011 [but see Chichilnisky and Kalmar, 2002]) while others have shown the existence of dark-dominant neurons in the primate primary visual cortex (Yeh, Xing, & Shapley, 2009; Xing et al., 2010, Jansen et al., 2018). Using a method similar to that of the present study, Yeh et al. (2009) demonstrated that most neurons located at the supragranular layers of the macaque V1 were dark dominant with an average dark response around three times larger than brights. This asymmetry for dark dominance was mostly confined in supragranular layers while the bright and dark response magnitudes of neurons at the thalamorecipient layer IV resemble those from the LGN and retina (Yeh, Xing, Williams, et al., 2009; Xing et al., 2010; Jin et al.,

2011). Thus, these results demonstrate that stronger responses to darks arise at the supragranular layers of the primary visual cortex which most likely contribute significantly to the enhanced dark dominance observed in area 21a. This assumption is, to some extent, further supported by our previous study (Piché et al., 2013) in which most PMLS neurons, an area that equally receives its main inputs from supragranular layers of area 17, were dark dominant (~ 57%). Still, the average dark response of neurons from area 21a was around 2.5 times larger than PMLS neurons, supporting the notion that the contribution from the area 17 to the responses to luminance processing across the visual hierarchy is heterogenous with a much greater influence along the ventral stream. To our knowledge, there are no studies that investigated this issue in both areas V4 and MT (putatively, the homologues of area 21a and PMLS), precluding us from making comparisons between species.

Possible Mechanisms and Functional Significance of Dark Preferences in Area 21a

Past studies have raised different hypotheses in order to explain the emergence of asymmetries in the spatiotemporal properties of ON/OFF channels in V1. For instance, a study performed in juvenile cats demonstrated that at the first two postnatal weeks, the visual cortex (areas 17 and 18) is mostly comprised of dark-dominated neurons and that their number tends to be reduced as the cortex develops (Albus & Wolf, 1984). Although this study did not target extrastriate areas, one can hypothesize that the large proportion of dark-dominated neurons in area 21a is reminiscent of this developmental process.

Another possible explanation is that the response profile of 21a neurons may arise from the substantial projections of neurons from the supragranular layers of area 17, as proposed above. Studies in primates and cats support this idea since the RF of neurons in layers II/III in V1 (area 17) exhibit larger and more responsive dark subfields (Liu et al., 2007; Yeh, Xing, & Shapley, 2009; Xing et al., 2010). Our results demonstrated that the differences in size and response strength between bright and dark subfields seem to be amplified in area 21a.The differences between the response profiles of area 21a and PMLS suggest that these areas receive distinct inputs from the supragranular layers of area 17.

In a previous study, Xing et al. (Xing et al., 2010) proposed different mechanistic models in order to explain the dark preference in supragranular layers of the primate V1. In association

with single-unit data collected in another study (Yeh, Xing, & Shapley, 2009), they assessed the spatiotemporal response profile to brights and darks of multi-unit activity and local field potentials across the cortical layers of the macaque V1. Their experimental data supports the existence of two possible mechanisms that are not mutually exclusive: a selective feedforward input from a subset of dark-dominated neurons of layer IV and a process of local recurrent excitation and/or inhibition that would amplify the response asymmetries by enhancing dark responses, inhibiting bright ones or both. Interestingly, the response profile of 21a neurons observed in the present study could equally be explained by both models (Figure 7). For instance, the dark preference of 21a neurons could arise from inputs from subpopulations of neurons from supragranular layers of area 17 (selective feedforward model). This last assumption is supported by anatomical evidence demonstrating that area 17 neurons projecting to area 21a are not uniformly distributed throughout the cortical surface, but rather grouped in clusters (Conway et al., 2000). Therefore, this spatial compartmentalization could facilitate the convergence of inputs with similar spatiotemporal response properties giving rise to the dark preference observed in area 21a. Furthermore, Conway et al. (Conway et al., 2000) demonstrated that neurons projecting to area 21a and to the lateral suprasylvian cortex (which comprises the PMLS area) are separated across layer III depth, indicating the presence of two distinct pathways to the ventral (area 21a) and dorsal (PMLS) streams. Similarly, in the LPl, the main thalamic input for both cortical areas, neurons projecting to area 21a and PMLS are almost completely segregated into distinct subpopulations (Dreher, Djavadian, et al., 1996). Thus, differences between the bright and dark responses in area 21a and PMLS may be explained by the existence of two inputs carrying distinct spatiotemporal features.

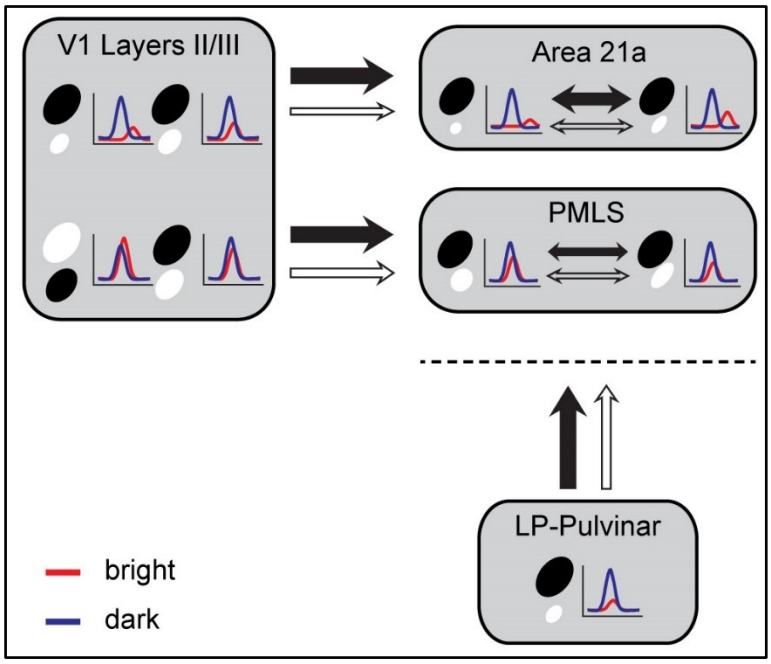

Figure 7. Schematic representation of two putative mechanisms giving rise to the response profile in area 21a and PMLS cortex. The first mechanism corresponds to a selective feedforward input (single arrows) from neurons in the supragranular layers (II/III) of the primary visual cortex (V1) and putatively from the LP-Pulvinar to the higher order areas (21a and PMLS). The second mechanism corresponds to a recurrent cortical local network of excitation/inhibition (double arrows) within higher order areas. Black and white ellipses represent the spatial profile and the curves represent the time course of the responses to darks and brights.

Another possible mechanism compatible with our findings involves local recurrent excitation/inhibition processes in area 21a. The greater dark responsiveness of neurons in area 21a in comparison to that in PMLS cortex (Piché et al., 2013), LPl nucleus (Piché et al., 2015) and V1 (Yeh, Xing, & Shapley, 2009; Xing et al., 2010) could be explained by distinct recurrent cortical local networks favoring larger dark subfields with increased responses to dark stimuli. Previous studies suggest that recurrent networks may be a ubiquitous mechanism in cortical processing among different modalities (Ben-Yishai et al., 1995; Wehr & Zador, 2003; Douglas & Martin, 2007). Thus, one cannot rule out the possibility that recurrent cortical local networks are involved in the dark dominance of 21a neurons. A recent study showed that the dark-dominance of neurons in the primate V1 may vary as a function of the size and spatial frequency of sinusoidal gratings stimuli (Jansen et al., 2018). We did not test the influence of size and the stimuli used here (squares) precluded us from investigating the impact of spatial frequency in the dark preference of area 21a neurons.

In cats, areas PMLS and 21a exhibit distinct functional and anatomical features placing them as gateway areas of the dorsal (motion processing) and ventral streams (form processing),

respectively (Wimborne & Henry, 1992; Dreher et al., 1993; Payne, 1993; Dreher, Djavadian, et al., 1996; Dreher, Wang, et al., 1996; Conway et al., 2000; Li et al., 2000). Taken together, our data on the response profile of neurons in areas 21a (the present study) and PMLS (Piché et al., 2013) to light increments and decrements adds to the current knowledge on the distinct functional properties of both areas. Additionally, the differences in the spatiotemporal profile of bright and dark responses suggest that there is a relationship between the magnitude of response asymmetry and the functional specialization of those cortical areas (i.e., motion vs form), with an increased sensitivity to dark for form processing. Indeed, evidence from psychophysical studies suggest the notion that bright/dark asymmetry play an important role in form recognition (Anstis et al., 2000; Motoyoshi et al., 2007) but not in motion detection (Edwards & Badcock, 1994).

The present study provides, for the first time, a description of the response profile to brights and darks of a higher-order area of the ventral stream, giving an important insight into the processing of luminance across the cortical hierarchy. The results suggest that the neural processing of darks is enhanced in the ventral cortical pathway, pinpointing the key role of darks in the analysis of form. Nonetheless, further studies in other animal models (e.g., primates) are necessary to determine whether dark-dominance is a ubiquitous feature in form processing along the mammalian visual cortex.

ACKNOWLEDGMENTS

This work was supported by a CIHR grant to CC (PJT-148959). BOFS received scholarships from EOUM-FESP. We thank Geneviève Cyr for her technical help, Sébastien Thomas and Samuel Bélanger for their valuable help in data analysis.

COMPETING INTERESTS

The authors declare no conflicts of interest.

AUTHOR CONTRIBUTIONS

CC conceived the research project; CC and BOFS designed the experimental protocol; BOFS performed experiments, data analysis and drafted the manuscript and figures; CC edited and revised the manuscript.

DATA ACCESSIBILITY

Raw electrophysiological data and MATLAB analysis code will be made available upon request by email to Dr. Christian Casanova (corresponding author).

ABBREVIATIONS

BA = bright subfield area; BARS = Bayesian adaptive regression splines; Cb = center of mass of bright subfield; Cd = center of mass of dark subfield; DA = dark subfield area; ECG = electrocardiogram; FS = fast spiking; LGN = lateral geniculate nucleus; OA = overlapped area; PMLS = posteromedial lateral suprasylvian cortex; PSTH = peri-stimulus time histogram; RF = receptive field; RS = regular spiking; SEM = standard error of the mean; SNR = signal to noise ratio; SOI = subfield overlap index; SSI = subfield size index.

REFERENCES

Albus, K. & Wolf, W. (1984) Early post-natal development of neuronal function in the kitten's visual cortex: a laminar analysis. J. Physiol., 348, 153–185.

Anstis, S.M., Smith, D.R.R., & Mather, G. (2000) Luminance processing in apparent motion, Vernier offset and stereoscopic depth. Vision Res., 40, 657–675.

Benardete, E.A. & Kaplan, E. (1999) Dynamics of primate P retinal ganglion cells: responses to chromatic and achromatic stimuli. J. Physiol., 519, 775–790.

Ben-Yishai, R., Bar-Or, R.L., & Sompolinsky, H. (1995) Theory of orientation tuning in visual cortex. Proc. Natl. Acad. Sci., 92, 3844–3848.

Burkhardt, D.A. (2011) Contrast processing by ON and OFF bipolar cells. Vis. Neurosci., 28, 69–75.

Burkhardt, D.A., Fahey, P.K., & Sikora, M. (1998) Responses of ganglion cells to contrast steps in the light-adapted retina of the tiger salamander. Vis. Neurosci., 15, 219–229.

Casanova, C., Savard, T., & Darveau, S. (1997) Contribution of area 17 to cell responses in the striate-recipient zone of the cat's lateral posterior-pulvinar complex. Eur. J. Neurosci., 9, 1026–1036.

Chichilnisky, E.J. & Kalmar, R.S. (2002) Functional Asymmetries in ON and OFF Ganglion Cells of Primate Retina. J. Neurosci., 22, 2737–2747.

Chubb, C. & Nam, J.-H. (2000) Variance of high contrast textures is sensed using negative half-wave rectification. Vision Res., 40, 1677–1694.

Conway, B., Boyd, J.D., Stewart, T.H., & Matsubara, J.A. (2000) The Projection from V1 to Extrastriate Area 21a: A Second Patchy Efferent Pathway that Colocalizes with the CO Blob Columns in Cat Visual Cortex. Cereb. Cortex, 10, 149–159.

Copenhagen, D.R., Ashmore, J.F., & Schnapf, J.K. (1983) Kinetics of synaptic transmission from photoreceptors to horizontal and bipolar cells in turtle retina. Vision Res., 23, 363–369.

DeAngelis, G.C., Ohzawa, I., & Freeman, R.D. (1993) Spatiotemporal organization of simple-cell receptive fields in the cat's striate cortex. I. General characteristics and postnatal development. J. Neurophysiol., 69, 1091–1117.

DeAngelis, G.C., Ohzawa, I., & Freeman, R.D. (1995) Receptive-field dynamics in the central visual pathways. Trends Neurosci., 18, 451–458.

Demb, J.B., Zaghloul, K., & Sterling, P. (2001) Cellular Basis for the Response to Second-Order Motion Cues in Y Retinal Ganglion Cells. Neuron, 32, 711–721.

Douglas, R.J. & Martin, K.A.C. (2007) Recurrent neuronal circuits in the neocortex. Curr. Biol., 17, R496–R500.

Dreher, B., Djavadian, R.L., Turlejski, K.J., & Wang, C. (1996) Areas PMLS and 21a of cat visual cortex are not only functionally but also hodologically distinct. Prog. Brain Res., 112, 251–276.

Dreher, B., Michalski, A., Ho, R.H., Lee, C.W., & Burke, W. (1993) Processing of form and motion in area 21a of cat visual cortex. Vis. Neurosci., 10, 93–115.

Dreher, B., Wang, C., Turlejski, K.J., Djavadian, R.L., & Burke, W. (1996) Areas PMLS and 21a of cat visual cortex: two functionally distinct areas. Cereb. Cortex N. Y. N 1991, 6, 585–599.

Edwards, M. & Badcock, D.R. (1994) Global motion perception: Interaction of the ON and OFF pathways. Vision Res., 34, 2849–2858.

Enroth-Cugell, C. & Robson, J.G. (1966) The contrast sensitivity of retinal ganglion cells of the cat. J. Physiol., 187, 517–552.

Ferster, D. (1990) X- and Y-mediated current sources in areas 17 and 18 of cat visual cortex. Vis. Neurosci., 4, 135–145.

Gollisch, T. & Meister, M. (2008) Rapid Neural Coding in the Retina with Relative Spike Latencies. Science, 319, 1108–1111.

Grant, S. & Hilgetag, C.C. (2005) Graded classes of cortical connections: quantitative analyses of laminar projections to motion areas of cat extrastriate cortex. Eur. J. Neurosci., 22, 681–696.

Hartline, H.K. (1938) The response of single optic nerve fibers of the vertebrate eye to illumination of the retina. Am. J. Physiol., 121, 400–415.

Henry, G.H. (1977) Receptive field classes of cells in the striate cortex of the cat. Brain Res., 133, 1–28.

Jansen, M., Jin, J., Li, X., Lashgari, R., Kremkow, J., Bereshpolova, Y., Swadlow, H.A., Zaidi, Q., & Alonso, J.-M. (2018) Cortical Balance Between ON and OFF Visual Responses Is Modulated by the Spatial Properties of the Visual Stimulus. Cereb. Cortex N. Y. N 1991.

Jin, J., Wang, Y., Lashgari, R., Swadlow, H.A., & Alonso, J.-M. (2011) Faster Thalamocortical Processing for Dark than Light Visual Targets. J. Neurosci., 31, 17471–17479.

Jin, J.Z., Weng, C., Yeh, C.-I., Gordon, J.A., Ruthazer, E.S., Stryker, M.P., Swadlow, H.A., & Alonso, J.-M. (2008) On and off domains of geniculate afferents in cat primary visual cortex. Nat. Neurosci., 11, 88–94.

Jones, J.P. & Palmer, L.A. (1987) The two-dimensional spatial structure of simple receptive fields in cat striate cortex. J. Neurophysiol., 58, 1187–1211.

Kass, R.E., Ventura, V., & Cai, C. (2003) Statistical smoothing of neuronal data. Netw. Bristol Engl., 14, 5–15.

Komban, S.J., Alonso, J.-M., & Zaidi, Q. (2011) Darks Are Processed Faster Than Lights. J. Neurosci., 31, 8654–8658.

Komban, S.J., Kremkow, J., Jin, J., Wang, Y., Lashgari, R., Li, X., Zaidi, Q., & Alonso, J.-M. (2014) Neuronal and Perceptual Differences in the Temporal Processing of Darks and Lights. Neuron, 82, 224–234.

Kremers, J., Lee, B.B., Pokorny, J., & Smith, V.C. (1993) Responses of macaque ganglion cells and human observers to compound periodic waveforms. Vision Res., 33, 1997–2011.

Krüger, J. & Fischer, B. (1975) Symmetry between the visual B- and D-systems and equivalence of center and surround: studies of light increment and decrement in retinal and geniculate neurons of the cat. Biol. Cybern., 20, 223–236.

Kuffler, S.W. (1953) Discharge Patterns and Functional Organization of Mammalian Retina. J. Neurophysiol., 16, 37–68.

Li, B., Li, B.-W., Chen, Y., Wang, L.-H., & Diao, Y.-C. (2000) Response properties of PMLS and PLLS neurons to simulated optic flow patterns. Eur. J. Neurosci., 12, 1534–1544.

Lien, A.D. & Scanziani, M. (2018) Cortical direction selectivity emerges at convergence of thalamic synapses. Nature, 558, 80–86.

Liu, S., Liu, Y.-J., & Li, B. (2007) Spatiotemporal structure of complex cell receptive fields and influence of GABAergic inhibition: NeuroReport, 18, 1577–1581.

Mata, M.L. & Ringach, D.L. (2005) Spatial Overlap of on and off Subregions and Its Relation to Response Modulation Ratio in Macaque Primary Visual Cortex. J. Neurophysiol., 93, 919–928.

Merabet, L., Minville, K., Ptito, M., & Casanova, C. (2000) Responses of neurons in the cat posteromedial lateral suprasylvian cortex to moving texture patterns. Neuroscience, 97, 611–623.

Michalski, A., Wimborne, B.M., & Henry, G.H. (1993) The effect of reversible cooling of cat's primary visual cortex on the responses of area 21a neurons. J. Physiol., 466, 133–156.

Mizobe, K., Itoi, M., Kaihara, T., & Toyama, K. (1988) Neuronal responsiveness in area 21a of the cat. Brain Res., 438, 307–310.

Morley, J.W., Yuan, L., & Vickery, R.M. (1997) Corticocortical connections between area 21a and primary visual cortex in the cat. NeuroReport, 8, 1263.

Motoyoshi, I., Nishida, S., Sharan, L., & Adelson, E.H. (2007) Image statistics and the perception of surface qualities. Nature, 447, 206–209.

Nassi, J.J. & Callaway, E.M. (2009) Parallel processing strategies of the primate visual system. Nat. Rev. Neurosci., 10, nrn2619.

Nichols, Z., Nirenberg, S., & Victor, J. (2013) Interacting Linear and Nonlinear Characteristics Produce Population Coding Asymmetries between ON and OFF Cells in the Retina. J. Neurosci., 33, 14958–14973.

Olman, C., Boyaci, H., Fang, F., & Doerschner, K. (2008) V1 responses to different types of luminance histogram contrast. J. Vis., 8, 345–345.

Payne, B.R. (1993) Evidence for visual cortical area homologs in cat and macaque monkey. Cereb. Cortex N. Y. N 1991, 3, 1–25.

Piché, M., Thomas, S., & Casanova, C. (2013) Spatiotemporal profiles of neurons receptive fields in the cat posteromedial lateral suprasylvian cortex. Neuroscience, 248, 319–332.

Piché, M., Thomas, S., & Casanova, C. (2015) Spatiotemporal profiles of receptive fields of neurons in the lateral posterior nucleus of the cat LP-pulvinar complex. J. Neurophysiol., 114, 2390–2403.

Raczkowski, D. & Rosenquist, A.C. (1980) Connections of the parvocellular C laminae of the dorsal lateral geniculate nucleus with the visual cortex in the cat. Brain Res., 199, 447–451.

Sakata, S. & Harris, K.D. (2009) Laminar Structure of Spontaneous and Sensory-Evoked Population Activity in Auditory Cortex. Neuron, 64, 404–418.

Sherk, H. (1989) Visual response properties of cortical inputs to an extrastriate cortical area in the cat. Vis. Neurosci., 3, 249–265.

Sherman, S.M. & Spear, P.D. (1982) Organization of visual pathways in normal and visually deprived cats. Physiol. Rev., 62, 738–855.

Sirota, A., Montgomery, S., Fujisawa, S., Isomura, Y., Zugaro, M., & Buzsáki, G. (2008) Entrainment of Neocortical Neurons and Gamma Oscillations by the Hippocampal Theta Rhythm. Neuron, 60, 683–697.

Szulborski, R.G. & Palmer, L.A. (1990) The two-dimensional spatial structure of nonlinear subunits in the receptive fields of complex cells. Vision Res., 30, 249–254.

Tardif, E., Bergeron, A., Lepore, F., & Guillemot, J.-P. (1996) Spatial and temporal frequency tuning and contrast sensitivity of single neurons in area 21a of the cat. Brain Res., 716, 219–223.

Taylor, M.M., Sedigh-Sarvestani, M., Vigeland, L., Palmer, L.A., & Contreras, D. (2018) Inhibition in Simple Cell Receptive Fields Is Broad and OFF-Subregion Biased. J. Neurosci., 38, 595–612.

Toyama, K., Mizobe, K., Akase, E., & Kaihara, T. (1994) Neuronal responsiveness in areas 19 and 21a, and the posteromedial lateral suprasylvian cortex of the cat. Exp. Brain Res., 99, 289–301.

Van Der Gucht, E., Vandesande, F., & Arckens, L. (2001) Neurofilament protein: A selective marker for the architectonic parcellation of the visual cortex in adult cat brain. J. Comp. Neurol., 441, 345–368.

Vickery, R.M. & Morley, J.W. (1997) Orientation-dependent binocular interactions in area 21a of the cat. [Miscellaneous Article]. Neuroreport Sept. 29 1997, 8, 3173–3176.

Villeneuve, M.Y., Ptito, M., & Casanova, C. (2006) Global motion integration in the postero-medial part of the lateral suprasylvian cortex in the cat. Exp. Brain Res., 172, 485–497.

Wang, Y., Wang, L., Li, B., Wang, L.H., & Diao, Y.C. (1995) How is direction selectivity organized in the extrastriate visual area PMLS of the cat? Neuroreport, 6, 1969–1974.

Wehr, M. & Zador, A.M. (2003) Balanced inhibition underlies tuning and sharpens spike timing in auditory cortex. Nature, 426, 442–446.

Wimborne, B.M. & Henry, G.H. (1992) Response characteristics of the cells of cortical area 21a of the cat with special reference to orientation specificity. J. Physiol., 449, 457–478.

Xing, D., Yeh, C.-I., & Shapley, R.M. (2010) Generation of Black-Dominant Responses in V1 Cortex. J. Neurosci., 30, 13504–13512.

Yeh, C.-I., Xing, D., & Shapley, R.M. (2009) “Black” Responses Dominate Macaque Primary Visual Cortex V1. J. Neurosci., 29, 11753–11760.

Yeh, C.-I., Xing, D., Williams, P.E., & Shapley, R.M. (2009) Stimulus ensemble and cortical layer determine V1 spatial receptive fields. Proc. Natl. Acad. Sci., 106, 14652–14657.

Zemon, V., Eisner, W., Gordon, J., Grose-Fifer, J., Tenedios, F., & Shoup, H. (1995) Contrast-dependent responses in the human visual system: childhood through adulthood. Int. J. Neurosci., 80, 181–201.

7 Article # 2

Manuscript in preparation for publication in the journal *Cerebral Cortex*

Pulvinar modulates contrast responses in visual cortex as a function of cortical hierarchy

Bruno Oliveira Ferreira de Souza*, Nelson Cortes* and Christian Casanova**

School of Optometry, Université de Montréal, CP 6128 succursale centre-ville, Montreal, Quebec, Canada

* These authors equally contributed to this manuscript.

** Corresponding author:

Christian Casanova

E-mail: christian.casanova@umontreal.ca

School of Optometry

Université de Montréal

CP 6128, Succ Centre-Ville

Montréal, Québec

Canada, H3C-3J7

Tel: (514)-343-6948

Fax: (514)-343-2382

Running title: Impact of pulvinar inactivation across the cat ventral stream

ABSTRACT

The pulvinar is the largest extrageniculate visual nucleus in mammals. Given its extensive reciprocal connectivity with the visual cortex, it allows the cortico-thalamo-cortical transfer of visual information. Nonetheless, the nature of the pulvinar inputs to the cortex remains elusive. We investigated the impact of silencing the pulvinar on the contrast response function of neurons in two distinct hierarchical cortical areas in the cat (areas 17 and 21a). Pulvinar inactivation altered the response gain in both areas, but with larger changes observed in area 21a. A theoretical model was proposed, simulating the pulvinar contribution to cortical contrast responses by modifying the excitation-inhibition balanced state of neurons across the cortical hierarchy. Our experimental and theoretical data showed that the pulvinar exerts a greater modulatory influence on neuronal activity in area 21a than in the primary visual cortex, indicating that the pulvinar impact on cortical visual neurons varies along the cortical hierarchy.

Keywords: cat, lateral posterior nucleus, reversible inactivation, transthalamic pathway, ventral stream.

INTRODUCTION

The perception of external stimuli is traditionally considered to result solely from the processing of thalamic signals through direct cortico-cortical connections between areas organized in a hierarchical manner (Panagiotaropoulos et al. 2014). This corticocentric view has been challenged in recent years since, besides direct communication between cortical areas through cortico-cortical connections, indirect communication through cortico-thalamocortical projections can also occur (Casanova 2004; Sherman and Guillery 2013). In the visual system, the pulvinar, which is the largest extrageniculate nucleus in mammals, is a key structure for the transfer of information between cortical areas (Casanova 2004; Chalfin et al. 2007). It receives a main input from the primary visual cortex and from most if not all higher-order visual areas and in turn, projects back to these areas (Leh et al. 2008; Arcaro et al. 2015; Barron et al. 2015). Pulvinar neurons have cortex-like receptive fields and this structure has been associated with a number of normal vision processing such as higher-order motion, feature binding, and attention (Petersen et al. 1987; Chalupa and Abramson 1989; Casanova and Savard 1996; Merabet et al. 1998; Ward et al. 2002; Villeneuve et al. 2005). It has recently been suggested that deficits in sensory processing observed in disorders such as schizophrenia results from a dysfunction in transthalamic cortical communication involving the pulvinar (Byne et al. 2009; Benarroch 2015).

While much is known about the geniculo-cortical pathway, we have virtually no information about the functional properties of the much more extensive pulvinar-cortical circuits. Consequently, their contribution in cortical processing, and ultimately in perception, remains elusive. Attempts to define the function of these pathways are mainly based on anatomical grounds (Sherman and Guillery 2013). Two types of inputs, drivers and modulators, have been described along the well-characterized retino-geniculate-cortical pathway on the basis of electrophysiological and anatomical criteria (Sherman and Guillery 1998). In essence, drivers determine the properties of their target cells whereas modulators provide contextual activity modulation of the recipient neurons, and it has been proposed that, a general rule, thalamic terminals ending in layer I and IV are modulatory and drivers, respectively (Crick and Koch 1998; Jones 2001; Lee and Sherman 2008; Viaene et al. 2011). In addition, drivers and

modulators would yield correspondingly additive/subtractive and multiplicative/divisive changes on the membrane potential of a cortical neuron (Anderson et al. 2000; Chance et al. 2002; Abbott and Chance 2005).

The pulvinar receives its main input from layers V neurons in the primary visual cortex and from layers VI neurons in higher-order areas (Lund et al. 1975; Trojanowski and Jacobson 1977; Raczkowski and Rosenquist 1983; Abramson and Chalupa 1985). Anatomical and physiological data indicate that the signals from V1 are almost exclusively drivers while those from higher-order areas are drivers and modulators (Theyel et al. 2010), with an increase of the modulators/driver ratio along the cortical hierarchy (Huppé-Gourgues et al. 2006). Pulvinar projections to the visual cortex are two-fold: for the most part, they reach layer I of the primary visual cortex and end in layer IV of all other visual areas (Benevento and Rezak 1976; Ogren and Hendrickson 1977; Rezak and Benevento 1979; Symonds et al. 1981; Roth et al. 2016). Based on this organization, one would suggest that the pulvinar modulates entrant activity in V1 and drive neurons in higher-order areas. We tested this assumption by investigating the impact of pulvinar on the contrast response function of two hierarchically distinct areas in the cat, the primary visual cortex and area 21a (the homologue of V4 in primates, (Payne 1993)). In this animal model, the pulvinar consists on a group of three main nuclei and is named the lateral posterior-pulvinar complex (LP-pulvinar, (Hutchins and Updyke 1989)). The lateral part of the LP (LPl) is the striato-recipient zone of the LP while the medial part is the tecto-recipient zone (Abramson and Chalupa 1985; Casanova et al. 1997). LPl neurons project to layer I of area 17 while those in LPl and LPm project to layer IV of area 21a (Miller et al. 1980; Symonds et al. 1981; Berson and Graybiel 1983).

In this study, we pharmacologically inactivated subregions of the pulvinar to determine the nature of the thalamic signals reaching lower and higher-order visual areas. According to the framework described above, we assumed that the contrast response function of cortical neurons will be distinctly affected in the two cortical areas: pulvinar should principally modulate activity (response gain; slope control) in the primary visual cortex, while it should mainly drive neuronal discharges (contrast gain; baseline control) in area 21a (Figure 1). Results indicate that there is no such clear difference. While some neurons in area 17 exhibited a change in contrast gain, the effects observed were mostly characterized by modifications in the response dynamic range

(i.e., response gain) of neurons in both areas, but at different strength levels. A theoretical model which simulates the impact of the LP inactivation on the cortical contrast sensitivity responses by modifying the excitation-inhibition balanced state of neurons throughout the visual cortical hierarchy is proposed.

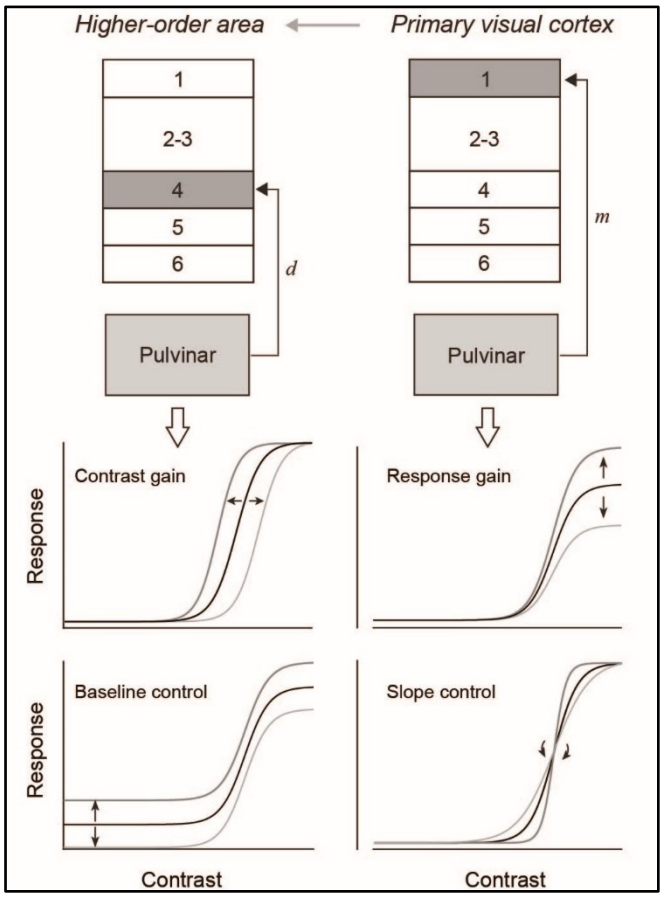

Figure 1. Hypothetical scheme of the nature of pulvino-cortical inputs to the primary visual cortex and an extrastriate area. A putative modulator (m) input would yield non-linear effects on the contrast response function (CRF) of neurons from the primary visual cortex represented as changes in the response gain and slope. On the other hand, a putative driver (d) input in higher-order cortical areas would yield linear effects on the neurons' CRFs, characterized by changes in the contrast gain and baseline.

MATERIAL AND METHODS

Animals and surgery

Experiments were performed on normal male and female adult cats (2.5-3.5 Kg). All surgical and experimental procedures were undertaken according to the guidelines of the Canadian Council on Animal Care and were approved by the Ethics Committee of the University of Montreal. First, atropine (0.1mg/Kg) and acepromazine (Atravet®, 1mg/Kg) were

administered subcutaneously to reduce parasympathetic effects of anesthesia and to provoke sedation, respectively. Anesthesia induction was performed with 3.5% Isofluorane in a 50:50 (vol/vol) gas mixture of O2 and N2O. Isofluorane concentration was maintained at 1.5% throughout surgical procedures. During recording sessions, Halothane (0.5-0.8%) was used in order to ensure cortical responsiveness (Villeneuve and Casanova 2003). A tracheotomy was performed, and animals were immobilized using an intravenous bolus injection of 2% gallamine triethiodide. Then, animals were artificially ventilated and a 1:1 (vol/vol) solution of 2% gallamine triethiodide (10 mg/kg/h) in 5% of dextrose in lactated ringer was continuously administered intravenously to maintain muscular relaxation and to provide nutrition and electrolytes. Expired level of CO2 was maintained between 35 and 40 mmHg by adjusting the tidal volume and respiratory rate. Heart rate was continuously monitored during the experiment and the temperature was maintained at 37°C by means of a feedback controlled heated blanket. Local anesthetic (lidocaine hydrochloride 2%) was used in all incisions and pressure points. Dexamethasone (4 mg, I.M.) was administered every 12 hours in order to avoid cortical swelling. Pupils were dilated using atropine (Mydriacyl®) and nictitating membranes were retracted using phenylephrine (Midfrin®). Rigid contact lenses with the appropriate power were used to correct eyes refraction and eye lubricants were used to avoid corneal dehydration. Three craniotomies were performed in order to gain access to the LP nucleus (5-8A; 3-7L, Horsley-Clarke coordinates) and to cortical areas 17 (4-8P;0.5-2L) and 21a (2-6P;7-11L). Small durectomies were performed for each electrode penetration. A 2% Agar solution in saline was applied over the exposed regions to increase recordings stability and to avoid the drying of the cortical surface.

Visual Stimuli

Visual stimuli were generated using the VPixx software (VPixx Technologies Inc., St-Bruno, Qc, Canada), projected onto an isoluminant screen located at 57 cm of viewing distance and covering 116° by 150° of visual angle with a mean luminance of 25 cd/m2. Stimuli consisted on drifting sinusoidal gratings with spatial and temporal frequencies set at 0.3 cpd and 3 Hz for

all stimuli, respectively. Neurons' direction tuning was obtained with 50% contrast gratings moving over 360° at 12 steps of 30°. The contrast response function (CRF) was evaluated by varying contrast values between 6 and 100% at the neuron's optimal direction. Two sets of contrast increments were used: 0, 16, 33, 50, 66 and 100%; 0, 6, 12, 25, 50 and 100%. For all tests, trials were fully randomized and each stimulus was presented for at least 10 times. Stimulus presentation lasted 1 and 2 s for contrast and direction tests, respectively, separated by a mean luminance gray screen (blank) used to assess spontaneous activity.

Electrophysiological recordings and signal preprocessing

Neural activity in areas 17 and 21a was recorded using 32-channel linear probes (~1MΩ, 1x32-6mm-100-177, Neuronexus). Prior to insertion, the probes were covered with a fluorescent dye (DiI) allowing the histologic assessment of the electrode position in the cortex. Electrophysiological signals were acquired at 30KHz and band pass filtered between 1-7500 Hz using an open-source system (Open-Ephys platform, (Siegle et al. 2017)). Single units were identified using the software package Klusta (Rossant et al. 2016). In brief, signals were high-pass filtered at 500 Hz and a threshold was used to detect the spikes. Subsequently, the spikes were separated by an unsupervised automatic clustering algorithm using principal component analysis. Finally, a manual validation of the clustering process was undertaken. Units exhibiting low spike amplitudes or ill-defined cluster margins were excluded. Peri-stimulus time histograms (PSTHs) were obtained from the neuronal responses to drifting gratings and the responses of each unit was calculated as the average firing rate during the stimulus presentation for each trial. Units with low firing rates (maximal discharge below 5 spikes/s) in the control condition were excluded from the analysis.

Thalamic inactivation

The lateral (LPl) and medial (LPm) subdivisions of the LP nucleus were pharmacologically inactivated by the intracerebral injection of a solution of 20mM GABA stained with Chicago Sky Blue (0.5%) for the histologic assessment of the location and extent of the injection (Figure S1A). The GABA solution was injected using a custom-made injectrode (Lai et al. 2015). First, the solution was injected at a rate of 80 nL/min until the inhibition of the neuronal activity was achieved. A successful inactivation was characterized by the silencing of the local multi-unit activity recorded through the injectrode. Subsequently, the injection rate was reduced to 20-40 nL/min in order to silence neural activity throughout the testing period. The local neuronal activity was continuously monitored and a recovery from inhibition was observed about 30-45 min after the completion of the GABA injection. Cortical responses were recorded before (control), during (injection), and after (recovery) GABA injection in the thalamus (Figure S1B).

Curve fitting and Data analysis

The CRF was generated by fitting the Naka-Rushton equation to experimental data:

$$R(C) = \mathrm{Rmax}\frac{C^n}{C^n + C50^n} + \mathrm{Bsln}, \qquad (1)$$

where $R(C)$ is the output response at contrast C, Bsln is the baseline response, n represents the slope of the curve, Rmax is the maximum response above the baseline, and $C50$ is the contrast that evokes half of Rmax.

The goodness of fit was assessed by a modified version of the Chi-squared (χ^2) test that takes into account the linear correlation between the cortical neuronal activity and the response variance. The χ^2 term was considered as:

$$\chi^2 = \sum_i \frac{(e_i - o_i)^2}{k + o_i \frac{\rho_i}{t}}, \qquad (2)$$

where i represents the index of the contrast level, o is the observed neuronal response, e is the expected response from the fit, ρ corresponds to the ratio between the response variance and the average firing rate at a particular contrast, t represents the response duration in seconds and k is a small factor (k = 0.01(p*max(o))) used to avoid infinite values at zero response (Cavanaugh

et al., 2002). Due to the nature of our experimental protocol (long lasting recordings), several factors could affect the recording reliability over time. Consequently, we excluded from the analysis neurons that showed χ^2 values from the recovery period that were higher than twice the one from the control curve.

The parameters extracted from the curve fit were used to compare the cortical activity recorded during the control, injection and recovery periods. The Rmax and baseline (Bsln) were normalized to the average firing rate at maximum contrast in the control condition. In addition, the percentage of variation (*%Var*) for each CRF parameter (*Par*) was calculated as

$$\%\,Var = 100 * \frac{Par_{control} - Par_{injection}}{Par_{control} + Par_{injection}} \qquad (4)$$

The response modulation to drifting gratings was assessed in order to identify simple and complex-like cells. Fourier transformation of the PSTH was performed and a modulation index was obtained by calculating the ratio of the amplitude of the first harmonic over the DC amplitude (F1/F0). Cells with F1/F0 values greater than one were classified as simple while those with values below one where considered as complex (Skottun et al., 1991).

Selection of CRF based on the percentage of overlap between conditions

For each unit, a qualitative analysis of the CRFs obtained in control, injection and recovery conditions was performed by considering the degree of overlap between the confidence intervals of each curve. The confidence intervals were estimated by a bootstrapping method. For each CRF, a distribution of CRFs was generated by applying the curve fit (equation 1) to resampled datasets over 1000 iterations. The central 95% of the curves distribution was considered as the confidence interval. Subsequently, the percentages of overlapped areas between the CRFs confidence intervals at control and injection (Ctr-Inj), control and recovery (Ctr-Rec) and injection and recovery (Inj-Rec) were calculated. A 100% overlap between CRF areas indicates that they are equal, while 0% shows that the CRFs are completely different. Neurons exhibiting lower Inj-Rec overlap (Inj-Rec < 50%) and higher Ctr-Rec overlap (Ctr-Rec > 50%) recovered completely from the GABA injection. On the other hand, those with high Inj-Rec overlap were considered partially recovered. However, neurons were only considered

partially recovered when their recovery CRFs tended towards the control condition, otherwise they were eliminated from the analysis.

Spike waveform classification

Putative inhibitory and excitatory neurons were classified as fast (FS) and regular (RS) spiking respectively, based on the analysis of their spike waveform profile (Sirota et al., 2008; Sakata and Harris, 2009). Prior to the analysis, the temporal resolution was increased using spline interpolation. Two parameters were calculated: the half-width of the spike negative deflection and the delay between the negative and the positive peaks (trough-to-peak). Cells were classified in two groups using a K-means clustering algorithm. The validation of the clustering method was performed using the *silhouette* MATLAB (RRID:SCR_001622) function, which calculates an index (silhouette value) ranging from -1 to 1 where values indicate how similar a data point is from its respective group, with negative values indicating a probable misclassified data point. Thus, neurons with negative silhouette values were considered as unclassifiable and were excluded from the analysis (Figure S2).

Histology

At the end of the experiment, animals were euthanized with an intravenous injection of sodium pentobarbital (Euthanyl, 110mg/Kg). Animals were transcardially perfused with a phosphate buffer solution (PBS 0.1M, pH 7.4) followed by a fixative (Paraformaldehyde 4%). Brain tissue was cryoprotected using sucrose solutions at different concentrations (10 to 30%), frozen and stored at -80°C. Then, 40 µm coronal sections were obtained and subsequently stained. LP subdivisions were revealed using Acetylcholinesterase staining (Graybiel and Berson 1980). The location and extent of GABA injections were assessed by analyzing the Chicago Sky Blue staining (Figure S1A). Cortical layers were identified using DAPI and the DiI fluorescence signal was used to reconstruct the electrode position. Furthermore,

immunostaining of nonphosphorylated neurofilament protein was used to confirm the position of recordings in area 21a (Figure 5C; Van Der Gucht et al. 2001).

Statistical analysis

Statistical analysis was undertaken using the computing environment R (RRID:SCR_001905) with the additional software package PMCMR. Data are expressed as mean ± SEM, unless otherwise stated. Data normality was verified using Kolmogorov-Smirnov test. Since data were not normally distributed, different non-parametric statistical approaches were used. Pairwise data comparison was performed using Wilcoxon rank-sum test. Results from LPl and LPm inactivation were analyzed together using Kruskal-Wallis test and Dunn's post hoc with Holm adjustment. Correlation analysis was performed and Pearson's correlation coefficient (r) and significance values are shown. Data obtained from direction tuning curves were compared using the Quade test. The relationship between categories was assessed using Fisher's exact test.

The network model

We modelled a layered network of four areas connected feedforwardly, which receive and send additional inputs from and to a parallel structure. The feedforward network (FFN) represents the transmission of visual information throughout the hierarchy of the cat visual cortex. The parallel structure mimics the LP nucleus. The first cortical area receives an excitatory LGN spiking firing rate input modeled by Poisson spike trains modulated by different contrast levels (see Cortical interactions). We considered four levels to mimic processing from areas 17 to 21a, passing across areas 18 and 19. Because we studied the effect of the LP on cortical neurons, for simplicity, we did not consider the direct connection from the LGN to extrastriate cortical areas described in the cat and the feedforward connections from area 17 to 21a (Wimborne and Henry, 1992). Each component of the network consisted of N_E excitatory and N_I inhibitory neurons organized to generate the balanced state. We characterized neurons as $i = 1,2,\ldots,N_A^{\alpha}$ of excitatory, E, or inhibitory, I, population, from cortical or thalamic

structures ($\alpha = ctx, lp$, where $ctx = 1,2,...L$ with $L = 4$ and lp as the LP). For each area, including the LP, we simulated $N = 10000$ neurons with 80% and 75% of excitatory cells for the cortex and the LP, respectively. We considered an additional 5% of inhibitory neurons in the LP based on available empirical data (Rinvik et al., 1987). This additional 5% produced a slight, but significant increase in thalamic activity, when compared with cortical responses. Both recurrent and afferent connectivity for each layer were random with probability c of connection, in which c is different for E and I populations.

Neuron dynamics

We used the adaptive exponential integrate-and fire model (Brette and Gerstner, 2005) to describe the dynamics of cortical and thalamic neurons. This neural model consists of two coupled differential equations. The membrane potential of neuron *i*, of the E or I population *A*, and cortical or thalamic structure α, were defined by:

$$C_m \frac{dV_i^{A,\alpha}}{dt} = -I_{L,i}^{A,\alpha} - w_i^{A,\alpha} + I_{input,i}^{A,\alpha}, (5)$$

where C_m is the capacitance of the neuron. The first term on the right-hand side of the above equation, given by $I_{L,i}^{A,\alpha} = -g_L^{A,\alpha}\left(V_i^{A,\alpha} - V_L^{A,\alpha}\right) + g_L^{A,\alpha}\Delta_T exp\left(\frac{V_i^{A,\alpha} - V_T}{\Delta_T}\right)$, consists of a linear component which is the leak current, and a second term which is the exponential function which characterizes the spike generation process where V_L is the leak reversal potential, V_T is the threshold and Δ_T is the slope factor. The adaptation current, w, obeyed:

$$\frac{dw_i^{A,\alpha}}{dt} = \frac{a\left(V_i^{A,\alpha} - V_L\right) - w_i^{A,\alpha}}{\tau_{adapt}}, (6)$$

where τ_{adapt} is a time constant and a describes the level of subthreshold adaptation. Every time that the neuron i fires, w is increased by a current b (spike-triggered adaptation), and the membrane potential is reset to a fixed voltage, V_r. Only excitatory neurons have adaptation current dynamics.

The input current that a neuron (i, A, α) receives is:

$$I_{input,i}^{A,\alpha} = I_{rec,i}^{A,\alpha} + I_{ext,i}^{A}, (7)$$

where $I_{rec,i}^{A,\alpha}$ characterizes the synaptic current from recurrent connections of each area, and the external current, $I_{ext,i}^{A}$, comprises two or four terms if the unit is from the cortex or the thalamus, respectively.

Recurrent connections

The recurrent synaptic interactions activate current input to a neuron (i,A,α) as

$$I_{rec,i}^{A,\alpha}(t) = -\sum_{B=E,I} g_i^{AB}(t)\left(V_i^A - V_B\right)$$
$$g_i^{AB}(t) = \frac{\bar{g}_i^{AB}}{\tau_{syn}^A}\sum_{j=1}^{N_{ff}} C_{ij}^{AB}\sum_k e^{-\left(t-t_{j,k}^B\right)/\tau_{syn}^A}, \quad (8)$$

where $C_{ij}^{AB} = 0{,}1$ is the connectivity matrix, τ_{syn} is the synaptic time constant, and $t_{j,k}^B$ is the time of the kth action potential of neuron j of population B and brain region α. So, for simplicity we assumed an instantaneous rise of the synaptic currents followed by an exponential decay. Recurrent connections were random and the probability varied according to the nature of the cell (i.e., excitatory or inhibitory). The probability of connections was set such as to guarantee that the total number of presynatic inputs to neuron (i, A, α) is on average K. Thus, we requested that the conductance $\bar{g}^{AB}$ is scaled by K as $\bar{g}^{AB} = G_{AB}/\sqrt{K}$, where G_{AB} and K are independent. Thus, the probability of connection was $c_A = K_A/N_A$, for $A = E, I$. This scaling lead to cells to fire closed to the maximum rate. However, the strong recurrent connections between excitatory and inhibitory cells balanced each other out leading to a net input on the order of the threshold. Under this regime, without any fine-tuning of parameters, neural populations dynamically arise in the balanced state. As a result, the firing rate of these neurons changes only very weakly if one rescales all the synaptic strengths by the same factor.

Cortical interactions

Cortical neurons between different areas interacted in a feedforward and a recurrent manner. They received two types of external inputs:

$$I_{ext,i}^{A}(t) = I_{ff,i}^{A,ctx}(t) + I_{i}^{A,lp}(t), (9)$$

where $I_{ff,i}^{A,ctx}$ is the feedforward cortical input and $I_{i}^{A,lp}$is the input coming from the LP. Feedforward inputs throughout the chain of cortical areas were defined as $ctx = 1,2,\ldots,L$. Therefore, the feedforward pathway for the neuron (i, A, ctx) in cortical area $ctx = l$, was defined by the incoming excitatory presynaptic inputs from the previous area $l-1$. Excitatory inputs targeted excitatory and inhibitory populations. Thus, the feedforward input current was defined as $I_{ff,i}^{A,ctx}(t) = -g_{ff,i}^{A,l-1}(t)\left(V_i^A - V_E^{l-1}\right)$, where the term on the right-hand side of the equation is the sum of all conductances from all presynaptic inputs on neuron $(i, A, l-1)$. It was described as

$$g_{ff,i}^{A,l}(t) = \frac{\bar{g}_{ff}^{A,l}}{\tau_{syn}^{A}} \sum_{j=1}^{N_{ff}} C_{ij}^{Aff,l} \sum_{k} e^{-\left(t - t_{j,k}^{ff}\right)/\tau_{syn}^{A}}, (10)$$

where $t_{j,k}^{ff}$ is the time of the kth spike on neuron (j, ff). The coupling matrices $C_{ij}^{Aff,l}$ for $A = E, I$ and $ff = E$, are random, i.e. C=1 with probability $c_{ff}\,K/N_{ff}$ and $C_{ij}^{Aff,l} = 0$ otherwise. Thus, a neuron (i, A, l) receives, on average, $K_{ff} = c_{ff}K$ inputs from area $l-1$. The conductance $\bar{g}_{ff}^{A,l}$ that describes the weight of the feedforward presynaptic inputs is scaled with K as $\bar{g}_{ff}^{A,l} = G_{ff}^{A}/\sqrt{K}$, where G_{ff}^{A} is independent of K and has equal strength for all cortical areas. The first cortical area received N_{inp} inputs from a population of LGN excitatory cells. These cells were not modeled explicitly, but they are assumed to have Poisson statistics. The firing rate of a LGN cell (i, ff) depended on the contrast C, which is given by

$$R_{i}^{ff}(C, t) = R^{ff}(C) g_i(t), (11)$$

where $R^{ff}(C) = R^{ff} log_{10}(C + 1)$ is the response amplitude due to the visual contrast. The excitatory LGN input, when $l = 1$, to excitatory and inhibitory cortical populations, is modeled with the conductance, $g_i(t)$. $g_i(t)$ is the total conductance described in Equation 10, where $t_{i,j}^{ff,0}$ is the time of the *j*th action potential by neuron (i, LGN), and ff =E.

The other source of external currents to the cortical neurons in area l was the LP. Each cortical area received at the same time inputs from an excitatory population of thalamic neurons. This source of LP neurons were chosen randomly. Therefore, the input current from the LP to cortical

neuron (i, A, l) follows $I_{lp,i}^{A,l}(t) = -g_{ctx\leftarrow lp,i}^{A}(t)\left(V_i^A - V_E^{ctx\leftarrow lp}\right)$, where the term on the right-hand side of the equation is the total conductance of neuron (i, A, l) from all presynaptic LP inputs. Note that we changed $I_i^{A,lp} = I_{ctx\leftarrow lp,i}^{A,l}$, to specify the cortical area l that receives inputs from the LP. It obeyed,

$$g_{ctx\leftarrow lp,i}^{A,l}(t) = \frac{\bar{g}_{ctx\leftarrow lp}^{A,l}}{\tau_{syn}^{A}} \sum_{j=1}^{N_{lp}} C_{ij}^{ctx_A\leftarrow lp_E,l} \sum_{k} e^{-\left(t-t_{j,k}^{lp}\right)/\tau_{syn}^{A}}, \quad (12)$$

where $t_{j,k}^{lp}$ is the time of the kth action potential by neuron (j, lp). To avoid confusion, we considered the thalamic conductance such as $g_{ctx\leftarrow lp,i}^{A,l}$ for $g_i^{AB,l}$, with $B = E_l$ being the excitatory population of neuron from the LP that connects to cortical area l. The connection matrices $C_{ij}^{ctx_A\leftarrow lp_E,l}$, for $A = E, I$, were random with probability $c_{ctx\leftarrow lp}\, K/N_{ctx\leftarrow lp}$ and $C_{ij}^{ctx_A\leftarrow lp_E,l} = 0$ otherwise. On average, cortical neurons received $K_{ctx\leftarrow lp} = c_{ctx\leftarrow lp}K$ presynaptic connections from LP. Here, the conductance $\bar{g}_{ctx\leftarrow lp}^{A,l}$ describes the strength of the thalamic presynaptic input, which is scaled by K as $\bar{g}_{ctx\leftarrow lp}^{A,l} = G_{ctx\leftarrow lp}^{A}/\sqrt{K}$, where $G_{ctx\leftarrow lp}^{A}$ is independent of K.

Thalamic interactions

Although the LP receives inputs from subcortical areas (Chalupa et al., 1983), the model considered that the external current for the thalamic neurons depended only on cortical inputs as shown by empirical data (Bender, 1983). A thalamic neuron (i, A, lp) received current inputs simultaneously from the four cortical areas. It obeyed,

$$\begin{aligned} I_{ext,i}^{A}(t) &= \frac{-\sum_l^L g_{lp\leftarrow ctx,i}^{A,l}(t)}{W(PC, l)}\left(V_i^A - V_E^{lp\leftarrow ctx}\right) \\ \bar{g}_{lp\leftarrow ctx,i}^{A,l}(t) &= \frac{\bar{g}_{lp\leftarrow ctx}^{A,l}}{\tau_{syn}^{A}} \sum_{j=1}^{N_l} C_{ij}^{lp_A\leftarrow ctx_E,l} \sum_{k} e^{-\left(t-t_{j,k}^{l}\right)/\tau_{syn}^{A}}, \end{aligned} \quad (13)$$

where $t_{j,k}^{lp}$ is the time of the kth action potential of neuron (j, lp). The weight $W(PC, l)$ scales the input from the cortical layer l to the LP, and it can be independent for each corticothalamic projection. The coupling matrices $C_{ij}^{lp_A \leftarrow ctx_E, l}$, for $A = E, I$, were random, i.e. C=1 with probability $c_{lp \leftarrow ctx} K / N_{lp \leftarrow ctx}$ and $C_{ij}^{lp_A \leftarrow ctx_E, l} = 0$ otherwise. On average, thalamic neurons received $K_{lp \leftarrow ctx} = c_{lp \leftarrow ctx} K$ presynaptic connections from each cortex. Here, the conductance $\bar{g}_{lp \leftarrow ctx}^{A,l}$describes the strength of the cortical presynaptic input, which is scaled by Kas $\bar{g}_{lp \leftarrow ctx}^{A,l} = G_{lp \leftarrow ctx}^{A} / \sqrt{K}$, where $G_{lp \leftarrow ctx}^{A}$ is independent of K.

Parameters

The parameters for the cell dynamics were $Cm = 1\,\mu F / c\,m^2$, with conductances of leak currents of $g_{L,E} = 0.1 m\,S / c\,m^2$and $g_{L,I} = 0.05\,mS / c\,m^2$for excitatory and inhibitory neurons, respectively. The other parameters that characterized the dynamic of neurons are: $V_L = -70.6mV, V_T = -50.4mV$ and $\Delta_T = 2mV$. The parameters for the adaptation current were $a = 24nS$, $b = 0.01nA$, and $\tau_{adapt} = 60ms$. For each area, the synapses' parameters were: $G_{E0} = 1.425ms \cdot n\,S / c\,m^2$, $G_{I0} = 1.89ms \cdot n\,S / c\,m^2$, $G_{EI} = 9.0ms \cdot n\,S / c\,m^2$, $G_{II} = 13.5ms \cdot n\,S / c\,m^2$, $G_{EE} = 22.5ms \cdot p\,S / c\,m^2$, $G_{IE} = 67.5ms \cdot p\,S / c\,m^2$, with $\tau_{syn} = 3ms$ and $V_E = 0mV$ and $V_I = -80mV$. Recurrent connectivity for each cortical layer and the LP is $K = 400$, the probability of connection was $c_A = K_A / N_A$, for $A = ff, E, I$.

Variation of pathway connections

We used the factors *WFF, WCP*, and *WPC* to change the weights of feedforward, pulvino-cortical and cortico-pulvinar projections. These factors multiply the ratio $G_{E0}^{\alpha} / G_{I0}^{\alpha}$for those entry inputs. However, for some simulations (Figure 9, Figures S4 and S5), the ratio $G_{E0}^{lp} / G_{I0}^{lp}$ of *WCP* changed across cortical areas to ensure a stable firing rate propagation until the last level of the system. *WPC* was normalized by the number of feedforward areas

($W(PC, l)$, N=4), to avoid an oversaturation of thalamic activity due to an overload of cortical inputs.

RESULTS

In the present study, from the total number of neurons recorded, 97 (area 17) and 83 (area 21a) units were analysed. The remaining neurons were discarded due to several factors such as: high response variability, loss of signal during recording sessions, units' failure to recover after the thalamic injections of GABA, or unsuccessful thalamic inactivation (Figure S5). Descriptive statistics (mean, median and SEM values) of all CRF parameters and respective significance levels (p-values) from statistical comparisons are summarized in tables provided as supplementary material.

Effects of LPl inactivation on the CRF of area 17 neurons

The lateral part of the LP nucleus (LPl) is the only subdivision of the cat pulvinar that is directly connected to the primary visual cortex in a reciprocal manner (Berson and Graybiel 1983; Casanova 1993). Silencing the LPl yielded changes in the CRF profile of 59 out of 97 area 17 neurons (CI overlap mean of 20,96% ± 2,29). Most changes in the CRF profile were observed at a contrast levels greater than 25%. Figure 2 shows three representative examples of the impact of LPl inactivation on the contrast response of neurons in area 17. In panel A, the LPl inactivation yielded an increase in firing rate (facilitation) of the cortical neuron. This enhancement of activity was observed in 19 units (~32%). Panel B depicts the most frequently observed effect, i.e. a decrease (suppression) in the firing rate (37 cells; ~63%). Three neurons exhibited a rightward shift of the contrast function (Panel C) and four out of the 19 units showing an increase in firing rate also displayed such rightward shift. In most cases, these changes of activity were not accompanied by significant modification in the cells' preferred orientation and direction and in corresponding tuning functions. Thus, two main groups of cells were identified based on the effect of LPl inactivation: those with facilitated and suppressed responses.

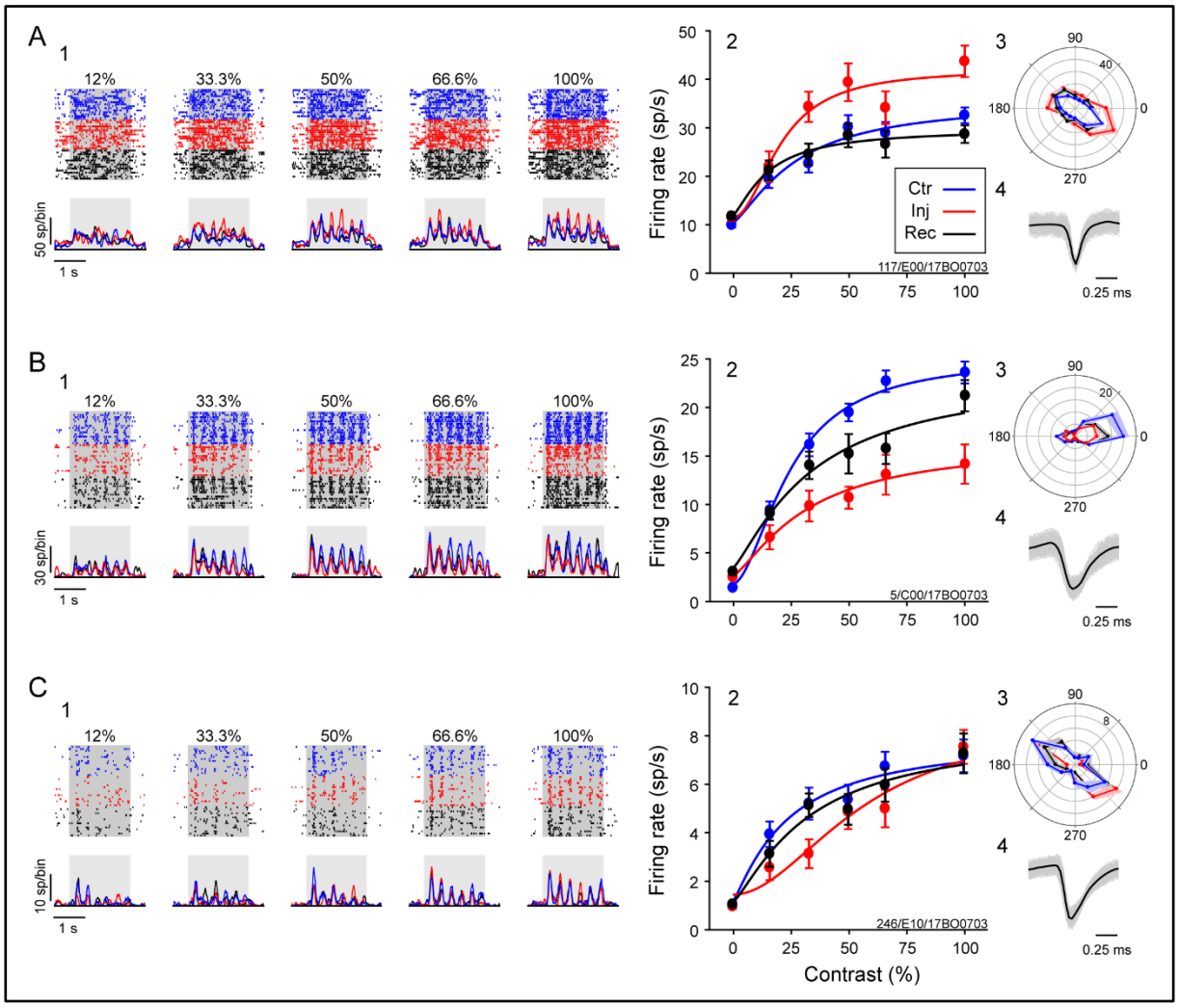

Figure 2. Effects of the reversible inactivation of LPl on the contrast response function (CRF) of three neurons from area 17. Neuronal responses during control (blue), thalamic inactivation (red) and recovery (black) are shown. In panels 1-4, Raster plots and PSTHs (1), CRFs (2), direction tunings (3) and spike waveforms (4) are presented for each neuron. A) The LPl inactivation yielded an increase on the neuron's firing rate at contrast levels higher than 25 % (A2). B) The neuron exhibited a reduction of the firing rate at higher contrast levels (> 25%) during LPl inactivation (B2). C) Here, the LPl inactivation yielded a rightward shift of the neuron's CRF (C2). Note that no changes on the direction selectivity was observed in none of the units shown (Panels 3's). In PSTHs, gray areas represent the duration of the presentation of the visual stimulus (drifting gratings). In CRF plots (panels 2's), dots and error bars represent the average and SEM of neurons' firing rates at different contrasts and lines represent the curve fitting by the Naka-Rushton function. In panels 3's, SEM are represented as shaded areas. In panels 4's, average spike waveforms are depicted as black lines. Ctr = control; Inj = thalamic inactivation; Rec = recovery.

The effects of the LPl inactivation were further characterized by analyzing the parameters of the Naka-Rushton function (equation 1). Changes on each variable of the equation represented a specific type of gain control of the contrast response curve. Here we identified four contrast-tuning parameters (Figure 1). The first, contrast gain, is characterized by changes in C50 and represented by a horizontal shift of the curve. The second, response gain, is distinguished by changes of the Rmax and consequently of the contrast curve dynamic range. The third, baseline control, is described by a change in Blsn and represented by a vertical shift of the contrast response curve. Finally, slope control is characterized by changes in the exponential factor (n). In order to characterize the type of modulation exerted by the pulvinar, each parameter was compared between control and GABA injection conditions for the 59 area 17 cells that showed a significant change of activity. Overall, the impact of the LPl inactivation consisted on a change in response gain (Rmax) and baseline control of neurons in the primary visual cortex. Figure 3 illustrates that the neurons in the "facilitated" group exhibited increased response gain and baseline (Panels A and B) while for the "suppressed" group, the LPl inactivation yielded a significant reduction of these two parameters (panels C and D).

Percentage of variation for the two populations in area 17

The magnitude of the effects of the LPl inactivation was assessed by calculating the percentage of variation (%Var) of the CRF parameters (see Methods for details). Positive and negative %Var values indicate a decrease and increase of a given parameter during inactivation, respectively. Here, we compared the %Var of the CRF parameters between the two previously defined cell groups (facilitated and suppressed) and the total neuronal sample. In accord with the previous analysis, facilitated and suppressed groups exhibited an increase and decrease in the percentage of variation of the response gain and baseline computed from their CRF (Figure 4). In addition, both groups exhibited larger variations on these parameters in comparison with the total sample (i.e. all 59 cells) that exhibited a slight decrease in response gain and baseline. These data corroborate our previous analysis supporting the notion that two neuronal populations in area 17 were distinctly affected by the LPl inactivation.

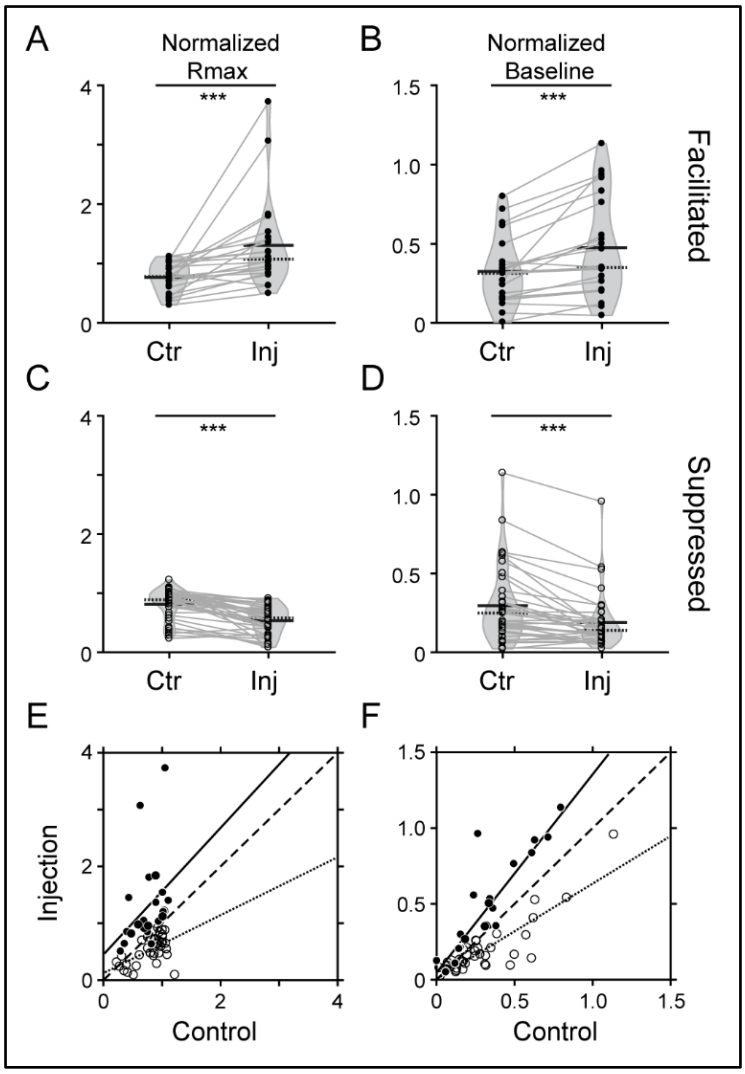

Figure 3. Impact of LPl inactivation on the CRF parameters Rmax and baseline of neurons from area 17. The normalized Rmax and baseline were compared between control (Ctr) and thalamic inactivation (Inj) conditions for two distinct neuronal populations with facilitated (A-B) and suppressed (C-D) responses at high contrast levels during inactivation. Neurons from the facilitated group exhibited an increase in Rmax (A) and baseline (B) during LPl inactivation whereas those from the suppressed group showed a decrease in both parameters (C-D). E-F) Scatter plots of Rmax and baseline of the two groups. Linear regression lines for facilitated (solid line over filled circles) and suppressed (dotted line over empty circles) groups are depicted. For the facilitated group, the regression lines of Rmax ($p = 0.09$, $r2 = 0.13$) and baseline ($p < 0.001$, $r2 = 0.8$) lie above the unity line (dashed line), while the inverse is observed for the suppressed group (Rmax: $p < 0.001$, $r2 = 0.3$; baseline: $p < 0.001$, $r2 = 0.7$). *** $p<0.001$. In A-D, solid and dotted lines indicate mean and median values.

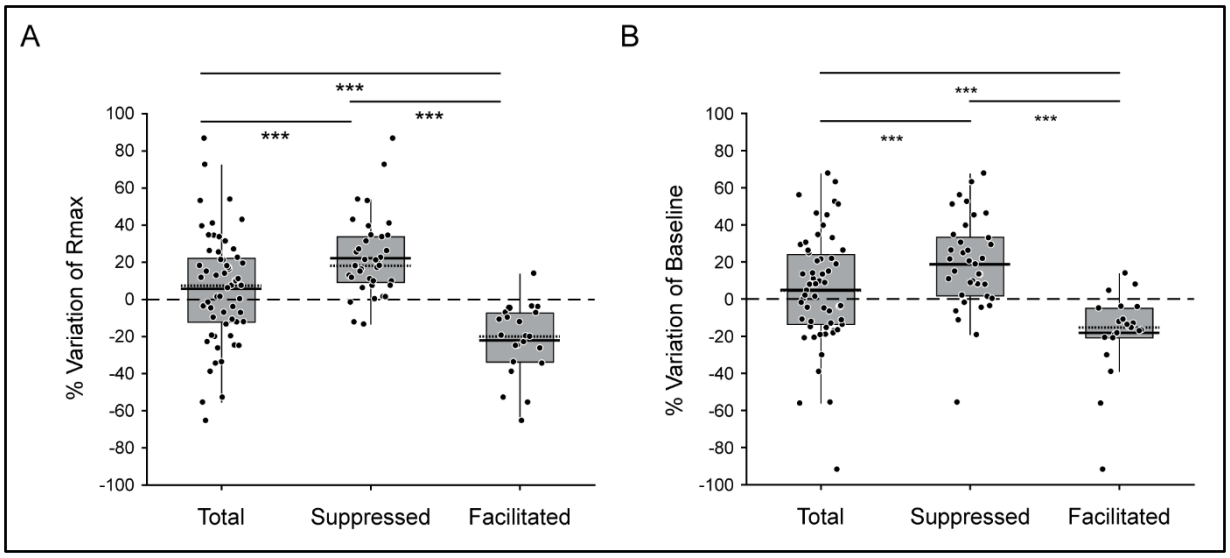

Figure 4. Comparison the percentage of variation (%Var) of the CRF parameters Rmax and baseline of neurons from area 17. Here, the total population is compared with the facilitated and suppressed groups. A) %Var of Rmax. In average, facilitated neurons exhibited negative %Var values indicating an increase in the CRF response gain during LPl inactivation. In contrary, suppressed neurons showed positive %Var values representing a decrease of the CRF response gain. The pooled dataset (Total) exhibited a slight decrease of the CRF response gain as a smaller average positive Rmax %Var value. B) %Var of baseline. As for the Rmax, facilitated neurons exhibited negative %Var values while the suppressed group showed positive values indicating a decrease and increase of baseline levels, respectively. The total population exhibited small positive %Var baseline values indicating a slight decrease on this parameter. In boxplots, solid and dotted lines indicate mean and median values, respectively. *** $p<0.001$.

Effects of LPl inactivation as a function of cortical depth and cell type in area 17

The %Var of the effects of LPl inactivation on the CRF of area 17 neurons was analyzed as a function of their laminar position, their response modulation to gratings (simple and complex cells) and their spike waveform (putative excitatory or inhibitory neurons; Figure 5; Table S3).

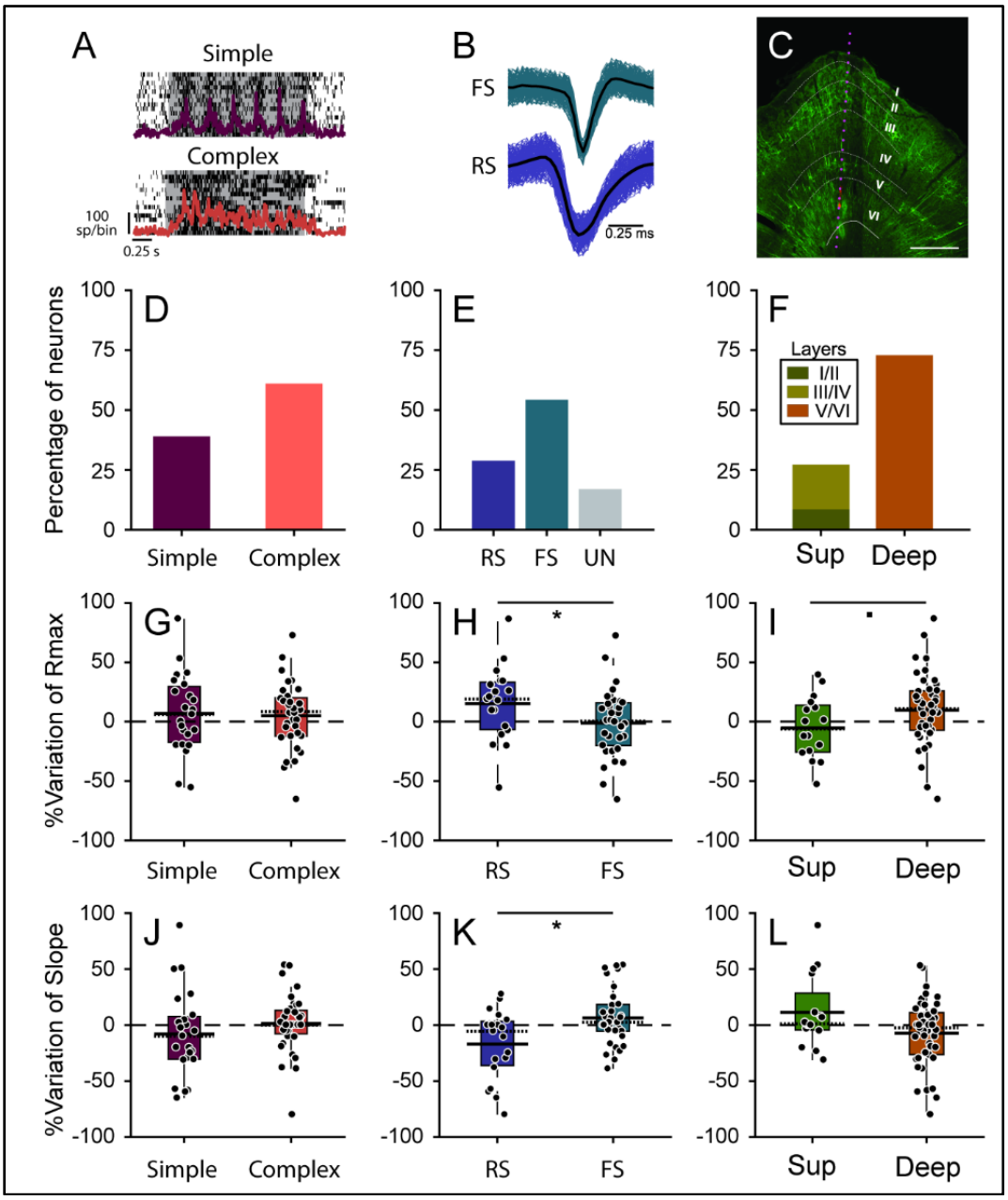

Figure 5. Comparison the percentage of variation (%Var) of Rmax and slope of neurons from area 17 in function of their physiological properties and cortical laminar position. Data were compared between simple and complex cells (A, D, G, J), putative excitatory (regular spiking) and inhibitory (fast spiking) cells (B, E, H, K) and cortical laminar position (C, F, I, L). A) PSTH and raster plots of a simple and a complex cell. B) Spike waveforms of a regular spiking (RS) and a fast spiking (FS) neurons. C) Reconstruction of recording contacts (magenta dots) across the cortical depth of area 17. D-F) Proportion of neurons in the different categories compared. G-I) %Var plots for Rmax. In H, RS neurons were more impacted by LPl inactivation exhibiting an decrease in the response gain (i.e., positive %Var values). In

I, there was a tendency that neurons from deep layers exhibiting an average decrease in the response gain as well. J-K) %Var plots for slope. UN = unclassified, Sup = superficial layers. ■ $p<0.1$, * $p<0.05$. IN boxplots, solid and dotted lines indicate mean and median values, respectively. In A, shadowed regions indicate the duration of the stimulus presentation (drifting gratings).

Simple vs complex cells

Out of the 59 units analyzed, 39% and 61% were classified as simple and complex cells respectively (Figure 5D). The proportion observed in our study resemble that previously reported in the cat primary visual cortex (Skottun et al. 1991). No differences were observed between simple and complex cells regarding the CRF parameters.

Putative excitatory vs inhibitory cells

From the total number of neurons recorded, 823 units were submitted to the analysis of the spike waveform (Figure S2). From those, a total of 780 units were classified as putative excitatory (72%) and inhibitory (28%) neurons. The proportion of excitatory/inhibitory neurons found in our study agrees with previous observations in cat visual cortex (Gabbott and Somogyi 1986). From the 59 area 17 neurons included in the analysis, 32% and 58% were classified as putative excitatory and inhibitory, while 10% were unclassified (Figure 5E). The comparison of the CRF parameters between the two neuronal categories revealed that putative excitatory neurons exhibited greater changes in the response gain and slope control in comparison with inhibitory neurons during LPl inactivation (Figure 5H,K). For instance, putative excitatory neurons showed an average decrease of 15,52% while inhibitory neurons showed a slight increase of 0,8% in response gain during inactivation. Similarly, excitatory neurons showed a large increase (17,1%) in the slope while inhibitory neurons exhibited a smaller decrease (6,4%).

Superficial vs deep layers

The analysis of laminar position showed that 8.6%, 18.6%, and 72.8% were neurons from layers I/II, III/IV, and V/VI, respectively (Figure 5F). Thus, most neurons were recorded from deep cortical layers (V/VI). This sampling bias was most likely due to the angle of insertion of the probe in the cortex where a larger number of contacts was located in layers V/VI. Therefore, for statistical comparison, neurons were grouped into superficial (I-IV) and deep layers (V/VI). Figure 5I shows that the LPl inactivation tended to preferentially enhance the

response gain in the superficial layers while reducing it in the deep layers (P = 0,07, Wilcoxon rank sum test).

Finally, we investigated the potential association between the two groups found in area 17 (facilitated and suppressed) and the anatomo-physiological parameters. No significant relationship (Fisher's exact test) was found in any of the parameters indicating that the distinct effects in area 17 induced by the LPl inactivation were independent of the cell type (simple vs complex; excitatory vs inhibitory) and its gross laminar position (superficial vs deep layers).

Effect of LP inactivation on the CRF of neurons from area 21a

In contrast to area 17, area 21a receives direct projections from neurons in the medial and lateral parts of the LP nucleus. Consequently, both subregions were targeted in distinct experiments. Out of the 83 neurons tested in area 21a, 45 and 38 were recorded during the LPl and LPm inactivation experiments, respectively. The evaluation of the CIs overlaps revealed that the inactivation yielded changes in the CRF profile of a large number of cells: 35 out of 45 in LPl experiments and 34 out of 38 in LPm.

Figure 6 shows four representative examples of the impact of LPl (A-B) and LPm (C-D) on the contrast response of area 21a neurons. For both LPl and LPm experiments, most changes occurred at contrast levels above ~26%. In LPl experiments, the inactivation yielded a facilitation of the visual responses in most neurons (~86; Figure 6A-B). For the remaining neurons (5 out of 35), the inactivation yielded a suppression of responses from which two units also exhibited a rightward shift of the CRF. The LPm inactivation also yielded a facilitation of visual responses at higher contrast levels for most units (31 units, ~ 91%; Figure 6C-D). However, 11 of these cells also showed a rightward shift of the CRF, and only three units (~9%) exhibited suppression in their visual responses during thalamic inactivation. Thus, the inactivation of both LP subdivisions yielded more homogenous effects on the CRF of 21a neurons that those observed in area 17 after LPl inactivation and these effects were mainly characterized by a response facilitation.

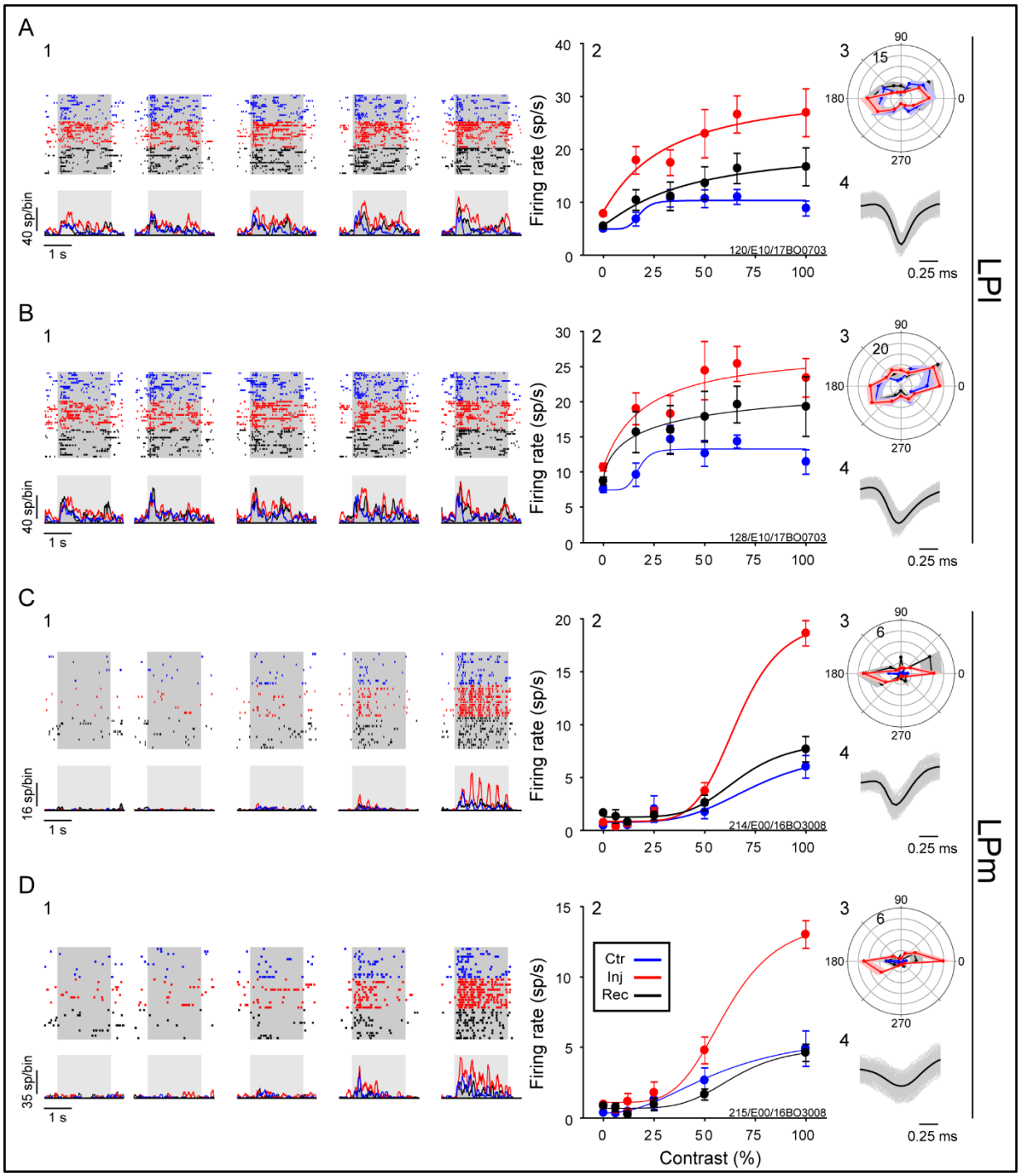

Figure 6. Effects of the reversible inactivation of LP on the contrast response function (CRF) of four neurons from area 21a. A-B) Examples of the effects of the inactivation of the lateral LP subdivision (LPl). C-D) Examples of the impact of the medial LP (LPm) inactivation. Note that the main impact in both subdivisions was an increase in the firing rate at high contrast levels (Panels 2's) with a

larger impact during LPm inactivation (C2 and D2). No changes on the direction selectivity were observed (Panels 3's). The same layout from figure 2 is applied here.

Next, the effects of the inactivation of both subdivisions were further characterized by analyzing the CRF parameters (Table S4). Figure 7 shows the main effects of LPl and LPm inactivation on the contrast response of 21a neurons. The LPl inactivation yielded an increase in response gain and baseline (panels A-B). As in LPl experiments, the main effects of LPm inactivation consisted on increases in response gain and baseline (panels C-D). In addition, the LPm inactivation yielded an increase in the contrast gain (C50) and a reduction in the curve slope.

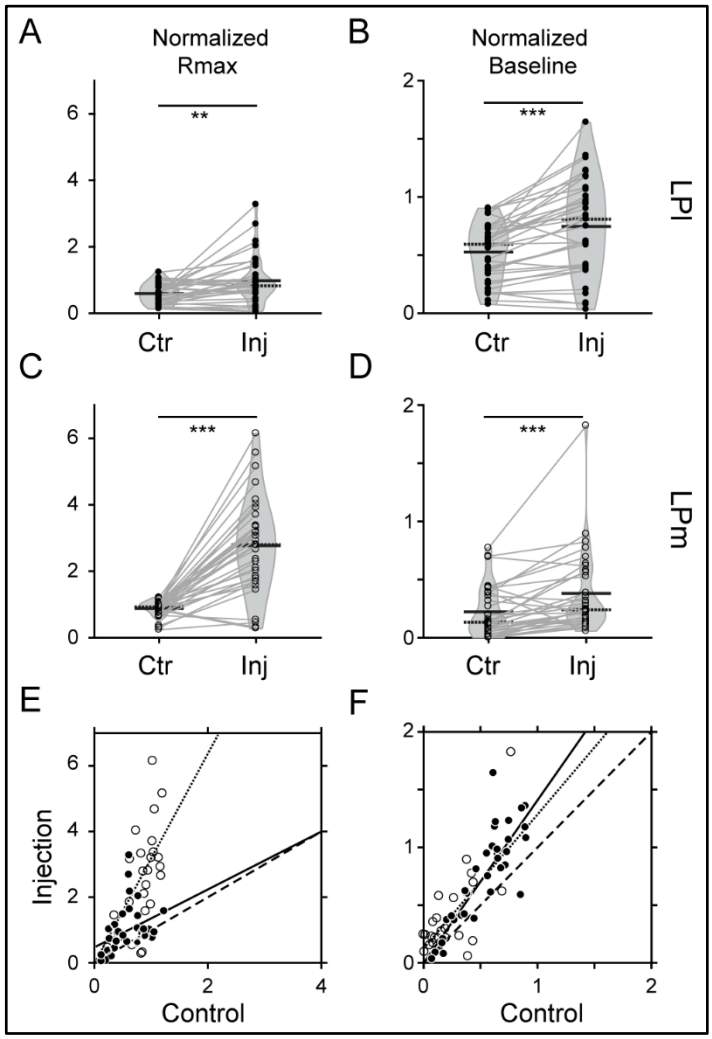

Figure 7. Impact of LP inactivation on the CRF parameters Rmax and baseline of neurons from area 21a. The normalized Rmax and baseline were compared between control (Ctr) and thalamic inactivation (Inj) conditions during inactivation of the LPl (A-B) and LPm (C-D)**.** The LPl inactivation yielded an increase in Rmax (A) and baseline (B). In comparison, the inactivation of the medial LP subdivision (LPm) yielded a greater increase in Rmax (C) and a similar increase in baseline (D). E-F) Scatter plots of Rmax and baseline of LPl (filled circles) and LPm (empty circles) inactivation. Note that most of data points and of both groups were located above the unity line (dashed line) showing an increase in Rmax (linear regression LPl: $p < 0.05$, $r2 = 0.13$; LPm: $p < 0.01$, $r2 = 0.29$) and baseline (linear regression LPl:

$p < 0.001$, $r2 = 0.72$; LPm: $p < 0.001$, $r2 = 0.52$). The same layout from figure 3 is applied here. ** $p<0.01$, *** $p<0.001$.

Effects of LP inactivation as a function of cortical depth and cell type of area 21a neurons

Out of the 69 neurons analyzed, most were complex-like (N = 66) with only three were classified as simple-like cells. This proportion is in accordance with previous reports showing that most area 21a neurons have complex-like receptive fields (Wimborne and Henry 1992; Dreher et al. 1993; Tardif et al. 1996). Regarding the other properties, the percentage of variation (%Var) of the CRF parameters of 21a neurons were compared in function of the cell type (putative excitatory vs inhibitory cells; Table S5) and laminar position (superficial vs deep layers; Tables S6).

Putative excitatory vs inhibitory cells

The spike waveform analysis revealed that 37 and 23 neurons were classified as putative excitatory (RS) and inhibitory (FS) cells, respectively. In LPl experiments, the proportion of putative excitatory and inhibitory cells was ~ 43% (15 units) and ~ 57% (20 units), while in LPm, they composed ~ 86% (22 units) and ~ 12% (3 units) of the sample, respectively. Due to the low number of FS neurons recorded during LPm inactivation (N= 3), no statistical analysis was performed. Regarding the LPl experiments, the CRF slope of excitatory and inhibitory neurons were distinctively affected during inactivation (P = 0,02, Wilcoxon rank sum test) where excitatory neurons showed a larger decrease (31,26% vs 0,37%).

Superficial vs deep layers

In LPl experiments, ~17% and ~83% were from layers III/IV and V/VI, respectively. In LPm experiments, ~ 10%, ~ 31%, and ~ 59% were neurons from layers I/II, III/IV, and V/VI, respectively. The same sampling bias observed in area 17 was thus also present here, where neurons from deep layers were more represented in the sample. Thus, for statistical comparison, we grouped the neurons in superficial (layers I-IV) and deep (layer V/VI) layers.

Neurons from superficial and deep layers were distinctively impacted by LPl inactivation. Differences were observed in the response gain and slope control. For instance, the LPl

inactivation yielded an average increase of the response gain in both superficial (%Var Rmax mean of -46,55% ± 9,28) and deep layers (%Var Rmax mean of -9,71% ± 5,05), but with more pronounced effect in the former (by a factor of 4.8 times; $P < 0,01$, Wilcoxon rank sum test). In addition, neurons from superficial layers exhibited a more pronounced decreased in the CRF slope (%Var n mean of 50,22% ± 12,74) in comparison with neurons from deep layers (%Var n mean of 6,03% ± 8,01; $P < 0,05$, Wilcoxon rank sum test). In contrast to the above observations, there was no relationship between the changes in response and the laminar position of the cells when the LPm was inactivated.

Comparison of LP effects across cortical areas

The amplitude of the effects of thalamic inactivation between areas 17 and 21a was assessed by comparing the %Var of the CRF parameters. Since our goal was to evaluate the global impact of thalamic inactivation on both cortical areas (LPl for areas 17 and 21a; LPm for area 21a only), in this analysis, the total sample from area 17 was considered. In area 17, the net impact of LPl inactivation was characterized by a small decrease in the response gain and baseline. Conversely, in area 21a, the LPl yielded a larger increase of response gain and baseline (Figure 8). However, the LPm inactivation yielded even larger changes on response gain and baseline. For instance, the average %Var of response gain during LPm inactivation was ~ 2.7 and ~ 7.7 times larger than those induced by LPl inactivation on area 21a and 17, respectively. Additionally, the increase of the baseline was ~ 2.97 and ~ 7.27 times larger than that observed in area 21a and 17 during LPl inactivation, respectively.

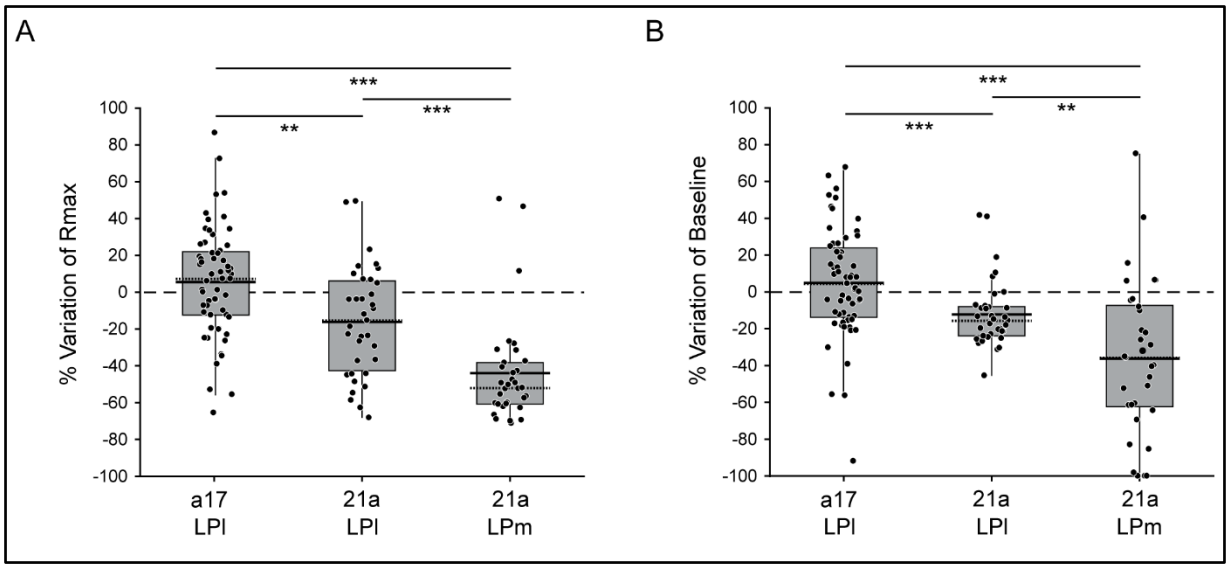

Figure 8. Comparison the percentage of variation (%Var) of Rmax and baseline between area 17 and 21a during LP inactivation. The net effects of LPl and LPm inactivation on areas 17 and 21a were compared. A) Rmax %Var. In area 17, LPl inactivation yielded a small positive Rmax variation while in area 21a, both LPl and LPm inactivation yielded stronger negative variations of this parameter. Thus, the effect of LPl inactivation was a slight decrease in the CRF response gain in area 17 whereas in area 21a, an increase was observed. B) Baseline %Var. Similarly, LPl yielded a slight positive change in the baseline %Var in area 17, while in area 21a, LPl and LPm inactivation yielded a larger negative change in this parameter. Note that the largest changes on both Rmax (A) and baseline (B) were observed in area 21a during LPm inactivation. Solid and dotted lines indicate mean and median values, respectively. ** $p<0.01$, *** $p<0.001$.

Modelling the transthalamic pathway

Our experimental data showed that the main impact of the LP inactivation in the CRF of areas 17 and 21a was characterized by small decreases and large increases in the response gain, respectively. Here, we created a theoretical model in order to mimic those effects. The theoretical cortical visual system was simulated by a network of four layers connected in a feedforward way with excitatory inputs (Feedforward network, FFN). The LP was represented by an external and parallel population of neurons interacting with the FFN through reciprocal excitatory connections (Figure 9A). The first area of the network received an external input mimicking the LGN projections. The LGN firing rate consisted on uncorrelated Poisson excitatory spikes which varied logarithmically with contrast. This signal mimicked the visual

contrast used in our experiments. This arrangement of connections between areas allowed a stable propagation of the signals across the FFN. For instance, in each level of the FFN, the activity increased in function of the contrast mimicking the CRF (Figure 9B). This was previously observed in other theoretical studies proposing that the pulvinar allows a stable propagation of visual signals across the cortex preserving the contrast sensitivity at higher levels of the hierarchy (Cortes and Van Vreeswijk 2012; Cortes and van Vreeswijk 2015).

After creating the corticothalamic system, the GABA injection in LP was simulated as a global reduction of its connectivity strength (50% of the initial strength). The robust recurrent connectivity between excitatory and inhibitory neurons produced a net increase of the LP output firing rate at higher contrast levels. Then, the effects of the GABA injection with LP-cortical projections targeting either excitatory or inhibitory cortical populations was assessed (Figure S3). First, excitatory neurons of the FFN received LP projections with equal strength of connectivity. During the control period, the neuronal activity was transmitted nonlinearly throughout the visual cortex, creating a stair-shaped CRF in the last area (Figure S3A). This unrealistic response was avoided by gradually increasing the strength of LP connections from the first to the last cortical area. Here, the dynamic range of cortical areas showed a greater increase during LP inactivation than during control periods (Figure S3B). In contrast, when only inhibitory neurons were targeted, the CRF dynamic range decreased during LP inactivation (Figure S3C-D). Interestingly, as revealed in our experimental findings, the neurons' CRFs were modulated mostly at high contrast levels. Indeed, the CRF in all cortical areas were scaled up or down when excitatory or inhibitory neurons were targeted mimicking the response gain control observed in the present study. The model produced these results when the cortico-LP connectivity strengths were weak while the LP-cortical ones were strong. In this setting, the LP controlled the cortical response gain, as previously described (Cortes and Van Vreeswijk 2012; Cortes and van Vreeswijk 2015). Next, another scenario was created in which the LP-cortical inputs targeted both excitatory and inhibitory cortical populations (Figure 9). Here, the weights of LP-cortical connections targeting inhibitory populations were equal for each cortical area while the weight of connections targeting excitatory populations was progressively increased across the FFN (Figure 9A). This solution was found when LP-cortical weights were stronger than the cortico-LP ones. This possible solution is supported by our experimental findings where

both putative excitatory and inhibitory neurons were impacted by LP inactivation, but with greater effects observed in excitatory neurons.

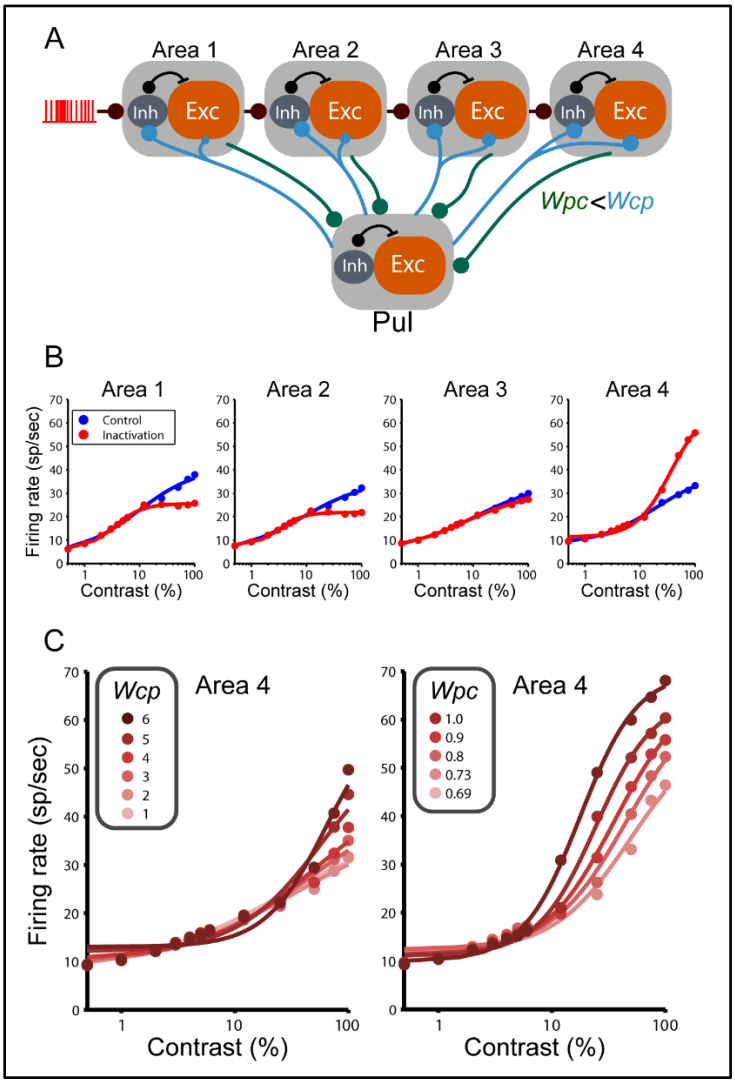

Figure 9. Modelling the transthalamic pathway. A) Model of a layered feedforward network (FFN) of four areas connected reciprocally to an external structure (pulvinar). Each area of the model, including pulvinar, consists of excitatory and inhibitory neurons connected strongly to reach the balanced state. The input to area 1 is K=400 excitatory uncorrelated Poisson spikes. The excitatory population of one area connects homogeneously in a random manner the neurons of the next area. The feedforward connections has on average K numbers of synapses, wit equal strength of connectivity (W_{FF}) across the four areas. Pulvinar receives and sends excitatory projections from and to the FFN, with weights W_{PC} and W_{CP}, respectively. Note, however, that the excitatory connectivity from the pulvinar to the excitatory neurons in area 1 is weaker than the connectivity to the excitatory population in the last area. B) Firing

rate as a function of contrast for the four cortical areas. Dots represent simulation results for control (blue) and inactivation (red) conditions. Solid lines are fits of contrast response functions (CRF). Note that the first area decreases and the last increases its firing rate during inactivation. Inactivation consists of a reduction of pulvinar internal weights by 25%. C) Left graph shows firing rate of last area when pulvino-cortical weights (W_{PC}) increase while magnitudes of cortico-pulvinar connections remain fixed ($W_{CP}= 0.6$). Right graph shows firing rate of last area when pulvino-cortical weights (W_{PC}) increases and $W_{PC}= 4$. The two set of simulations have equal cortico-cortical strength of connectivity ($W_{FF}= 10$).

In the above-mentioned solutions, the simulation of the GABA injections yielded a net increase of the LP output. In order to mimic a decrease of the LP output firing rate, only the weights of inhibitory connections were reduced (50% decrease of initial strength). In this setting, the weights of LP-cortical inputs targeting excitatory populations were the same across the cortical areas while the weights to inhibitory populations gradually increased from the first to the last area. In addition, the LP-cortical weights were weaker than the cortico-LP ones. In this setting, a qualitatively similar solution was obtained where the LP inactivation yielded a decrease and an increase of the response gain in the first and last cortical areas (Figure S4). However, in this case, our model could not mimic the greater increase of the response gain at the last cortical area.

In our simulation, the LP inactivation resulted in a decrease and increase of the firing rate at high contrast levels in the first and last areas of the FFN, respectively. The progressive increase of the weights of LP-cortical connections on the FFN induced a considerable increase of the firing rate in the last area of the chain, mimicking the increased response gain shown by neurons in area 21a (Figure 9B). Thus, our model supports the notion that the LP controls the contrast response in areas 17 and 21a by modulating the excitatory and inhibitory inputs in a balanced way (Abbott and Chance 2005), characterized by changes in the response gain rather than a contrast gain. None of the solutions proposed in our theoretical model showed changes in the contrast gain, as observed in neurons from area 21a during LPm inactivation.

DISCUSSION

In this study, we investigated the impact of the reversible pharmacological inactivation of the LP nucleus on the contrast response of neurons in a low (area 17) and a higher-level area of the cortical hierarchy (area 21a). Our findings demonstrated that LP inactivation yielded distinct changes on the CRF of cortical neurons. In area 17, the main impact of LPl inactivation on the neurons' CRFs was characterized by a small decrease in the response gain. Conversely, in area 21a, the LPl inactivation yielded a more pronounced increase in the neurons` response gain. During LPm inactivation, changes were observed in all CRF parameters of 21a neurons with a strikingly large increase in the response gain and an increase in contrast gain, baseline and a reduction in the slope.

The area 21a is placed at a higher level in the cortical hierarchy in relation to area 17 and is considered as a gateway area of the cat ventral stream (Payne 1993; Scannell et al. 1995). Several distinctions are also observed at a functional level where the response profile of 21a neurons is more similar to LP neurons (e.g. binocularity, complex-like RFs) than to those from area 17 (Tardif et al. 1996; Vickery and Morley 1999). Thus, in order to obtain comparable measures of the effects of the thalamic inactivation, it was imperative to use a visual stimulus that reliably elicits neuronal response in both cortical areas. In the present study, drifting gratings with varying contrasts were found to be a suitable stimulus as neurons from both cortical areas were sensitive to contrast changes. Indeed, contrast sensitivity is observed in several areas across the visual system (Enroth-Cugell and Robson 1966; Tardif et al. 1996; Avidan et al. 2002; Burkhardt 2011) and, with some exceptions (Sani et al. 2013), the contrast response is stereotypically described as a sigmoidal curve better characterized by a hyperbolic function (Naka and Rushton 1966). Here, the responses of neurons from both cortical areas were well fitted by the Naka-Rushton function which allowed us to characterize, quantify and compare the distinct types of gain control of the CRF during thalamic inactivation.

The CRF as a measure of the nature of thalamocortical projections

Projections to and from distinct thalamic nuclei involved in visual, auditory and somatosensory processing were previously characterized based on their anatomical and physiological properties (Sherman and Guillery 1996; Reichova and Sherman 2004; Lee and

Sherman 2008; Ji et al. 2016). Two main categories were identified: drivers and modulators. Driver inputs carry the main message while modulators modify that message (Sherman and Guillery 1998). Alternatively, drivers and modulators can be distinguished based on how the excitatory and inhibitory inputs are integrated affecting a neuron's firing rate (Chance et al. 2002; Abbott and Chance 2005). In this classification framework, a driver control is characterized by a push-pull mechanism between excitatory and inhibitory inputs (Anderson et al. 2000) while a modulatory effect occurs by the combination of both input types in a balanced mode (Vreeswijk and Sompolinsky 1996; Chance et al. 2002). Indeed, theoretical and experimental data have shown that push-pull excitation and inhibition yield additive/subtractive effects in a neuron's firing rate (Gabbiani et al. 1994; Anderson et al. 2000). On the other hand, multiplicative/divisive changes of a neuron's firing rate occur when the level of balanced inputs (i.e., combined excitatory and inhibitory signals) is modified (Chance et al. 2002; Abbott and Chance 2005). Here, we applied this principle to the interpretation of the effects of LP inactivation on the contrast response curve. For instance, additive/subtractive changes of the CRF are translated by changes in the contrast gain and baseline control while multiplicative/divisive effects are observed as changes in the response gain and slope control (Figure 1). Thus, based on this interpretation, we observed that the LP inactivation yielded mainly modulatory effects on the CRF of areas 17 and 21a.

The nature of LP inputs in the primary visual cortex

Our findings showed that the influence of LPl on neuronal responses in area 17 was mostly modulatory, as revealed by an increase (facilitated group) and a decrease (suppressed group) in the response gain during inactivation. In a study aimed at determining the impact of pulvinar on oscillatory activity in the cat (Molotchnikoff and Shumikhina 1996) reported increased and decreased responses to high contrast (50 and 80%) drifting gratings during LPl inactivation. These changes can be explained by the modulation of the CRF response gain observed in the present study. In primates, the visually evoked and spontaneous activity of neurons from V1 supragranular layers was strikingly reduced during pulvinar inactivation (Purushothaman et al. 2012). These results suggest that the pulvinar would be essential for the activity of neurons in this region which can be interpreted as a driver input. Our findings are at odds with this assumption since the impact LPl inactivation was almost exclusively modulatory

as shown by the effects on the response gain. Previous theoretical studies have investigated the potential role of the pulvinar in visual cortical circuitry (Crick and Koch 1998; Cortes and Van Vreeswijk 2012; Cortes and van Vreeswijk 2015). For instance, Crick and Koch (Crick and Koch 1998) proposed the so-called "no-strong-loop" hypothesis which predicts that two reciprocally connected areas cannot drive each other, which otherwise would inevitably cause the system to oscillate uncontrollably. Based on this hypothesis, since LPl receives its main driving inputs from area 17 (Abramson and Chalupa 1985; Chalupa and Abramson 1989; Casanova et al. 1997), it would be unlikely that the thalamocortical projections would be a driver in nature. Indeed, our findings further supports this hypothesis where the nature of the LPl inputs to area 17 is modulatory.

The nature of LP inputs in area 21a

Our findings demonstrated that the LP nucleus exerts a stronger modulatory influence on area 21a than on area 17. Previous studies indicated a modulatory role of pulvinar on higher order cortical areas. For instance, in primate area V2, Soares et al. (Soares et al. 2004) showed that the pulvinar inactivation yielded an increase in the neurons' spontaneous activity and visual responses. Here, we provided evidence that these effects may originate from changes in baseline and response gain of cortical neurons. In cats, a previous study from our group (Minville and Casanova 1998) showed that the LPl inactivation had a small impact on the basic properties of neurons from the PMLS area (e.g., spatial frequency and direction tunings), an extrastriate area from the cat dorsal stream (Dreher et al. 1996). Thus, one may conclude that the LP does not participate on the creation of basic properties in this higher order visual area, therefore in agreement with a modulatory rather than a driver input. Similarly, our results showed that LPl exerts a modulatory influence on the contrast processing in area 21a. The modulatory nature of the LP input to area 21a was not expected since most projections end in layer IV and thus, be considered as drivers, i.e. contributing to basic receptive field structure of neurons (Felleman and Van Essen 1991; Jones 2001; Sherman and Guillery 2013). This suggests that the general scheme of organization described along the geniculo-cortical pathway may not be applied to extrageniculate pathways. Indeed, it is well known that LGN neurons reaching layer IV provide a driver input to the primary visual cortex (Kandel and Schwartz 2013; Sherman and Guillery 2013).

However, nothing is black and white here. Although the main influence of LPm on area 21a was modulatory (as for LPl), characterized by an increase in the response gain, a driver component was equally present since an increase in the contrast gain was also observed (Figure 10). The weight of the LP driver signals with respect to that of the LP modulatory signals remains to be determined. Similarly, we do not know how it compares to cortical signals. It is unlikely that this driver component exerts a stronger impact in area 21a than the cortico-cortical feedforward pathway given the fact that the latter is essential for the maintenance of the contrast sensitivity in the cortical network (Litvak et al. 2003; Kumar et al. 2010; Cortes and van Vreeswijk 2015).

While both lateral and medial subdivisions of the LP are connected to area 21a, they receive their main excitatory inputs from area 17 and superior colliculus, respectively (Berson and Graybiel 1983; Raczkowski and Rosenquist 1983; Abramson and Chalupa 1985). Therefore, distinct neuronal properties are observed between the LP subdivisions which resemble their respective main inputs (Chalupa et al. 1983; Chalupa and Abramson 1989; Casanova et al. 1991, 1997). Interestingly, the distinct effects of the inactivation of the two LP subdivisions on the CRF of area 21a neurons may reflect their respective functional roles. For instance, the predominantly modulatory inputs from LPl may be related to the modulation of the processing of visual information through the transthalamic pathway. On the other hand, the presence of driving components in the LPm inputs may be related to the processing of visuo-motor signals originated from the superior colliculus.

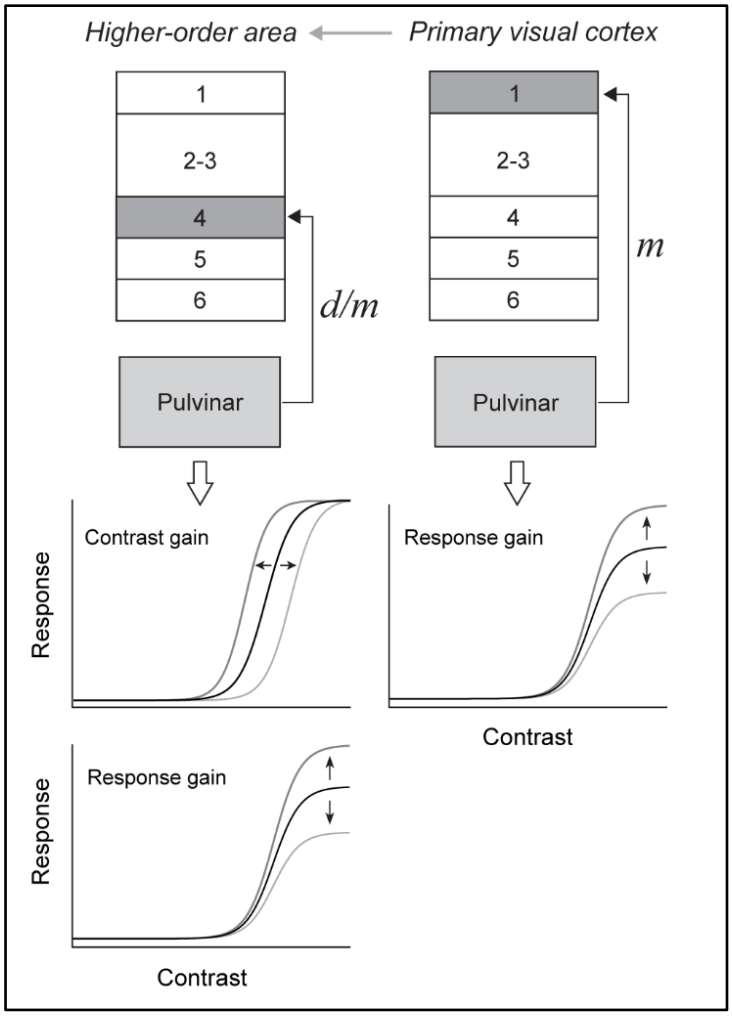

Figure 10. Scheme of the nature of pulvino-cortical connections with the primary visual cortex and an extrastriate area based on our findings. The hypothetical scheme shown in figure 1 is updated here taking into account our findings. The prediction made for the nature of pulvino-cortical inputs in the primary visual cortex (e.g., area 17) was confirmed indicating that it is mostly modulatory. This was exemplified in our study mainly by non-linear changes (i.e., response gain) in the CRF of neurons from area 17 during LPl inactivation. On the other hand, the impact of LP (LPl and LPm) inactivation was mostly characterized by changes on the response gain and contrast gain of the CRF of neurons from area 21a. This indicates that the pulvino-cortical projections exert both a modulatory (LPl) and driver (LPm) actions on the neuronal activity in a higher-order area from the ventral stream (area 21a), challenging our initial predictions (see figure 1).

Functional implications of the role of the pulvinar on cortical processing

Our findings showed that the LP exerts distinct modulatory influences on the contrast processing in areas 17 and 21a. In addition, the stronger impact of LP inactivation in area 21a suggests that the pulvinar may play a more important role on visual processing at higher levels of the cortical hierarchy. What mechanisms could underlie these distinct effects? In our theoretical model, differences in the target population as well as in the strength of thalamocortical connections could represent a possible mechanism for the distinct effects of LP inactivation on the visual cortex. Our simulation strongly suggests that the LP regulates cortical contrast responses by a gain control mechanism based on the variation of the balanced forces between excitatory and inhibitory cortical populations (Abbott and Chance 2005; Cortes and van Vreeswijk 2015). Thus, our experimental and theoretical data support the notion that the pulvinar impact on the visual processing at higher levels of the cortical hierarchy is mostly modulatory.

It is well known that the pulvinar participates in modulatory visual processes such as attention and visual salience (Petersen et al. 1987; Desimone et al. 1990; Robinson and Petersen 1992; Saalmann and Kastner 2009, 2011; Snow et al. 2009; Saalmann et al. 2012). In the primate area V4, an homolog of area 21a in cats (Payne 1993), the neuronal responses are extensively modulated by attention (Saalmann et al. 2012; Zhou et al. 2016). Previous studies reported changes on the CRF of V4 neurons when animals were engaged in attention-demanding tasks (Reynolds and Desimone 1999; Reynolds et al. 2000; Williford and Maunsell 2006; Hudson et al. 2009). Interestingly, one study (Williford and Maunsell 2006) demonstrated that the attentional modulation of the contrast response of neurons from V4 was predominantly characterized by changes on the response gain. Recent evidence indicated that the pulvinar mediates the attentional effects in area V4 (Zhou et al. 2016). Thus, one may hypothesize that the pulvinar plays an essential role on the attentional modulation of the contrast response in area V4. In our study, given that the experiments were carried out in anesthetized cats, we could not test this hypothesis. However, the mechanisms underlying the changes observed here may be those involved in awake animals. On the other hand, Zhou et al. (Zhou et al. 2016) observed that the pulvinar inactivation affected the neuronal responses in area V4 regardless of the attentional effects suggesting that the pulvinar is actively implicated in the basic processing of

visual information in this cortical area. Indeed, this was corroborated by our findings supporting the notion that the pulvinar is actively implicated in the modulation of the visual processing in extrastriate areas of the ventral stream.

The present study demonstrates that the pulvinar plays an important role in high-level processing of visual information by distinctively influencing the cortical neuronal activity. The pulvinar is extensively connected with several cortical areas that perform high level sensory and cognitive processes. Thus, in order to better understand these processes, the classical "corticocentric" view should be revisited by including of the pulvinar as an active part of the network.

ACKNOWLEDGMENTS

This work was supported by a CIHR grant to CC (PJT-148959). BOFS received scholarships from EOUM-FESP. NC was supported by the Chilean fellowship BecasChile and CONICYT. We thank Geneviève Cyr for her technical help and Alessandro Barry for comments on the theoretical model.

AUTHOR CONTRIBUTIONS

CC conceptualized the research project; CC and BOFS designed the experimental protocol; BOFS performed experiments; NC conceived the interpretation of experimental data based on the work of Abbott and Chance (2005); NC created the theoretical model; BOFS and NC implemented the computer codes, algorithms, analysed the data, and drafted the manuscript and figures; CC edited and revised the manuscript; BOFS and NC equally contributed to this manuscript.

DECLARATION OF INTERESTS

The authors declare no conflicts of interest.

REFERENCES

Aasebø, I.E.J., Lepperød, M.E., Stavrinou, M., Nøkkevangen, S., Einevoll, G., Hafting, T., and Fyhn, M. (2017). Temporal Processing in the Visual Cortex of the Awake and Anesthetized Rat. ENeuro *4*.

Abbott, L.F., and Chance, F.S. (2005). Drivers and modulators from push-pull and balanced synaptic input. Progress in Brain Research *149*, 147–155.

Abramson, B.P., and Chalupa, L.M. (1985). The laminar distribution of cortical connections with the tecto- and cortico-recipient zones in the cat's lateral posterior nucleus. Neuroscience *15*, 81–95.

Abramson, B.P., and Chalupa, L.M. (1988). Multiple pathways from the superior colliculus to the extrageniculate visual thalamus of the cat. J. Comp. Neurol. *271*, 397–418.

Adams, M.M., Hof, P.R., Gattass, R., Webster, M.J., and Ungerleider, L.G. (2000). Visual cortical projections and chemoarchitecture of macaque monkey pulvinar. J. Comp. Neurol. *419*, 377–393.

Ajina, S., Kennard, C., Rees, G., and Bridge, H. (2015). Motion area V5/MT+ response to global motion in the absence of V1 resembles early visual cortex. Brain *138*, 164–178.

Albrecht, D., and Hamilton, D. (1982). Striate cortex of monkey and cat - contrast response function. J Neurophysiol *48*, 217–237.

Anstis, S.M., Smith, D.R.R., and Mather, G. (2000). Luminance processing in apparent motion, Vernier offset and stereoscopic depth. Vision Research *40*, 657–675.

Arcaro, M.J., Pinsk, M.A., Chen, J., and Kastner, S. (2018). Organizing principles of pulvino-cortical functional coupling in humans. Nature Communications *9*, 5382.

Arcizet, F., Jouffrais, C., and Girard, P. (2008). Natural textures classification in area V4 of the macaque monkey. Exp Brain Res *189*, 109–120.

Arend, I., Machado, L., Ward, R., McGrath, M., Ro, T., and Rafal, R.D. (2008). The role of the human pulvinar in visual attention and action: evidence from temporal-order judgment, saccade decision, and antisaccade tasks. In Progress in Brain Research, Christopher Kennard and R. John Leigh, ed. (Elsevier), pp. 475–483.

Avidan, G., Harel, M., Hendler, T., Ben-Bashat, D., Zohary, E., and Malach, R. (2002). Contrast Sensitivity in Human Visual Areas and Its Relationship to Object Recognition. Journal of Neurophysiology *87*, 3102–3116.

Bachatene, L., Bharmauria, V., Cattan, S., Chanauria, N., Rouat, J., and Molotchnikoff, S. (2015). Electrophysiological and firing properties of neurons: Categorizing soloists and choristers in primary visual cortex. Neuroscience Letters *604*, 103–108.

Bahmani, H., Murayama, Y., Logothetis, N.K., and Keliris, G.A. (2014). Binocular flash suppression in the primary visual cortex of anesthetized and awake macaques. PLoS ONE *9*, e107628.

Baldwin, M.K.L., Balaram, P., and Kaas, J.H. (2017). The evolution and functions of nuclei of the visual pulvinar in primates. J. Comp. Neurol. *525*, 3207–3226.

Bender, D. (1981). Retinotopic organization of macaque pulvinar. J Neurophysiol *46*, 672–693.

Bender, D. (1982). Receptive-field properties of neurons in the macaque inferior pulvinar. J Neurophysiol *48*, 1–17.

Bender, D., and Butter, C. (1987). Comparison of the effects of superior colliculus and pulvinar lesions on visual-search and tachistoscopic pattern-discrimination in monkeys. Experimental Brain Research *69*, 140–154.

Berman, R.A., and Wurtz, R.H. (2011). Signals Conveyed in the Pulvinar Pathway from Superior Colliculus to Cortical Area MT. J. Neurosci. *31*, 373–384.

Berson, D.M., and Graybiel, A.M. (1978). Parallel thalamic zones in the LP-pulvinar complex of the cat identified by their afferent and efferent connections. Brain Research *147*, 139–148.

Berson, D.M., and Graybiel, A.M. (1980). Some cortical and subcortical fiber projections to the accessory optic nuclei in the cat. Neuroscience *5*, 2203–2217.

Berson, D.M., and Graybiel, A.M. (1983). Organization of the striate-recipient zone of the cat's lateralis posterior-pulvinar complex and its relations with the geniculostriate system. Neuroscience *9*, 337–372.

Bickford, M.E. (2016). Thalamic Circuit Diversity: Modulation of the Driver/Modulator Framework. Frontiers in Neural Circuits 86.

Blanke, O., Landis, T., Safran, A.B., and Seeck, M. (2002). Direction-specific motion blindness induced by focal stimulation of human extrastriate cortex. European Journal of Neuroscience *15*, 2043–2048.

Boire, D., Matteau, I., Casanova, C., and Ptito, M. (2004). Retinal projections to the lateral posterior-pulvinar complex in intact and early visual cortex lesioned cats. Exp Brain Res *159*, 185–196.

Bokor, H., Frère, S.G.A., Eyre, M.D., Slézia, A., Ulbert, I., Lüthi, A., and Acsády, L. (2005). Selective GABAergic Control of Higher-Order Thalamic Relays. Neuron *45*, 929–940.

Borghuis, B.G., Perge, J.A., Vajda, I., van Wezel, R.J.A., van de Grind, W.A., and Lankheet, M.J.M. (2003). The motion reverse correlation (MRC) method:: A linear systems approach in the motion domain. Journal of Neuroscience Methods *123*, 153–166.

Bowen, R.W., Pokorny, J., and Smith, V.C. (1989). Sawtooth contrast sensitivity: Decrements have the edge. Vision Research *29*, IN1-1509.

Boynton, G.M. (2005). Contrast Gain in the Brain. Neuron *47*, 476–477.

Bridge, H., Leopold, D., and Bourne, J. (2015). Adaptive Pulvinar Circuitry Supports Visual Cognition. Trends Cogn Sci *20*, 146–157.

Brosseau-Lachaine, O., Faubert, J., and Casanova, C. (2001). Functional Sub-regions for Optic Flow Processing in the Posteromedial Lateral Suprasylvian Cortex of the Cat. Cereb Cortex *11*, 989–1001.

Burke, Dreher, and Wang (1998). Selective block of conduction in Y optic nerve fibres: significance for the concept of parallel processing. European Journal of Neuroscience *10*, 8–19.

Burkhardt, D.A. (2011). Contrast processing by ON and OFF bipolar cells. Visual Neuroscience *28*, 69–75.

Burkhardt, D.A., Fahey, P.K., and Sikora, M. (1998). Responses of ganglion cells to contrast steps in the light-adapted retina of the tiger salamander. Visual Neuroscience *15*, 219–229.

Byne, W., Fernandes, J., Haroutunian, V., Huacon, D., Kidkardnee, S., Kim, J., Tatusov, A., Thakur, U., and Yiannoulos, G. (2007). Reduction of right medial pulvinar volume and neuron number in schizophrenia. Schizophrenia Research *90*, 71–75.

Campos-Ortega, J., Hayhow, W., and Cluver, P. (1970). A note on the problem of retinal projections to the inferior pulvinar nucleus of primates. Brain Research *22*, 126–130.

Casanova, C. (1993). Response properties of neurons in area-17 projecting to the striate-recipient zone of the cats lateralis posterior-pulvinar complex - comparison with cortico-tectal cells. Experimental Brain Research *96*.

Casanova, C. (2002). In search of the role of extrageniculate cortico-thalamic loops in visual processing using deactivation techniques. In Virtual Lesions: Understanding Behaviour and Perception with Reversible Deactivation Techniques, S.G. Lomber, and R.A.W. Galuske, eds. (New York: Oxford University Press), pp. 61–81.

Casanova, C. (2004). The Visual Functions of the Pulvinar. In The Visual Neurosciences, (MIT Press), pp. 592–608.

Casanova, C., and Savard, T. (1996). Responses to moving texture patterns of cells in the striate-recipient zone of the cat's lateral posterior-pulvinar complex. Neuroscience *70*, 439–447.

Casanova, C., Freeman, R., and Nordmann, J. (1989). Monocular and binocular response properties of cells in the striate-recipient zone of the cats lateral posterior-pulvinar complex. J Neurophysiol *62*, 544–557.

Casanova, C., Savard, T., and Darveau, S. (1997). Contribution of area 17 to cell responses in the striate-recipient zone of the cat's lateral posterior-pulvinar complex. Eur. J. Neurosci. *9*, 1026–1036.

Casanova, C., Piché, M., and Ouellette, B. (2008). Spatiotemporal properties of LP-pulvinar visual receptive fields. J Vis *8*, 809–809.

Chalfin, B.P., Cheung, D.T., Muniz, J.A.P.C., de Lima Silveira, L.C., and Finlay, B.L. (2007). Scaling of neuron number and volume of the pulvinar complex in new world primates: Comparisons with humans, other primates, and mammals. J. Comp. Neurol. *504*, 265–274.

Chalupa, L.M., and Abramson, B.P. (1989). Visual receptive fields in the striate-recipient zone of the lateral posterior-pulvinar complex. J. Neurosci. *9*, 347–357.

Chalupa, L.M., Coyle, R.S., and Lindsley, D.B. (1976). Effect of pulvinar lesions on visual pattern discrimination in monkeys. Journal of Neurophysiology *39*, 354–369.

Chalupa, L.M., Williams, R.W., and Hughes, M.J. (1983). Visual response properties in the tectorecipient zone of the cat's lateral posterior-pulvinar complex: a comparison with the superior colliculus. J. Neurosci. *3*, 2587–2596.

Chen, L.L., Goffart, L., and Sparks, D.L. (2001). A simple method for constructing microinjectrodes for reversible inactivation in behaving monkeys. Journal of Neuroscience Methods *107*, 81–85.

Chichilnisky, E.J. (2001). A simple white noise analysis of neuronal light responses. Network *12*, 199–213.

Chubb, C., and Nam, J.-H. (2000). Variance of high contrast textures is sensed using negative half-wave rectification. Vision Research *40*, 1677–1694.

Churan, J., Guitton, D., and Pack, C.C. (2012). Spatiotemporal structure of visual receptive fields in macaque superior colliculus. Journal of Neurophysiology *108*, 2653–2667.

Conway, B., Boyd, J.D., Stewart, T.H., and Matsubara, J.A. (2000). The Projection from V1 to Extrastriate Area 21a: A Second Patchy Efferent Pathway that Colocalizes with the CO Blob Columns in Cat Visual Cortex. Cereb. Cortex *10*, 149–159.

Copenhagen, D.R., Ashmore, J.F., and Schnapf, J.K. (1983). Kinetics of synaptic transmission from photoreceptors to horizontal and bipolar cells in turtle retina. Vision Research *23*, 363–369.

Cowey, A., Stoerig, P., and Bannister, M. (1994). Retinal ganglion-cells labeled from the pulvinar nucleus in macaque monkeys. Neuroscience *61*, 691–705.

Crick, F., and Koch, C. (1998). Constraints on cortical and thalamic projections: the no-strong-loops hypothesis. Nature *391*, 245–250.

Curtis, D.R., and Crawford, J.M. (1969). Central synaptic transmission--microelectrophoretic studies. Annu Rev Pharmacol *9*, 209–240.

Curtis, D.R., and Johnston, G.A. (1974). Amino acid transmitters in the mammalian central nervous system. Ergeb Physiol *69*, 97–188.

Cusick, C.G., Scripter, J.L., Darensbourg, J.G., and Weber, J.T. (1993). Chemoarchitectonic subdivisions of the visual pulvinar in monkeys and their connectional relations with the middle temporal and rostral dorsolateral visual areas, MT and DLr. J. Comp. Neurol. *336*, 1–30.

Cutrone, E.K., Heeger, D.J., and Carrasco, M. (2014). Attention enhances contrast appearance via increased input baseline of neural responses. J Vis *14*, 16.

David, S.V., Hayden, B.Y., and Gallant, J.L. (2006). Spectral Receptive Field Properties Explain Shape Selectivity in Area V4. J Neurophysiol *96*, 3492–3505.

De Valois, R.L., Albrecht, D.G., and Thorell, L.G. (1982). Spatial frequency selectivity of cells in macaque visual cortex. Vision Res. *22*, 545–559.

DeAngelis, G.C., Ohzawa, I., and Freeman, R.D. (1993a). Spatiotemporal organization of simple-cell receptive fields in the cat's striate cortex. I. General characteristics and postnatal development. J Neurophysiol *69*, 1091–1117.

DeAngelis, G.C., Ohzawa, I., and Freeman, R.D. (1993b). Spatiotemporal organization of simple-cell receptive fields in the cat's striate cortex. II. Linearity of temporal and spatial summation. Journal of Neurophysiology *69*, 1118–1135.

DeAngelis, G.C., Ohzawa, I., and Freeman, R.D. (1995). Receptive-field dynamics in the central visual pathways. Trends in Neurosciences *18*, 451–458.

Delli Pizzi, S., Maruotti, V., Taylor, J.-P., Franciotti, R., Caulo, M., Tartaro, A., Thomas, A., Onofrj, M., and Bonanni, L. (2014). Relevance of subcortical visual pathways disruption to visual symptoms in dementia with Lewy bodies. Cortex *59*, 12–21.

Desimone, R., Wessinger, M., Thomas, L., and Schneider, W. (1990). Attentional control of visual perception: cortical and subcortical mechanisms. Cold Spring Harb. Symp. Quant. Biol. *55*, 963–971.

DeValois, K.K., DeValois, R.L., and Yund, E.W. (1979). Responses of striate cortex cells to grating and checkerboard patterns. The Journal of Physiology *291*, 483–505.

Dreher, B., Michalski, A., Ho, R.H., Lee, C.W., and Burke, W. (1993). Processing of form and motion in area 21a of cat visual cortex. Vis. Neurosci. *10*, 93–115.

Dreher, B., Wang, C., Turlejski, K.J., Djavadian, R.L., and Burke, W. (1996a). Areas PMLS and 21 a of Cat Visual Cortex: Two Functionally Distinct Areas. Cereb. Cortex *6*, 585–599.

Dreher, B., Djavadian, R.L., Turlejski, K.J., and Wang, C. (1996b). Areas PMLS and 21a of cat visual cortex are not only functionally but also hodologically distinct. Prog. Brain Res. *112*, 251–276.

Dreher, B., Wang, C., Turlejski, K.J., Djavadian, R.L., and Burke, W. (1996c). Areas PMLS and 21a of cat visual cortex: two functionally distinct areas. Cereb. Cortex *6*, 585–599.

Dumbrava, D., Faubert, J., and Casanova, C. (2001). Global motion integration in the cat's lateral posterior-pulvinar complex. European Journal of Neuroscience *13*, 2218–2226.

Duong, T., and Freeman, R.D. (2008). Contrast Sensitivity Is Enhanced by Expansive Nonlinear Processing in the Lateral Geniculate Nucleus. Journal of Neurophysiology *99*, 367–372.

Durand, S., Iyer, R., Mizuseki, K., Vries, S. de, Mihalas, S., and Reid, R.C. (2016). A Comparison of Visual Response Properties in the Lateral Geniculate Nucleus and Primary Visual Cortex of Awake and Anesthetized Mice. J. Neurosci. *36*, 12144–12156.

Eggermont, J.J., Johannesma, P.M., and Aertsen, A.M. (1983). Reverse-correlation methods in auditory research. Q. Rev. Biophys. *16*, 341–414.

Enroth-Cugell, C., and Robson, J.G. (1966). The contrast sensitivity of retinal ganglion cells of the cat. The Journal of Physiology *187*, 517–552.

Felleman, D.J., and Van Essen, D.C. (1991). Distributed Hierarchical Processing in the Primate Cerebral Cortex. Cerebral Cortex *1*, 1–47.

Fenno, L., Yizhar, O., and Deisseroth, K. (2011). The Development and Application of Optogenetics. Annual Review of Neuroscience *34*, 389–412.

Ferster, D. (1990). X- and Y-mediated current sources in areas 17 and 18 of cat visual cortex. Vis. Neurosci. *4*, 135–145.

Fetter, M., Zee, D.S., and Proctor, L.R. (1988). Effect of lack of vision and of occipital lobectomy upon recovery from unilateral labyrinthectomy in rhesus monkey. Journal of Neurophysiology *59*, 394–407.

Freund, T.F., Martin, K. a. C., and Whitteridge, D. (1985). Innervation of cat visual areas 17 and 18 by physiologically identified X- and Y- type thalamic afferents. I. Arborization patterns and quantitative distribution of postsynaptic elements. J. Comp. Neurol. *242*, 263–274.

Gallant, J.L., Braun, J., and Essen, D.V. (1993). Selectivity for polar, hyperbolic, and Cartesian gratings in macaque visual cortex. Science *259*, 100–103.

Gallant, J.L., Connor, C.E., Rakshit, S., Lewis, J.W., and Van Essen, D.C. (1996). Neural responses to polar, hyperbolic, and Cartesian gratings in area V4 of the macaque monkey. Journal of Neurophysiology *76*, 2718–2739.

Ganel, T., and Goodale, M.A. (2017). Still holding after all these years: An action-perception dissociation in patient DF. Neuropsychologia.

Gardner, J.L., Sun, P., Waggoner, R.A., Ueno, K., Tanaka, K., and Cheng, K. (2005). Contrast Adaptation and Representation in Human Early Visual Cortex. Neuron *47*, 607–620.

Gattass, R., Galkin, T.W., Desimone, R., and Ungerleider, L.G. (2013). Subcortical connections of area V4 in the macaque. Journal of Comparative Neurology n/a–n/a.

Gehring, W.J. (2014). The evolution of vision. Wiley Interdisciplinary Reviews: Developmental Biology *3*, 1–40.

Goodale, M.A., and Milner, A.D. (1992). Separate visual pathways for perception and action. Trends in Neurosciences *15*, 20–25.

Govindaiah, G., and Cox, C.L. (2006). Depression of retinogeniculate synaptic transmission by presynaptic D2-like dopamine receptors in rat lateral geniculate nucleus. European Journal of Neuroscience *23*, 423–434.

Grant, S., and Hilgetag, C.C. (2005). Graded classes of cortical connections: quantitative analyses of laminar projections to motion areas of cat extrastriate cortex. Eur. J. Neurosci. *22*, 681–696.

Graybiel, A.M., and Berson, D.M. (1980). Histochemical identification and afferent connections of subdivisions in the lateralis posterior-pulvinar complex and related thalamic nuclei in the cat. Neuroscience *5*, 1175–1238.

Green, M.F., Butler, P.D., Chen, Y., Geyer, M.A., Silverstein, S., Wynn, J.K., Yoon, J.H., and Zemon, V. (2009). Perception Measurement in Clinical Trials of Schizophrenia: Promising Paradigms From CNTRICS. Schizophr Bull *35*, 163–181.

Gregoriou, G.G., Rossi, A.F., Ungerleider, L.G., and Desimone, R. (2014). Lesions of prefrontal cortex reduce attentional modulation of neuronal responses and synchrony in V4. Nat Neurosci *17*, 1003–1011.

Grieve, K.L., Acuña, C., and Cudeiro, J. (2000). The primate pulvinar nuclei: vision and action. Trends in Neurosciences *23*, 35–39.

Grill-Spector, K., and Malach, R. (2004). The human visual cortex. Annu. Rev. Neurosci. *27*, 649–677.

Guillery, R.W., and Sherman, S.M. (2002). Thalamic Relay Functions and Their Role in Corticocortical Communication: Generalizations from the Visual System. Neuron *33*, 163–175.

Gulcebi, M.I., Ketenci, S., Linke, R., Hacıoğlu, H., Yanalı, H., Veliskova, J., Moshé, S.L., Onat, F., and Çavdar, S. (2012). Topographical connections of the substantia nigra pars reticulata to higher-order thalamic nuclei in the rat. Brain Research Bulletin *87*, 312–318.

Gutierrez, C., Cola, M.G., Seltzer, B., and Cusick, C. (2000). Neurochemical and connectional organization of the dorsal pulvinar complex in monkeys. J. Comp. Neurol. *419*, 61–86.

de Haan, E.H.F., and Cowey, A. (2011). On the usefulness of 'what' and 'where' pathways in vision. Trends in Cognitive Sciences *15*, 460–466.

Hamos, J.E., Van Horn, S.C., Raczkowski, D., and Sherman, S.M. (1987). Synaptic circuits involving an individual retinogeniculate axon in the cat. J. Comp. Neurol. *259*, 165–192.

Hartline, H.K. (1938). THE RESPONSE OF SINGLE OPTIC NERVE FIBERS OF THE VERTEBRATE EYE TO ILLUMINATION OF THE RETINA. American Journal of Physiology *121*, 400–415.

Hegde, J., and Felleman, D.J. (2007). A comparative study of shape representation in macaque visual areas V2 and V4. Cerebral Cortex *17*, 1100–1116.

Hess, R., and Murata, K. (1974). Effects of glutamate and GABA on specific response properties of neurones in the visual cortex. Exp Brain Res *21*, 285–297.

Hubel, D., and Wiesel, T. (1968). Receptive fields and functional architecture of monkey striate cortex. Journal of Physiology-London *195*, 215–243.

Hubel, D.H., and Wiesel, T.N. (1962). Receptive fields, binocular interaction and functional architecture in the cat's visual cortex. J Physiol *160*, 106-154.2.

Humphrey, A.L., Sur, M., Uhlrich, D.J., and Sherman, S.M. (1985). Projection patterns of individual X- and Y-cell axons from the lateral geniculate nucleus to cortical area 17 in the cat. J. Comp. Neurol. *233*, 159–189.

Hupé, J.M., Chouvet, G., and Bullier, J. (1999). Spatial and temporal parameters of cortical inactivation by GABA. J. Neurosci. Methods *86*, 129–143.

Huppé-Gourgues, F., Bickford, M. e., Boire, D., Ptito, M., and Casanova, C. (2006). Distribution, morphology, and synaptic targets of corticothalamic terminals in the cat lateral posterior-pulvinar complex that originate from the posteromedial lateral suprasylvian cortex. The Journal of Comparative Neurology *497*, 847–863.

Hutchins, B., and Updyke, B.V. (1989). Retinotopic organization within the lateral posterior complex of the cat. J. Comp. Neurol. *285*, 350–398.

Ikeda, H., and Wright, M.J. (1974). Sensitivity of neurones in visual cortex (area 17) under different levels of anaesthesia. Exp Brain Res *20*, 471–484.

Imas, O.A., Ropella, K.M., Wood, J.D., and Hudetz, A.G. (2004). Halothane augments event-related gamma oscillations in rat visual cortex. Neuroscience *123*, 269–278.

Isbell, L.A. (2006). Snakes as agents of evolutionary change in primate brains. Journal of Human Evolution *51*, 1–35.

Itaya, S., and Vanhoesen, G. (1983). Retinal projections to the inferior and medial pulvinar nuclei in the old-world monkey. Brain Research *269*, 223–230.

Jay Hegdé, and Daniel J. Felleman (2007). Reappraising the Functional Implications of the Primate Visual Anatomical Hierarchy. Neuroscientist *13*, 416–421.

Jin, J., Wang, Y., Lashgari, R., Swadlow, H.A., and Alonso, J.-M. (2011). Faster Thalamocortical Processing for Dark than Light Visual Targets. J. Neurosci. *31*, 17471–17479.

Jin, J.Z., Weng, C., Yeh, C.-I., Gordon, J.A., Ruthazer, E.S., Stryker, M.P., Swadlow, H.A., and Alonso, J.-M. (2008). On and off domains of geniculate afferents in cat primary visual cortex. Nat Neurosci *11*, 88–94.

Jones, E.G. (2001). The thalamic matrix and thalamocortical synchrony. Trends in Neurosciences *24*, 595–601.

Jones, J.P., and Palmer, L.A. (1987). The two-dimensional spatial structure of simple receptive fields in cat striate cortex. J Neurophysiol *58*, 1187–1211.

Jones, J.P., Stepnoski, A., and Palmer, L.A. (1987). The two-dimensional spectral structure of simple receptive fields in cat striate cortex. Journal of Neurophysiology *58*, 1212–1232.

Kaas, J.H., and Collins, C.E. (2001). The organization of sensory cortex. Current Opinion in Neurobiology *11*, 498–504.

Kaas, J.H., and Lyon, D.C. (2007). Pulvinar contributions to the dorsal and ventral streams of visual processing in primates. Brain Research Reviews *55*, 285–296.

Kandel, E.R., Schwartz, J.H., and Jessell, T.M. (2000). Principles of Neural Science (McGraw-Hill Medical).

Kawamura, S., Sprague, J.M., and Niimi, K. (1974). Corticofugal projections from the visual cortices to the thalamus, pretectum and superior colliculus in the cat. J. Comp. Neurol. *158*, 339–362.

Kayser, C. a, and Konig, P. a (2006). Feature selectivity in area 21a of the cat. [Miscellaneous Article]. Neuroreport May 29, 2006 *17*, 809–812.

Kim, T., Allen, E.A., Pasley, B.N., and Freeman, R.D. (2015). Transcranial magnetic stimulation changes response selectivity of neurons in the visual cortex. Brain Stimul *8*, 613–623.

King, J.L., Lowe, M.P., Stover, K.R., Wong, A.A., and Crowder, N.A. (2016). Adaptive Processes in Thalamus and Cortex Revealed by Silencing of Primary Visual Cortex during Contrast Adaptation. Current Biology *26*, 1295–1300.

Kobatake, E., and Tanaka, K. (1994). Neuronal selectivities to complex object features in the ventral visual pathway of the macaque cerebral cortex. Journal of Neurophysiology *71*, 856–867.

Komban, S.J., Alonso, J.-M., and Zaidi, Q. (2011). Darks Are Processed Faster Than Lights. J. Neurosci. *31*, 8654–8658.

Komban, S.J., Kremkow, J., Jin, J., Wang, Y., Lashgari, R., Li, X., Zaidi, Q., and Alonso, J.-M. (2014). Neuronal and Perceptual Differences in the Temporal Processing of Darks and Lights. Neuron *82*, 224–234.

Kravitz, D.J., Saleem, K.S., Baker, C.I., and Mishkin, M. (2011). A new neural framework for visuospatial processing. Nature Reviews Neuroscience *12*, 217.

Kuffler, S.W. (1953). Discharge Patterns and Functional Organization of Mammalian Retina. Journal of Neurophysiology *16*, 37–68.

Lai, J., Legault, M.-A., Thomas, S., and Casanova, C. (2015). Simultaneous Electrophysiological Recording and Micro-injections of Inhibitory Agents in the Rodent Brain. J Vis Exp.

Laties, A.M., and Sprague, J.M. (1966). The projection of optic fibers to the visual centers in the cat. Journal of Comparative Neurology *127*, 35–70.

Le, Q.V., Isbell, L.A., Matsumoto, J., Nguyen, M., Hori, E., Maior, R.S., Tomaz, C., Tran, A.H., Ono, T., and Nishijo, H. (2013). Pulvinar neurons reveal neurobiological evidence of past selection for rapid detection of snakes. PNAS *110*, 19000–19005.

Le, Q.V., Isbell, L.A., Matsumoto, J., Le, V.Q., Hori, E., Tran, A.H., Maior, R.S., Tomaz, C., Ono, T., and Nishijo, H. (2014). Monkey Pulvinar Neurons Fire Differentially to Snake Postures. PLoS ONE *9*, e114258.

Lee, C.C., and Sherman, S.M. (2008). Synaptic Properties of Thalamic and Intracortical Inputs to Layer 4 of the First- and Higher-Order Cortical Areas in the Auditory and Somatosensory Systems. J Neurophysiol *100*, 317–326.

Letinic, K., and Rakic, P. (2001). Telencephalic origin of human thalamic GABAergic neurons. Nature Neuroscience *4*, 931–936.

Li, B., Li, B.-W., Chen, Y., Wang, L.-H., and Diao, Y.-C. (2000a). Response properties of PMLS and PLLS neurons to simulated optic flow patterns. European Journal of Neuroscience *12*, 1534–1544.

Li, B., Li, B.-W., Chen, Y., Wang, L.-H., and Diao, Y.-C. (2000b). Response properties of PMLS and PLLS neurons to simulated optic flow patterns. European Journal of Neuroscience *12*, 1534–1544.

Li, X., Sroubek, A., Kelly, M.S., Lesser, I., Sussman, E., He, Y., Branch, C., and Foxe, J.J. (2012). Atypical Pulvinar–Cortical Pathways During Sustained Attention Performance in Children With Attention-Deficit/Hyperactivity Disorder. Journal of the American Academy of Child & Adolescent Psychiatry *51*, 1197-1207.e4.

Liddell, B.J., Brown, K.J., Kemp, A.H., Barton, M.J., Das, P., Peduto, A., Gordon, E., and Williams, L.M. (2005). A direct brainstem–amygdala–cortical 'alarm' system for subliminal signals of fear. NeuroImage *24*, 235–243.

Lien, A.D., and Scanziani, M. (2018). Cortical direction selectivity emerges at convergence of thalamic synapses. Nature *558*, 80–86.

Lin, C.-S., and Kaas, J.H. (1979). The inferior pulvinar complex in owl monkeys: Architectonic subdivisions and patterns of input from the superior colliculus and subdivisions of visual cortex. J. Comp. Neurol. *187*, 655–678.

Lin, C.-S., and Kaas, J.H. (1980). Projections from the medial nucleus of the inferior pulvinar complex to the middle temporal area of the visual cortex. Neuroscience *5*, 2219–2228.

Ling, S., and Carrasco, M. (2006). Sustained and transient covert attention enhance the signal via different contrast response functions. Vision Res *46*, 1210–1220.

Liu, S., Liu, Y.-J., and Li, B. (2007). Spatiotemporal structure of complex cell receptive fields and influence of GABAergic inhibition: NeuroReport *18*, 1577–1581.

Liu, X.-B., Honda, C. n., and Jones, E. g. (1995). Distribution of four types of synapse on physiologically identified relay neurons in the ventral posterior thalamic nucleus of the cat. Journal of Comparative Neurology *352*, 69–91.

Livingstone, M.S., Pack, C.C., and Born, R.T. (2001). Two-Dimensional Substructure of MT Receptive Fields. Neuron *30*, 781–793.

Lomber, S.G. (2001). Behavioral cartography of visual functions in cat parietal cortex: areal and laminar dissociations. Prog. Brain Res. *134*, 265–284.

Lomber, S.G., Payne, B.R., Cornwell, P., and Long, K.D. (1996). Perceptual and Cognitive Visual Functions of Parietal and Temporal Cortices in the Cat. Cereb. Cortex *6*, 673–695.

Lomber, S.G., Payne, B.R., and Horel, J.A. (1999). The cryoloop: an adaptable reversible cooling deactivation method for behavioral or electrophysiological assessment of neural function. Journal of Neuroscience Methods *86*, 179–194.

Lyon, D.C., Nassi, J.J., and Callaway, E.M. (2010). A Disynaptic Relay from Superior Colliculus to Dorsal Stream Visual Cortex in Macaque Monkey. Neuron *65*, 270–279.

Maior, R.S., Hori, E., Tomaz, C., Ono, T., and Nishijo, H. (2010). The monkey pulvinar neurons differentially respond to emotional expressions of human faces. Behavioural Brain Research *215*, 129–135.

Mason, R. (1981). Differential responsiveness of cells in the visual zones of the cat's LP-pulvinar complex to visual stimuli. Exp Brain Res *43*, 25–33.

Masson, G., Mestre, D., and Blin, O. (1993). Dopaminergic modulation of visual sensitivity in man. Fundam Clin Pharmacol *7*, 449–463.

Matteau, I., Boire, D., and Ptito, M. (2003). Retinal projections in the cat: A cholera toxin B subunit study. Visual Neuroscience *20*, 481–493.

May, K.A., and Solomon, J.A. (2015). Connecting psychophysical performance to neuronal response properties II: Contrast decoding and detection. Journal of Vision *15*, 9–9.

Meikle, T.H., and Sprague, J.M. (1964). THE NEURAL ORGANIZATION OF THE VISUAL PATHWAYS IN THE CAT. Int. Rev. Neurobiol. *6*, 149–189.

Merabet, L., Desautels, A., Minville, K., and Casanova, C. (1998). Motion integration in a thalamic visual nucleus. Nature *396*, 265–268.

Merabet, L., Minville, K., Ptito, M., and Casanova, C. (2000). Responses of neurons in the cat posteromedial lateral suprasylvian cortex to moving texture patterns. Neuroscience *97*, 611–623.

Michalski, A., Wimborne, B.M., and Henry, G.H. (1993). The effect of reversible cooling of cat's primary visual cortex on the responses of area 21a neurons. J Physiol *466*, 133–156.

Miller, K.J., Hermes, D., Pestilli, F., Wig, G.S., and Ojemann, J.G. (2017). Face percept formation in human ventral temporal cortex. Journal of Neurophysiology *118*, 2614–2627.

Milner, A.D. (2017). How do the two visual streams interact with each other? Exp Brain Res *235*, 1297–1308.

Minville, K., and Casanova, C. (1998). Spatial frequency processing in posteromedial lateral suprasylvian cortex does not depend on the projections from the striate-recipient zone of the cat's lateral posterior-pulvinar complex. Neuroscience *84*, 699–711.

Mishkin, M., and Ungerleider, L. (1982). Contribution of striate inputs to the visuospatial functions of parieto-preoccipital cortex in monkeys. Behavioural Brain Research *6*, 57–77.

Mishkin, M., Ungerleider, L.G., and Macko, K.A. (1983). Object vision and spatial vision: Two cortical pathways. Trends in Neurosciences *10*, 414–417.

Mizobe, K., Itoi, M., Kaihara, T., and Toyama, K. (1988). Neuronal responsiveness in area 21a of the cat. Brain Res. *438*, 307–310.

Molotchnikoff, S., and Shumikhina, S. (1996). The lateral posterior-pulvinar complex modulation of stimulus-dependent oscillations in the cat visual cortex. Vision Research *36*, 2037–2046.

Morin, E.L., Hadj-Bouziane, F., Stokes, M., Ungerleider, L.G., and Bell, A.H. (2015). Hierarchical Encoding of Social Cues in Primate Inferior Temporal Cortex. Cereb Cortex *25*, 3036–3045.

Morley, J.W., and Vickery, R.M. (1997). Spatial and temporal frequency selectivity of cells in area 21a of the cat. J Physiol *501*, 405–413.

Morley, J.W., and Vickery, R.M. (1999). Binocular interactions in area 21a of the cat. [Miscellaneous Article]. Neuroreport August 2, 1999 *10*, 2241–2244.

Motoyoshi, I., Nishida, S., Sharan, L., and Adelson, E.H. (2007). Image statistics and the perception of surface qualities. Nature *447*, 206–209.

Movshon, J.A., Thompson, I.D., and Tolhurst, D.J. (1978a). Spatial summation in the receptive fields of simple cells in the cat's striate cortex. The Journal of Physiology *283*, 53–77.

Movshon, J.A., Thompson, I.D., and Tolhurst, D.J. (1978b). Receptive field organization of complex cells in the cat's striate cortex. The Journal of Physiology *283*, 79–99.

Nahmani, M., and Turrigiano, G.G. (2014). Adult cortical plasticity following injury: Recapitulation of critical period mechanisms? Neuroscience *0*, 4–16.

Naito, J. (1986). Course of retinogeniculate projection fibers in the cat optic nerve. J. Comp. Neurol. *251*, 376–387.

Naka, K.I., and Rushton, W. a. H. (1966). S-potentials from colour units in the retina of fish (Cyprinidae). The Journal of Physiology *185*, 536–555.

Nassi, J.J., and Callaway, E.M. (2009). Parallel processing strategies of the primate visual system. Nature Reviews Neuroscience *10*, nrn2619.

Nguyen, M.N., Hori, E., Matsumoto, J., Tran, A.H., Ono, T., and Nishijo, H. (2013). Neuronal responses to face-like stimuli in the monkey pulvinar. Eur J Neurosci *37*, 35–51.

Nichols, Z., Nirenberg, S., and Victor, J. (2013). Interacting Linear and Nonlinear Characteristics Produce Population Coding Asymmetries between ON and OFF Cells in the Retina. J. Neurosci. *33*, 14958–14973.

Niimi, K., and Sprague, J.M. (1970). Thalamo-cortical organization of the visual system in the cat. Journal of Comparative Neurology *138*, 219–249.

Nishimoto, S., Arai, M., and Ohzawa, I. (2005). Accuracy of Subspace Mapping of Spatiotemporal Frequency Domain Visual Receptive Fields. Journal of Neurophysiology *93*, 3524–3536.

Nishimoto, S., Ishida, T., and Ohzawa, I. (2006). Receptive Field Properties of Neurons in the Early Visual Cortex Revealed by Local Spectral Reverse Correlation. J. Neurosci. *26*, 3269–3280.

Noudoost, B., and Moore, T. (2011). A reliable microinjectrode system for use in behaving monkeys. Journal of Neuroscience Methods *194*, 218–223.

Öhman, A., Flykt, A., and Esteves, F. (2001). Emotion drives attention: Detecting the snake in the grass. Journal of Experimental Psychology: General *130*, 466–478.

Ohzawa, I., Sclar, G., and Freeman, R. (1982). Contrast gain-control in the cat visual-cortex. Nature *298*, 266–268.

Ohzawa, I., DeAngelis, G.C., and Freeman, R.D. (1990). Stereoscopic depth discrimination in the visual cortex: neurons ideally suited as disparity detectors. Science *249*, 1037–1041.

Olshausen, B.A., Anderson, C.H., and Van, E. (1993). A neurobiological model of visual attention and invariant pattern recognition based on dynamic routing of information. Journal of Neuroscience *13*, 4700–4719.

Olszewski, J. (1952). The thalamus of the Macaca mulatta (Basel and New York: S. Karger AG).

Orban, G.A. (2008). Higher Order Visual Processing in Macaque Extrastriate Cortex. Physiological Reviews *88*, 59–89.

Pack, C.C., Berezovskii, V.K., and Born, R.T. (2001). Dynamic properties of neurons in cortical area MT in alert and anaesthetized macaque monkeys. Nature *414*, 905–908.

Pack, C.C., Conway, B.R., Born, R.T., and Livingstone, M.S. (2006). Spatiotemporal Structure of Nonlinear Subunits in Macaque Visual Cortex. J. Neurosci. *26*, 893–907.

Pasupathy, A., and Connor, C.E. (1999). Responses to Contour Features in Macaque Area V4. Journal of Neurophysiology *82*, 2490–2502.

Pasupathy, A., and Connor, C.E. (2001). Shape Representation in Area V4: Position-Specific Tuning for Boundary Conformation. Journal of Neurophysiology *86*, 2505–2519.

Pasupathy, A., and Connor, C.E. (2002). Population coding of shape in area V4. Nature Neuroscience *5*, 1332.

Payne, B.R. (1993). Evidence for visual cortical area homologs in cat and macaque monkey. Cereb. Cortex *3*, 1–25.

Payne, B.R., and Peters, A. (2002). 1 - The Concept of Cat Primary Visual Cortex. In The Cat Primary Visual Cortex, (San Diego: Academic Press), pp. 1–129.

Petersen, S.E., Robinson, D.L., and Keys, W. (1985). Pulvinar nuclei of the behaving rhesus monkey: visual responses and their modulation. Journal of Neurophysiology *54*, 867–886.

Petersen, S.E., Robinson, D.L., and Morris, J.D. (1987). Contributions of the pulvinar to visual spatial attention. Neuropsychologia *25*, 97–105.

Petrof, I., Viaene, A.N., and Sherman, S.M. (2012). Two populations of corticothalamic and interareal corticocortical cells in the subgranular layers of the mouse primary sensory cortices. J. Comp. Neurol. *520*, 1678–1686.

Petry, H.M., and Bickford, M.E. (2018). The Second Visual System of the Tree Shrew. J. Comp. Neurol.

Piché, M., Thomas, S., and Casanova, C. (2013). Spatiotemporal profiles of neurons receptive fields in the cat posteromedial lateral suprasylvian cortex. Neuroscience *248*, 319–332.

Piché, M., Thomas, S., and Casanova, C. (2015). Spatiotemporal profiles of receptive fields of neurons in the lateral posterior nucleus of the cat LP-pulvinar complex. Journal of Neurophysiology *114*, 2390–2403.

Purushothaman, G., Marion, R., Li, K., and Casagrande, V.A. (2012). Gating and control of primary visual cortex by pulvinar. Nat Neurosci *15*, 905–912.

Quax, S., Jensen, O., and Tiesinga, P. (2017). Top-down control of cortical gamma-band communication via pulvinar induced phase shifts in the alpha rhythm. PLOS Computational Biology *13*, e1005519.

Raczkowski, D., and Rosenquist, A.C. (1981). Retinotopic organization in the cat lateral posterior-pulvinar complex. Brain Research *221*, 185–191.

Raczkowski, D., and Rosenquist, A.C. (1983). Connections of the multiple visual cortical areas with the lateral posterior-pulvinar complex and adjacent thalamic nuclei in the cat. J. Neurosci. *3*, 1912–1942.

Rauschecker, J.P. (2017). Where, When, and How: Are they all sensorimotor? Towards a unified view of the dorsal pathway in vision and audition. Cortex.

Reichova, I., and Sherman, S. (2004). Somatosensory corticothalamic projections: Distinguishing drivers from modulators. J Neurophysiol *92*, 2185–2197.

Reid, R.C., Victor, J.D., and Shapley, R.M. (1997). The use of m-sequences in the analysis of visual neurons: linear receptive field properties. Vis. Neurosci. *14*, 1015–1027.

Rey, H.G., Pedreira, C., and Quian Quiroga, R. (2015). Past, present and future of spike sorting techniques. Brain Research Bulletin.

Reynolds, J.H., and Desimone, R. (1999). The Role of Neural Mechanisms of Attention in Solving the Binding Problem. Neuron *24*, 19–29.

Reynolds, J.H., Pasternak, T., and Desimone, R. (2000). Attention Increases Sensitivity of V4 Neurons. Neuron *26*, 703–714.

Richert, M., Albright, T.D., and Krekelberg, B. (2013). The complex structure of receptive fields in the middle temporal area. Front. Syst. Neurosci. *7*, 2.

Ringach, D., and Shapley, R. (2004). Reverse correlation in neurophysiology. Cognitive Science *28*, 147–166.

Ringach, D.L., Sapiro, G., and Shapley, R. (1997). A subspace reverse-correlation technique for the study of visual neurons. Vision Research *37*, 2455–2464.

Robinson, D.L., and Petersen, S.E. (1992). The pulvinar and visual salience. Trends in Neurosciences *15*, 127–132.

Rossant, C., Kadir, S.N., Goodman, D.F.M., Schulman, J., Hunter, M.L.D., Saleem, A.B., Grosmark, A., Belluscio, M., Denfield, G.H., Ecker, A.S., et al. (2016). Spike sorting for large, dense electrode arrays. Nat Neurosci *19*, 634–641.

Rovó, Z., Ulbert, I., and Acsády, L. (2012). Drivers of the Primate Thalamus. J. Neurosci. *32*, 17894–17908.

Saalmann, Y.B., and Kastner, S. (2009). Gain control in the visual thalamus during perception and cognition. Current Opinion in Neurobiology *19*, 408–414.

Saalmann, Y.B., and Kastner, S. (2011). Cognitive and Perceptual Functions of the Visual Thalamus. Neuron *71*, 209–223.

Saalmann, Y.B., Pinsk, M.A., Wang, L., Li, X., and Kastner, S. (2012). The Pulvinar Regulates Information Transmission Between Cortical Areas Based on Attention Demands. Science *337*, 753–756.

Sakai, H.M., Naka, K., and Korenberg, M.J. (1988). White-noise analysis in visual neuroscience. Vis. Neurosci. *1*, 287–296.

Sanderson, K.J. (1971). The projection of the visual field to the lateral geniculate and medial interlaminar nuclei in the cat. J. Comp. Neurol. *143*, 101–117.

Sandkühler, J., and Gebhart, G.F. (1991). Production of Reversible Local Blockage of Neuronal Function. In Methods in Neurosciences, P.M. Conn, ed. (Academic Press), pp. 122–138.

Scannell, J., Blakemore, C., and Young, M. (1995). Analysis of connectivity in the cat cerebral-cortex. J Neurosci *15*, 1463–1483.

Sclar, G., Maunsell, J., and Lennie, P. (1990). Coding of image-contrast in central visual pathways of the macaque monkey. Vision Research *30*, 1–10.

Sekuler, A.B., and Bennett, P.J. (2001). Visual neuroscience: Resonating to natural images. Current Biology *11*, R733–R736.

Sellers, K.K., Bennett, D.V., Hutt, A., Williams, J.H., and Fröhlich, F. (2015). Awake vs. anesthetized: layer-specific sensory processing in visual cortex and functional connectivity between cortical areas. J. Neurophysiol. *113*, 3798–3815.

Sherk, H. (1989). Visual response properties of cortical inputs to an extrastriate cortical area in the cat. Vis. Neurosci. *3*, 249–265.

Sherman, S.M. (2007). The thalamus is more than just a relay. Current Opinion in Neurobiology *17*, 417–422.

Sherman, S.M. (2016). Thalamus plays a central role in ongoing cortical functioning. Nat Neurosci *16*, 533–541.

Sherman, S.M. (2017). Functioning of Circuits Connecting Thalamus and Cortex. Compr Physiol *7*, 713–739.

Sherman, S., and Guillery, R. (2002). The role of the thalamus in the flow of information to the cortex. Philosophical Transactions of the Royal Society B-Biological Sciences *357*, 1695–1708.

Sherman, S., and Guillery, R. (2013a). Functional Connections of Cortical Areas: A New View from the Thalamus (Cambridge, MA: MIT Press).

Sherman, S.M., and Guillery, R.W. (1996). Functional organization of thalamocortical relays. Journal of Neurophysiology *76*, 1367–1395.

Sherman, S.M., and Guillery, R.W. (1998). On the actions that one nerve cell can have on another: Distinguishing "drivers" from "modulators." PNAS *95*, 7121–7126.

Sherman, S.M., and Guillery, R.W. (2013b). Functional Connections of Cortical Areas: A New View from the Thalamus (MIT Press).

Sherman, S.M., and Koch, C. (1986). The control of retinogeniculate transmission in the mammalian lateral geniculate nucleus. Exp Brain Res *63*, 1–20.

Shibasaki, M., and Kawai, N. (2009). Rapid detection of snakes by Japanese monkeys (Macaca fuscata): An evolutionarily predisposed visual system. Journal of Comparative Psychology *123*, 131–135.

Shipp, S. (2003). The functional logic of cortico-pulvinar connections. Philos Trans R Soc Lond B Biol Sci *358*, 1605–1624.

Shipp, S. (2004). The brain circuitry of attention. Trends in Cognitive Sciences *8*, 223–230.

Shipp, S., and Grant, S. (1991). Organization of reciprocal connections between area 17 and the lateral suprasylvian area of cat visual cortex. Vis. Neurosci. *6*, 339–355.

Shumikhina, S., and Molotchnikoff, S. (1999). Pulvinar participates in synchronizing neural assemblies in the visual cortex, in cats. Neuroscience Letters *272*, 135–139.

Silverstein, S.M., and Keane, B.P. (2011). Vision Science and Schizophrenia Research: Toward a Re-view of the Disorder Editors' Introduction to Special Section. Schizophr Bull *37*, 681–689.

Simoncelli, E.P., and Olshausen, B.A. (2001). Natural Image Statistics and Neural Representation. Annual Review of Neuroscience *24*, 1193–1216.

Skottun, B.C., De Valois, R.L., Grosof, D.H., Movshon, J.A., Albrecht, D.G., and Bonds, A.B. (1991). Classifying simple and complex cells on the basis of response modulation. Vision Research *31*, 1078–1086.

Smith, M.A., Majaj, N.J., and Movshon, J.A. (2005). Dynamics of motion signaling by neurons in macaque area MT. Nature Neuroscience *8*, 220.

Snow, J.C., Allen, H.A., Rafal, R.D., and Humphreys, G.W. (2009). Impaired attentional selection following lesions to human pulvinar: Evidence for homology between human and monkey. PNAS *106*, 4054–4059.

Soares, J., Diogo, A., Fiorani, M., Souza, A., and Gattass, R. (2004). Effects of inactivation of the lateral pulvinar on response properties of second visual area cells in Cebus monkeys. Clinical and Experimental Pharmacology and Physiology *31*, 580–590.

Soma, S., Shimegi, S., Osaki, H., and Sato, H. (2012). Cholinergic modulation of response gain in the primary visual cortex of the macaque. Journal of Neurophysiology *107*, 283–291.

Soma, S., Shimegi, S., Suematsu, N., and Sato, H. (2013). Cholinergic modulation of response gain in the rat primary visual cortex. Sci. Rep. *3*.

Stepniewska, I. (2003). The Pulvinar complex. In The Primate Visual System, J. Kaas, and C. Collins, eds. (Boca Raton, FL:CRC Press), pp. 53–80.

Stone, J., and Dreher, B. (1973). Projection of X- and Y-cells of the cat's lateral geniculate nucleus to areas 17 and 18 of visual cortex. Journal of Neurophysiology *36*, 551–567.

Symonds, L.L., and Rosenquist, A.C. (1984a). Laminar origins of visual corticocortical connections in the cat. J. Comp. Neurol. *229*, 39–47.

Symonds, L.L., and Rosenquist, A.C. (1984b). Corticocortical connections among visual areas in the cat. J. Comp. Neurol. *229*, 1–38.

Symonds, L.L., Rosenquist, A.C., Edwards, S.B., and Palmer, L.A. (1981). Projections of the pulvinar-lateral posterior complex to visual cortical areas in the cat. Neuroscience *6*, 1995–2020.

Szulborski, R.G., and Palmer, L.A. (1990). The two-dimensional spatial structure of nonlinear subunits in the receptive fields of complex cells. Vision Research *30*, 249–254.

Talebi, V., and Baker, C.L. (2012). Natural versus Synthetic Stimuli for Estimating Receptive Field Models: A Comparison of Predictive Robustness. J. Neurosci. *32*, 1560–1576.

Talebi, V., and Baker, C.L. (2016). Categorically distinct types of receptive fields in early visual cortex. Journal of Neurophysiology jn.00659.2015.

Tao, X., Zhang, B., Smith, E.L., Nishimoto, S., Ohzawa, I., and Chino, Y.M. (2012). Local sensitivity to stimulus orientation and spatial frequency within the receptive fields of neurons in visual area 2 of macaque monkeys. J Neurophysiol *107*, 1094–1110.

Tardif, E., Bergeron, A., Lepore, F., and Guillemot, J.-P. (1996). Spatial and temporal frequency tuning and contrast sensitivity of single neurons in area 21a of the cat. Brain Research *716*, 219–223.

Taylor, J.C., and Downing, P.E. (2011). Division of Labor between Lateral and Ventral Extrastriate Representations of Faces, Bodies, and Objects. Journal of Cognitive Neuroscience *23*, 4122–4137.

Toyama, K., Mizobe, K., Akase, E., and Kaihara, T. (1994). Neuronal responsiveness in areas 19 and 21a, and the posteromedial lateral suprasylvian cortex of the cat. Exp Brain Res *99*, 289–301.

Tusa, R.J., and Palmer, L.A. (1980). Retinotopic organization of areas 20 and 21 in the cat. J. Comp. Neurol. *193*, 147–164.

Uhl, R.R., Squires, K.C., Bruce, D.L., and Starr, A. (1980). Effect of halothane anesthesia on the human cortical visual evoked response. Anesthesiology *53*, 273–276.

Ungerleider, L.G., and Haxby, J.V. (1994). "What" and "where" in the human brain. Curr. Opin. Neurobiol. *4*, 157–165.

Ungerleider, L.G., Desimone, R., Galkin, T.W., and Mishkin, M. (1984). Subcortical projections of area MT in the macaque. J. Comp. Neurol. *223*, 368–386.

Ungerleider, L.G., Galkin, T.W., Desimone, R., and Gattass, R. (2014). Subcortical Projections of Area V2 in the Macaque. Journal of Cognitive Neuroscience *26*, 1220–1233.

Updyke, B.V. (1977). Topographic organization of the projections from cortical areas 17, 18, and 19 onto the thalamus, pretectum and superior colliculus in the cat. J. Comp. Neurol. *173*, 81–121.

Updyke, B.V. (1981). Projections from visual areas of the middle suprasylvian sulcus onto the lateral posterior complex and adjacent thalamic nuclei in cat. J. Comp. Neurol. *201*, 477–506.

Updyke, B.V. (1983). A reevaluation of the functional organization and cytoarchitecture of the feline lateral posterior complex, with observations on adjoining cell groups. J. Comp. Neurol. *219*, 143–181.

Usrey, W.M., Reppas, J.B., and Reid, R.C. (1999). Specificity and Strength of Retinogeniculate Connections. Journal of Neurophysiology *82*, 3527–3540.

USREY, W.M., SCENIAK, M.P., and CHAPMAN, B. (2003). Receptive Fields and Response Properties of Neurons in Layer 4 of Ferret Visual Cortex. J Neurophysiol *89*, 1003–1015.

Vajda, I., Lankheet, M.J.M., and van de Grind, W.A. (2005). Spatio-temporal requirements for direction selectivity in area 18 and PMLS complex cells. Vision Research *45*, 1769–1779.

Van der Stigchel, S., Arend, I., van Koningsbruggen, M.G., and Rafal, R.D. (2010). Oculomotor integration in patients with a pulvinar lesion. Neuropsychologia *48*, 3497–3504.

Van Hooser, S.D. (2007). Similarity and Diversity in Visual Cortex: Is There a Unifying Theory of Cortical Computation? , Similarity and Diversity in Visual Cortex: Is There a Unifying Theory of Cortical Computation? Neuroscientist *13*, 639–656.

Van horn, S., and Sherman, S. (2004). Differences in projection patterns between large and small corticothalamic terminals. Journal of Comparative Neurology *475*, 406–415.

Van Horn, S.C., Erişir, A., and Sherman, S.M. (2000). Relative distribution of synapses in the A-laminae of the lateral geniculate nucleus of the cat. J. Comp. Neurol. *416*, 509–520.

Viaene, A.N., Petrof, I., and Sherman, S.M. (2011). Synaptic Properties of Thalamic Input to the Subgranular Layers of Primary Somatosensory and Auditory Cortices in the Mouse. J Neurosci *31*, 12738–12747.

Vickery, R.M., and Morley, J.W. (1997). Orientation-dependent binocular interactions in area 21a of the cat. [Miscellaneous Article]. Neuroreport September 29, 1997 *8*, 3173–3176.

Vickery, R.M., and Morley, J.W. (1999). Binocular phase interactions in area 21a of the cat. J Physiol *514*, 541–549.

Villeneuve, M.Y., and Casanova, C. (2003). On the use of isoflurane versus halothane in the study of visual response properties of single cells in the primary visual cortex. Journal of Neuroscience Methods *129*, 19–31.

Villeneuve, M.Y., Kupers, R., Gjedde, A., Ptito, M., and Casanova, C. (2005). Pattern–motion selectivity in the human pulvinar. NeuroImage *28*, 474–480.

Villeneuve, M.Y., Ptito, M., and Casanova, C. (2006). Global motion integration in the postero-medial part of the lateral suprasylvian cortex in the cat. Exp Brain Res *172*, 485–497.

Villeneuve, M.Y., Vanni, M.P., and Casanova, C. (2009). Modular organization in area 21a of the cat revealed by optical imaging: comparison with the primary visual cortex. Neuroscience *164*, 1320–1333.

Wamer, C., Goldshmit, Y., and Bourne, J. (2010). Retinal afferents synapse with relay cells targeting the middle temporal area inthe pulvinar and lateral geniculate nuclei. Frontiers in Neuroanatomy *4*, 1–16.

Wang, H.X., and Movshon, J.A. (2015). Properties of pattern and component direction-selective cells in area MT of the macaque. Journal of Neurophysiology *115*, 2705–2720.

Wang, S., Eisenback, M.A., and Bickford, M.E. (2002). Relative distribution of synapses in the pulvinar nucleus of the cat: Implications regarding the "driver/modulator" theory of thalamic function. J. Comp. Neurol. *454*, 482–494.

Wang, Y., Wang, L., Li, B., Wang, L.H., and Diao, Y.C. (1995). How is direction selectivity organized in the extrastriate visual area PMLS of the cat? Neuroreport *6*, 1969–1974.

Ward, R., Danziger, S., Owen, V., and Rafal, R. (2002). Deficits in spatial coding and feature binding following damage to spatiotopic maps in the human pulvinar. Nat Neurosci *5*, 99–100.

Ward, R., Danziger, S., and Bamford, S. (2005). Response to Visual Threat Following Damage to the Pulvinar. Current Biology *15*, 571–573.

Ward, R., Calder, A.J., Parker, M., and Arend, I. (2007). Emotion recognition following human pulvinar damage. Neuropsychologia *45*, 1973–1978.

White, B.J., Kan, J.Y., Levy, R., Itti, L., and Munoz, D.P. (2017). Superior colliculus encodes visual saliency before the primary visual cortex. PNAS 201701003.

Wilke, M., Turchi, J., Smith, K., Mishkin, M., and Leopold, D.A. (2010). Pulvinar Inactivation Disrupts Selection of Movement Plans. J. Neurosci. *30*, 8650–8659.

Williford, T., and Maunsell, J.H.R. (2006). Effects of Spatial Attention on Contrast Response Functions in Macaque Area V4. Journal of Neurophysiology *96*, 40–54.

Wilson, D.E., Smith, G.B., Jacob, A.L., Walker, T., Dimidschstein, J., Fishell, G., and Fitzpatrick, D. (2017). GABAergic Neurons in Ferret Visual Cortex Participate in Functionally Specific Networks. Neuron *93*, 1058-1065.e4.

Wimborne, B.M., and Henry, G.H. (1992). Response characteristics of the cells of cortical area 21a of the cat with special reference to orientation specificity. J Physiol *449*, 457–478.

Xia, S., Li, X., Kimball, A.E., Kelly, M.S., Lesser, I., and Branch, C. (2012). Thalamic shape and connectivity abnormalities in children with attention- deficit/hyperactivity disorder. Psychiatry Research: Neuroimaging *204*, 161–167.

Xing, D., Yeh, C.-I., and Shapley, R.M. (2010). Generation of Black-Dominant Responses in V1 Cortex. J. Neurosci. *30*, 13504–13512.

Yau, J.M., Pasupathy, A., Brincat, S.L., and Connor, C.E. (2013). Curvature Processing Dynamics in Macaque Area V4. Cereb Cortex *23*, 198–209.

Yeh, C.-I., Xing, D., Williams, P.E., and Shapley, R.M. (2009a). Stimulus ensemble and cortical layer determine V1 spatial receptive fields. PNAS *106*, 14652–14657.

Yeh, C.-I., Xing, D., and Shapley, R.M. (2009b). "Black" Responses Dominate Macaque Primary Visual Cortex V1. J. Neurosci. *29*, 11753–11760.

Yu, C., Sellers, K.K., Radtke-Schuller, S., Lu, J., Xing, L., Ghukasyan, V., Li, Y., Shih, Y.-Y.I., Murrow, R., and Frohlich, F. (2015). Structural and Functional Connectivity between the Lateral Posterior-Pulvinar Complex and Primary Visual Cortex in the Ferret. Eur J Neurosci n/a-n/a.

Zabouri, N., Ptito, M., and Casanova, C. (2008). Complex motion sensitivity of neurons, in the visual part of the anterior ectosylvian cortex in cats. Neuroscience *152*, 106–118.

Zhao, Y., Kerscher, N., Eysel, U., and Funke, K. (2001). Changes of contrast gain in cat dorsal lateral geniculate nucleus by dopamine receptor agonists. NeuroReport *12*, 2939–2945.

Zhou, H., Schafer, R.J., and Desimone, R. (2016). Pulvinar-Cortex Interactions in Vision and Attention. Neuron *89*, 209–220.

Zhou, N., Maire, P.S., Masterson, S.P., and Bickford, M.E. (2017a). The mouse pulvinar nucleus: Organization of the tectorecipient zones. Visual Neuroscience *34*.

Zhou, N., Masterson, S.P., Damron, J.K., Guido, W., and Bickford, M.E. (2017b). The mouse pulvinar nucleus links the lateral extrastriate cortex, striatum, and amygdala. J. Neurosci. 1279–17.

SUPPLEMENTARY MATERIAL

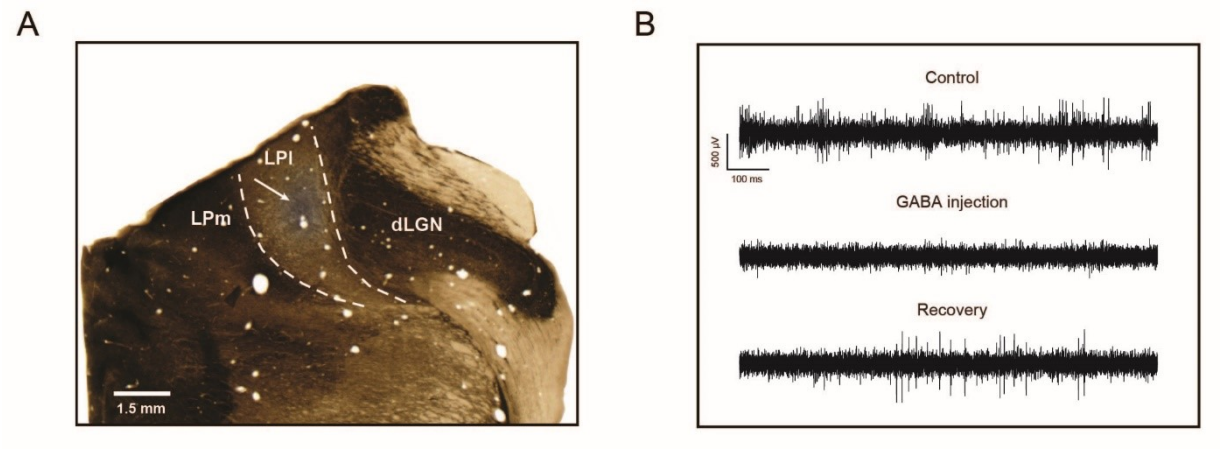

Figure S1. Validation of GABA injection in LP nucleus. A) Acetylchlolinesterase staining of cat thalamus showing the extent of GABA injection in the lateral subdivision of LP (arrow). B) Extract of high-passed signal recordings from GABA injection site during control, injection and recovery using a custom build injectrode (Lai et al. 2015). Successful inhibition of local neuronal population was achieved during GABA injection. After cessation of the injection, a recovery of neuronal activity was observed.

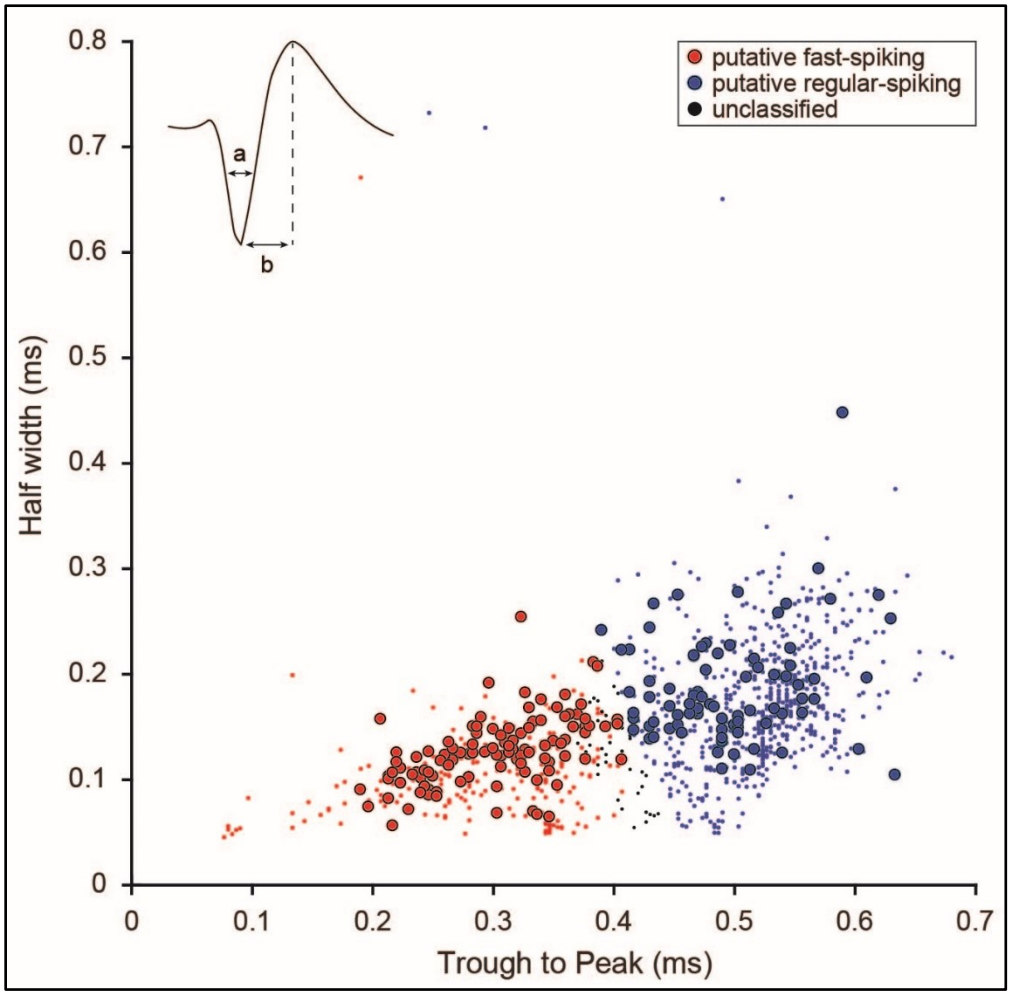

Figure S2. Spike waveform classification. Neurons were classified into two categories, regular (RS) and fast-spiking (FS) using the half width of the negative deflection (a) and the time between the negative peak and the following positive peak (trough to peak, b) of the spike waveform as parameters (Sakata and Harris 2009). K-means clustering algorithm was used to group the data into two clusters. Silhouette values were used to assess the quality of the clustering. Neurons with silhouette values lower than zero were considered as unclassified. Small dots represent all units used in the spike waveform analysis (N = 823) while large dots represent those kept for the analysis of the contrast response function (N = 200).

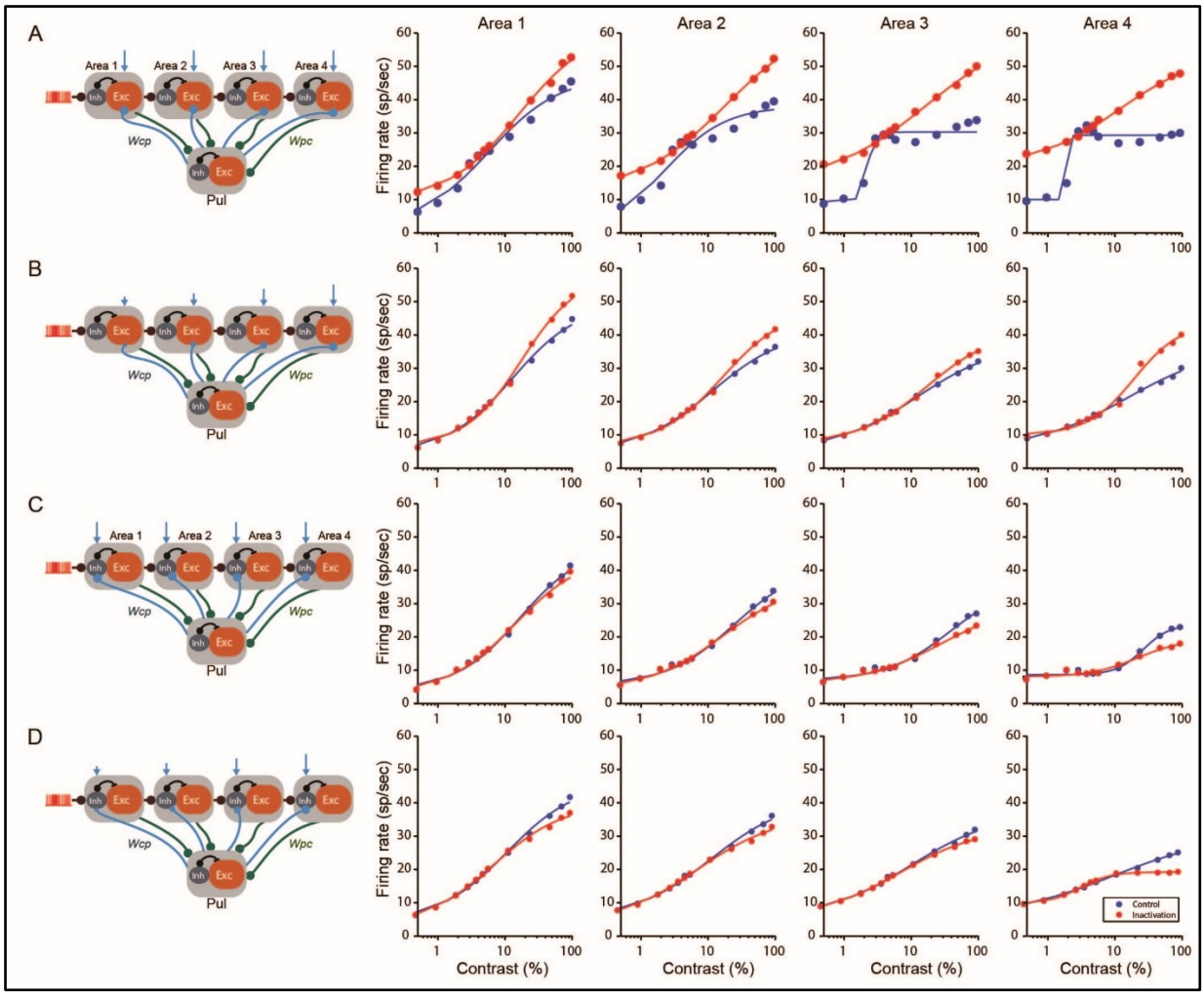

Figure S3. Settings of the transthalamic pathway. Different arrangements of connections to explain the modulation of response gain. The corticothalamic strength of connections is fixed, while the force of thalamocortical projections varies for population targeted. A) Contrast response function (CRF) of neurons when only the excitatory populations are targeted, and the strength of the connections is homogeneous. B) CRF of neurons when only the excitatory populations are targeted, and the strength of the connections increases from lower to higher areas. C) CRF of neurons when only the inhibitory populations are targeted, and the strength of the connections is homogeneous. D) CRF of neurons when only the inhibitory populations are targeted, and the strength of the connections increases from lower to higher areas.

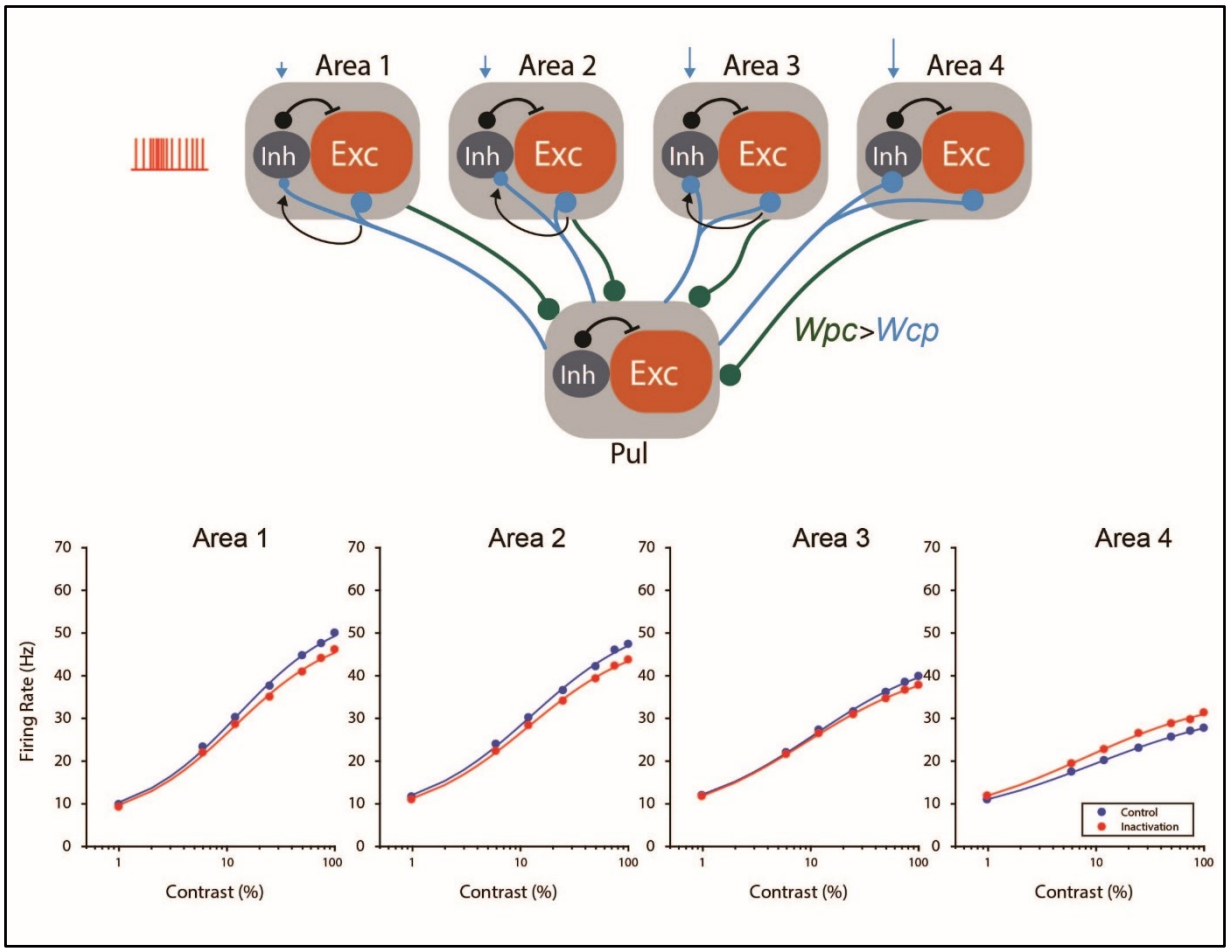

Figure S4. Reciprocal connections provide a symmetrical solution when the net effect of GABA in the LP is inhibitory. In this network, LP connections target primarily cortical excitatory populations, and LP-cortical projections are weaker than cortico-LP. This arrangement of strengths produces that the system responds qualitatively as a part our experimental findings. In this new regime, the LP output can still modulate the firing rate of cortical neurons, preserving the thalamic gain control mechanism into cortical neurons. Thus, this symmetrical quality of our theoretical thalamocortical system can also explain the net inactivation of the LP neurons by the injection of GABA.

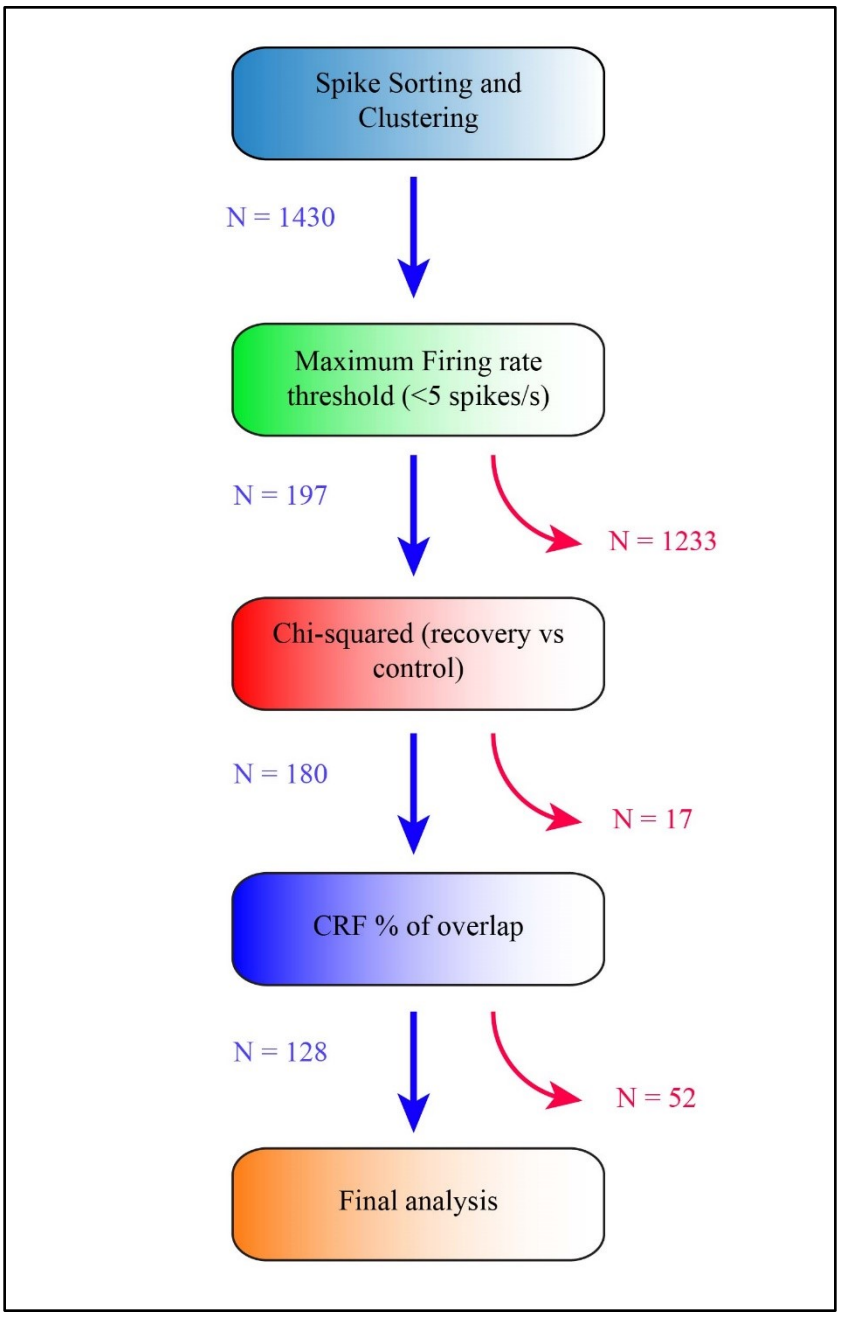

Figure S5. Workflow of exclusion criteria used in the study. Details of each step are described in methods. Blue and red arrows indicate included and excluded units at each step.

Tables

Table S1. Effect of LPl inactivation on the CRF parameters of neurons from area 17. Descriptive statistics (mean (median) ± SEM) and significance level (p-value, Z-value, Wilcoxon signed rank test) of CRF parameters comparison between control (Ctr) and LPl inactivation (Inj) are shown.

	Facilitated			**Suppressed**			**Total**		
	Ctr	**Inj**	***p*(z)**	**Ctr**	**Inj**	***p*(z)**	**Ctr**	**Inj**	***p*(z)**
Rmax	0.77(0.78) ± 0.05	1.31(1.07) ± 0.16	**< 0.001 (-3.82)**	0.81(0.89) ± 0.04	0.54(0.58) ± 0.04	**< 0.001 (5.06)**	0,80(0,87) ± 0,03	0,82(0,7) ± 0,08	0.24 (1.17)
Baseline	0.33(0.31) ± 0.05	0.47(0.35) ± 0.07	**< 0.001 (-3.84)**	0.3(0.25) ± 0.04	0.19(0.14) ± 0.03	**< 0.001 (4.4)**	0.31(0.26) ± 0.03	0.3 (0.2) ± 0.04	0.38 (0.88)
C50	35.44(34.19) ± 2.83	43.68(39.1) ± 5.76	0.5 (-0.66)	38.06(34.76) ± 3.26	40.81(38.06) ± 3.61	0.19 (-1.29)	37.08(34.76) ± 2.29	41.88 (38.06) ± 3.09	0.15 (-1.43)
Slope	3.28(2.69) ± 0.42	3.00(2.14) ± 0.32	0.68 (0.41)	2.91(1.85) ± 0.33	3.27(2.02) ± 0.36	0.61 (-0.51)	3.04(1.98) ± 0.26	3.17 (2.09) ± 0.26	0.76 (-0.31)

Table S2. Percentage of variation (%Var) of CRF parameters of neurons from area 17 during LPl inactivation. The values of %Var for the facilitated, suppressed and all (total) units are shown separately. Values are expressed as Mean% (Median%) ± SEM, and positive and negative changes indicate a decrease or increase of the parameter during thalamic inactivation, respectively.

	Rmax	**Slope**	**C50**	**Baseline**
Facilitated	-22.10 (-19.99) ± 4.06	0.50 (-2.94) ± 6.24	-3.15 (1.75) ± 5.85	-18.15 (-15.32) ± 4.74
Suppressed	22.18 (18.09) ± 3.48	-3.52 (0) ± 5.38	-1.21 (-4.74) ± 3.63	18.72 (18.67) ± 4.08
Total	5.67 (7.36) ± 3.86	-2.02 (0) ± 4.07	-2.06 (-2.19) ±3 .13	4.98 (4.51) ± 3.87

Table S3. Percentage of variation (%Var) of CRF parameters of neurons from area 17 during LPl inactivation as a function of the cortical laminar position and neuronal physiological properties. Values are expressed as Mean% (Median%) ± SEM, and positive and negative changes indicate a decrease or increase of the parameter during thalamic inactivation, respectively.

	Rmax	Slope	C50	Baseline
Simple	6.77 (6.07) ± 6.92	-7.94 (-9.84) ± 8.00	-2.77 (-4.74) ± 6.47	0.11 (-3.74) ± 7.34
Complex	4.95 (8.57) ± 4.59	1.46 (0) ± 4.29	-1.61 (0.17) ± 3.13	8.08 (7.80) ± 4.29
RS	15.52 (19.31) ±7.18	-17.1 (-5.5) ± 7.2	-11.11 (-11.23) ± 5.15	-4.37 (0.17) ± 7.38
FS	-0.8 (0.69) ± 4.84	6.4 (2.4) ± 4.2	-1.36 (1.08) ± 3.23	9.8 (7.8) ± 4.51
Sup	-5.23 (-6.05) ± 6.56	11.41 (1.14) ± 8.04	4.44 (-3.28) ± 7.28	12.61 (15.04) ± 6.25
Deep	9.72 (10.95) ± 4.58	-7.27 (-2.45) ± 4.54	-4.48 (-1.18) ± 3.31	2.13 (1.28) ± 4.75

Table S4. Effect of LPl and LPm inactivation on the CRF parameters of neurons from area 21a. Descriptive statistics (mean (median) ± SEM) and significance level (p-value, Z-value, Wilcoxon signed rank test) of CRF parameters comparison between control (Ctr) and LPl inactivation (Inj) are shown. Results from the analysis of the combined datasets from LPl and LPm (LP) is shown.

	LPl			LPm		
	Ctr	**Inj**	***p*(z)**	**Ctr**	**Inj**	***p*(z)**
Rmax	0.59 (0.61) ± 0.05	0.98 (0.82) ± 0.12	**< 0.01 (-3.06)**	0.87 (0.92) ± 0.04	2.77 (2.8) ± 0.25	**< 0.001 (-4.87)**
Baseline	0.53 (0.59) ± 0.04	0.75 (0.81) ± 0.07	**< 0.001 (-4.38)**	0.22 (0.13) ± 0.04	0.38 (0.24) ± 0.06	**< 0.001 (-3.74)**
C50	39.73 (38) ± 4.44	39.63 (32.46) ± 4.58	0.91 (-0.11)	47.34 (39.78) ± 3.12	52.6 (54.23) ± 2.18	**<0.05 (-2.1)**
Slope	4.27 (6) ± 0.38	3.29 (2.39) ± 0.39	0.36 (0.91)	4.58(5.09) ± 0.23	3.53 (3.1) ± 0.3	**<0.05 (2.48)**

Table S5. Percentage of variation (%Var) of CRF parameters of neurons from area 21a during LPl and LPm inactivation as a function of the spike waveform classification - regular (RS) and fast-spiking (FS) cells- and laminar position – superior (Sup) vs deep layers. The values of %Var of the pooled dataset (LP) are shown. Values are expressed as Mean% (Median%) ± SEM, and positive and negative changes indicate a decrease or increase of the parameter during thalamic inactivation, respectively.

		Rmax	Slope	C50	Baseline
LPl	**RS**	-22.84 (-26.66) ± 9.68	31.26 (0) ± 10.44	-11.88 (-20.28) ± 10	-11.78 (-17.31) ± 5.47
	FS	-10.91 (-6.42) ± 4.91	0.37 (-0.46) ± 9.69	7.73 (-5.10) ± 11.51	-12.47 (-15.29) ± 3.68
LPm	**RS**	-39.95 (-48.38) ± 6.72	13.71 (20.06) ± 5.9	-2.37 (-6.52) ± 4.53	-37.56 (-37.77) ± 8.3
	FS	-55.25 (-60.25) ± 6.3	14.64 (0) ± 21.38	-14.03 (-2.12) ± 14.24	-26.22 (-32.12) ± 17.1
LPl	**Sup**	-46.55 (-50.03) ± 9.28	50.22 (63.96) ± 12.74	2.22 (-8.17) ± 11.67	-13.09 (-16.52) ± 5.70
	Deep	-9.71 (-8.92) ± 5.05	6.03 (0) ± 8.01	-1.69 (-5.94) ± 9.30	-11.99 (-15.62) ± 3.59
LPm	**Sup**	-49.75 (-52.35) ± 3.39	17.60 (20.71) ± 5.38	-12.42 (-9.93) ± 5.58	-38.77 (-35.63) ± 9.56
	Deep	-38.92 (-49.20) ± 8.37	12.45 (7.26) ± 7.69	-3.19 (-4.53) ± 4.70	-32.85 (-32.12) ± 10.83

8 Discussion

8.1 Results summary

The object of study in the present thesis was the area 21a of the cat ventral stream and how the pulvinar impacts its activity. First, we characterized the spatiotemporal response profile of 21a neurons to light increments (brights) and decrements (darks). We found that the receptive field of most neurons exhibited a preference to darks that was represented by larger OFF subfields with stronger responses to darks. In a second approach, we assessed the impact of LP pharmacological inactivation on the contrast response in area 21a and the primary visual cortex (area 17). The main effects of the inactivation were changes in the CRF dynamic range in both cortical areas. However, the contrast response dynamic range was slightly reduced in area 17 while it increased in area 21a.

8.1.1 Processing of brights and darks in area 21a

Light increments and decrements are distinctly processed across the early visual system. Indeed, evidence shows that the processing of darks is faster than brights in the retina and in the visual thalamus (Burkhardt, 2011; Burkhardt et al., 1998; Copenhagen et al., 1983; Jin et al., 2008; Nichols et al., 2013). However, in the primary visual cortex, neurons not only process darks faster (Komban et al., 2014) but also respond more strongly to light decrements (Yeh et al., 2009b). In addition to the neurophysiological evidence, this asymmetry in luminance processing is present at a perceptual level as dark stimuli are detected faster than brights. This suggests that the distinct processing of brights and darks is preserved across the visual hierarchy (Komban et al., 2011, 2014). Here, we tested this hypothesis by assessing the responses of neurons from area 21a to bright and dark stimuli.

We observed that the area 21a is composed mostly of neurons that respond preferentially to darks. This asymmetry was mainly constrained at the spatial level in which the neurons' receptive fields exhibited larger dark subfield. In addition, 21a neurons' responses to darks were significantly stronger than to brights. However, no significant differences were observed between the peak responses to brights and darks indicating that both stimuli are processed similarly in the temporal domain. Therefore, our results provide further neurophysiological evidence for the assumption that the preference for darks is preserved in higher order visual areas. That being said, we also showed that the asymmetries between bright and dark responses

are not the same across the visual system. For instance, while in early visual areas (i.e., retina and LGN) most differences were constrained to the temporal domain (faster processing of darks), in area 21a, the preference for darks was expressed as asymmetries in the spatial structure of the neurons' receptive fields and in response strength. Interestingly, stronger responses to darks were previously observed in neurons from supragranular layers from the primate V1 (Yeh et al., 2009b). These results suggest that the preference to darks observed in our study could originate from neurons at supragranular layers in the primary visual cortex, since they represent the main excitatory input to 21a (Conway et al., 2000; Dreher et al., 1993; Grant and Hilgetag, 2005; Michalski et al., 1993; Sherk, 1989).

Yet, our results raised another interesting question: are there any differences in luminance processing between areas from the ventral and dorsal streams? In previous studies from our lab, the responses to brights and darks of PMLS neurons were assessed (Piché et al., 2015). PMLS is considered as the gateway of the dorsal stream and a large body of evidence demonstrated that this area and area 21a are distinct in an anatomical and functional level (Dreher et al., 1993, 1996a). Similar to our findings in area 21a, the receptive field of PMLS neurons exhibits an asymmetric spatial structure with larger dark subfields showing stronger responses in comparison to brights. On the other hand, both the spatial and response strength asymmetries in area 21a were more important than in PMLS indicating that higher order areas process light increments and decrements differently. These observations support our hypothesis (see section 5.1) in which neurons from the ventral and dorsal streams exhibit distinct response properties regarding luminance encoding.

8.1.2 Impact of pulvinar inactivation on the CRF of neurons from area 17 and 21a

The pulvinar is a higher order thalamic nucleus involved in several complex processes such as visual attention and emotion-driven detection of visual stimuli (Maior et al., 2010; Saalmann et al., 2012; Ward et al., 2007; Zhou et al., 2016). Due to its extensive reciprocal connectivity with the cortex (Berson and Graybiel, 1983; Graybiel and Berson, 1980; Jones, 2001; Kaas and Lyon, 2007; Raczkowski and Rosenquist, 1981; Updyke, 1983), the presence

of the pulvinar creates a transthalamic pathway that parallels the well-known cortico-cortical transmission of visual information (Crick and Koch, 1998).

The thalamo-cortical projections can be classified into two main categories based on anatomical and physiological criteria: drivers and modulators (Abbott and Chance, 2005; Sherman and Guillery, 1998). Regarding the pulvinar, the nature of these connections remains elusive. Here, we addressed this issue by investigating the impact of the pharmacological inactivation of the LP nucleus in cats, a pulvinar homolog, on the response to contrast at two levels of the cortical hierarchy: the primary visual cortex (area 17) and a higher order area from the ventral stream (area 21a). The study of two distinct cortical areas allowed us to understand the nature of the pulvino-cortical inputs in those areas and to determine whether they differ across the cortical hierarchy. In addition, the use of the CRF as a measure of the neuronal input/output function served as a functional assessment of the net driver/modulator influence of the LP yielding linear and nonlinear effects in the contrast response of cortical neurons, respectively. Those linear/nonlinear changes in the neurons' CRFs were interpreted as driver/modulator effects.

Our results demonstrated that the LP inactivation yielded a mix of linear and nonlinear changes in areas 17 and 21a. However, the most predominant effects were nonlinear with changes in the response gain in both cortical areas. Despite this, those changes were distinct between areas. Indeed, while in area 17 the net effect of LP inactivation was translated as a slight reduction in the response gain, in area 21a, the opposite was observed with a great increase of the response gain.

In contrast with our initial hypothesis (see section 5.2), our results demonstrated that the pulvinar exerts mostly a modulatory influence on the cortical processing with distinct effects across the ventral stream. In addition, our results are in agreement with previous studies supporting the modulatory role of the pulvinar in the primary visual cortex and higher order cortical areas (Soares et al. 2004; Molotchnikoff and Shumikhina 1996 [but see Purushothaman et al. 2012]).

8.2 Methodological considerations

8.2.1 The animal model

In the present thesis, the experiments described in both studies were performed in cats. This animal model was extensively used in the past, such as in the seminal work by Hubel and Wiesel in the 1960s (Hubel and Wiesel, 1962), contributing to great advancements in the field of visual neuroscience. Still, the cat remains a suitable tool in the modern-day research to investigate the neuronal mechanisms underlying visual perception along with other animal models such as primates, rodents and other carnivore species (Bachatene et al., 2015; Le et al., 2014; Quax et al., 2017; Wilson et al., 2017).

Several aspects of the structure and functional organization of the cat visual cortex resemble those in primates (Payne, 1993). Common features include the presence of orientation and direction columns, hierarchical connectivity between areas and specialized high-level processing of visual features (e.g., global motion and form processing) segregated into parallel visual pathways (i.e., dorsal and ventral streams) (Dreher et al., 1996a; Li et al., 2000b; Scannell et al., 1995; Villeneuve et al., 2009). In addition, the cat LP-Pulvinar complex was extensively studied in the past and a large body of evidence on the anatomical and physiological properties of the pulvinar is available (Berson and Graybiel, 1983; Casanova and Savard, 1996; Casanova et al., 1989; Graybiel and Berson, 1980; Jones, 2001; Raczkowski and Rosenquist, 1981; Updyke, 1983). This makes the cat a suitable model for the investigation of the role of the pulvinar on the cortical processing of visual information.

Despite the similarities between cats and primates, it is important to point out that extrapolations from the results obtained in the cat should be taken carefully. For instance, in phylogenetic terms, carnivores are farther from primates than rodents, suggesting that the similarities observed between the cat and primate visual cortices are most likely to be the result of evolutionary convergence (Van Hooser, 2007). An example of the distinctions between the visual systems of cats and primates is the connectivity pattern of thalamocortical projections from the LGN. In cats, in addition to the projections to area 17, the LGN is directly connected to areas 18 and 19. In contrast, parallel projections from the primate LGN to areas V2 and V3 are significantly less prominent (Payne, 1993; Payne and Peters, 2002). Therefore,

understanding the similarities and distinctions between the functional structures of the visual systems in different species largely contributes to the knowledge of the underlying mechanisms that support the cortical processing of sensory information.

8.2.1.1 Potential influence of anaesthesia

The studies described in this thesis were performed using animals under anaesthesia. For instance, halothane was the anaesthetic agent used during the electrophysiological recordings in cat experiments. This volatile anaesthetic was chosen based on a previous study from our lab demonstrating that halothane induced less depression of cortical neurons in comparison with isofluorane, a commonly used anaesthetic in neuroscience research (Villeneuve and Casanova, 2003). Despite this, it is likely that the anaesthesia exerted some influence upon the neuronal responses in our experiments. Indeed, several effects of halothane and other anaesthetics on the visual system have been known for decades and recent studies continue to report the impacts of anaesthesia on the cortical activity in different species (Bahmani et al., 2014; Ikeda and Wright, 1974; Imas et al., 2004; Pack et al., 2001; Sellers et al., 2015; Uhl et al., 1980).

In the past, *in vivo* single-unit recordings had to be performed in anaesthetized animals due to the nature of the procedure. In a typical experiment, a craniotomy was performed and an electrode, often a varnished tungsten needle or a glass pipette, was inserted into the brain to acquire neuronal evoked potentials. Nowadays, due to technological advances in recording equipment (e.g., implantable chronic probes and miniaturized signal amplifiers) and computational power, *in vivo* single-unit electrophysiological recordings are suitable for awake preparations. This allowed the comparison of recordings performed under anaesthesia with those performed in awake setups (Aasebø et al., 2017; Durand et al., 2016).

Even though anaesthesia could introduce unknown artifacts while measuring the neuronal responses to visual stimuli, several neuronal properties – from the most basic to higher order ones – are present in anaesthetized animals and are comparable to those obtained in awake settings (Durand et al., 2016). This is true for the properties of neurons in the pulvinar (Bender, 1982; Casanova and Savard, 1996; Casanova et al., 1989; Chalupa et al., 1983; Merabet et al., 1998; Petersen et al., 1985).

In our study #2, we investigated the role of the pulvinar in cortical processing. The anaesthetized setting is particularly suitable for this study since the experimental setup involved several intracortical injections and recording of neuronal activity for long periods of time. These experiments would be very difficult to carry out in awake preparations, in particular with cats.

In addition, it is well known that the pulvinar is implicated in the attentional modulation of the visual cortex activity. Since there is no evidence that conscience is present during anaesthesia, our experimental setup represents an opportunity to investigate the impact of the pulvinar in the basic cortical processing of visual information without the interference of attentional modulation. However, the last statement does not preclude that the mechanisms revealed are not involved in attentional processes in awake animals.

8.2.2 Electrophysiological recordings of cortical neurons ensembles

In the two studies described in this thesis, the cortical activity was assessed by means of extracellular electrophysiological recordings of individual neurons. This recording technique is particularly suitable to assess neuronal responses during in vivo preparations in which action potentials (spikes) are recorded without the need to touch or penetrate the cellular membrane. Instead, the rationale of the technique is that the electrodes inserted in the neuropil are able to detect the spikes of neurons located in their immediate surroundings.

The extracellular acquisition of single units can be performed using different methods. In the case of our studies, we used two distinct approaches: single and multi-electrode probes. The first one consisted on the use of varnished tungsten electrodes with high impedances (>2MOhms) to isolate the signal from normally one or two units. The second approach was completely different. Multi-electrode probes consisted of a silicon needle where a number of low impedance (~ 1MOhm) electrodes – in our case, 32 contacts – are distributed in a specific topographical arrangement. Both approaches differ, not only in the number of electrodes inserted in the cortex at a time, but also in the method to isolate signals of individual neurons from the background noise.

The first approach was used in the study #1. The electrodes' high impedance allowed the detection of signals from few neurons located at close distance from their tip. One advantage of this method is that the isolation of spikes from single neurons is relatively simply done by

applying a threshold on the signal amplitude. On the other hand, some disadvantages are associated with the use of this recording method in *in vivo* preparations. Since the electrodes only record neurons very close to them, this technique is highly sensitive to cortical movements which could draw the neurons apart from the electrode, losing the signals over time. In an *in vivo* setting, there are several sources of such movements. For instance, the cortex is subject to movement artifacts caused by the respiration, heart beats or inflammation (i.e., cortical swelling). In the case of our study, several measures were taken in order to mitigate those artifacts. For instance, we applied a 3% solution of agar over the craniotomy to maintain some pressure over the cortex to reduce the movement artifacts caused by the respiration and heartbeats. In addition, we preserved as much dura mater as possible which helped to maintain pressure over the cortex. Cortical swelling was avoided by the administration of anti-inflammatory drugs (i.e., dexamethasone). Finally, the experimental setup itself was compatible with the use of high impedance single electrodes because the neurons were tested for a relatively short period of time, which reduced the risk of losing its signal due to slow drifts (e.g., cortical swelling).

In the experiments performed in the study #2, we used multi-electrode probes. The greatest advantages of this method include the large number of electrodes and lower impedance contacts that favour the detection of a larger number of units with less sensitivity to cortical movements. Additionally, the different arrangements of available probes allow the simultaneous recording of neurons located at distinct regions. For instance, in the case of our study, we used a linear probe with electrodes distributed across the cortical depth of areas 21a and 17 that could provide additional information regarding the relationship between cortical layers. On the other hand, the recording of a large number of electrodes generates a larger volume of data per experiment in comparison with the single electrode approach. Additionally, the use of these probes requires a more complex a posteriori processing of the data to isolate the signals from single neurons (i.e., spike sorting) which, therefore, requires larger computational power and is more time consuming.

8.2.2.1 Spike sorting

The spike sorting is a procedure that is essential for the isolation of neurons recorded through multi-electrode probes. In brief, it consists of three main steps. First, the raw broadband signal acquired is band passed for the visualization of higher frequencies (300 – 6000Hz). Then, a threshold is set in the amplitude of the signal in order to detect the spikes that pass the noise level. Finally, the spikes are separated based on their waveforms by means of a clustering algorithm. Normally, principal component analysis (PCA) or wavelet analysis is used to isolate single units during spike sorting (Rey et al., 2015). All this procedure can be performed through an automatic unsupervised procedure. In the case of our study, we used the klusta suite (Rossant et al., 2016), an open-source software package that performs an unsupervised spike detection and clustering by PCA followed by a manual validation through a graphical user interface (GUI). The GUI provided different tools such as the PCA plots and correlograms, which were crucial to verify the quality of spike separation and to apply corrections when needed.

Despite the advantages from the use of multi-site probes, its use was not without problems. For instance, in our study #2, several units were discarded because they were lost during the experiment. Although these electrodes are less sensitive to cortical drifts, they are still susceptible to it. In our case, the recordings were undertaken over long periods of time (sometimes more than five hours) which increased the possibility of losing the neuron's signal.

8.2.3 Reversible thalamic inactivation

In neuroscience, one way to understand the function of brain structures is through the interference of the neuronal circuity. One way of achieving this is by provoking permanent lesions in specific brain regions and to examine the neurophysiological changes associated with it (Bender and Butter, 1987; Chalupa et al., 1976; Gregoriou et al., 2014). Despite the advantages of this method and its undeniable contribution to the understanding of the brain physiology, current knowledge on neuronal plasticity indicates that lesions may induce significant changes in the neuronal circuitry which could influence the interpretation of the results (Fetter et al., 1988; Nahmani and Turrigiano, 2014). Alternatively, different methods were developed that reversibly impact the neuronal activity in the brain without causing permanent damage to the cells. Most common techniques involve the use of physical (cold), chemical (anesthetics or

pharmacological agents), magnetic (TMS) and, more recently, genetic (optogenetics or chemogenetics) approaches (Fenno et al., 2011; Kim et al., 2015; Lomber et al., 1999; Soares et al., 2004).

In our study #2, we used the technique of the reversible pharmacological inactivation of the LP nucleus by means of the injection of a GABA solution. This method was long established in our lab and previously used by others to reversibly inactivate deep brain regions such as the thalamus (Casanova, 2002; Shumikhina and Molotchnikoff, 1999; Soares et al., 2004). The technical aspects of the procedure vary among studies (Chen et al., 2001; Lai et al., 2015; Noudoost and Moore, 2011), but in principle, it consists of the slow infusion of the pharmacological agent in the brain tissue. Common methods include the use of iontophoresis and pressure-based injection systems (Hupé et al., 1999; Purushothaman et al., 2012; Wilke et al., 2010). In our study, we used a custom-built injection system that was coupled to an electrode (injectrode, Lai et al. 2015). The use of the injectrode allowed us to examine the thalamic inactivation during and after the GABA injection. Since GABA is quickly metabolized (Curtis and Johnston, 1974; Hupé et al., 1999), a continuous monitoring of the activity at the injection site was crucial in order to adjust the injection rate during the experiment. Another advantage of this method is that larger volumes of brain tissue can be inactivated. This was particularly interesting for our study given the fact that the LP is a large thalamic structure and the blockage of a greater group of neurons is needed to assess the net impact of this thalamic structure on cortical activity. The use of GABA in comparison with local anaesthetics (e.g., lidocaine) was preferred. For instance, GABA affects only the local neuronal network by bounding to $GABA_A$ and $GABA_B$ receptors, without affecting passing-by fibres (Curtis and Crawford, 1969; Hess and Murata, 1974), which happens when lidocaine, a sodium channel blocker, is used (Sandkühler and Gebhart, 1991). This was particularly important in our case since a large number of passing axons from the cortex to the superior colliculus is present in the LP-pulvinar complex area (Casanova, 2002).

8.3 Functional implications

8.3.1 The processing of light increments and decrements in the cat ventral stream

In the study #1, we demonstrated that the responses to light increments (brights) and decrements (darks) were distinct in area 21a in which the receptive field of neurons exhibited larger and stronger (i.e., greater response amplitude) dark subfields. To our knowledge, our study was the first to report a bias towards dark responses in a higher level cortical area of the ventral stream (area 21a). However, this kind of asymmetry between bright and dark responses was previously found by our group in area PMLS (Piché, Thomas, and Casanova 2013), in the thalamic nucleus LP (Piché et al., 2015) and by others in the primary visual cortex (Liu et al., 2007; Xing et al., 2010; Yeh et al., 2009b). Nonetheless, it is worth noting that the asymmetries observed in area 21a were considerably larger than those in PMLS and primary visual cortex. Taken together, these results suggest that a bias towards the detection of light decrements might be ubiquitous in the visual cortex but with varying degrees across the cortical hierarchy.

Distinctions between ON and OFF pathways were long known to exist in early visual areas such as the retina and LGN but they were mostly limited to differences between their temporal dynamic in which darks are processed faster than brights (Burkhardt, 2011; Burkhardt et al., 1998; Copenhagen et al., 1983; Jin et al., 2011, 2008; Nichols et al., 2013). More recently, this temporal asymmetry was equally demonstrated in neurons from the thalamorecipient layer IV of the cat area 17 (Komban et al., 2014). Nevertheless, these studies failed to show any significant differences between the response amplitude to light increments and decrements. Instead, dark-dominant responses were first observed in the supragranular layers (II/III) of the primary visual cortex (Xing et al., 2010; Yeh et al., 2009b), indicating that those features arise at cortical level and, as demonstrated by our results, are transmitted across the cortical hierarchy. Despite this, our findings indicate that the nature of the signals originated at the supragranular layers of the primary visual cortex is not the same between the dorsal and ventral streams. For instance, the comparison of the data from the study #1 with our previous study (Piché et al., 2015) indicates that area 21a and PMLS cortex process light increments and decrements differently. Interestingly, although neurons from both areas were dark dominant, neurons from

area 21a showed significantly larger asymmetries with dark subfields ~ 26% times larger with a response amplitude ~ 2.5 times greater than PMLS neurons.

Several properties of the connectivity and neuronal response features of area 21a and PMLS cortex indicate that these areas play distinct roles on the cortical processing of visual information (Conway et al., 2000; Dreher et al., 1993, 1996b, 1996c; Li et al., 2000a; Payne, 1993; Wimborne and Henry, 1992). For instance, most PMLS neurons respond to complex moving stimuli supporting the notion that this area participates in the high order processing of motion (Li et al., 2000b; Merabet et al., 2000). On the other hand, neurons from area 21a are more sensitive to the spatial features of complex visual stimuli (i.e., natural images) rather than motion suggesting that this area is concerned with higher level processing of form (Dreher et al., 1993; Kayser and Konig, 2006). In the context of the responses to light increments and decrements, the larger and stronger dark subfields of 21a neurons in comparison with PMLS neurons provide further evidence that these cortical areas encode distinct features of the visual scene. Therefore, one may suggest that the larger asymmetries on the spatial structure of neurons from area 21a could be associated with the functional specialization of this extrastriate area (form processing). Given that in early subcortical areas darks are processed faster than brights, one would expect that this temporal asymmetry would equally be transmitted across the cortical hierarchy (Komban et al., 2011, 2014). Our results are at odds with this assumption since neurons from area 21a exhibited similar response latencies to bright and dark stimuli. One possible explanation for this is that the lack of differences in the temporal domain could be associated with the functional specialization of area 21a (form processing). Since 21a encodes mostly spatial features of the visual information, it is likely – and expected – that the temporality of the stimulus might not be relevant for the visual processing in this area. A recent study demonstrated that the temporal dynamics of thalamic signals were crucial for the development of direction selectivity in cortical neurons (Lien and Scanziani, 2018). Given that the majority of neurons from area 21a lack direction selectivity (Mizobe et al., 1988; Tardif et al., 1996; Toyama et al., 1994; Vickery and Morley, 1997), one could hypothesize that the most relevant features for this area are related to the spatial aspect of the visual signal whereas no significant information is processed regarding the temporality of the visual stimulus. Still, we cannot rule out that potential differences in the temporal domain could be undetected by our methodological approach. For

instance, the smoothing process of the PSTH may decrease the temporal resolution of our analysis masking potential subtle differences between the latencies of brights and darks responses. This hypothesis is plausible given the fact that the latencies between brights and darks are relatively small in the primary visual cortex (3-14 ms; Komban et al. 2014).

In another study from our group, we investigated the responses of brights and darks in the LP thalamic nucleus (Piché et al., 2015). Interestingly, a large proportion of LP neurons exhibited receptive fields with dark subfields significantly larger than bright ones resembling those from area 21a. Given the fact that 21a receives projections from LP nucleus, it is likely that the latter contributes to the neuronal response properties in this cortical area. This hypothesis was tested in the study #2 where the impact of the LP inactivation on the CRF of 21a neurons was assessed.

Taken together, our findings and the data from the PMLS study contribute to the growing body of evidence demonstrating that the parallel processing of visual signals in early subcortical visual areas is selectively integrated in the primary visual cortex giving rise to new outputs that are transmitted across the dorsal and ventral streams (Figure 13; Nassi and Callaway 2009). In addition, our findings add to the growing body of neurophysiological evidence supporting the notion that the dark preference is a common feature of the visual system. Indeed, this dark bias was previously reported in different psychophysical experiments (Anstis et al., 2000; Bowen et al., 1989; Chubb and Nam, 2000; Komban et al., 2011; Motoyoshi et al., 2007). Interestingly, previous studies demonstrated that changes in luminance increments and decrements exerted more influence on the detection of static (Anstis et al. 2000; Motoyoshi et al. 2007) rather than moving stimuli (Edwards and Badcock 1994). Thus, our findings provide neurophysiological evidence to these studies supporting the notion that the dark preference could play a more important role in form recognition but less in motion detection.

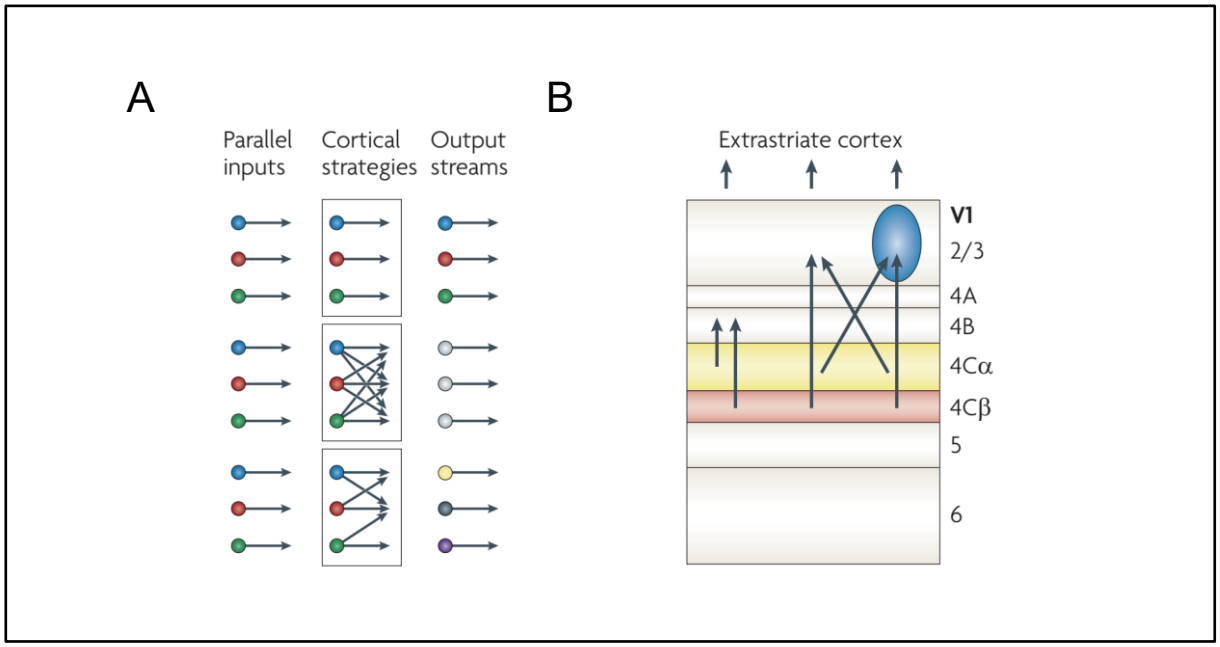

Figure 13. Putative models of cortical integration of visual inputs in primates. A) Possible cortical strategies for the processing of parallel inputs from early subcortical visual areas (i.e., retina and LGN) by V1 where the parallel signals remain segregated (top), are randomly integrated in V1 resulting in a homogenous output to higher levels areas (middle), are selectively integrated in V1 giving rise to new distinct parallel outputs (bottom). B) Representation of the integration of subcortical signals in V1 (as in the bottom scheme in A) where distinct parallel pathways (represented by the yellow and red areas in layer IV) are selectively integrated in supragranular layers (blue ellipsis representing a distinct subpopulation of neurons in layers II/III). Adapted from Nassi and Callaway (2009).

8.3.2 The role of pulvinar in the ventral stream

In the study #2, we characterized the impact of the inactivation of the lateral (LPl) and medial (LPm) subdivisions of the LP nucleus on the CRF of neurons from area 21a. For comparison, the effects of LPl inactivation on the CRF of neurons in the primary visual cortex (area 17) were assessed. Overall, the LP inactivation yielded distinct changes in the CRF profile in both cortical areas. For instance, the most noticeable effect was characterized by changes in the response gain (see Figure 6 in section 2.3 for an example). In area 21a, the inactivation of both LP subdivisions (LPl and LPm) yielded a significant increase in the neurons' CRF response gain. On the other hand, in area 17, although a larger variability of effects was observed across the neuronal population, the net impact of LPl inactivation on the CRF was represented as a slight decrease of the response gain.

In the context of our study, the comparison of the impact of LP inactivation on areas 21a and 17 allowed us to draw a more general portrait of the role of this higher order thalamic nucleus on the processing of visual information along the ventral stream. In order to achieve this, it was imperative to use one common visual stimulus that could be compared between cortical areas. In our study, drifting gratings with varying contrasts were used as a stimulus of choice which successfully elicited reliable responses from neurons in both cortical areas. Contrast sensitivity is present across several levels of the visual system (Duong and Freeman, 2008; Enroth-Cugell and Robson, 1966; Ohzawa et al., 1982) and responses to contrast were previously used to assess the role of neurotransmitters (Masson et al., 1993; Soma et al., 2012, 2013), visual adaptation (Gardner et al., 2005; King et al., 2016; Ohzawa et al., 1982) and attention (Avidan et al., 2002; Cutrone et al., 2014; Ling and Carrasco, 2006) on visual cortex processes, to name a few. One advantage of the CRF is that the changes observed in the neuronal responses can be straightforwardly explained by analysing the parameters of the model (Naka-Rushton function) applied to the dataset. In addition, the CRF could be interpreted as a measure of the product of the total thalamic synaptic input on a cortical neuron.

Alternatively to the predominantly anatomical-based classification of thalamocortical inputs (Sherman and Guillery, 2013b), Abbot and Chance (2005) proposed that drivers and modulators could be characterized respectively by linear (additive/subtractive) and nonlinear (multiplicative/divisive) effects of the total synaptic input to a neuron. In our study, we applied

the same principle in the analysis of the CRF in which contrast and baseline gains were interpreted as the result of driver inputs whereas response gains corresponded to modulatory effects.

In our initial hypothesis (see section 5.2), we predicted that the LP projections to area 21a would be mostly drivers. This hypothesis was based on previous anatomical evidence in other sensory modalities (auditory and somatosensory cortices), as well as in vision, supporting the notion that inputs from higher order thalamic nuclei to primary areas are mainly modulators whereas those projecting to extrastriate areas are drivers (Sherman and Guillery, 2013a). In addition, evidence suggests that thalamocortical driver inputs terminate mainly in layer IV while modulators terminate in layers I and VI (Felleman and Van Essen, 1991; Jones, 2001). In cats, LP projections to area 21a terminate mostly in layer IV with some in layer I whereas the projections to area 17 terminate mostly in layer I (Abramson and Chalupa, 1985). Thus, our hypothesis was that the LP inputs to area 21a would be mostly drivers while those projecting to area 17 would be modulators. However, our results are at odds with this assumption as the net impact of the LP projections to area 21a was found to be modulatory. Despite this, it is noteworthy to point out that, at the single unit level, both driver and modulator effects were observed on the CRF across the neuronal population of both cortical areas. Thus, one cannot rule out the possibility that a certain percentage of LP projections could be drivers even though the net impact of the LP inactivation was predominantly modulatory in areas 21a and 17.

Similarly to our findings, previous studies indicated that the pulvinar inputs to extrastriate areas can be modulatory (Minville and Casanova, 1998; Soares et al., 2004; Zhou et al., 2016). For instance, Soares et al. (2004) assessed the impact of pulvinar inactivation on the neuronal activity of the primate extrastriate area V2. Interestingly, the main effect of the thalamic inactivation was modulatory where most changes were limited to the neurons' orientation and direction tunings. In addition, a previous study from our lab (Minville and Casanova, 1998) showed that the LP inactivation had a small impact on basic properties of PMLS neurons (e.g., spatial frequency and direction tunings), indicating that the former does not participate on the creation of basic receptive field structure of neurons in this higher order visual area which is not compatible with a driver input. In contrary, other studies have shown a greater impact of pulvinar inactivation on the activity of striate and extrastriate visual areas which could be

interpreted as a driver input. For instance, Purushothaman et al. (2012) investigated the impact of pulvinar inactivation in the responses of neurons from the supragranular layers of the primate V1. Surprisingly, they observed a striking reduction of the neuronal spontaneous and evoked activity due to the injection of a $GABA_A$ agonist, muscimol, in the lateral pulvinar of a bush baby monkey (*Otolemur garnettii*). These results suggest that the pulvinar would be essential for the activity of neurons in this region which can be interpreted as a driver input. Our findings disagree with this assumption since the main impact of LP inactivation in area 17 was characterized as a decreased response gain (i.e., modulatory). Nonetheless, our findings from the study #2 could provide an explanation for the seemingly driver effect of pulvinar on V1. For instance, in their study, the impact of pulvinar inactivation was assessed using a fixed contrast level of 50%. In our study, the effects of LPl inactivation on the CRF of neurons from area 17 were observed in contrast levels ranging from about 25 to 100%. Thus, the reduction of the neuronal activity at 50% contrast could be a result of a decrease in the neuron's response gain.

Previous studies have demonstrated that attentional modulation yielded distinct changes in the CRF of neurons from the primate homolog of the cat area 21a, area V4 (Reynolds and Desimone, 1999; Reynolds et al., 2000; Williford and Maunsell, 2006). For instance, Williford and Maunsel (2006) observed similar results to our study where the attentional modulation yielded mostly changes in the response gain of V4 neurons. Interestingly, evidence indicates that the pulvinar plays a central role on complex modulatory mechanisms of the visual signal such as attention and visual salience (Desimone et al., 1990; Petersen et al., 1987; Robinson and Petersen, 1992; Saalmann and Kastner, 2009, 2011; Saalmann et al., 2012; Snow et al., 2009). Indeed, a recent study investigated the role of the pulvinar on the attentional modulation of V4 neurons (Zhou et al., 2016). Unsurprisingly, they observed that the pulvinar inactivation significantly impaired the animals' performance during attentional tasks. Moreover, the neuronal activity in area V4 was reduced during trials with and without attentional demand suggesting that the pulvinar is not only involved in the attentional modulation but also on basic visual processing in V4. Indeed, in our study, since the animals were anaesthetized, we assumed that the cortical activity was not influenced by attentional mechanisms. Thus, our results are aligned with the notion that the pulvinar is not a simple relay of the attentional modulation network but is also actively implicated in the visual processing of the ventral stream.

In nature, the fast detection of behaviourally relevant stimuli among non-relevant ones is crucial for an individual's survival. Generally, the visual environment is composed of several distinct visual stimuli, and knowing which one is relevant is a complex task in which the pulvinar is actively implicated (Robinson and Petersen, 1992). Indeed, previous neurophysiological studies in primates and psychophysical studies in humans with pulvinar lesions demonstrated several impairments in the detection and discrimination of visual stimuli in the presence of distractors (Chalupa et al., 1976; Robinson and Petersen, 1992; Snow et al., 2009; Ward et al., 2002; Zhou et al., 2016). For instance, Snow et al. (Snow et al., 2009) compared the performance of two patients with lesions in the ventral part of the pulvinar with normal subjects in a visual discrimination tasks. As expected, the lesioned patients underperformed in comparison with the control subjects when the targeted visual stimulus was presented along with a distractor. However, when the contrast of the distractors was reduced, or the contrast of the target was increase, the patients performed better in the task. These results suggest that the pulvinar plays a role on the modulation of the visual salience, either by filtering out irrelevant stimuli or increasing the salience of relevant ones, by means of a contrast modulation mechanism. In our study #2, the contrast responses of cortical neurons were deeply impacted by the pulvinar inactivation. Thus, our findings provide an explanation for the mechanisms underlying the modulation of stimulus salience by the pulvinar. Nonetheless, it is worth noting that our study was focused on one particular aspect of the visual processing (i.e., contrast). Thus, one cannot rule out the possibility that other visual features are impacted by the pulvinar inactivation. For instance, in monkeys and humans, a large number of cortical areas from the ventral stream are functionally connected to subdivisions of the ventral pulvinar (Arcaro et al., 2018; Kaas and Lyon, 2007; Shipp, 2003). In addition, groups of neurons in the pulvinar were selectively activated by complex visual stimuli (e.g., faces and body parts) that are known to be processed in areas from the ventral stream (Maior et al., 2010; Miller et al., 2017; Morin et al., 2015; Nguyen et al., 2013). Thus, one may hypothesize that the pulvinar inactivation could impact the cortical activity at more complex levels of the visual processing in the ventral stream.

8.4 Future investigations

The studies described in the present thesis contributed to a better comprehension of the mechanisms underlying the neuronal processing of visual information in the cat ventral stream. In addition, we added to the current knowledge on the role of the pulvinar on the modulation of the neuronal activity in the ventral stream and in the primary visual cortex. Nevertheless, our findings allowed the proposition of new questions about functional properties of the cat ventral stream and its relationship with the pulvinar. Therefore, different research avenues are open in order to pursue a more complete understanding of the visual cortex functional organization as a whole. Some possible research projects are proposed here.

8.4.1 The origin of the response profile of 21a neurons to brights and darks

In our study #1, one of the putative mechanisms for the response profile of 21a neurons to brights and darks was a significant contribution of neurons from the supragranular layers of area 17. This assumption was based on previous studies in the primate (Xing et al., 2010; Yeh et al., 2009b). Despite the similarities of the structure and function of the primary visual cortex between primates and cats, it would be thoughtful to apply the same methodological approach from our study #1 in the cat area 17. This would not only provide more evidence for the understanding of the mechanisms underlying the responses in area 21a, but also complement the current knowledge (Jin et al., 2011; Komban et al., 2014) on the visual processing of brights and darks in the cat primary visual cortex.

Additionally, given the fact that LP and area 21a share similar response features to brights and darks (Piché, Thomas, and Casanova 2015; our study #1), it would be interesting to evaluate the contribution of the LP nucleus on the spatiotemporal response profile of 21a neurons. By combining the methodologies of the two studies described in the present thesis, we would be able to assess the impact of LP inactivation on the response to brights and darks in area 21a. This would allow us to better understand the contribution of this thalamic area on the spatiotemporal structure of 21a neurons' receptive fields. In fact, this was already part of our research project but, due to chronological constrains, we were not able to accomplish this goal before the conclusion of the present thesis.

8.4.2 Further characterization of 21a neuronal properties

Besides the changes in the CRF, it would be interesting to investigate more specific features of 21a neurons that would be more related to the processing of form. Despite the amount of information on the response properties of 21a neurons (Mizobe et al., 1988; Tardif et al., 1996; Toyama et al., 1994; Vickery and Morley, 1997), there area few studies that tested the responses of neurons from this area to complex visual stimuli such as natural images (Kayser and Konig, 2006). In contrast, several studies characterized the neuronal properties of the primate area V4 (a homolog of area 21a) to complex visual stimuli (David et al., 2006; Gallant et al., 1993, 1996; Hegde and Felleman, 2007). Therefore, despite the similarities between those areas, the limited knowledge on the response properties of 21a neurons makes it difficult to extrapolate certain observations from primate studies to the cat.

In order to address this issue, one interesting project would be the characterization of the response profile of 21a neurons to non-cartesian gratings. Differently to standard gratings, non-cartesian gratings are more complex stimuli that were found to be more adapted to test form processing (Gallant et al., 1996). Interestingly, previous studies in primates revealed that V4 neurons are selective to such visual stimulus type (David et al., 2006; Gallant et al., 1993, 1996; Hegde and Felleman, 2007). Thus, it is reasonable to hypothesize that 21a neurons would exhibit similar tuning for these complex stimuli. This hypothesis could be tested using different approaches. For instance, the single-unit response profile could be obtained by means of electrophysiological techniques such as those used in the studies from the present thesis. In addition, optical imaging of intrinsic signals (technique used in co-authored publications; see Appendix) could be used to assess the overall response magnitude to non-cartesian gratings. Indeed, in a previous study from our lab, optical imaging was used in order to reveal the modular organization of area 21a to orientation (Villeneuve et al., 2009). Thus, it would be interesting to investigate if similar modular structure (i.e., orientation columns) would be present for non-cartesian gratings as well.

Another potential research avenue would be to further investigate the receptive field properties of area 21a neurons. For instance, one of the advantages of the reverse correlation method used in the study #1 is that one can correlate the several features of a neuron's receptive field with its basic properties such as spatial frequency and orientation tuning. Unfortunately, the sparse noise

stimulus used in our study does not provide any information regarding the neuronal response properties to gratings of complex-like cells in area 21a (DeAngelis et al., 1993b). One solution for this is to use more sophisticated/appropriate reverse correlation methods (Borghuis et al., 2003; Nishimoto et al., 2005, 2006; Richert et al., 2013; Tao et al., 2012). For instance, the receptive field structure of complex cells from cat areas 17 and 18 was previously analysed using a tertiary white noise stimulus and a local spectral reverse correlation method (Nishimoto et al., 2006; Tao et al., 2012). We believe that this could represent an useful tool to investigate the receptive field structure of neurons from area 21a.

8.4.3 The role of LP on the cortical oscillations in the cat ventral stream

Previous studies indicate that the pulvinar participates actively in the synchronization of the oscillatory activity between cortical areas (Molotchnikoff and Shumikhina, 1996; Saalmann and Kastner, 2009, 2011; Saalmann et al., 2012; Shumikhina and Molotchnikoff, 1999; Zhou et al., 2016). This phenomenon was previously observed in primates during attention demanding tasks (Saalmann et al., 2012; Zhou et al., 2016). Furthermore, previous studies in anesthetized cats have shown that the LP inactivation yielded profound changes in the oscillatory activity of areas 17 and 18 (Molotchnikoff and Shumikhina, 1996; Shumikhina and Molotchnikoff, 1999). In our context, it would be interesting to evaluate the impact of LP inactivation on the oscillatory patterns and synchronization between area 21a and area 17. This could be achieved by the analysis of local field potentials, from which the coherence between LP and the cortical areas would be compared. In addition, the simultaneous recording of the LP, area 17 and 21a would allow us to calculate the Granger causality which would give us an insight on the directionality of the signal between the areas implicated. In fact, in a subset of experiments in our study #2, we performed simultaneous recordings in both areas 21a and 17 during LP inactivation. Thus, these data can be used for the analysis of the impact of LP inactivation on the synchronization of oscillatory activity between those areas. Indeed, this project is currently being carried out by another member of our group.

9 Conclusion

The studies shown in the present thesis allowed a better comprehension of the hierarchical processing of visual information in the ventral stream. In addition, we contributed for a better understanding of the role of the pulvinar on the cortico-thalamo-cortical interactions between areas of the ventral stream. More specifically, the results of the study #1 showed that the dark preference in area 21a was mostly constrained to the spatial domain and to the response strength. In contrast with the data on the processing of brights and darks in the PMLS, a gateway area in the dorsal stream, the distinct response profile of 21a neurons observed in our study further contributes to the notion that this area plays an important role in form processing.

In addition, the study #2 provided evidence supporting the notion that the pulvinar is actively implicated in the processing of visual information across the ventral stream. Its influence on the cortex was characterized by a modulation of the cortical local processing by controlling the gain of the neuronal responses. Given the extensive connectivity of the pulvinar with several cortical areas processing high level features of the visual scene (complex motion, face recognition etc.), it is likely that this thalamic region is implicated in even higher level processes involved in sensory perception and even cognition (Saalmann and Kastner, 2011). Therefore, our studies support the idea that the classical "corticocentric" approach should be reviewed by including the pulvinar as an active part of the network in order to better understand the neurophysiological mechanisms underlying sensory perception.

While, our studies provided a greater understanding of the function of the cat ventral stream and the role of LP inputs in area 21a processing, a complete comprehension of the nature of the numerous reciprocal connections between this thalamic structure and the visual cortex remains to be attained.

10 References

Aasebø, I.E.J., Lepperød, M.E., Stavrinou, M., Nøkkevangen, S., Einevoll, G., Hafting, T., and Fyhn, M. (2017). Temporal Processing in the Visual Cortex of the Awake and Anesthetized Rat. ENeuro *4*.

Abbott, L.F., and Chance, F.S. (2005). Drivers and modulators from push-pull and balanced synaptic input. Progress in Brain Research *149*, 147–155.

Abramson, B.P., and Chalupa, L.M. (1985). The laminar distribution of cortical connections with the tecto- and cortico-recipient zones in the cat's lateral posterior nucleus. Neuroscience *15*, 81–95.

Abramson, B.P., and Chalupa, L.M. (1988). Multiple pathways from the superior colliculus to the extrageniculate visual thalamus of the cat. J. Comp. Neurol. *271*, 397–418.

Adams, M.M., Hof, P.R., Gattass, R., Webster, M.J., and Ungerleider, L.G. (2000). Visual cortical projections and chemoarchitecture of macaque monkey pulvinar. J. Comp. Neurol. *419*, 377–393.

Ajina, S., Kennard, C., Rees, G., and Bridge, H. (2015). Motion area V5/MT+ response to global motion in the absence of V1 resembles early visual cortex. Brain *138*, 164–178.

Albrecht, D., and Hamilton, D. (1982). Striate cortex of monkey and cat - contrast response function. J Neurophysiol *48*, 217–237.

Anstis, S.M., Smith, D.R.R., and Mather, G. (2000). Luminance processing in apparent motion, Vernier offset and stereoscopic depth. Vision Research *40*, 657–675.

Arcaro, M.J., Pinsk, M.A., Chen, J., and Kastner, S. (2018). Organizing principles of pulvino-cortical functional coupling in humans. Nature Communications *9*, 5382.

Arcizet, F., Jouffrais, C., and Girard, P. (2008). Natural textures classification in area V4 of the macaque monkey. Exp Brain Res *189*, 109–120.

Arend, I., Machado, L., Ward, R., McGrath, M., Ro, T., and Rafal, R.D. (2008). The role of the human pulvinar in visual attention and action: evidence from temporal-order judgment, saccade decision, and antisaccade tasks. In Progress in Brain Research, Christopher Kennard and R. John Leigh, ed. (Elsevier), pp. 475–483.

Avidan, G., Harel, M., Hendler, T., Ben-Bashat, D., Zohary, E., and Malach, R. (2002). Contrast Sensitivity in Human Visual Areas and Its Relationship to Object Recognition. Journal of Neurophysiology *87*, 3102–3116.

Bachatene, L., Bharmauria, V., Cattan, S., Chanauria, N., Rouat, J., and Molotchnikoff, S. (2015). Electrophysiological and firing properties of neurons: Categorizing soloists and choristers in primary visual cortex. Neuroscience Letters *604*, 103–108.

Bahmani, H., Murayama, Y., Logothetis, N.K., and Keliris, G.A. (2014). Binocular flash suppression in the primary visual cortex of anesthetized and awake macaques. PLoS ONE *9*, e107628.

Baldwin, M.K.L., Balaram, P., and Kaas, J.H. (2017). The evolution and functions of nuclei of the visual pulvinar in primates. J. Comp. Neurol. *525*, 3207–3226.

Bender, D. (1981). Retinotopic organization of macaque pulvinar. J Neurophysiol *46*, 672–693.

Bender, D. (1982). Receptive-field properties of neurons in the macaque inferior pulvinar. J Neurophysiol *48*, 1–17.

Bender, D., and Butter, C. (1987). Comparison of the effects of superior colliculus and pulvinar lesions on visual-search and tachistoscopic pattern-discrimination in monkeys. Experimental Brain Research *69*, 140–154.

Berman, R.A., and Wurtz, R.H. (2011). Signals Conveyed in the Pulvinar Pathway from Superior Colliculus to Cortical Area MT. J. Neurosci. *31*, 373–384.

Berson, D.M., and Graybiel, A.M. (1978). Parallel thalamic zones in the LP-pulvinar complex of the cat identified by their afferent and efferent connections. Brain Research *147*, 139–148.

Berson, D.M., and Graybiel, A.M. (1980). Some cortical and subcortical fiber projections to the accessory optic nuclei in the cat. Neuroscience *5*, 2203–2217.

Berson, D.M., and Graybiel, A.M. (1983). Organization of the striate-recipient zone of the cat's lateralis posterior-pulvinar complex and its relations with the geniculostriate system. Neuroscience *9*, 337–372.

Bickford, M.E. (2016). Thalamic Circuit Diversity: Modulation of the Driver/Modulator Framework. Frontiers in Neural Circuits 86.

Blanke, O., Landis, T., Safran, A.B., and Seeck, M. (2002). Direction-specific motion blindness induced by focal stimulation of human extrastriate cortex. European Journal of Neuroscience *15*, 2043–2048.

Boire, D., Matteau, I., Casanova, C., and Ptito, M. (2004). Retinal projections to the lateral posterior-pulvinar complex in intact and early visual cortex lesioned cats. Exp Brain Res *159*, 185–196.

Bokor, H., Frère, S.G.A., Eyre, M.D., Slézia, A., Ulbert, I., Lüthi, A., and Acsády, L. (2005). Selective GABAergic Control of Higher-Order Thalamic Relays. Neuron *45*, 929–940.

Borghuis, B.G., Perge, J.A., Vajda, I., van Wezel, R.J.A., van de Grind, W.A., and Lankheet, M.J.M. (2003). The motion reverse correlation (MRC) method:: A linear systems approach in the motion domain. Journal of Neuroscience Methods *123*, 153–166.

Bowen, R.W., Pokorny, J., and Smith, V.C. (1989). Sawtooth contrast sensitivity: Decrements have the edge. Vision Research *29*, IN1-1509.

Boynton, G.M. (2005). Contrast Gain in the Brain. Neuron *47*, 476–477.

Bridge, H., Leopold, D., and Bourne, J. (2015). Adaptive Pulvinar Circuitry Supports Visual Cognition. Trends Cogn Sci *20*, 146–157.

Brosseau-Lachaine, O., Faubert, J., and Casanova, C. (2001). Functional Sub-regions for Optic Flow Processing in the Posteromedial Lateral Suprasylvian Cortex of the Cat. Cereb Cortex *11*, 989–1001.

Burke, Dreher, and Wang (1998). Selective block of conduction in Y optic nerve fibres: significance for the concept of parallel processing. European Journal of Neuroscience *10*, 8–19.

Burkhardt, D.A. (2011). Contrast processing by ON and OFF bipolar cells. Visual Neuroscience *28*, 69–75.

Burkhardt, D.A., Fahey, P.K., and Sikora, M. (1998). Responses of ganglion cells to contrast steps in the light-adapted retina of the tiger salamander. Visual Neuroscience *15*, 219–229.

Byne, W., Fernandes, J., Haroutunian, V., Huacon, D., Kidkardnee, S., Kim, J., Tatusov, A., Thakur, U., and Yiannoulos, G. (2007). Reduction of right medial pulvinar volume and neuron number in schizophrenia. Schizophrenia Research *90*, 71–75.

Campos-Ortega, J., Hayhow, W., and Cluver, P. (1970). A note on the problem of retinal projections to the inferior pulvinar nucleus of primates. Brain Research *22*, 126–130.

Casanova, C. (1993). Response properties of neurons in area-17 projecting to the striate-recipient zone of the cats lateralis posterior-pulvinar complex - comparison with cortico-tectal cells. Experimental Brain Research *96*.

Casanova, C. (2002). In search of the role of extrageniculate cortico-thalamic loops in visual processing using deactivation techniques. In Virtual Lesions: Understanding Behaviour and Perception with Reversible Deactivation Techniques, S.G. Lomber, and R.A.W. Galuske, eds. (New York: Oxford University Press), pp. 61–81.

Casanova, C. (2004). The Visual Functions of the Pulvinar. In The Visual Neurosciences, (MIT Press), pp. 592–608.

Casanova, C., and Savard, T. (1996). Responses to moving texture patterns of cells in the striate-recipient zone of the cat's lateral posterior-pulvinar complex. Neuroscience *70*, 439–447.

Casanova, C., Freeman, R., and Nordmann, J. (1989). Monocular and binocular response properties of cells in the striate-recipient zone of the cats lateral posterior-pulvinar complex. J Neurophysiol *62*, 544–557.

Casanova, C., Savard, T., and Darveau, S. (1997). Contribution of area 17 to cell responses in the striate-recipient zone of the cat's lateral posterior-pulvinar complex. Eur. J. Neurosci. *9*, 1026–1036.

Casanova, C., Piché, M., and Ouellette, B. (2008). Spatiotemporal properties of LP-pulvinar visual receptive fields. J Vis *8*, 809–809.

Chalfin, B.P., Cheung, D.T., Muniz, J.A.P.C., de Lima Silveira, L.C., and Finlay, B.L. (2007). Scaling of neuron number and volume of the pulvinar complex in new world primates: Comparisons with humans, other primates, and mammals. J. Comp. Neurol. *504*, 265–274.

Chalupa, L.M., and Abramson, B.P. (1989). Visual receptive fields in the striate-recipient zone of the lateral posterior-pulvinar complex. J. Neurosci. *9*, 347–357.

Chalupa, L.M., Coyle, R.S., and Lindsley, D.B. (1976). Effect of pulvinar lesions on visual pattern discrimination in monkeys. Journal of Neurophysiology *39*, 354–369.

Chalupa, L.M., Williams, R.W., and Hughes, M.J. (1983). Visual response properties in the tectorecipient zone of the cat's lateral posterior-pulvinar complex: a comparison with the superior colliculus. J. Neurosci. *3*, 2587–2596.

Chen, L.L., Goffart, L., and Sparks, D.L. (2001). A simple method for constructing microinjectrodes for reversible inactivation in behaving monkeys. Journal of Neuroscience Methods *107*, 81–85.

Chichilnisky, E.J. (2001). A simple white noise analysis of neuronal light responses. Network *12*, 199–213.

Chubb, C., and Nam, J.-H. (2000). Variance of high contrast textures is sensed using negative half-wave rectification. Vision Research *40*, 1677–1694.

Churan, J., Guitton, D., and Pack, C.C. (2012). Spatiotemporal structure of visual receptive fields in macaque superior colliculus. Journal of Neurophysiology *108*, 2653–2667.

Conway, B., Boyd, J.D., Stewart, T.H., and Matsubara, J.A. (2000). The Projection from V1 to Extrastriate Area 21a: A Second Patchy Efferent Pathway that Colocalizes with the CO Blob Columns in Cat Visual Cortex. Cereb. Cortex *10*, 149–159.

Copenhagen, D.R., Ashmore, J.F., and Schnapf, J.K. (1983). Kinetics of synaptic transmission from photoreceptors to horizontal and bipolar cells in turtle retina. Vision Research *23*, 363–369.

Cowey, A., Stoerig, P., and Bannister, M. (1994). Retinal ganglion-cells labeled from the pulvinar nucleus in macaque monkeys. Neuroscience *61*, 691–705.

Crick, F., and Koch, C. (1998). Constraints on cortical and thalamic projections: the no-strong-loops hypothesis. Nature *391*, 245–250.

Curtis, D.R., and Crawford, J.M. (1969). Central synaptic transmission--microelectrophoretic studies. Annu Rev Pharmacol *9*, 209–240.

Curtis, D.R., and Johnston, G.A. (1974). Amino acid transmitters in the mammalian central nervous system. Ergeb Physiol *69*, 97–188.

Cusick, C.G., Scripter, J.L., Darensbourg, J.G., and Weber, J.T. (1993). Chemoarchitectonic subdivisions of the visual pulvinar in monkeys and their connectional relations with the middle temporal and rostral dorsolateral visual areas, MT and DLr. J. Comp. Neurol. *336*, 1–30.

Cutrone, E.K., Heeger, D.J., and Carrasco, M. (2014). Attention enhances contrast appearance via increased input baseline of neural responses. J Vis *14*, 16.

David, S.V., Hayden, B.Y., and Gallant, J.L. (2006). Spectral Receptive Field Properties Explain Shape Selectivity in Area V4. J Neurophysiol *96*, 3492–3505.

De Valois, R.L., Albrecht, D.G., and Thorell, L.G. (1982). Spatial frequency selectivity of cells in macaque visual cortex. Vision Res. *22*, 545–559.

DeAngelis, G.C., Ohzawa, I., and Freeman, R.D. (1993a). Spatiotemporal organization of simple-cell receptive fields in the cat's striate cortex. I. General characteristics and postnatal development. J Neurophysiol *69*, 1091–1117.

DeAngelis, G.C., Ohzawa, I., and Freeman, R.D. (1993b). Spatiotemporal organization of simple-cell receptive fields in the cat's striate cortex. II. Linearity of temporal and spatial summation. Journal of Neurophysiology *69*, 1118–1135.

DeAngelis, G.C., Ohzawa, I., and Freeman, R.D. (1995). Receptive-field dynamics in the central visual pathways. Trends in Neurosciences *18*, 451–458.

Delli Pizzi, S., Maruotti, V., Taylor, J.-P., Franciotti, R., Caulo, M., Tartaro, A., Thomas, A., Onofrj, M., and Bonanni, L. (2014). Relevance of subcortical visual pathways disruption to visual symptoms in dementia with Lewy bodies. Cortex *59*, 12–21.

Desimone, R., Wessinger, M., Thomas, L., and Schneider, W. (1990). Attentional control of visual perception: cortical and subcortical mechanisms. Cold Spring Harb. Symp. Quant. Biol. *55*, 963–971.

DeValois, K.K., DeValois, R.L., and Yund, E.W. (1979). Responses of striate cortex cells to grating and checkerboard patterns. The Journal of Physiology *291*, 483–505.

Dreher, B., Michalski, A., Ho, R.H., Lee, C.W., and Burke, W. (1993). Processing of form and motion in area 21a of cat visual cortex. Vis. Neurosci. *10*, 93–115.

Dreher, B., Wang, C., Turlejski, K.J., Djavadian, R.L., and Burke, W. (1996a). Areas PMLS and 21 a of Cat Visual Cortex: Two Functionally Distinct Areas. Cereb. Cortex *6*, 585–599.

Dreher, B., Djavadian, R.L., Turlejski, K.J., and Wang, C. (1996b). Areas PMLS and 21a of cat visual cortex are not only functionally but also hodologically distinct. Prog. Brain Res. *112*, 251–276.

Dreher, B., Wang, C., Turlejski, K.J., Djavadian, R.L., and Burke, W. (1996c). Areas PMLS and 21a of cat visual cortex: two functionally distinct areas. Cereb. Cortex *6*, 585–599.

Dumbrava, D., Faubert, J., and Casanova, C. (2001). Global motion integration in the cat's lateral posterior-pulvinar complex. European Journal of Neuroscience *13*, 2218–2226.

Duong, T., and Freeman, R.D. (2008). Contrast Sensitivity Is Enhanced by Expansive Nonlinear Processing in the Lateral Geniculate Nucleus. Journal of Neurophysiology *99*, 367–372.

Durand, S., Iyer, R., Mizuseki, K., Vries, S. de, Mihalas, S., and Reid, R.C. (2016). A Comparison of Visual Response Properties in the Lateral Geniculate Nucleus and Primary Visual Cortex of Awake and Anesthetized Mice. J. Neurosci. *36*, 12144–12156.

Eggermont, J.J., Johannesma, P.M., and Aertsen, A.M. (1983). Reverse-correlation methods in auditory research. Q. Rev. Biophys. *16*, 341–414.

Enroth-Cugell, C., and Robson, J.G. (1966). The contrast sensitivity of retinal ganglion cells of the cat. The Journal of Physiology *187*, 517–552.

Felleman, D.J., and Van Essen, D.C. (1991). Distributed Hierarchical Processing in the Primate Cerebral Cortex. Cerebral Cortex *1*, 1–47.

Fenno, L., Yizhar, O., and Deisseroth, K. (2011). The Development and Application of Optogenetics. Annual Review of Neuroscience *34*, 389–412.

Ferster, D. (1990). X- and Y-mediated current sources in areas 17 and 18 of cat visual cortex. Vis. Neurosci. *4*, 135–145.

Fetter, M., Zee, D.S., and Proctor, L.R. (1988). Effect of lack of vision and of occipital lobectomy upon recovery from unilateral labyrinthectomy in rhesus monkey. Journal of Neurophysiology *59*, 394–407.

Freund, T.F., Martin, K. a. C., and Whitteridge, D. (1985). Innervation of cat visual areas 17 and 18 by physiologically identified X- and Y- type thalamic afferents. I. Arborization patterns and quantitative distribution of postsynaptic elements. J. Comp. Neurol. *242*, 263–274.

Gallant, J.L., Braun, J., and Essen, D.V. (1993). Selectivity for polar, hyperbolic, and Cartesian gratings in macaque visual cortex. Science *259*, 100–103.

Gallant, J.L., Connor, C.E., Rakshit, S., Lewis, J.W., and Van Essen, D.C. (1996). Neural responses to polar, hyperbolic, and Cartesian gratings in area V4 of the macaque monkey. Journal of Neurophysiology *76*, 2718–2739.

Ganel, T., and Goodale, M.A. (2017). Still holding after all these years: An action-perception dissociation in patient DF. Neuropsychologia.

Gardner, J.L., Sun, P., Waggoner, R.A., Ueno, K., Tanaka, K., and Cheng, K. (2005). Contrast Adaptation and Representation in Human Early Visual Cortex. Neuron *47*, 607–620.

Gattass, R., Galkin, T.W., Desimone, R., and Ungerleider, L.G. (2013). Subcortical connections of area V4 in the macaque. Journal of Comparative Neurology n/a–n/a.

Gehring, W.J. (2014). The evolution of vision. Wiley Interdisciplinary Reviews: Developmental Biology *3*, 1–40.

Goodale, M.A., and Milner, A.D. (1992). Separate visual pathways for perception and action. Trends in Neurosciences *15*, 20–25.

Govindaiah, G., and Cox, C.L. (2006). Depression of retinogeniculate synaptic transmission by presynaptic D2-like dopamine receptors in rat lateral geniculate nucleus. European Journal of Neuroscience *23*, 423–434.

Grant, S., and Hilgetag, C.C. (2005). Graded classes of cortical connections: quantitative analyses of laminar projections to motion areas of cat extrastriate cortex. Eur. J. Neurosci. *22*, 681–696.

Graybiel, A.M., and Berson, D.M. (1980). Histochemical identification and afferent connections of subdivisions in the lateralis posterior-pulvinar complex and related thalamic nuclei in the cat. Neuroscience *5*, 1175–1238.

Green, M.F., Butler, P.D., Chen, Y., Geyer, M.A., Silverstein, S., Wynn, J.K., Yoon, J.H., and Zemon, V. (2009). Perception Measurement in Clinical Trials of Schizophrenia: Promising Paradigms From CNTRICS. Schizophr Bull *35*, 163–181.

Gregoriou, G.G., Rossi, A.F., Ungerleider, L.G., and Desimone, R. (2014). Lesions of prefrontal cortex reduce attentional modulation of neuronal responses and synchrony in V4. Nat Neurosci *17*, 1003–1011.

Grieve, K.L., Acuña, C., and Cudeiro, J. (2000). The primate pulvinar nuclei: vision and action. Trends in Neurosciences *23*, 35–39.

Grill-Spector, K., and Malach, R. (2004). The human visual cortex. Annu. Rev. Neurosci. *27*, 649–677.

Guillery, R.W., and Sherman, S.M. (2002). Thalamic Relay Functions and Their Role in Corticocortical Communication: Generalizations from the Visual System. Neuron *33*, 163–175.

Gulcebi, M.I., Ketenci, S., Linke, R., Hacıoğlu, H., Yanalı, H., Veliskova, J., Moshé, S.L., Onat, F., and Çavdar, S. (2012). Topographical connections of the substantia nigra pars reticulata to higher-order thalamic nuclei in the rat. Brain Research Bulletin *87*, 312–318.

Gutierrez, C., Cola, M.G., Seltzer, B., and Cusick, C. (2000). Neurochemical and connectional organization of the dorsal pulvinar complex in monkeys. J. Comp. Neurol. *419*, 61–86.

de Haan, E.H.F., and Cowey, A. (2011). On the usefulness of 'what' and 'where' pathways in vision. Trends in Cognitive Sciences *15*, 460–466.

Hamos, J.E., Van Horn, S.C., Raczkowski, D., and Sherman, S.M. (1987). Synaptic circuits involving an individual retinogeniculate axon in the cat. J. Comp. Neurol. *259*, 165–192.

Hartline, H.K. (1938). THE RESPONSE OF SINGLE OPTIC NERVE FIBERS OF THE VERTEBRATE EYE TO ILLUMINATION OF THE RETINA. American Journal of Physiology *121*, 400–415.

Hegde, J., and Felleman, D.J. (2007). A comparative study of shape representation in macaque visual areas V2 and V4. Cerebral Cortex *17*, 1100–1116.

Hess, R., and Murata, K. (1974). Effects of glutamate and GABA on specific response properties of neurones in the visual cortex. Exp Brain Res *21*, 285–297.

Hubel, D., and Wiesel, T. (1968). Receptive fields and functional architecture of monkey striate cortex. Journal of Physiology-London *195*, 215–243.

Hubel, D.H., and Wiesel, T.N. (1962). Receptive fields, binocular interaction and functional architecture in the cat's visual cortex. J Physiol *160*, 106-154.2.

Humphrey, A.L., Sur, M., Uhlrich, D.J., and Sherman, S.M. (1985). Projection patterns of individual X- and Y-cell axons from the lateral geniculate nucleus to cortical area 17 in the cat. J. Comp. Neurol. *233*, 159–189.

Hupé, J.M., Chouvet, G., and Bullier, J. (1999). Spatial and temporal parameters of cortical inactivation by GABA. J. Neurosci. Methods *86*, 129–143.

Huppé-Gourgues, F., Bickford, M. e., Boire, D., Ptito, M., and Casanova, C. (2006). Distribution, morphology, and synaptic targets of corticothalamic terminals in the cat lateral posterior-pulvinar complex that originate from the posteromedial lateral suprasylvian cortex. The Journal of Comparative Neurology *497*, 847–863.

Hutchins, B., and Updyke, B.V. (1989). Retinotopic organization within the lateral posterior complex of the cat. J. Comp. Neurol. *285*, 350–398.

Ikeda, H., and Wright, M.J. (1974). Sensitivity of neurones in visual cortex (area 17) under different levels of anaesthesia. Exp Brain Res *20*, 471–484.

Imas, O.A., Ropella, K.M., Wood, J.D., and Hudetz, A.G. (2004). Halothane augments event-related gamma oscillations in rat visual cortex. Neuroscience *123*, 269–278.

Isbell, L.A. (2006). Snakes as agents of evolutionary change in primate brains. Journal of Human Evolution *51*, 1–35.

Itaya, S., and Vanhoesen, G. (1983). Retinal projections to the inferior and medial pulvinar nuclei in the old-world monkey. Brain Research *269*, 223–230.

Jay Hegdé, and Daniel J. Felleman (2007). Reappraising the Functional Implications of the Primate Visual Anatomical Hierarchy. Neuroscientist *13*, 416–421.

Jin, J., Wang, Y., Lashgari, R., Swadlow, H.A., and Alonso, J.-M. (2011). Faster Thalamocortical Processing for Dark than Light Visual Targets. J. Neurosci. *31*, 17471–17479.

Jin, J.Z., Weng, C., Yeh, C.-I., Gordon, J.A., Ruthazer, E.S., Stryker, M.P., Swadlow, H.A., and Alonso, J.-M. (2008). On and off domains of geniculate afferents in cat primary visual cortex. Nat Neurosci *11*, 88–94.

Jones, E.G. (2001). The thalamic matrix and thalamocortical synchrony. Trends in Neurosciences *24*, 595–601.

Jones, J.P., and Palmer, L.A. (1987). The two-dimensional spatial structure of simple receptive fields in cat striate cortex. J Neurophysiol *58*, 1187–1211.

Jones, J.P., Stepnoski, A., and Palmer, L.A. (1987). The two-dimensional spectral structure of simple receptive fields in cat striate cortex. Journal of Neurophysiology *58*, 1212–1232.

Kaas, J.H., and Collins, C.E. (2001). The organization of sensory cortex. Current Opinion in Neurobiology *11*, 498–504.

Kaas, J.H., and Lyon, D.C. (2007). Pulvinar contributions to the dorsal and ventral streams of visual processing in primates. Brain Research Reviews *55*, 285–296.

Kandel, E.R., Schwartz, J.H., and Jessell, T.M. (2000). Principles of Neural Science (McGraw-Hill Medical).

Kawamura, S., Sprague, J.M., and Niimi, K. (1974). Corticofugal projections from the visual cortices to the thalamus, pretectum and superior colliculus in the cat. J. Comp. Neurol. *158*, 339–362.

Kayser, C. a, and Konig, P. a (2006). Feature selectivity in area 21a of the cat. [Miscellaneous Article]. Neuroreport May 29, 2006 *17*, 809–812.

Kim, T., Allen, E.A., Pasley, B.N., and Freeman, R.D. (2015). Transcranial magnetic stimulation changes response selectivity of neurons in the visual cortex. Brain Stimul *8*, 613–623.

King, J.L., Lowe, M.P., Stover, K.R., Wong, A.A., and Crowder, N.A. (2016). Adaptive Processes in Thalamus and Cortex Revealed by Silencing of Primary Visual Cortex during Contrast Adaptation. Current Biology *26*, 1295–1300.

Kobatake, E., and Tanaka, K. (1994). Neuronal selectivities to complex object features in the ventral visual pathway of the macaque cerebral cortex. Journal of Neurophysiology *71*, 856–867.

Komban, S.J., Alonso, J.-M., and Zaidi, Q. (2011). Darks Are Processed Faster Than Lights. J. Neurosci. *31*, 8654–8658.

Komban, S.J., Kremkow, J., Jin, J., Wang, Y., Lashgari, R., Li, X., Zaidi, Q., and Alonso, J.-M. (2014). Neuronal and Perceptual Differences in the Temporal Processing of Darks and Lights. Neuron *82*, 224–234.

Kravitz, D.J., Saleem, K.S., Baker, C.I., and Mishkin, M. (2011). A new neural framework for visuospatial processing. Nature Reviews Neuroscience *12*, 217.

Kuffler, S.W. (1953). Discharge Patterns and Functional Organization of Mammalian Retina. Journal of Neurophysiology *16*, 37–68.

Lai, J., Legault, M.-A., Thomas, S., and Casanova, C. (2015). Simultaneous Electrophysiological Recording and Micro-injections of Inhibitory Agents in the Rodent Brain. J Vis Exp.

Laties, A.M., and Sprague, J.M. (1966). The projection of optic fibers to the visual centers in the cat. Journal of Comparative Neurology *127*, 35–70.

Le, Q.V., Isbell, L.A., Matsumoto, J., Nguyen, M., Hori, E., Maior, R.S., Tomaz, C., Tran, A.H., Ono, T., and Nishijo, H. (2013). Pulvinar neurons reveal neurobiological evidence of past selection for rapid detection of snakes. PNAS *110*, 19000–19005.

Le, Q.V., Isbell, L.A., Matsumoto, J., Le, V.Q., Hori, E., Tran, A.H., Maior, R.S., Tomaz, C., Ono, T., and Nishijo, H. (2014). Monkey Pulvinar Neurons Fire Differentially to Snake Postures. PLoS ONE *9*, e114258.

Lee, C.C., and Sherman, S.M. (2008). Synaptic Properties of Thalamic and Intracortical Inputs to Layer 4 of the First- and Higher-Order Cortical Areas in the Auditory and Somatosensory Systems. J Neurophysiol *100*, 317–326.

Letinic, K., and Rakic, P. (2001). Telencephalic origin of human thalamic GABAergic neurons. Nature Neuroscience *4*, 931–936.

Li, B., Li, B.-W., Chen, Y., Wang, L.-H., and Diao, Y.-C. (2000a). Response properties of PMLS and PLLS neurons to simulated optic flow patterns. European Journal of Neuroscience *12*, 1534–1544.

Li, B., Li, B.-W., Chen, Y., Wang, L.-H., and Diao, Y.-C. (2000b). Response properties of PMLS and PLLS neurons to simulated optic flow patterns. European Journal of Neuroscience *12*, 1534–1544.

Li, X., Sroubek, A., Kelly, M.S., Lesser, I., Sussman, E., He, Y., Branch, C., and Foxe, J.J. (2012). Atypical Pulvinar–Cortical Pathways During Sustained Attention Performance in Children With Attention-Deficit/Hyperactivity Disorder. Journal of the American Academy of Child & Adolescent Psychiatry *51*, 1197-1207.e4.

Liddell, B.J., Brown, K.J., Kemp, A.H., Barton, M.J., Das, P., Peduto, A., Gordon, E., and Williams, L.M. (2005). A direct brainstem–amygdala–cortical 'alarm' system for subliminal signals of fear. NeuroImage *24*, 235–243.

Lien, A.D., and Scanziani, M. (2018). Cortical direction selectivity emerges at convergence of thalamic synapses. Nature *558*, 80–86.

Lin, C.-S., and Kaas, J.H. (1979). The inferior pulvinar complex in owl monkeys: Architectonic subdivisions and patterns of input from the superior colliculus and subdivisions of visual cortex. J. Comp. Neurol. *187*, 655–678.

Lin, C.-S., and Kaas, J.H. (1980). Projections from the medial nucleus of the inferior pulvinar complex to the middle temporal area of the visual cortex. Neuroscience *5*, 2219–2228.

Ling, S., and Carrasco, M. (2006). Sustained and transient covert attention enhance the signal via different contrast response functions. Vision Res *46*, 1210–1220.

Liu, S., Liu, Y.-J., and Li, B. (2007). Spatiotemporal structure of complex cell receptive fields and influence of GABAergic inhibition: NeuroReport *18*, 1577–1581.

Liu, X.-B., Honda, C. n., and Jones, E. g. (1995). Distribution of four types of synapse on physiologically identified relay neurons in the ventral posterior thalamic nucleus of the cat. Journal of Comparative Neurology *352*, 69–91.

Livingstone, M.S., Pack, C.C., and Born, R.T. (2001). Two-Dimensional Substructure of MT Receptive Fields. Neuron *30*, 781–793.

Lomber, S.G. (2001). Behavioral cartography of visual functions in cat parietal cortex: areal and laminar dissociations. Prog. Brain Res. *134*, 265–284.

Lomber, S.G., Payne, B.R., Cornwell, P., and Long, K.D. (1996). Perceptual and Cognitive Visual Functions of Parietal and Temporal Cortices in the Cat. Cereb. Cortex *6*, 673–695.

Lomber, S.G., Payne, B.R., and Horel, J.A. (1999). The cryoloop: an adaptable reversible cooling deactivation method for behavioral or electrophysiological assessment of neural function. Journal of Neuroscience Methods *86*, 179–194.

Lyon, D.C., Nassi, J.J., and Callaway, E.M. (2010). A Disynaptic Relay from Superior Colliculus to Dorsal Stream Visual Cortex in Macaque Monkey. Neuron *65*, 270–279.

Maior, R.S., Hori, E., Tomaz, C., Ono, T., and Nishijo, H. (2010). The monkey pulvinar neurons differentially respond to emotional expressions of human faces. Behavioural Brain Research *215*, 129–135.

Mason, R. (1981). Differential responsiveness of cells in the visual zones of the cat's LP-pulvinar complex to visual stimuli. Exp Brain Res *43*, 25–33.

Masson, G., Mestre, D., and Blin, O. (1993). Dopaminergic modulation of visual sensitivity in man. Fundam Clin Pharmacol *7*, 449–463.

Matteau, I., Boire, D., and Ptito, M. (2003). Retinal projections in the cat: A cholera toxin B subunit study. Visual Neuroscience *20*, 481–493.

May, K.A., and Solomon, J.A. (2015). Connecting psychophysical performance to neuronal response properties II: Contrast decoding and detection. Journal of Vision *15*, 9–9.

Meikle, T.H., and Sprague, J.M. (1964). THE NEURAL ORGANIZATION OF THE VISUAL PATHWAYS IN THE CAT. Int. Rev. Neurobiol. *6*, 149–189.

Merabet, L., Desautels, A., Minville, K., and Casanova, C. (1998). Motion integration in a thalamic visual nucleus. Nature *396*, 265–268.

Merabet, L., Minville, K., Ptito, M., and Casanova, C. (2000). Responses of neurons in the cat posteromedial lateral suprasylvian cortex to moving texture patterns. Neuroscience *97*, 611–623.

Michalski, A., Wimborne, B.M., and Henry, G.H. (1993). The effect of reversible cooling of cat's primary visual cortex on the responses of area 21a neurons. J Physiol *466*, 133–156.

Miller, K.J., Hermes, D., Pestilli, F., Wig, G.S., and Ojemann, J.G. (2017). Face percept formation in human ventral temporal cortex. Journal of Neurophysiology *118*, 2614–2627.

Milner, A.D. (2017). How do the two visual streams interact with each other? Exp Brain Res *235*, 1297–1308.

Minville, K., and Casanova, C. (1998). Spatial frequency processing in posteromedial lateral suprasylvian cortex does not depend on the projections from the striate-recipient zone of the cat's lateral posterior-pulvinar complex. Neuroscience *84*, 699–711.

Mishkin, M., and Ungerleider, L. (1982). Contribution of striate inputs to the visuospatial functions of parieto-preoccipital cortex in monkeys. Behavioural Brain Research *6*, 57–77.

Mishkin, M., Ungerleider, L.G., and Macko, K.A. (1983). Object vision and spatial vision: Two cortical pathways. Trends in Neurosciences *10*, 414–417.

Mizobe, K., Itoi, M., Kaihara, T., and Toyama, K. (1988). Neuronal responsiveness in area 21a of the cat. Brain Res. *438*, 307–310.

Molotchnikoff, S., and Shumikhina, S. (1996). The lateral posterior-pulvinar complex modulation of stimulus-dependent oscillations in the cat visual cortex. Vision Research *36*, 2037–2046.

Morin, E.L., Hadj-Bouziane, F., Stokes, M., Ungerleider, L.G., and Bell, A.H. (2015). Hierarchical Encoding of Social Cues in Primate Inferior Temporal Cortex. Cereb Cortex *25*, 3036–3045.

Morley, J.W., and Vickery, R.M. (1997). Spatial and temporal frequency selectivity of cells in area 21a of the cat. J Physiol *501*, 405–413.

Morley, J.W., and Vickery, R.M. (1999). Binocular interactions in area 21a of the cat. [Miscellaneous Article]. Neuroreport August 2, 1999 *10*, 2241–2244.

Motoyoshi, I., Nishida, S., Sharan, L., and Adelson, E.H. (2007). Image statistics and the perception of surface qualities. Nature *447*, 206–209.

Movshon, J.A., Thompson, I.D., and Tolhurst, D.J. (1978a). Spatial summation in the receptive fields of simple cells in the cat's striate cortex. The Journal of Physiology *283*, 53–77.

Movshon, J.A., Thompson, I.D., and Tolhurst, D.J. (1978b). Receptive field organization of complex cells in the cat's striate cortex. The Journal of Physiology *283*, 79–99.

Nahmani, M., and Turrigiano, G.G. (2014). Adult cortical plasticity following injury: Recapitulation of critical period mechanisms? Neuroscience *0*, 4–16.

Naito, J. (1986). Course of retinogeniculate projection fibers in the cat optic nerve. J. Comp. Neurol. *251*, 376–387.

Naka, K.I., and Rushton, W. a. H. (1966). S-potentials from colour units in the retina of fish (Cyprinidae). The Journal of Physiology *185*, 536–555.

Nassi, J.J., and Callaway, E.M. (2009). Parallel processing strategies of the primate visual system. Nature Reviews Neuroscience *10*, nrn2619.

Nguyen, M.N., Hori, E., Matsumoto, J., Tran, A.H., Ono, T., and Nishijo, H. (2013). Neuronal responses to face-like stimuli in the monkey pulvinar. Eur J Neurosci *37*, 35–51.

Nichols, Z., Nirenberg, S., and Victor, J. (2013). Interacting Linear and Nonlinear Characteristics Produce Population Coding Asymmetries between ON and OFF Cells in the Retina. J. Neurosci. *33*, 14958–14973.

Niimi, K., and Sprague, J.M. (1970). Thalamo-cortical organization of the visual system in the cat. Journal of Comparative Neurology *138*, 219–249.

Nishimoto, S., Arai, M., and Ohzawa, I. (2005). Accuracy of Subspace Mapping of Spatiotemporal Frequency Domain Visual Receptive Fields. Journal of Neurophysiology *93*, 3524–3536.

Nishimoto, S., Ishida, T., and Ohzawa, I. (2006). Receptive Field Properties of Neurons in the Early Visual Cortex Revealed by Local Spectral Reverse Correlation. J. Neurosci. *26*, 3269–3280.

Noudoost, B., and Moore, T. (2011). A reliable microinjectrode system for use in behaving monkeys. Journal of Neuroscience Methods *194*, 218–223.

Öhman, A., Flykt, A., and Esteves, F. (2001). Emotion drives attention: Detecting the snake in the grass. Journal of Experimental Psychology: General *130*, 466–478.

Ohzawa, I., Sclar, G., and Freeman, R. (1982). Contrast gain-control in the cat visual-cortex. Nature *298*, 266–268.

Ohzawa, I., DeAngelis, G.C., and Freeman, R.D. (1990). Stereoscopic depth discrimination in the visual cortex: neurons ideally suited as disparity detectors. Science *249*, 1037–1041.

Olshausen, B.A., Anderson, C.H., and Van, E. (1993). A neurobiological model of visual attention and invariant pattern recognition based on dynamic routing of information. Journal of Neuroscience *13*, 4700–4719.

Olszewski, J. (1952). The thalamus of the Macaca mulatta (Basel and New York: S. Karger AG).

Orban, G.A. (2008). Higher Order Visual Processing in Macaque Extrastriate Cortex. Physiological Reviews *88*, 59–89.

Pack, C.C., Berezovskii, V.K., and Born, R.T. (2001). Dynamic properties of neurons in cortical area MT in alert and anaesthetized macaque monkeys. Nature *414*, 905–908.

Pack, C.C., Conway, B.R., Born, R.T., and Livingstone, M.S. (2006). Spatiotemporal Structure of Nonlinear Subunits in Macaque Visual Cortex. J. Neurosci. *26*, 893–907.

Pasupathy, A., and Connor, C.E. (1999). Responses to Contour Features in Macaque Area V4. Journal of Neurophysiology *82*, 2490–2502.

Pasupathy, A., and Connor, C.E. (2001). Shape Representation in Area V4: Position-Specific Tuning for Boundary Conformation. Journal of Neurophysiology *86*, 2505–2519.

Pasupathy, A., and Connor, C.E. (2002). Population coding of shape in area V4. Nature Neuroscience *5*, 1332.

Payne, B.R. (1993). Evidence for visual cortical area homologs in cat and macaque monkey. Cereb. Cortex *3*, 1–25.

Payne, B.R., and Peters, A. (2002). 1 - The Concept of Cat Primary Visual Cortex. In The Cat Primary Visual Cortex, (San Diego: Academic Press), pp. 1–129.

Petersen, S.E., Robinson, D.L., and Keys, W. (1985). Pulvinar nuclei of the behaving rhesus monkey: visual responses and their modulation. Journal of Neurophysiology *54*, 867–886.

Petersen, S.E., Robinson, D.L., and Morris, J.D. (1987). Contributions of the pulvinar to visual spatial attention. Neuropsychologia *25*, 97–105.

Petrof, I., Viaene, A.N., and Sherman, S.M. (2012). Two populations of corticothalamic and interareal corticocortical cells in the subgranular layers of the mouse primary sensory cortices. J. Comp. Neurol. *520*, 1678–1686.

Petry, H.M., and Bickford, M.E. (2018). The Second Visual System of the Tree Shrew. J. Comp. Neurol.

Piché, M., Thomas, S., and Casanova, C. (2013). Spatiotemporal profiles of neurons receptive fields in the cat posteromedial lateral suprasylvian cortex. Neuroscience *248*, 319–332.

Piché, M., Thomas, S., and Casanova, C. (2015). Spatiotemporal profiles of receptive fields of neurons in the lateral posterior nucleus of the cat LP-pulvinar complex. Journal of Neurophysiology *114*, 2390–2403.

Purushothaman, G., Marion, R., Li, K., and Casagrande, V.A. (2012). Gating and control of primary visual cortex by pulvinar. Nat Neurosci *15*, 905–912.

Quax, S., Jensen, O., and Tiesinga, P. (2017). Top-down control of cortical gamma-band communication via pulvinar induced phase shifts in the alpha rhythm. PLOS Computational Biology *13*, e1005519.

Raczkowski, D., and Rosenquist, A.C. (1981). Retinotopic organization in the cat lateral posterior-pulvinar complex. Brain Research *221*, 185–191.

Raczkowski, D., and Rosenquist, A.C. (1983). Connections of the multiple visual cortical areas with the lateral posterior-pulvinar complex and adjacent thalamic nuclei in the cat. J. Neurosci. *3*, 1912–1942.

Rauschecker, J.P. (2017). Where, When, and How: Are they all sensorimotor? Towards a unified view of the dorsal pathway in vision and audition. Cortex.

Reichova, I., and Sherman, S. (2004). Somatosensory corticothalamic projections: Distinguishing drivers from modulators. J Neurophysiol *92*, 2185–2197.

Reid, R.C., Victor, J.D., and Shapley, R.M. (1997). The use of m-sequences in the analysis of visual neurons: linear receptive field properties. Vis. Neurosci. *14*, 1015–1027.

Rey, H.G., Pedreira, C., and Quian Quiroga, R. (2015). Past, present and future of spike sorting techniques. Brain Research Bulletin.

Reynolds, J.H., and Desimone, R. (1999). The Role of Neural Mechanisms of Attention in Solving the Binding Problem. Neuron *24*, 19–29.

Reynolds, J.H., Pasternak, T., and Desimone, R. (2000). Attention Increases Sensitivity of V4 Neurons. Neuron *26*, 703–714.

Richert, M., Albright, T.D., and Krekelberg, B. (2013). The complex structure of receptive fields in the middle temporal area. Front. Syst. Neurosci. *7*, 2.

Ringach, D., and Shapley, R. (2004). Reverse correlation in neurophysiology. Cognitive Science *28*, 147–166.

Ringach, D.L., Sapiro, G., and Shapley, R. (1997). A subspace reverse-correlation technique for the study of visual neurons. Vision Research *37*, 2455–2464.

Robinson, D.L., and Petersen, S.E. (1992). The pulvinar and visual salience. Trends in Neurosciences *15*, 127–132.

Rossant, C., Kadir, S.N., Goodman, D.F.M., Schulman, J., Hunter, M.L.D., Saleem, A.B., Grosmark, A., Belluscio, M., Denfield, G.H., Ecker, A.S., et al. (2016). Spike sorting for large, dense electrode arrays. Nat Neurosci *19*, 634–641.

Rovó, Z., Ulbert, I., and Acsády, L. (2012). Drivers of the Primate Thalamus. J. Neurosci. *32*, 17894–17908.

Saalmann, Y.B., and Kastner, S. (2009). Gain control in the visual thalamus during perception and cognition. Current Opinion in Neurobiology *19*, 408–414.

Saalmann, Y.B., and Kastner, S. (2011). Cognitive and Perceptual Functions of the Visual Thalamus. Neuron *71*, 209–223.

Saalmann, Y.B., Pinsk, M.A., Wang, L., Li, X., and Kastner, S. (2012). The Pulvinar Regulates Information Transmission Between Cortical Areas Based on Attention Demands. Science *337*, 753–756.

Sakai, H.M., Naka, K., and Korenberg, M.J. (1988). White-noise analysis in visual neuroscience. Vis. Neurosci. *1*, 287–296.

Sanderson, K.J. (1971). The projection of the visual field to the lateral geniculate and medial interlaminar nuclei in the cat. J. Comp. Neurol. *143*, 101–117.

Sandkühler, J., and Gebhart, G.F. (1991). Production of Reversible Local Blockage of Neuronal Function. In Methods in Neurosciences, P.M. Conn, ed. (Academic Press), pp. 122–138.

Scannell, J., Blakemore, C., and Young, M. (1995). Analysis of connectivity in the cat cerebral-cortex. J Neurosci *15*, 1463–1483.

Sclar, G., Maunsell, J., and Lennie, P. (1990). Coding of image-contrast in central visual pathways of the macaque monkey. Vision Research *30*, 1–10.

Sekuler, A.B., and Bennett, P.J. (2001). Visual neuroscience: Resonating to natural images. Current Biology *11*, R733–R736.

Sellers, K.K., Bennett, D.V., Hutt, A., Williams, J.H., and Fröhlich, F. (2015). Awake vs. anesthetized: layer-specific sensory processing in visual cortex and functional connectivity between cortical areas. J. Neurophysiol. *113*, 3798–3815.

Sherk, H. (1989). Visual response properties of cortical inputs to an extrastriate cortical area in the cat. Vis. Neurosci. *3*, 249–265.

Sherman, S.M. (2007). The thalamus is more than just a relay. Current Opinion in Neurobiology *17*, 417–422.

Sherman, S.M. (2016). Thalamus plays a central role in ongoing cortical functioning. Nat Neurosci *16*, 533–541.

Sherman, S.M. (2017). Functioning of Circuits Connecting Thalamus and Cortex. Compr Physiol *7*, 713–739.

Sherman, S., and Guillery, R. (2002). The role of the thalamus in the flow of information to the cortex. Philosophical Transactions of the Royal Society B-Biological Sciences *357*, 1695–1708.

Sherman, S., and Guillery, R. (2013a). Functional Connections of Cortical Areas: A New View from the Thalamus (Cambridge, MA: MIT Press).

Sherman, S.M., and Guillery, R.W. (1996). Functional organization of thalamocortical relays. Journal of Neurophysiology *76*, 1367–1395.

Sherman, S.M., and Guillery, R.W. (1998). On the actions that one nerve cell can have on another: Distinguishing "drivers" from "modulators." PNAS *95*, 7121–7126.

Sherman, S.M., and Guillery, R.W. (2013b). Functional Connections of Cortical Areas: A New View from the Thalamus (MIT Press).

Sherman, S.M., and Koch, C. (1986). The control of retinogeniculate transmission in the mammalian lateral geniculate nucleus. Exp Brain Res *63*, 1–20.

Shibasaki, M., and Kawai, N. (2009). Rapid detection of snakes by Japanese monkeys (Macaca fuscata): An evolutionarily predisposed visual system. Journal of Comparative Psychology *123*, 131–135.

Shipp, S. (2003). The functional logic of cortico-pulvinar connections. Philos Trans R Soc Lond B Biol Sci *358*, 1605–1624.

Shipp, S. (2004). The brain circuitry of attention. Trends in Cognitive Sciences *8*, 223–230.

Shipp, S., and Grant, S. (1991). Organization of reciprocal connections between area 17 and the lateral suprasylvian area of cat visual cortex. Vis. Neurosci. *6*, 339–355.

Shumikhina, S., and Molotchnikoff, S. (1999). Pulvinar participates in synchronizing neural assemblies in the visual cortex, in cats. Neuroscience Letters *272*, 135–139.

Silverstein, S.M., and Keane, B.P. (2011). Vision Science and Schizophrenia Research: Toward a Re-view of the Disorder Editors' Introduction to Special Section. Schizophr Bull *37*, 681–689.

Simoncelli, E.P., and Olshausen, B.A. (2001). Natural Image Statistics and Neural Representation. Annual Review of Neuroscience *24*, 1193–1216.

Skottun, B.C., De Valois, R.L., Grosof, D.H., Movshon, J.A., Albrecht, D.G., and Bonds, A.B. (1991). Classifying simple and complex cells on the basis of response modulation. Vision Research *31*, 1078–1086.

Smith, M.A., Majaj, N.J., and Movshon, J.A. (2005). Dynamics of motion signaling by neurons in macaque area MT. Nature Neuroscience *8*, 220.

Snow, J.C., Allen, H.A., Rafal, R.D., and Humphreys, G.W. (2009). Impaired attentional selection following lesions to human pulvinar: Evidence for homology between human and monkey. PNAS *106*, 4054–4059.

Soares, J., Diogo, A., Fiorani, M., Souza, A., and Gattass, R. (2004). Effects of inactivation of the lateral pulvinar on response properties of second visual area cells in Cebus monkeys. Clinical and Experimental Pharmacology and Physiology *31*, 580–590.

Soma, S., Shimegi, S., Osaki, H., and Sato, H. (2012). Cholinergic modulation of response gain in the primary visual cortex of the macaque. Journal of Neurophysiology *107*, 283–291.

Soma, S., Shimegi, S., Suematsu, N., and Sato, H. (2013). Cholinergic modulation of response gain in the rat primary visual cortex. Sci. Rep. *3*.

Stepniewska, I. (2003). The Pulvinar complex. In The Primate Visual System, J. Kaas, and C. Collins, eds. (Boca Raton, FL:CRC Press), pp. 53–80.

Stone, J., and Dreher, B. (1973). Projection of X- and Y-cells of the cat's lateral geniculate nucleus to areas 17 and 18 of visual cortex. Journal of Neurophysiology *36*, 551–567.

Symonds, L.L., and Rosenquist, A.C. (1984a). Laminar origins of visual corticocortical connections in the cat. J. Comp. Neurol. *229*, 39–47.

Symonds, L.L., and Rosenquist, A.C. (1984b). Corticocortical connections among visual areas in the cat. J. Comp. Neurol. *229*, 1–38.

Symonds, L.L., Rosenquist, A.C., Edwards, S.B., and Palmer, L.A. (1981). Projections of the pulvinar-lateral posterior complex to visual cortical areas in the cat. Neuroscience *6*, 1995–2020.

Szulborski, R.G., and Palmer, L.A. (1990). The two-dimensional spatial structure of nonlinear subunits in the receptive fields of complex cells. Vision Research *30*, 249–254.

Talebi, V., and Baker, C.L. (2012). Natural versus Synthetic Stimuli for Estimating Receptive Field Models: A Comparison of Predictive Robustness. J. Neurosci. *32*, 1560–1576.

Talebi, V., and Baker, C.L. (2016). Categorically distinct types of receptive fields in early visual cortex. Journal of Neurophysiology jn.00659.2015.

Tao, X., Zhang, B., Smith, E.L., Nishimoto, S., Ohzawa, I., and Chino, Y.M. (2012). Local sensitivity to stimulus orientation and spatial frequency within the receptive fields of neurons in visual area 2 of macaque monkeys. J Neurophysiol *107*, 1094–1110.

Tardif, E., Bergeron, A., Lepore, F., and Guillemot, J.-P. (1996). Spatial and temporal frequency tuning and contrast sensitivity of single neurons in area 21a of the cat. Brain Research *716*, 219–223.

Taylor, J.C., and Downing, P.E. (2011). Division of Labor between Lateral and Ventral Extrastriate Representations of Faces, Bodies, and Objects. Journal of Cognitive Neuroscience *23*, 4122–4137.

Toyama, K., Mizobe, K., Akase, E., and Kaihara, T. (1994). Neuronal responsiveness in areas 19 and 21a, and the posteromedial lateral suprasylvian cortex of the cat. Exp Brain Res *99*, 289–301.

Tusa, R.J., and Palmer, L.A. (1980). Retinotopic organization of areas 20 and 21 in the cat. J. Comp. Neurol. *193*, 147–164.

Uhl, R.R., Squires, K.C., Bruce, D.L., and Starr, A. (1980). Effect of halothane anesthesia on the human cortical visual evoked response. Anesthesiology *53*, 273–276.

Ungerleider, L.G., and Haxby, J.V. (1994). "What" and "where" in the human brain. Curr. Opin. Neurobiol. *4*, 157–165.

Ungerleider, L.G., Desimone, R., Galkin, T.W., and Mishkin, M. (1984). Subcortical projections of area MT in the macaque. J. Comp. Neurol. *223*, 368–386.

Ungerleider, L.G., Galkin, T.W., Desimone, R., and Gattass, R. (2014). Subcortical Projections of Area V2 in the Macaque. Journal of Cognitive Neuroscience *26*, 1220–1233.

Updyke, B.V. (1977). Topographic organization of the projections from cortical areas 17, 18, and 19 onto the thalamus, pretectum and superior colliculus in the cat. J. Comp. Neurol. *173*, 81–121.

Updyke, B.V. (1981). Projections from visual areas of the middle suprasylvian sulcus onto the lateral posterior complex and adjacent thalamic nuclei in cat. J. Comp. Neurol. *201*, 477–506.

Updyke, B.V. (1983). A reevaluation of the functional organization and cytoarchitecture of the feline lateral posterior complex, with observations on adjoining cell groups. J. Comp. Neurol. *219*, 143–181.

Usrey, W.M., Reppas, J.B., and Reid, R.C. (1999). Specificity and Strength of Retinogeniculate Connections. Journal of Neurophysiology *82*, 3527–3540.

USREY, W.M., SCENIAK, M.P., and CHAPMAN, B. (2003). Receptive Fields and Response Properties of Neurons in Layer 4 of Ferret Visual Cortex. J Neurophysiol *89*, 1003–1015.

Vajda, I., Lankheet, M.J.M., and van de Grind, W.A. (2005). Spatio-temporal requirements for direction selectivity in area 18 and PMLS complex cells. Vision Research *45*, 1769–1779.

Van der Stigchel, S., Arend, I., van Koningsbruggen, M.G., and Rafal, R.D. (2010). Oculomotor integration in patients with a pulvinar lesion. Neuropsychologia *48*, 3497–3504.

Van Hooser, S.D. (2007). Similarity and Diversity in Visual Cortex: Is There a Unifying Theory of Cortical Computation? , Similarity and Diversity in Visual Cortex: Is There a Unifying Theory of Cortical Computation? Neuroscientist *13*, 639–656.

Van horn, S., and Sherman, S. (2004). Differences in projection patterns between large and small corticothalamic terminals. Journal of Comparative Neurology *475*, 406–415.

Van Horn, S.C., Erişir, A., and Sherman, S.M. (2000). Relative distribution of synapses in the A-laminae of the lateral geniculate nucleus of the cat. J. Comp. Neurol. *416*, 509–520.

Viaene, A.N., Petrof, I., and Sherman, S.M. (2011). Synaptic Properties of Thalamic Input to the Subgranular Layers of Primary Somatosensory and Auditory Cortices in the Mouse. J Neurosci *31*, 12738–12747.

Vickery, R.M., and Morley, J.W. (1997). Orientation-dependent binocular interactions in area 21a of the cat. [Miscellaneous Article]. Neuroreport September 29, 1997 *8*, 3173–3176.

Vickery, R.M., and Morley, J.W. (1999). Binocular phase interactions in area 21a of the cat. J Physiol *514*, 541–549.

Villeneuve, M.Y., and Casanova, C. (2003). On the use of isoflurane versus halothane in the study of visual response properties of single cells in the primary visual cortex. Journal of Neuroscience Methods *129*, 19–31.

Villeneuve, M.Y., Kupers, R., Gjedde, A., Ptito, M., and Casanova, C. (2005). Pattern–motion selectivity in the human pulvinar. NeuroImage *28*, 474–480.

Villeneuve, M.Y., Ptito, M., and Casanova, C. (2006). Global motion integration in the postero-medial part of the lateral suprasylvian cortex in the cat. Exp Brain Res *172*, 485–497.

Villeneuve, M.Y., Vanni, M.P., and Casanova, C. (2009). Modular organization in area 21a of the cat revealed by optical imaging: comparison with the primary visual cortex. Neuroscience *164*, 1320–1333.

Wamer, C., Goldshmit, Y., and Bourne, J. (2010). Retinal afferents synapse with relay cells targeting the middle temporal area inthe pulvinar and lateral geniculate nuclei. Frontiers in Neuroanatomy *4*, 1–16.

Wang, H.X., and Movshon, J.A. (2015). Properties of pattern and component direction-selective cells in area MT of the macaque. Journal of Neurophysiology *115*, 2705–2720.

Wang, S., Eisenback, M.A., and Bickford, M.E. (2002). Relative distribution of synapses in the pulvinar nucleus of the cat: Implications regarding the "driver/modulator" theory of thalamic function. J. Comp. Neurol. *454*, 482–494.

Wang, Y., Wang, L., Li, B., Wang, L.H., and Diao, Y.C. (1995). How is direction selectivity organized in the extrastriate visual area PMLS of the cat? Neuroreport *6*, 1969–1974.

Ward, R., Danziger, S., Owen, V., and Rafal, R. (2002). Deficits in spatial coding and feature binding following damage to spatiotopic maps in the human pulvinar. Nat Neurosci *5*, 99–100.

Ward, R., Danziger, S., and Bamford, S. (2005). Response to Visual Threat Following Damage to the Pulvinar. Current Biology *15*, 571–573.

Ward, R., Calder, A.J., Parker, M., and Arend, I. (2007). Emotion recognition following human pulvinar damage. Neuropsychologia *45*, 1973–1978.

White, B.J., Kan, J.Y., Levy, R., Itti, L., and Munoz, D.P. (2017). Superior colliculus encodes visual saliency before the primary visual cortex. PNAS 201701003.

Wilke, M., Turchi, J., Smith, K., Mishkin, M., and Leopold, D.A. (2010). Pulvinar Inactivation Disrupts Selection of Movement Plans. J. Neurosci. *30*, 8650–8659.

Williford, T., and Maunsell, J.H.R. (2006). Effects of Spatial Attention on Contrast Response Functions in Macaque Area V4. Journal of Neurophysiology *96*, 40–54.

Wilson, D.E., Smith, G.B., Jacob, A.L., Walker, T., Dimidschstein, J., Fishell, G., and Fitzpatrick, D. (2017). GABAergic Neurons in Ferret Visual Cortex Participate in Functionally Specific Networks. Neuron *93*, 1058-1065.e4.

Wimborne, B.M., and Henry, G.H. (1992). Response characteristics of the cells of cortical area 21a of the cat with special reference to orientation specificity. J Physiol *449*, 457–478.

Xia, S., Li, X., Kimball, A.E., Kelly, M.S., Lesser, I., and Branch, C. (2012). Thalamic shape and connectivity abnormalities in children with attention- deficit/hyperactivity disorder. Psychiatry Research: Neuroimaging *204*, 161–167.

Xing, D., Yeh, C.-I., and Shapley, R.M. (2010). Generation of Black-Dominant Responses in V1 Cortex. J. Neurosci. *30*, 13504–13512.

Yau, J.M., Pasupathy, A., Brincat, S.L., and Connor, C.E. (2013). Curvature Processing Dynamics in Macaque Area V4. Cereb Cortex *23*, 198–209.

Yeh, C.-I., Xing, D., Williams, P.E., and Shapley, R.M. (2009a). Stimulus ensemble and cortical layer determine V1 spatial receptive fields. PNAS *106*, 14652–14657.

Yeh, C.-I., Xing, D., and Shapley, R.M. (2009b). "Black" Responses Dominate Macaque Primary Visual Cortex V1. J. Neurosci. *29*, 11753–11760.

Yu, C., Sellers, K.K., Radtke-Schuller, S., Lu, J., Xing, L., Ghukasyan, V., Li, Y., Shih, Y.-Y.I., Murrow, R., and Frohlich, F. (2015). Structural and Functional Connectivity between the Lateral Posterior-Pulvinar Complex and Primary Visual Cortex in the Ferret. Eur J Neurosci n/a-n/a.

Zabouri, N., Ptito, M., and Casanova, C. (2008). Complex motion sensitivity of neurons, in the visual part of the anterior ectosylvian cortex in cats. Neuroscience *152*, 106–118.

Zhao, Y., Kerscher, N., Eysel, U., and Funke, K. (2001). Changes of contrast gain in cat dorsal lateral geniculate nucleus by dopamine receptor agonists. NeuroReport *12*, 2939–2945.

Zhou, H., Schafer, R.J., and Desimone, R. (2016). Pulvinar-Cortex Interactions in Vision and Attention. Neuron *89*, 209–220.

Zhou, N., Maire, P.S., Masterson, S.P., and Bickford, M.E. (2017a). The mouse pulvinar nucleus: Organization of the tectorecipient zones. Visual Neuroscience *34*.

Zhou, N., Masterson, S.P., Damron, J.K., Guido, W., and Bickford, M.E. (2017b). The mouse pulvinar nucleus links the lateral extrastriate cortex, striatum, and amygdala. J. Neurosci. 1279–17.

11 Appendix: other authored and co-authored publications

frontiers in Integrative Neuroscience

ORIGINAL RESEARCH
published: 15 January 2018
doi: 10.3389/fnint.2017.00041

Spatial Frequency Selectivity Is Impaired in Dopamine D2 Receptor Knockout Mice

Bruno Oliveira Ferreira Souza[1], *Mira Abou Rjeili*[1], *Clémentine Quintana*[2], *Jean M. Beaulieu*[2] *and Christian Casanova*[1]*

[1] *Laboratory of Visual Neuroscience, Optometry School, University of Montreal, Montreal, QC, Canada,* [2] *Department of Pharmacology and Toxicology, University of Toronto, Toronto, ON, Canada*

Dopamine is a neurotransmitter implicated in several brain functions, including vision. In the present study, we investigated the impacts of the lack of D2 dopamine receptors on the structure and function of the primary visual cortex (V1) of D2-KO mice using optical imaging of intrinsic signals. Retinotopic maps were generated in order to measure anatomo-functional parameters such as V1 shape, cortical magnification factor, scatter, and ocular dominance. Contrast sensitivity and spatial frequency selectivity (SF) functions were computed from responses to drifting gratings. When compared to control mice, none of the parameters of the retinotopic maps were affected by D2 receptor loss of function. While the contrast sensitivity function of D2-KO mice did not differ from their wild-type counterparts, SF selectivity function was significantly affected as the optimal SF and the high cut-off frequency ($p < 0.01$) were higher in D2-KO than in WT mice. These findings show that the lack of function of D2 dopamine receptors had no influence on cortical structure whereas it had a significant impact on the spatial frequency selectivity and high cut-off. Taken together, our results suggest that D2 receptors play a specific role on the processing of spatial features in early visual cortex while they do not seem to participate in its development.

Keywords: dopamine receptor, cortical maps, optical imaging, primary visual cortex, mouse model

OPEN ACCESS

Edited by:
He Cui,
Institute of Neuroscience, Shanghai Institutes for Biological Sciences (CAS), China

Reviewed by:
Yao Chen,
Shanghai Jiao Tong University, China
Dongmin Yin,
East China Normal University, China

***Correspondence:**
Christian Casanova
christian.casanova@umontreal.ca

Received: *13 October 2017*
Accepted: *29 December 2017*
Published: *15 January 2018*

Citation:
Souza BOF, Abou Rjeili M, Quintana C, Beaulieu JM and Casanova C (2018) Spatial Frequency Selectivity Is Impaired in Dopamine D2 Receptor Knockout Mice. Front. Integr. Neurosci. 11:41. doi: 10.3389/fnint.2017.00041

INTRODUCTION

Dopamine (DA) is a neurotransmitter that plays a central role in several brain functions such as motor control, cognition and motivated behaviors. Dopamine modulates neuronal activity through a set of G-protein coupled receptors divided in two functionally distinct groups based on their effects on the intracellular levels of cyclic AMP, D1-class (D1 and D5) and D2-class (D2S, D2L, D3, and D4) receptors (Witkovsky, 2004; Beaulieu and Gainetdinov, 2011).

Dopamine receptors play an important role in the development and function of several brain regions (Money and Stanwood, 2013). Disruption of the DAergic system gives rise to several debilitating conditions such as Parkinson's disease and Schizophrenia (Howes and Kapur, 2009; Gama et al., 2014). Alterations of visual perception are symptoms frequently reported in those diseases (Bodis-Wollner, 2009; Green et al., 2009; Botha and Carr, 2012). For example, Parkinson's patients experience a variety of visual deficits such as reduced visual acuity, contrast sensitivity,

color perception and are prone to visual hallucinations (Büttner et al., 1996; Bodis-Wollner, 2009; Gama et al., 2014). Such spectrum of symptoms indicates that the DAergic system participates in multiple levels of neural processing of visual information. As such, numerous studies have investigated the presence and functional implications of the DAergic system in several key areas of the visual system.

In the retina, the release of dopamine from a subset of amacrine cells is involved in light adaptation, contrast sensitivity and spatial frequency (SF) selectivity (Bodis-Wollner and Tzelepi, 1998; Witkovsky, 2004; Huppé-Gourgues et al., 2005) as well as in non-visual processes such as the control of circadian rhythm and ocular growth (McCarthy et al., 2007; Feldkaemper and Schaeffel, 2013). Studies in primates revealed that the inactivation of D2-class receptors alters the SF tuning of ganglion cells (Tagliati et al., 1994) and the blockage of these receptors in humans reduced the signal amplitude of pattern ERG in a dose-dependent manner (Stanzione et al., 1995). A recent study investigated the impact of the absence of D1 and D2 dopamine receptors in respective knockout mice models (Lavoie et al., 2013). Interestingly, the lack of functional D2 receptors has little effect on the electroretinogram (ERG) of knockout mice suggesting that this receptor plays a minor role on DA modulation of retinal physiology in mice.

D2-class receptors are also found in the dorsal lateral geniculate nucleus (dLGN) (Khan et al., 1998) and are directly implicated in the modulation of excitatory glutamatergic synapses of relay neurons (Govindaiah and Cox, 2006). Interestingly, the local injection of D2 agonists influenced the contrast response gain of relay neurons from dLGN (Zhao et al., 2001). It is thus likely that these changes are reflected at the level of the recipient cells in the primary visual cortex.

While D2 receptors are also present in layers IV and V of the visual cortex (in primates, Lidow, 1995; Khan et al., 1998), very few studies have characterized the impact of the DAergic system on the visual cortex (Antal et al., 1997; Noudoost and Moore, 2011; Arsenault et al., 2013; Zaldivar et al., 2014). In monkeys, the systemic administration of D2 receptors antagonists during a visual discrimination task yielded alterations of components of V1 visual evoked potentials (Antal et al., 1997). Despite the evidence that the DAergic system influences the function of the primary visual cortex, the impact of dopamine receptors in the modulation of neuronal responses in the primary visual cortex to specific visual features (e.g., contrast response and SF tuning) remains unknown.

To shed more light on this issue, the present study investigated the contribution of D2 receptors in the organization and function of the primary visual cortex by studying cortical responses in an animal model lacking these receptors. In a first step, we confirmed the presence of D2 receptors in the primary visual cortex of mice. Then, we used optical imaging of intrinsic signals to assess the organization and function of primary visual cortex from D2-KO mice.

We found that the absence of D2 dopamine receptors influenced the cortical processing of spatial features in V1 of mice without alteration of the contrast response and cortical organization.

MATERIALS AND METHODS

Animals

Adult D2 receptor deficient mice ($n = 12$) (Kelly et al., 1997) and their control wild-type littermates ($n = 9$) were obtained from Jackson Laboratory (Bar Harbor, Maine). Mice were housed in a controlled environment with a 12 h light/dark cycle with food and water *ad libitum*. All procedures were carried out in agreement with the guidelines of the Canadian Council for the Protection of Animals, and the experimental protocol was approved by the Ethics Committee of the University of Montreal.

Surgical Procedures

Animals were anesthetized with an intraperitoneal injection of urethane (2 g/Kg, in saline). Atropine (0.05 mg/Kg) was injected subcutaneously to reduce tracheal secretion and to counteract the parasympathomimetic effects of the anesthesia. Injectable lidocaine (2%) was used at incision sites. Lidocaine gel was also used at all pressure points. In order to improve the animals' condition under prolonged anesthesia, a tracheotomy was performed (Moldestad et al., 2009). Animal core body temperature was maintained around 37°C using a heating pad feedback-controlled by a rectal thermoprobe. Viscous artificial tears were used when necessary to avoid corneal dehydration. Animals were placed in a stereotaxic apparatus and the scalp and connective tissues were removed to expose the occipital portion of the skull. A 10 mm wide metal ring was glued over the skull to serve as an imaging chamber. Low melting point agarose (1% in saline) was used to fill the chamber, which was then sealed with a glass cover slip. Electrocardiogram (ECG) and core body temperature were monitored throughout the experiment. After experiments, tissue samples were collected and individual genotypes were confirmed by PCR analysis.

Visual Stimuli

Visual stimuli were projected on a flat translucent screen at 21 cm from the animal's eyes covering 150 by 135 degrees of visual field. Stimuli were generated by the Vpixx software (version 2.8.9, Vpixx Technologies, Saint-Bruno, QC, Canada). Periodic stimulation consisted in full screen vertical or horizontal 2 degree thick white bars drifting over a black background in four directions (0, 90, 180, and 270 degrees) at 0.2 Hz for 10 min (**Figures 2C,E**) (Kalatsky and Stryker, 2003). In order to assess ocular dominance, the full-screen bar was replaced by a 10 × 2 degree bar that was presented along the elevation axis at the vertical meridian (Cang et al., 2005a). Episodic stimuli consisted in full-screen sinusoidal gratings drifting in four directions (0, 90, 180, and 270 degrees) at 2 Hz (**Figure 2G**). To evaluate contrast sensitivity, gratings at 0.02 cpd were shown at different contrasts (6, 12, 25, 50, and 100%). 100% contrast gratings with varying SFs (0.005 to 0.64 cpd) were used to assess the SF selectivity function and its cut-off values. Episodic trials lasted 20 s and consisted in the presentation of a uniform gray screen (blank stimulus) for 5 s, followed by 2 s of stimulation and a post-stimulus period of blank for 13 s. Trials were repeated 10 times, and conditions were randomly presented. Apart from ocular dominance tests, all stimuli were presented binocularly.

Data Acquisition and Processing

Images were obtained with a cooled 12-bit CCD camera (Dalsa 1M60, Colorado Springs, USA) coupled to a macro lens (Nikon, AF Micro Nikkor, 60 m, 1:2.8 D). Images were sampled at 2 Hz for experiments involving episodic stimulation and 1 Hz for retinotopic maps with a resolution of 512 × 512 pixels. Data acquisition was controlled by an Imager 3001 system and with VDAQ software (Optical Imaging Ltd., Rehovot, Israel). An anatomic reference image was taken under a 550 nm illumination for optimal contrast between the cortical matter and the blood vessels (**Figures 2A,B**). The focus was then set to approximately 300 µm deep from the cortical surface and intrinsic signals were acquired under 630 nm illumination. The imaged area encompassed the primary visual cortex of both hemispheres. The analysis was performed using custom scripts in MATLAB (The Mathworks, Natick, MA).

Cortical retinotopic maps were obtained from the spectral decomposition of data originating from periodic stimulation trials (Kalatsky and Stryker, 2003). This resulted in frequency power spectrum maps, accompanied by their respective phase maps. Retinotopic maps were created by the product of the phase component and amplitude of the periodic intrinsic signal (**Figures 2C–F**). Regions of interest (ROIs) delimiting each primary visual cortex were manually drawn based on the cortical activation maps as in Groleau et al. (2014) and Farishta et al. (2015). Different parameters drawn from both the amplitude and phase components of the retinotopic maps were used to trace a profile of cortical organization. The ROIs served to assess the cortical surface and shape, while the phase component comprised in the respective ROIs was used to assess the cortical magnification factor (CMF), scatter, and the extent of the visual field represented.

The shape of primary visual cortex was assessed by fitting ellipses to ROIs using the MATLAB built-in function *regionprops*. The ellipsis eccentricity was used as an "ovality index" in order to establish a parameter of cortical shape. This parameter provides an elongation index (ranging from 0 to 1) of the fitted ellipsis in which higher values represents more elongated ellipses. The phase scatter was calculated on a pixel-to-pixel basis by the subtraction of the phase value of each pixel by the mean phase of its 25 neighboring pixels. The scatter index represents the standard deviation of the mean phase scatter for the ROI and it is a measure of the "quality" of the retinotopy in which lower scatter values represent more uniform phases with "smoother" transitions (Cang et al., 2005a). The extent of cortical representation of the visual field, named here the apparent visual field, was calculated by fitting a Gaussian curve to the phase span for azimuth and elevation maps. The apparent visual field is represented by the 95% confidence interval of the curve and is expressed in degrees. The CMF was also drawn using the same above-mentioned procedures. CMF was determined as the distance between the centroid of the majoritarian phase and the centroid of the sigma from the Gaussian and it is expressed in millimeters per degree.

The ocular dominance index (ODI) was determined as described by Cang et al. (2005a). In brief, ipsilateral and contralateral retinotopic maps were generated from the stimulation of the central visual field. Ocular dominance values were calculated for each pixel using the following operation: (C – I) / (C + I), where C and I represent the amplitude values for the contralateral and ipsilateral stimulation paradigms respectively. The ODI was obtained by averaging the ocular dominance values from each pixel.

Responses from the episodic stimulation paradigm were used to assess the contrast response function and SF selectivity curve (**Figures 2G,H**). As done for the retinotopy, ROIs were manually traced on the amplitude maps obtained at optimal conditions (i.e., 100% contrast or 0.02 cpd, for contrast and SF respectively). The responses to the four drifting directions were averaged. Signal amplitude was calculated on a pixel-to-pixel basis and subsequently averaged across the ROI. A modified Naka-Rushton function (Equation 1) was used to fit the contrast responses, in which n is the exponent (slope coefficient), and C_{50} is the contrast corresponding to the half of the maximum response amplitude.

$$z = \frac{C^n}{C_{50}^n + C^n} \tag{1}$$

The spatial selectivity curve was obtained by the fitting of data with an asymmetric Gaussian curve (Equation 2), in which e is the Euler's constant, s is the standard deviation, p is the optimal SF and o is the log offset.

$$z = e^{\frac{-1}{2s^2} * \log\left(\frac{x+o}{p+o}\right)^2} \tag{2}$$

The SF high cut-off was considered as the SF value at which the model intercepts the level of noise present in the blank recordings from each neuron.

Statistics

Kolmogorov-Smirnov test was used to characterize data distributions. When data were normally distributed, Student's *t*-tests were performed, otherwise Wilcoxon Rank-sum tests were used. All results are presented as mean ± SEM, unless otherwise stated.

In order to compare the contrast and SF sensitivity response curves fitted to the datasets from D2-KO mice and their WT littermates, *F*-tests were performed. In brief, the *F*-test compares the sum of squared errors of prediction (SSE) from the curve fit of the control and D2-KO groups with values obtained from a curve fit to the pooled data. If the two datasets come from different populations, the SSE from the pooled data fit should increase and the null hypothesis is rejected. In case of a significant difference between the curve fits, Welch's *t*-test was performed on the model parameters (as shown in Equations 1 and 2). The levels of significance are indicated as follows: $^{*}p < 0.05$, $^{**}p < 0.01$ and $^{***}p < 0.001$.

Expression of D2 Receptors in Visual Cortex

A subgroup of WT mice was used to investigate the presence of D2 receptors in V1. Mice were killed by a rapid cervical dislocation. Heads of animals were immediately cooled by immersion in liquid nitrogen for 6 s. The brains were extracted

and 500 µm thick serial coronal sections were prepared using ice-cold adult mouse brain slicer and matrix (Zivic instruments). Visual cortices (**Figure 1**), striatum and liver tissues were dissected rapidly (within 90 s) on an ice-cold surface using microsurgical knife (KF Technology) and frozen in liquid nitrogen (one mouse per sample). Tissue samples were lysed by adding TRI reagent (Zymo research) and RNA was extracted by Direct-zol RNA kit according to the manufacturer's instructions (Zymo research). RNA concentration was quantified using ND-1000 Spectrophotometer (NanoDrop Technologies).

Complementary DNA was synthesized using a reverse transcriptase SuperScript III kit according to the manufacturer's instructions (Invitrogen). PCR was performed using following primers: Drd2 forward—TACGTGCCCTTCATCGTCAC, Drd2 reverse—CCATTGGGCATGGTCTGGAT, Gapdh forward—ACAGTCCATGCCATCACTGCC, Gapdh reverse—GCCTGCT TCACCACCTTCTTG.

RESULTS

Receptor Expression

Quantitative real time PCR was used to determine the presence of D2 receptors. **Figure 1** shows the presence of the receptor in the visual cortex comprising V1 and adjacent visual areas. As expected a strong band was observed in the striatum while no receptors were seen in the liver.

Anatomo-Functional Maps

In the present study, optical imaging of intrinsic signals was used to assess the cortical architecture from D2-KO mice. Retinotopic cortical maps were obtained using the periodic stimulus paradigm described by Kalatsky and Stryker (2003). Representative examples of azimuth and elevation cortical maps from D2-KO and WT mice are shown in **Figures 2C–F**. Initially, the qualitative analysis of the maps did not reveal any obvious alterations in cortical morphology (V1 shape) or visuotopic representation (number of phases) of D2-KO mice. Further analysis was performed on the amplitude and phase components of the cortical retinotopic maps in order to respectively quantify different features of the cortical morphology and functional organization. Our results are summarized in **Table 1**. V1 boundaries were drawn from the amplitude component of the retinotopic maps from which the cortical surface and ovality index were analyzed. The surface of V1 in D2-KO mice was not significantly different to that of their WT littermates. Similarly, no differences were observed between the ovality index of both groups. The functional organization of V1 from D2-KO mice was also examined. First, the extent of the visual field stimulated (apparent visual field) was assessed. D2-KO mice exhibited apparent visual field values similar to those of WT mice in both azimuth and elevation. The phase component was equally used to quantify the CMF (see Materials and Methods) for azimuth and elevation maps. No significant differences between CMF values of D2-KO and WT mice were observed, indicating that the lack of D2 receptors had no effect on the amount of cortical surface dedicated to the processing of a specific part of the visual field. Finally, the scatter index from D2-KO mice was computed. Again, no significant differences were noted between the quality of the retinotopic maps derived from azimuth and elevation phase maps of D2-KO and WT mice. Taken together, the analysis of cortical retinotopic maps from D2-KO mice revealed that the lack of D2 dopamine receptors had no significant impact on the functional organization of V1.

Further, the ocular dominance of D2-KO and WT mice was assessed by calculating the ocular dominance index (ODI). **Figure 3** shows the distribution of ODI values for D2-KO mice and their WT littermates. ODI values of D2-KO mice were not different from WT mice (0.173 ± 0.056 vs. 0.29 ± 0.07, Wilcoxon rank sum test, $p = 0.21$), indicating that the ocular dominance was not affected by the congenital lack of D2 dopamine receptors.

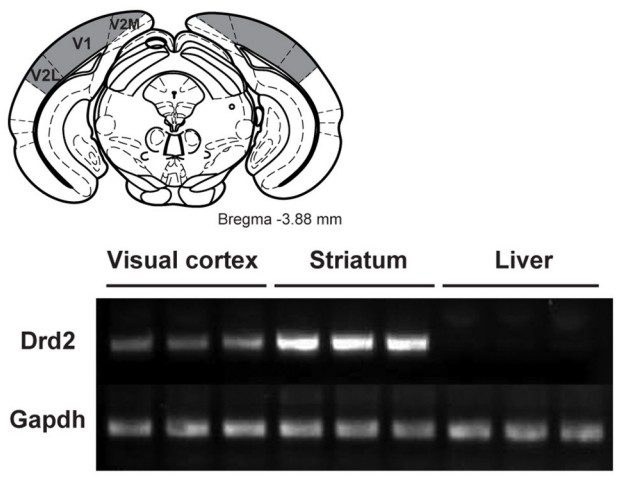

FIGURE 1 | Characterization of the expression of D2 receptors in the visual cortex of wild-type mice. **(Top)** Location of the visual cortex (gray areas) extracted for the quantitative real time PCR (qRT-PCR) analysis (Adapted from Paxinos and Franklin, 2008). **(Bottom)** qRT-PCR for Drd2 and GAPDH from visual cortex, striatum and liver tissues. GAPDH was used as a loading control. V1, primary visual cortex; V2L, secondary visual cortex lateral area; V2M, secondary visual cortex medial area.

Response Properties

In a next step, we measured and compared the SF selectivity and the contrast response of V1 from WT and D2-KO mice using drifting sinusoidal gratings.

Contrast Response Function

Contrast response curves were obtained from V1 of D2-KO and WT mice. Individual datasets were pooled, and data were fitted in order to obtain a response curve for each group. **Figure 4** shows the contrast response curves for D2-KO and WT mice as well as the comparison of the C50 values and slope coefficient drawn from the curve fits. While V1 of D2-KO mice tended to be less sensitive to contrast (lower C50 and slope) than WT mice, this trend, however, did not

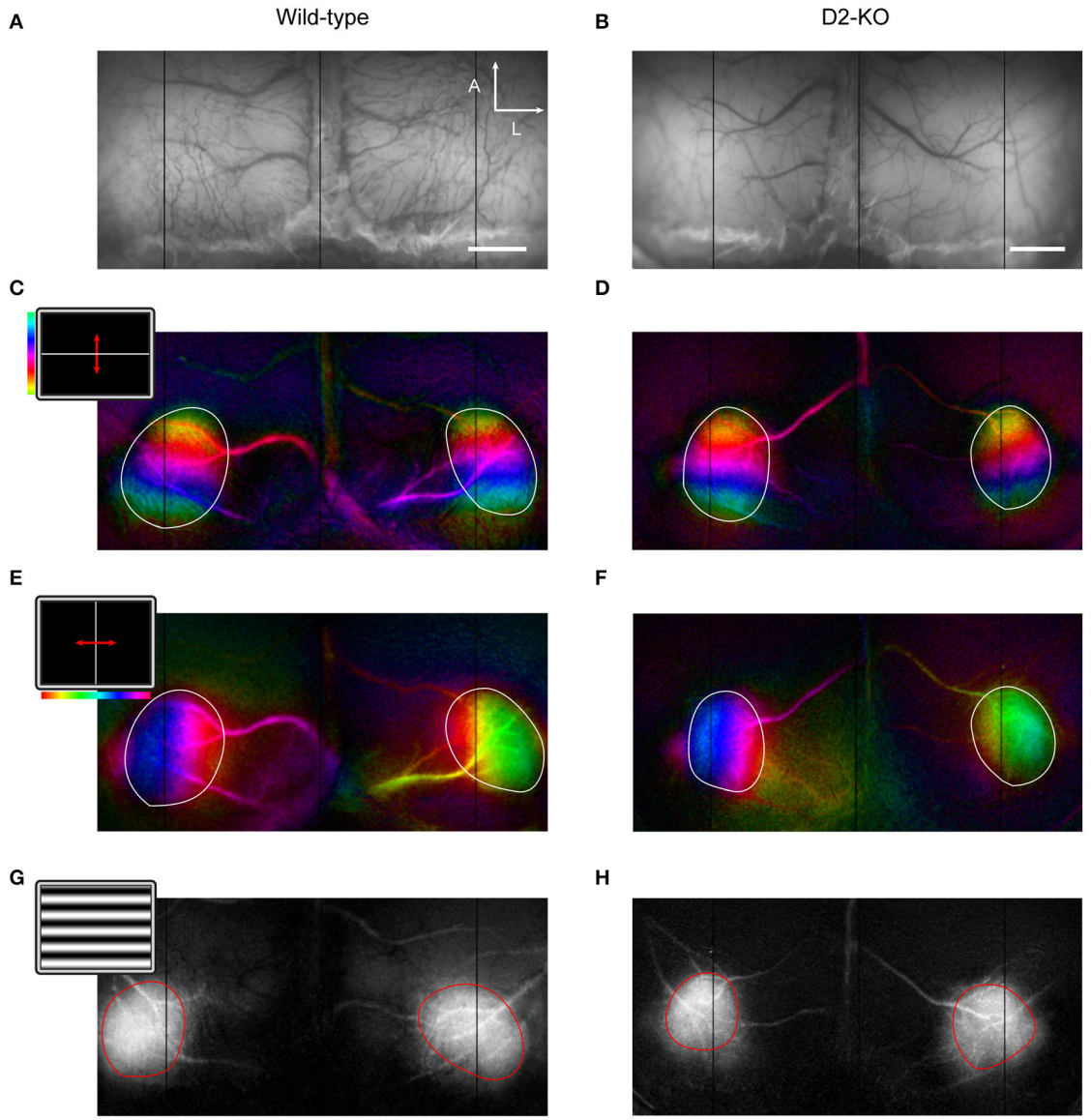

FIGURE 2 | Retinotopic maps in V1 of wild-type and D2-KO mice. **(A,B)** Anatomical reference images of cortical vessels at 545 nm illumination (scale bar = 1 mm; A, anterior; L, lateral). **(C–F)** Retinotopic maps along elevation and azimuth. The insets in **(C,E)** show the stimulus which consisted of a two degrees white bar drifting periodically at 0.2 Hz over a black background. The color bar indicates the position of the bar along the horizontal or vertical axis. The visual field covered in elevation and azimuth was 135 and 150 degree, respectively. **(G,H)** Cortical activation maps to episodic stimulation (inset in **G**, drifting gratings at 100% contrast). Regions of interest (ROIs) are represented by the white and red lines.

reach statistical significance. Indeed, F-statistics performed on the curve fits failed to reveal any differences between the two curves (F-test, $p = 0.27$) and comparison of C50 and slope coefficient values (Welch's t-test) revealed no significant differences between the response to contrast of D2-KO and WT mice.

Spatial Frequency Selectivity

The overall SF selectivity of V1 was also evaluated. As for contrast response functions, datasets in each group were pooled and curve fits were applied to obtain SF selectivity curves (**Figure 5A**). One may note that SF tuning function of D2-KO mice was shifted toward higher SFs when compared to the WT curve (F-test, $p < 0.05$). This was accompanied by changes in the optimal SF and high cut-off. D2-KO mice exhibited higher optimal SF (**Figure 5B**; 0.026 ± 0.009 vs. 0.0175 ± 0.0021, Welch's t-test, $p < 0.001$) and high cut-off (**Figure 5C**; 0.28 ± 0.019 vs. 0.24 ± 0.031, Welch's t-test, $p < 0.01$) compared to their WT littermates. Thus, the SF selectivity profile of D2-KO mice revealed that the lack of functional D2 dopamine receptors increased the sensitivity of V1 neuronal populations by shifting the optimal SF and increasing the SF high-cut-off.

TABLE 1 | Summary of analysis performed on wild-type and D2-KO mice azimuth and elevation retinotopic maps.

Parameters analyzed	D2-KO	Wild-type	*p*-value
AZIMUTH			
Activated cortical surface (mm^2)	3.956 ± 0.0269	3.816 ± 0.0385	$p = 0.357$
Ovality index	0.5469 ± 0.0046	0.5673 ± 0.0071	$p = 0.298$
Apparent visual field (°)	37.81 ± 0.7079	40.46 ± 1.2141	$p = 0.417$
Cortical Magnification Factor (mm/°)	0.03404 ± 0.001	0.03243 ± 0.0023	$p = 0.7908$
Scatter index (°)	43.94 ± 1.2142	53.62 ± 2.2030	$p = 0.179$
ELEVATION			
Activated cortical surface (mm^2)	3.971 ± 0.0271	3.8 ± 0.0523	$p = 0.099$
Ovality index	0.5778 ± 0.0050	0.5645 ± 0.0072	$p = 0.747$
Apparent visual field (°)	81.96 ± 0.8394	77.89 ± 1.0863	$p = 0.3328$
Cortical Magnification Factor (mm/°)	0.0298 ± 0.0003	0.03064 ± 0.0006	$p = 0.5856$
Scatter index (◦)	39.46 ± 0.6573	47.38 ± 1.6127	$p = 0.398$

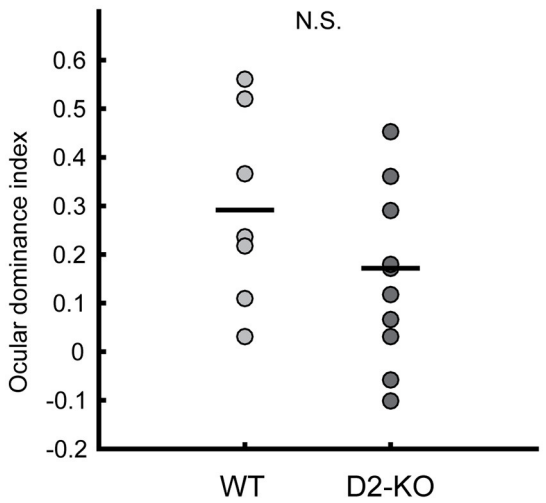

FIGURE 3 | Scatter plot of D2-KO and WT ocular dominance indices (ODIs). No significant differences were observed between groups (Wilcoxon rank sum test, $p = 0.2109$). Black bars represent the mean. N.S.: not significant.

DISCUSSION

In this study, taking advantage of knockout animal models, we present the first evidence of altered visual responses in the primary visual cortex of mice lacking functional D2 dopamine receptor. The main impact of the lack of these receptors was a significant change in the SF tuning function. This change was not accompanied by a modification of the response to the stimulus contrast. Further, the analysis of retinotopic maps indicated that V1 shape or retinotopic organization, as well as ocular dominance in binocular cortex were not altered in D2-KO mice.

Functional Structure of D2-KO Mice V1

In order to investigate if the lack of D2 receptor function could cause structural alterations in mice primary visual cortex, the present study analyzed the retinotopic maps obtained by the periodic paradigm described by Kalatsky and Stryker (2003). Previous studies from us and others have successfully applied this technique in order to assess the impact of different molecular pathways and receptors on the structural organization of V1 connectivity in different knockout mice models (Cang et al., 2005b; Groleau et al., 2014; Farishta et al., 2015). In the present study, the analysis of visual maps revealed that the cortical structure of D2-KO mice did not differ from their WT littermates, suggesting that D2 receptors are not involved in V1 structural organization. Furthermore, the lack of functional D2 dopamine receptors did not affect the ocular dominance in V1 of D2-KO mice.

DAergic receptors are known to play a role in brain development (see Money and Stanwood, 2013 for a review) and pharmacological approaches as well as knockout models have been extensively used to investigate the impact of the lack of these receptors in cortical structure (Jones et al., 2000; Stanwood et al., 2005; Zhang et al., 2010). In a D1-KO mouse model, Stanwood et al. (2005) observed that the lack of functional D1 receptors induced morphological alterations in the dendritic projection of the prefrontal and anterior cingulate cortex whereas the cellular morphology of neurons from the visual cortex remained intact, suggesting that the role of D1 receptors in development is confined to cortical areas with major DAergic input, such as the prefrontal cortex, without any detectable alterations in cortical circuitry of visual areas.

Our data shows that the absence of D2 receptors did not alter the cortical organization of V1 (as shown by the retinotopy and ocular dominance), suggesting that, as observed for D1 receptors, D2 receptors do not play a preponderant role in the organization of the circuitry in the visual cortex. However, given the experimental approach used here, we cannot rule out any morphological changes occurring at the cellular level or in other parts of the visual pathways. Although no structural alterations were observed in V1 of D2-KO mice, the lack of function of D2 receptors did influence cortical processing as described in the next section.

Contrast and SF Functions of D2-KO Mice V1

Visual areas are generally considered to have a less prominent DAergic innervation compared to other parts of the brain such as the prefrontal cortex (Papadopoulos and Parnavelas, 1990; Boumghar et al., 1997; Zhao et al., 2001; Govindaiah and Cox, 2005, 2006). Nevertheless, there is evidence that DA and its receptors are implicated in different aspects of the processing of visual information from the retina to the cortex (Papadopoulos and Parnavelas, 1990; Antal et al., 1997; Witkovsky, 2004; Lavoie et al., 2013; Zaldivar et al., 2014). In particular, previous studies have demonstrated modulatory effects of DAergic receptors on SF processing and contrast response function in the retina and visual thalamus, respectively (Zhao et al., 2001; Witkovsky, 2004).

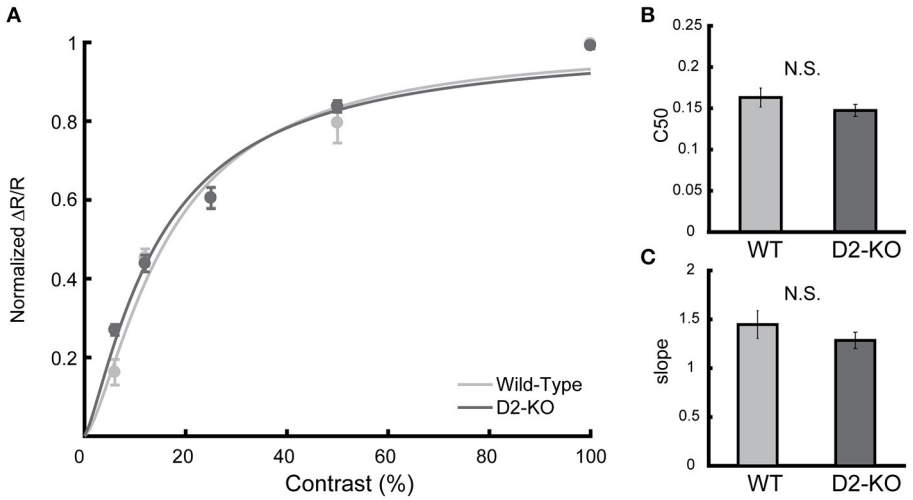

FIGURE 4 | Contrast response curve for D2-KO and wild-type mice V1. **(A)** Curve fitted on normalized response amplitude (mean ± SEM) of pooled individual data elicited by gratings of varying contrasts (6, 12, 50, and 100%). **(B,C)** Comparison of parameters drawn from the curve fits, c50 and slope coefficient respectively. No significant difference was observed between the datasets (F-test, $p = 0.27$). N.S.: not significant.

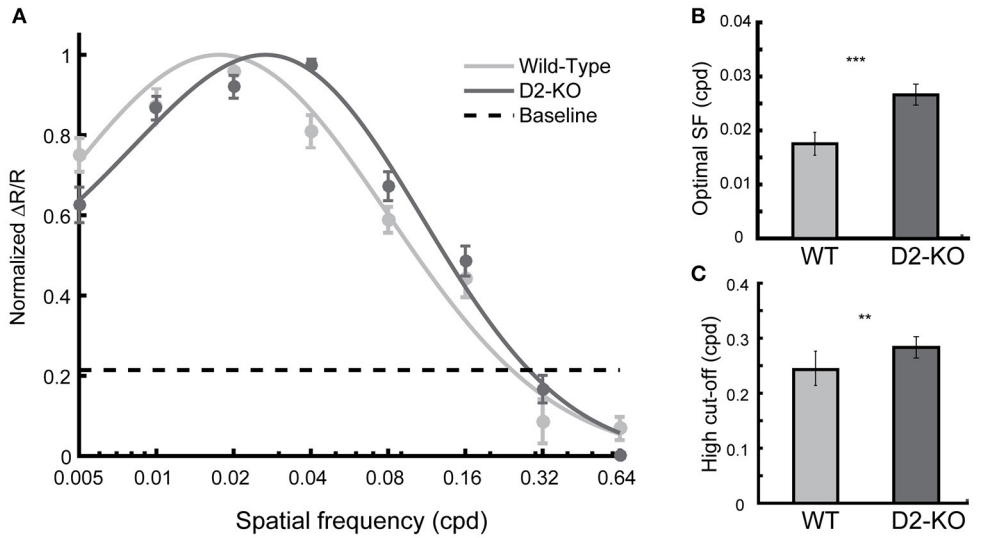

FIGURE 5 | Spatial frequency (SF) tuning function for D2-KO and wild-type mice V1. **(A)** The normalized response amplitude (mean ± SEM) of pooled individual data is plotted against the SFs tested. Note that the D2-KO mice curve is shifted toward higher SFs. The curves are statistically different (F-test, $p < 0.05$). **(B)** SF eliciting the maximal response (mean ± SEM) from V1 of D2-KO and wild-type. V1 neurons of D2-KO were optimally activated by higher SFs compared to wild-type mice (Welch's t-test, $^{***}p < 0.001$). **(C)** Predicted high cut-off for V1 of D2-KO and wild-type mice. The SF threshold was determined by the value at which the model intercepts the level of noise (example of cut-off level depicted in **A**) present in the blank recordings for each individual (Students t-test, $^{**}p < 0.01$).

One could thus hypothesize that V1 neurons will exhibit a similar modulation of the contrast response by inheriting the effects produced in the LGN relay neurons. Our findings do not support this assumption since the contrast response function of D2-KO mice was not significantly different from their WT littermates, indicating that D2 receptors do not influence the contrast sensitivity of V1 neurons. This result is thus at odds with Zhao et al. (2001) report that the injection of D2 receptor agonists provoked a facilitation or inhibition of the contrast response gain of relay neurons in the cat dLGN in a dose-dependent manner. It is worth emphasizing that the contrast responses obtained in the present study is the mean response of the whole primary visual cortex. Since D2 receptors activation gives rise to both facilitation and suppression in the thalamus (Zhao et al., 2001), it is possible that those modulatory effects are balanced or even nullified once the different thalamic signals are integrated in the cortex, avoiding any profound effects on the cortical processing of contrast. Alternatively, a recent study in mice indicated that

contrast adaptation in V1 arises primarily from the local circuitry, with less contribution from the thalamus (King et al., 2016). Hence, the compensatory mechanisms from local circuitry of V1 may dampen the potential modulatory D2-mediated changes observed in the thalamus on the contrast response.

There is little evidence of the specific role of D2 dopamine receptors on the modulation of the SF selectivity of neurons in the visual system. Until now, the effects of the DAergic system on the SF responses have been observed mostly at the retinal level. For instance, in anesthetized monkeys, the administration of l-sulpiride, a selective D2 receptor antagonist caused a reduction of the amplitude of the pattern-ERG (PERG) at the optimal SF (Tagliati et al., 1994). Similar effects were also reported in humans (Stanzione et al., 1995). In our study, the lack of D2 dopamine receptors induced an increased sensitivity to SF in V1, with D2-KO mice exhibiting higher optimal SFs and cut-off values. To our knowledge, this is the first demonstration of the impact of the lack of D2 dopamine receptors on the SF selectivity in V1. Aside obvious methodological differences between our study and the above-mentioned ones, our data suggest that the effects of the lack of D2 dopamine receptors on V1 SF tuning do not arise from the retina. Therefore, it is most likely that the increased SF sensitivity presented in D2-KO mice resulted from changes occurring in the visual thalamus or directly in the cortex since D2 receptors are present in the LGN (Zhao et al., 2001) and in the visual cortex, as revealed here. Nonetheless, it is worth noting that the animal model used in the present study lacks congenitally the D2 dopamine receptor and this takes place ubiquitously. Therefore, the effects observed in the primary visual cortex may result from changes arising at the subcortical level and/or in higher-order visual areas.

CONCLUSION

Our data shows that the lack of function of D2 receptors does not impair the structural organization of neuronal populations of V1. However, compared to WT littermates, D2-KO mice were characterized by an increase of the response amplitudes to higher SFs and of the high SF cut-off. These results suggest that D2 receptors are specifically implicated in the processing of spatial aspects of the visual scene in V1.

AUTHOR CONTRIBUTIONS

BS: performed the surgical procedures, part of data acquisition, performed data analysis and wrote the manuscript; MA: performed part of data acquisition; CQ: performed the PCR experiments; JB: provided the knockout mice and participated in the formulation of original scientific questions, study design and manuscript corrections; CC: participated on the formulation of original scientific questions, on the study design, provided guidance throughout the experiment, and provided helpful feedback on the manuscript writing.

FUNDING

This work was supported by an NSERC grant to CC (2014-06503). BS received scholarships from EOUM-FESP.

ACKNOWLEDGMENTS

We thank Sébastien Thomas for his valuable comments on a draft of the manuscript and Geneviève Cyr for her technical help.

REFERENCES

Antal, A., Kéri, S., and Bodis-Wollner, I. (1997). Dopamine D2 receptor blockade alters the primary and cognitive components of visual evoked potentials in the monkey, Macaca fascicularis. *Neurosci. Lett.* 232, 179–181. doi: 10.1016/S0304-3940(97)00596-X

Arsenault, J. T., Nelissen, K., Jarraya, B., and Vanduffel, W. (2013). Dopaminergic reward signals selectively decrease fMRI activity in primate visual cortex. *Neuron* 77, 1174–1186. doi: 10.1016/j.neuron.2013.01.008

Beaulieu, J.-M., and Gainetdinov, R. R. (2011). The Physiology, signaling, and pharmacology of dopamine receptors. *Pharmacol. Rev.* 63, 182–217. doi: 10.1124/pr.110.002642

Bodis-Wollner, I. (2009). Retinopathy in Parkinson disease. *J. Neural Transm.* 116, 1493–1501. doi: 10.1007/s00702-009-0292-z

Bodis-Wollner, I., and Tzelepi, A. (1998). The push–pull action of dopamine on spatial tuning of the monkey retina: the effects of dopaminergic deficiency and selective D1 and D2 receptor ligands on the pattern electroretinogram. *Vision Res.* 38, 1479–1487. doi: 10.1016/S0042-6989(98)00028-5

Botha, H., and Carr, J. (2012). Attention and visual dysfunction in Parkinson's disease. *Parkinsonism Relat. Disord.* 18, 742–747. doi: 10.1016/j.parkreldis.2012.03.004

Boumghar, L., Marois, A., Jolicoeur, F. J., and Casanova, C. (1997). Apomorphine modifies the visual responses of cells in the rabbit's lateral geniculate nucleus. *Can. J. Physiol. Pharmacol.* 75, 853–858. doi: 10.1139/y97-136

Büttner, T., Kuhn, W., Müller, T., Heinze, T., Pühl, C., and Przuntek, H. (1996). Chromatic and achromatic visual evoked potentials in Parkinson's disease. *Electroencephalogr. Clin. Neurophysiol.* 100, 443–447. doi: 10.1016/0168-5597(96)95700-7

Cang, J., Kalatsky, V. A., Löwel, S., and Stryker, M. P. (2005a). Optical imaging of the intrinsic signal as a measure of cortical plasticity in the mouse. *Vis. Neurosci.* 22, 685–691. doi: 10.1017/S0952523805225178

Cang, J., Kaneko, M., Yamada, J., Woods, G., Stryker, M. P., and Feldheim, D. A. (2005b). Ephrin-as guide the formation of functional maps in the visual cortex. *Neuron* 48, 577–589. doi: 10.1016/j.neuron.2005.10.026

Farishta, R. A., Robert, C., Turcot, O., Thomas, S., Vanni, M. P., Bouchard, J.-F., et al. (2015). Impact of CB1 receptor deletion on visual responses and organization of primary visual cortex in adult micefunctional effects of CBR1 deletion on mouse visual cortex. *Invest. Ophthalmol. Vis. Sci.* 56, 7697–7707. doi: 10.1167/iovs.15-17690

Feldkaemper, M., and Schaeffel, F. (2013). An updated view on the role of dopamine in myopia. *Exp. Eye Res.* 114, 106–119. doi: 10.1016/j.exer.2013.02.007

Gama, R. L., Bruin, V. M., Távora, D. G., Duran, F. L., Bittencourt, L., and Tufik, S. (2014). Structural brain abnormalities in patients with Parkinson's disease with visual hallucinations: a comparative voxel-based analysis. *Brain Cogn.* 87, 97–103. doi: 10.1016/j.bandc.2014.03.011

Govindaiah, G., and Cox, C. L. (2005). Excitatory actions of dopamine Via D1-like receptors in the rat lateral geniculate nucleus. *J. Neurophysiol.* 94, 3708–3718. doi: 10.1152/jn.00583.2005

Govindaiah, G., and Cox, C. L. (2006). Depression of retinogeniculate synaptic transmission by presynaptic D2-like dopamine receptors in rat lateral geniculate nucleus. *Eur. J. Neurosci.* 23, 423–434. doi: 10.1111/j.1460-9568.2005.04575.x

Green, M. F., Butler, P. D., Chen, Y., Geyer, M. A., Silverstein, S., Wynn, J. K., et al. (2009). Perception measurement in clinical trials of schizophrenia: promising paradigms from CNTRICS. *Schizophr. Bull.* 35, 163–181. doi: 10.1093/schbul/sbn156

Groleau, M., Nguyen, H. N., Vanni, M. P., Huppé-Gourgues, F., Casanova, C., and Vaucher, E. (2014). Impaired functional organization in the visual cortex of muscarinic receptor knock-out mice. *Neuroimage* 98, 233–242. doi: 10.1016/j.neuroimage.2014.05.016

Howes, O. D., and Kapur, S. (2009). The dopamine hypothesis of schizophrenia: version III—the final common pathway. *Schizophr. Bull.* 35, 549–562. doi: 10.1093/schbul/sbp006

Huppé-Gourgues, F., Coudé, G., Lachapelle, P., and Casanova, C. (2005). Effects of the intravitreal administration of dopaminergic ligands on the b-wave amplitude of the rabbit electroretinogram. *Vision Res.* 45, 137–145. doi: 10.1016/j.visres.2004.08.001

Jones, L. B., Stanwood, G. D., Reinoso, B. S., Washington, R. A., Wang, H.-Y., Friedman, E., et al. (2000). *In utero* cocaine-induced dysfunction of dopamine D1 receptor signaling and abnormal differentiation of cerebral cortical neurons. *J. Neurosci.* 20, 4606–4614. Available online at: http://www.jneurosci.org/content/20/12/4606

Kalatsky, V. A., and Stryker, M. P. (2003). New paradigm for optical imaging. *Neuron* 38, 529–545. doi: 10.1016/S0896-6273(03)00286-1

Kelly, M. A., Rubinstein, M., Asa, S. L., Zhang, G., Saez, C., Bunzow, J. R., et al. (1997). Pituitary lactotroph hyperplasia and chronic hyperprolactinemia in dopamine D2 RECEPTOR-DEFICIENT MICE. *Neuron* 19, 103–113. doi: 10.1016/S0896-6273(00)80351-7

Khan, Z. U., Gutiérrez, A., Martín, R., Peñafiel, A., Rivera, A., and De La Calle, A. (1998). Differential regional and cellular distribution of dopamine D2-like receptors: an immunocytochemical study of subtype-specific antibodies in rat and human brain. *J. Comp. Neurol.* 402, 353–371. doi: 10.1002/(SICI)1096-9861(19981221)402:3<353::AID-CNE5>3.0.CO;2-4

King, J. L., Lowe, M. P., Stover, K. R., Wong, A. A., and Crowder, N. A. (2016). Adaptive processes in thalamus and cortex revealed by silencing of primary visual cortex during contrast adaptation. *Curr. Biol.* 26, 1295–1300. doi: 10.1016/j.cub.2016.03.018

Lavoie, J., Illiano, P., Sotnikova, T. D., Gainetdinov, R. R., Beaulieu, J.-M., and Hébert, M. (2013). The electroretinogram as a biomarker of central dopamine and serotonin: potential relevance to psychiatric disorders. *Biol. Psychiatry* 75, 479–486. doi: 10.1016/j.biopsych.2012.11.024

Lidow, M. S. (1995). D1- and D2 dopaminergic receptors in the developing cerebral cortex of macaque monkey: a film autoradiographic study. *Neuroscience* 65, 439–452. doi: 10.1016/0306-4522(94)00475-K

McCarthy, C. S., Megaw, P., Devadas, M., and Morgan, I. G. (2007). Dopaminergic agents affect the ability of brief periods of normal vision to prevent form-deprivation myopia. *Exp. Eye Res.* 84, 100–107. doi: 10.1016/j.exer.2006.09.018

Moldestad, O., Karlsen, P., Molden, S., and Storm, J. F. (2009). Tracheotomy improves experiment success rate in mice during urethane anesthesia and stereotaxic surgery. *J. Neurosci. Methods* 176, 57–62. doi: 10.1016/j.jneumeth.2008.08.015

Money, K. M., and Stanwood, G. D. (2013). Developmental origins of brain disorders: roles for dopamine. *Front. Cell. Neurosci.* 7:260. doi: 10.3389/fncel.2013.00260

Noudoost, B., and Moore, T. (2011). Control of visual cortical signals by prefrontal dopamine. *Nature* 474, 372–375. doi: 10.1038/nature09995

Papadopoulos, G. C., and Parnavelas, J. G. (1990). Distribution and synaptic organization of dopaminergic axons in the lateral geniculate nucleus of the rat. *J. Comp. Neurol.* 294, 356–361. doi: 10.1002/cne.902940305

Paxinos, G., and Franklin, K. B. J. (2008). *The Mouse Brain in Stereotaxic Coordinates*. New York, NY: Elsevier Academic Press.

Stanwood, G. D., Parlaman, J. P., and Levitt, P. (2005). Anatomical abnormalities in dopaminoceptive regions of the cerebral cortex of dopamine D1 receptor mutant mice. *J. Comp. Neurol.* 487, 270–282. doi: 10.1002/cne.20548

Stanzione, P., Pierantozzi, M., Semprini, R., Tagliati, M., Traversa, R., Peppe, A., et al. (1995). Increasing doses of l-sulpiride reveal dose- and spatial frequency-dependent effects of D2 selective blockade in the human electroretinogram. *Vision Res.* 35, 2659–2664. doi: 10.1016/0042-6989(95)00037-Z

Tagliati, M., Bodis-Wollner, I., Kovanecz, I., and Stanzione, P. (1994). Spatial frequency tuning of the monkey pattern erg depends on d2 receptor-linked action of dopamine. *Vision Res.* 34, 2051–2057. doi: 10.1016/0042-6989(94)90316-6

Witkovsky, P. (2004). Dopamine and retinal function. *Doc. Ophthalmol. Adv. Ophthalmol.* 108, 17–40. doi: 10.1023/B:DOOP.0000019487.88486.0a

Zaldivar, D., Rauch, A., Whittingstall, K., Logothetis, N. K., and Goense, J. (2014). Dopamine-induced dissociation of BOLD and neural activity in macaque visual cortex. *Curr. Biol.* 24, 2805–2811. doi: 10.1016/j.cub.2014.10.006

Zhang, X., Bearer, E. L., Boulat, B., Hall, F. S., Uhl, G. R., and Jacobs, R. E. (2010). Altered neurocircuitry in the dopamine transporter knockout mouse brain. *PLoS ONE* 5:e11506. doi: 10.1371/journal.pone.0011506

Zhao, Y., Kerscher, N., Eysel, U., and Funke, K. (2001). Changes of contrast gain in cat dorsal lateral geniculate nucleus by dopamine receptor agonists. *Neuroreport* 12, 2939–2945. doi: 10.1097/00001756-200109170-00037

Conflict of Interest Statement: The authors declare that the research was conducted in the absence of any commercial or financial relationships that could be construed as a potential conflict of interest.

Neuroscience Letters 616 (2016) 177–181

Contents lists available at ScienceDirect

Neuroscience Letters

journal homepage: www.elsevier.com/locate/neulet

Research paper

Correlation of hemodynamic and fluorescence signals under resting state conditions in mice's barrel field cortex

Samuel Bélanger[a,b,*], Bruno Oliveira Ferreira de Souza[c], Christian Casanova[c], Frédéric Lesage[a,b]

[a] Institut de Génie Biomédical, Dpt. de Génie Électrique, École Polytechnique de Montréal, C.P. 6079, succ. Centre-ville, Montréal, QC H3C 3A7, Canada
[b] Montreal Heart Institute, 5000 rue Bélanger, Montréal, QC H1T 1C8, Canada
[c] École d'Optométrie, Université de Montréal, 3744 Jean-Brillant, Montréal, QC H3T 1P1, Canada

HIGHLIGHTS

- A bimodal IOI—calcium imaging system was used to record resting state activity.
- Neuronal and glial parts of fluorescence signal were retrieved with frequency filters.
- Hemodynamic response and fluorescence signals correlation was computed.
- Differences in correlation patterns were found between high and low spectrum.

ARTICLE INFO

Article history:
Received 28 October 2015
Received in revised form 22 January 2016
Accepted 29 January 2016
Available online 2 February 2016

Keywords:
Neurovascular coupling
Resting state
Astrocytes
Intrinsic signal imaging
Calcium fluorescence signal imaging
Barrel field cortex

ABSTRACT

Both neurons and astrocytes are known to affect local vascular response in the brain following neuronal activity. In order to differentiate the contributions of each cell type to the hemodynamic response during stimulation and resting state, intrinsic optical signal (IOI) was recorded synchronized with fluorescence imaging of calcium concentration sensitive dye Oregon Green BAPTA-1 AM. By changing the stimulation parameters (frequency and duration), it was possible to individually promote neuronal and glial responses and to compare them to levels of oxy (HbO), deoxy (HbR) and total (HbT) hemoglobin concentrations. Finally, resting state recordings were done to investigate the possible correlation between hemoglobin fluctuation and calcium transients, based on different frequency bands associated either with neuronal or glial activity.

1. Introduction

Following neuronal activity, a cascade of events induces a local change in vascular dynamics. This phenomenon, known as neurovascular coupling, is well-documented in literature. As described in a recent review [1], multiple actors influence vascular tone in the brain. Starting at the capillaries and then propagating backward to ascending arterioles and to pial arteries, the dilatation process induced by local neuronal activity affects hemoglobin concentration levels. The ensuing hemodynamic response associated with these events consists of a local increase in oxy-hemoglobin (HbO) and a decrease in deoxy-hemoglobin (HbR) concentration. Multiple cell types are known to influence hemodynamics, primarily neurons and astrocytes, although through different pathways. As oxygenation changes are used as a way to quantify brain activity, it is important to understand more precisely how different cellular populations are involved in this process. In particular, to assess whether the causality observed during stimulation translates in the context of resting state signals.

Using a bimodal acquisition setup for simultaneous fluorescence calcium level and fMRI recordings, Schultz et al. [2] were able to differentiate the neuronal and glial contributions to the BOLD signal. They showed that a strong correlation exists between the BOLD signal and changes in calcium levels in neurons, measured by calcium sensitive fluorescent probes. Comparing the BOLD response with a simple model based on neuronal response, they observed some dissimilarities explained by glial activity. By analyzing these

* Corresponding author at: Institut de Génie Biomédical, Dpt. de Génie Électrique, École Polytechnique de Montréal, C.P. 6079, succ. Centre-ville, Montréal QC H3C 3A7, Canada.
E-mail address: samuel.belanger@polymtl.ca (S. Bélanger).

http://dx.doi.org/10.1016/j.neulet.2016.01.067
0304-3940/

differences, they were able to extract the neuronal and the glial components from the BOLD response. However, these results were measured using stimulation and anesthesia. The question remains as to whether the astrocyte contribution to BOLD, measured under isoflurane anesthesia in [2] was diminished compared to awake signals, given that there is a known reduction in astrocyte activity under anesthesia [3]. Separately, one might ask whether a similar relationship to what Schultz et al. [2] observed exists between signals measured at rest. BOLD fMRI signals are now commonly used to assess brain region connections during resting state conditions [4–6] and while some work has tried to pin down the neural origin of resting state signals [7], it remains to be investigated whether part of the signal has a glial origin.

The bimodality scheme developed by Schultz can be reproduced by a simpler optical system. Intrinsic optical signal imaging (IOI) techniques have been used for many years in order to measure hemodynamic at the surface of the cortex [8–10]. More recently, the ability to record both hemodynamic and fluorescence changes of calcium probes was demonstrated [11]. As IOI signals are akin to BOLD signals, they offer a simple means to reproduce the dual approach investigated by Shultz et al. [2], with increased control on hemodynamic parameters and the ability to measure more than a single spatial point in the cortex.

Likewise, the idea of measuring both fluorescence and hemodynamic signals during the same experiment is not new. Other recent work has used genetically modified mouse models to image both calcium activity (GCaMP3) and hemodynamics in resting state paradigm [12–14]. Evidence of correlation between neuronal calcium transient and hemodynamics was observed using such an approach. However, the contribution from astrocytes was not able to be determined since GCaMP3 transgenic mice fluorescence is specific to neuronal activity. In our investigation, we used a fluorescent dye that is not specific to either neurons or astrocytes, and based the analysis on the frequency of the recorded calcium signal. As shown in previous work [2,15], glial and neuronal calcium transient do not have support in the same frequency bands enabling their distinction in recordings (less than 0.5 Hz for astrocytes and over 1 Hz for neurons).

The goal of this study was to use a bimodal IOI-Calcium imaging technique in order to measure simultaneous hemodynamic and calcium transients during resting state (RS) experiments. Fluorescence staining was done using Oregon Green Bapta-1 AM in order to measure both neuronal and glial calcium activity. Doing so, we tried to determine the separate neuronal and glial influences on the HbO/HbR fluctuations seen in RS.

2. Material and methods

2.1. Animal model and preparation

A total of N = 8 Male C57BL/6 mice (weight between 18 and 22 g, 8 weeks old, Charles River) were imaged for this study. From this group, three mice were rejected (dehydration, poor tracheostomy surgery and abnormal physiological signals respectively). The Animal Research Ethics Committee of the Montreal Heart Institute approved all surgical procedures, which were performed according to the recommendations of the Canadian Council on Animal Care.

All animals were anesthetized using urethane (1–1.5 mg/kg, intraperitoneal injection (IP)). A tracheostomy was performed to reduce the risk of respiratory depression often seen with the use of this anesthetic. The mice were then attached to a stereotaxic device with monitoring capabilities to record physiology throughout the experiment (Small Animal Monitoring Station, Labeotech Inc.). After the injection of a local anesthetic (Xylocaine, subcutaneous (SC), 0.2%) under the scalp, a surgical procedure was done to expose the skull covering the whole cortex area. A small hole was drilled through the bone over the barrel field cortex of each hemisphere (based on a stereotaxic atlas [16] over the barrel field cortex: −1.25 mm AP, ±3 mm ML) to have access to the brain for injections with a glass pipette. Artificial Cerebrospinal Fluid (aCSF: 125 mM NaCl, 10 mM HEPES, 10 mM glucose, 5 mM KCl, 1,5 mM $CaCl_2$, 1 mM $MgSO_4$) was used to keep the scalp moist for clear imaging. Injections of fluorophore (Oregon Green BAPTA-1, Invitrogen) diluted to a final concentration of 1 mM (first in 3.97 μl of 20% Pluronic acid in DMSO to reach a 10 mM solution, then, in 35 ml of aCSF to obtain the 1 μM final solution) were done with a microinjection pump (UMP3, WPI) according to procedures found in the literature [17,18]. To complete the surgical procedure, a small imaging chamber was installed around the skull and fixed with dental cement (Ortho-Jet, Lang). Next, agarose (0.8 mg/ml, Sigma-Aldrich) was poured to cover the skull and completely fill the chamber. A small cover slip was then installed on the top of the agarose to prevent exposure to air and to help re-establish normal intracranial pressure on the brain.

2.2. Physiology monitoring

Physiological monitoring was done continuously, from the beginning of anesthesia to the end of the experiment. Cardiac and respiratory rates were recorded; body temperature was maintained between 36.5 and 37.5 °C. The mice's hydration was preserved by injecting 0.25 ml of saline (SC) every hour. After the tracheostomy, an air mixture of 0.8 l/min of medical air and 0.2 l/min of oxygen was delivered close to the tracheal tube to reduce slow CO_2 level increases that can occur with time and ensure constant blood gas levels among the animals.

Finally, blood pressure was measured through volume-pressure recordings (VPR) during the procedure performed immediately preceding imaging in order to validate the physiological status during IOI recordings.

2.3. Stimulation

Activity in the barrel fields of the sensory cortex of each mouse was modulated by the stimulation of its whiskers with a controlled airflow (Picospritzer II, Parker). A series of air puffs were directed toward the whiskers unilaterally, with a pressure of 25 PSI for a duration of 100 ms. Length and frequency of the series were modulated so as to favor either the neuronal or the astrocytic response [2]. Frequencies were set to 1, 3 or 5 Hz and for a duration of 5 s or 30 s. Each series of stimulations were followed by an inter-stimulation period of rest of 30 ± 3 s, repeated 10 times. For each animal, 8 recordings were done: 2 resting state sessions of 5 min and 6 stimulations sessions (1 Hz for 5 s, 1 Hz for 30 s, 3 Hz for 5 s, etc.). The order of session recording was set randomly for each acquisition to avoid effects from habituation or physiology (e.g. fatigue, anesthesia, etc.) in the recorded data.

2.4. Optical imaging

Both IOI and fluorescence were acquired with a 12-bit charge-coupled device (CCD) camera (MV-D1024E-160-cl, PhotonFocus) with a full resolution of 1024 × 1024 pixels. The camera was linked to a computer through a frame grabber (Neon-CLB, Bitflow), allowing high frame rate acquisitions. A custom-made interface was programmed in Matlab (Matlab, MathWorks) to control the illumination, the stimulation, and the acquisition of images and vital signs. A macro-photo camera lens (EF-S 60 mm f/2.8 Macro USM, Canon) was used to image the brain on the CCD camera. With this particular lens set in macro mode, we were able to get a field of view

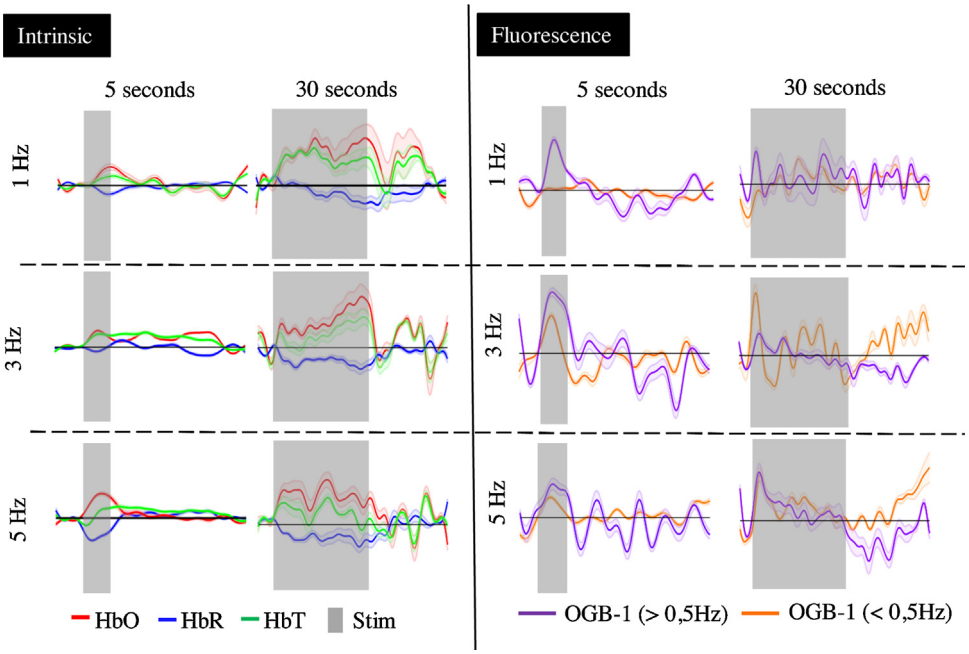

Fig. 1. Typical responses to stimulation block-averaged from the signal measured on the contralateral barrel cortex of a mouse. (For interpretation of the references to colour in this figure legend, the reader is referred to the web version of this article.)
On the left: HbO (in red), HbR (in blue) and HbT (in green) concentrations changes computed from the IOI acquisitions made according to the different stimulation paradigms (3 frequencies and two total durations). The gray areas represent when the stimulations were ON. On the right: the normalized power spectrum density computed on a 2 s window swept along the time dimension on each acquisition. The spectrum was separated in two frequency bands: greater than 1 Hz to quantify neuronal activity and lower than 0.5 Hz for glial activity.

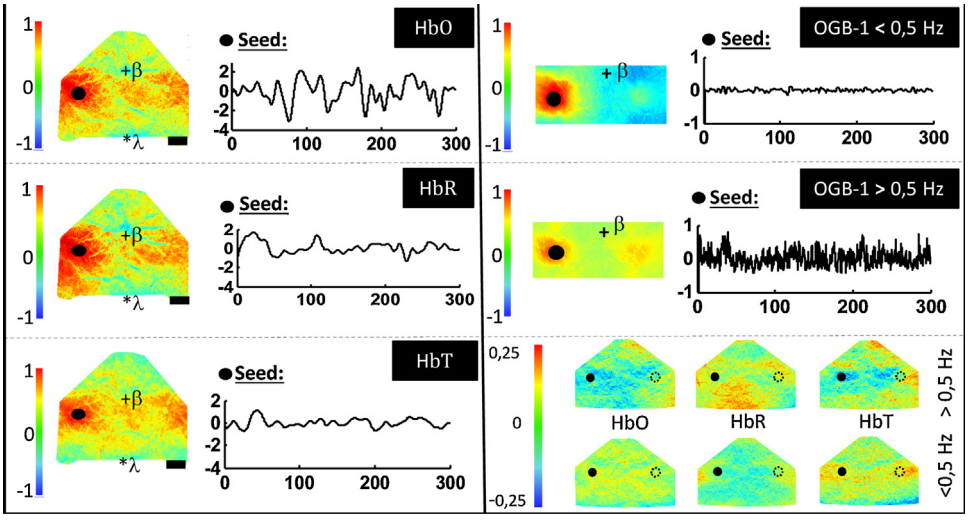

Fig. 2. Correlation maps for resting state sessions for both IOI and fluorescence signals.
All correlation values shown here are Pearson's coefficients. On the left: co-registered averaged maps across animals for the hemoglobin concentrations. The seed is indicated with a black dot on each map and the time course of its variation for one animal is shown next to each maps. Scale bars in black represent 1 mm. On the right: correlation maps for the power spectrum variation of the fluorescence signal over and under 0.5 Hz. Bottom-right: group-averaged correlations maps between the two OGB-1 seeds and the three Hb data set.

of 10 mm^2 on a region of interest (ROI) of 512 × 512 pixels (20 μm per pixel in both directions). The depth of view (the distance on the optical axis for which the image remains at focus) was determined by both the focal distance (200 mm) and the stop number (3, for an aperture opening of 2.8) of the lens, giving a focal depth of 1.2 mm.

Reflectance changes on the surface of the cortex were recorded with time-multiplexed illumination (488, 525, 590, 625 nm) produced by 3.5 W LED (LZ4-00MA00, Led Engin; XP-E blue, CREE). The four temporally multiplexed wavelengths led to a full-frame rate of 5 Hz for IOI and 15 Hz for fluorescence imaging. Illumination was further adjusted so that no part of the brain was under- or oversaturated by any of the wavelengths. The exposure time of the camera was set to 30 ms. Finally, filters were used to ensure that there was no contamination between the fluorescence channel and IOI channels (FF01-480/40-25 and FF01-515/LP-25, Semrock).

2.5. Analysis

Prior to data analysis, camera frames were filtered to remove electric noise [19]. They were then classified according to their corresponding illumination color. To reduce the influence of noise sources on the data, a generalized linear model (GLM) was

computed from multiple nuisance regressors: the EEG (X_{EEG}), the heart rate (X_{BPM}), the respiratory signal (X_{RESP}), the respiratory rate (X_{RPM}) and the averaged reflectance measure on a ROI including all the cortical pixels (X_G). Once the estimate was obtained, it was used to normalize data and thus, remove (or reduce) the effects of those regressors on the signal of interest.

For IOI channels (530 nm, 590 nm and 630 nm), each pixel's intensity time course was then filtered with a low pass filter (4th order Butterworth, cutoff frequency at 1 Hz). The use of a filter is necessary to reduce higher frequency noise unrelated to the hemodynamic response: predominantly respiration (from 2 Hz to 4 Hz) and heart-rate (between 6.5 Hz and 10 Hz). Butterworth filters are the most common choice to achieve this task because of their relatively flat (i.e. free of ripples) bandpass gain and their fast decrease after the cutoff frequency [20,21]. Moreover, the hemodynamic response is a slow process, having most of its frequency support below 1 Hz. To get HbO, HbR and HbT measures, the modified Beer–Lambert's law was used as described in Ref. [20].

For fluorescence recordings, the images (480 nm) were filtered into two distinct bandwidth signals, noted LF for the lower band and HF for the higher one. The bandpass cutoff frequencies were set between 0.01 to 0.1 Hz for LF and between 0.5 and 6 Hz for HF. In order to have comparable signals with the hemodynamic signal, the final LF and HF components were calculated by doing the summation of the power spectral density function of the two bandwidths on a 1 s moving window.

To compare hemodynamic activity with LF and HF fluorescence variations through the stimulation protocol, each signal (LF, HF, HbO, HbR and HbT) was averaged over every stimulation event for the contralateral barrel field area. As for resting state paradigm, correlation maps were generated from a seed (0.25–0.3 mm) selected in the barrel field cortex of one hemisphere (same seed area for every signal, positioned based on a stereotaxic atlas [16] over the barrel field cortex: −1.25 mm AP, 3 mm ML, next to the holes drilled for the OGB-1 injections) [20,22]. In addition, correlation coefficients were computed to compare both LF and HF calcium transient with HbO/HbR/HbT resting state signals (0.009–0.08 Hz) in order to evaluate the influence that each calcium frequency band might have on hemodynamics. From those Pearson's coefficient r values, Fisher Z measures were built using Fisher's Z-transform before performing a random effect *t*-tests on the seeds. Statistical significance was determined by using a standard Student's unpaired *t*-test of all pixels. Values were considered significant at $p < 0,05$, after adjusting the p values with the Benjamini–Hochberg procedure [20].

3. Results

Fig. 1 shows the mean block-averaged results for acquisition sessions with whisker stimulation. The fluorescence curves represent the power spectrum summation over high (HF) and low (LF) frequencies associated with neuronal (>0.5 Hz) and glial (<0.5 Hz) activity. For the long-duration stimulation sessions, the effect of habituation can be seen on the HF curves and the response was strongest when stimulation was set to 3 Hz. In comparison, LF responses were stronger for long-duration as compared to short-duration stimulation. This is in accordance with previous work [2].

There were no notable differences when comparing hemodynamic response at different stimulation frequencies using IOI measurements. But, when comparing the short and long stimulation periods some differences are noticeable. During the short-stimulation period (5 s), the signal returns quickly to its basal level, without the large oscillations seen after the long-duration stimulation period (30 s). This behavior is also present when looking at the fluorescence measures.

Correlation maps created with IOI data show a strong relationship between the somatosensory cortices of both hemispheres. As shown on Fig. 2, this relationship appears to be weaker with the OGB-1 signal. Also, the correlation spread for LF, related to astrocytes, is stronger and spatially larger than for the HF maps in the ipsilateral hemisphere. This relationship is reversed when looking at the contralateral side, associated with an increased bilateral correlation for HF signals. Finally, when looking at the correlation maps between the LF and HF power spectrum variations and the HbO/HbR/HbT signals, HF signals had a statistically significant (anti-) correlation with HbO ($p = 0.03$ ipsilateral seed, $p = 0.03$, contralateral seed) and HbT ($p = 0.04$ ipsilateral seed, $p = 0.03$, contralateral seed). No significant correlations were found between LF and hemodynamic signals.

4. Discussion

4.1. Changes measured with the stimulation paradigm

The link between stimulation parameters and the signal measured in fluorescence shows the same trends as what has been reported previously in literature [2]. Lower frequency calcium signals have a stronger response to longer stimulation periods. In comparison, higher frequencies return to a normal level a few seconds after the start of stimulation, probably caused by the habituation effect the stimulation has on neurons [2].

It has been shown that astrocytes have significantly slower calcium transients than neurons [15], a finding that was used in this study as a basis for the separation of calcium signal between neuronal and glial components. However, one cannot exclude crosstalk. Other works have shown low frequency correlation maps from fluorescence measurements on GCaMP3 mice, on which fluorescence is neuron-specific [13]. One hypothesis could be that neuronal activity is present in both frequency bands, while astrocytes only have support in the low frequency band. This could be validated by imaging with fluorophores that are astrocyte-specific (i.e. rhod-2 or fluo-4). In this study, imaging of fluo-4 signals was unsuccessful due to a weak fluorescence signal after staining when using the large-spatial scale IOI technique. The use of this fluorophore in wide field imaging might be more difficult in part because of its position close to blood vessels in the brain. Further investigation is needed in order to be able to measure both signals distinctively.

Furthermore, as shown in Ref. [3], isoflurane anesthesia has a significant effect on both neuron and astrocyte activity. Questions about a similar outcome should be raised with respect to urethane anesthesia, as the effects of this particular agent on cells and blood vessels might also have an impact on the recorded signals. To explore this, future studies should be conducted on both awake and anesthetized mice.

4.2. Correlation maps from resting state sessions

The correlation maps of hemoglobin changes in resting state show a strong relationship in both ipsilateral and contralateral barrel field's cortices, as could be expected considering previous works [20]. The added value of the current study is the investigation of hemoglobin change in correlation with fluorescence signals, which provides insight into the nature of the resting state signal origins.

As seen on Fig. 2, there are noticeable differences between the seed-based spatial-correlation of LF and HF fluorescence signals. The size and the strength of the highly correlated area on the LF map might be a sign of a stronger ipsilateral local network in this frequency range (from both neurons and astrocytes). In opposition, the HF correlation map shows a more uniform correlation between contra- and ipsi- lateral areas. We found that only HF

signals correlated with significance with hemodynamics (HbO and HbT) suggesting that RS signals have a neuronal substrate in this anesthetized preparation.

An important limitation to keep in mind when comparing these two signals is the fact that OGB-1 is excited at 488 nm and emits fluorescence at 530 nm. This range of wavelength is greatly absorbed by hemoglobin and thus can be influenced by hemodynamics. Perhaps LF signals were more affected than HF signals in this particular case since they share support in the same frequency band. The fluorescence maps presented in Fig. 2 were normalized by fluctuations of the IOI data based on known extinction coefficients of hemoglobin. In doing this procedure, we observed a stronger correction on LF signals, indicating that despite this correction, there may be a remaining confound due to partial volume effects. A second limitation is the use of a global regressor: we cannot exclude that introducing such a regressor may induce spurious negative correlations in RS maps. However, the IOI technique used here does not provide a clear alternative and more work needs to be done to investigate this issue.

5. Conclusions

In conclusion, this study provided multimodal measurements linking calcium transients in neurons and astrocytes to changes seen in hemoglobin concentration during resting state imagery. By separating the calcium-related fluorescence signal in two distinctive frequency bands, we were able to show differences in the way these signals correlate with hemodynamics.

Disclosure

The authors Bélanger and Lesage have partial ownership in Labeotech inc.

All procedures were approved by the animal ethics committee of the research center of the Montreal Heart Institute.

Acknowledgements

The authors would like to thank Alison Prendergast for her assistance in the writing of this article. We also would like to thank Marc-Antoine Gillis for his advice regarding the animal preparation.

References

[1] E.M.C. Hillman, Coupling mechanism and significance of the BOLD signal: a status report, Annu. Rev. Neurosci. 37 (2014) 161–181, http://dx.doi.org/10.1146/annurev-neuro-071013-014111.
[2] K. Schulz, E. Sydekum, R. Krueppel, C.J. Engelbrecht, F. Schlegel, A. Schröter, et al., Simultaneous BOLD fMRI and fiber-optic calcium recording in rat neocortex, Nat. Methods 9 (2012) 597–602, http://dx.doi.org/10.1038/nmeth.2013.
[3] A.S. Thrane, V.R. Thrane, D. Zeppenfeld, N. Lou, Q. Xu, E.A. Nagelhus, et al., General anesthesia selectively disrupts astrocyte calcium signaling in the awake mouse cortex, Proc. Natl. Acad. Sci. U. S. A. 109 (2012) 18974–18979, http://dx.doi.org/10.1073/pnas.1209448109.
[4] J.R. Binder, J.A. Frost, T.A. Hammeke, P.S.F. Bellgowan, S.M. Rao, R.W. Cox, Conceptual processing during the conscious resting state: a functional MRI study, J. Cogn. Neurosci. 11 (1999) 80–93, http://dx.doi.org/10.1162/089892999563265.
[5] J.S. Damoiseaux, S.A.R.B. Rombouts, F. Barkhof, P. Scheltens, C.J. Stam, S.M. Smith, et al., Consistent resting-state networks across healthy subjects, Proc. Natl. Acad. Sci. U. S. A. 103 (2006) 13848–13853, http://dx.doi.org/10.1073/pnas.0601417103.
[6] P. Fransson, Spontaneous low-frequency BOLD signal fluctuations: an fMRI investigation of the resting-state default mode of brain function hypothesis, Hum. Brain Mapp. 26 (2005) 15–29, http://dx.doi.org/10.1002/hbm.20113.
[7] A. Shmuel, D.A. Leopold, Neuronal correlates of spontaneous fluctuations in fMRI signals in monkey visual cortex: implications for functional connectivity at rest, Hum. Brain Mapp. 29 (2008) 751–761, http://dx.doi.org/10.1002/hbm.20580.
[8] A. Grinvald, D. Shoam, D.E. Shmuel, In-vivo optical imaging of cortical architecture and dynamics, in: Modern Techniques in Neuroscience Research, Springer, Heidelberg, 1999.
[9] V.A. Kalatsky, M.P. Stryker, New paradigm for optical imaging: temporally encoded maps of intrinsic signal, Neuron 38 (2003) 529–545, http://dx.doi.org/10.1016/S0896-6273(03)00286-1.
[10] M. Vanni, M. Villeneuve, M. Bickford, H. Petry, C. Casanova, Functional organization of the primary visual cortex (areas 17 and 18) of the tree shrew revealed by optical brain imaging, J. Vis. 9 (2009) 770, http://dx.doi.org/10.1167/9.8.770.
[11] M.B. Bouchard, B.R. Chen, S.A. Burgess, E.M.C. Hillman, Ultra-fast multispectral optical imaging of cortical oxygenation, blood flow, and intracellular calcium dynamics, Opt. Express 17 (2009) 15670, http://dx.doi.org/10.1364/OE.17.015670.
[12] M. Shaik, S.H. Kim, H.T. Zhao, E.M. Hillman, Simultaneous multi-region imaging of neuronal activity, hemodynamics and speckle flow In awake mice, OSA (2015), http://dx.doi.org/10.1364/BRAIN.2015.BrT2B.2 (BrT2B.2).
[13] M.P. Vanni, T.H. Murphy, Mesoscale transcranial spontaneous activity mapping in GCaMP3 transgenic mice reveals extensive reciprocal connections between areas of somatomotor cortex, J. Neurosci. 34 (2014) 15931–15946.
[14] A.L. Vazquez, M.C. Murphy, S.-G. Kim, Neuronal and physiological correlation to hemodynamic resting-state fluctuations in health and disease, Brain Connect. 4 (2014) 727–740, http://dx.doi.org/10.1089/brain.2014.0276.
[15] H. Ma, S. Harris, R. Rahmani, C.O. Lacefield, M. Zhao, A.G.S. Daniel, et al., Wide-field in vivo neocortical calcium dye imaging using a convection-enhanced loading technique combined with simultaneous multiwavelength imaging of voltage-sensitive dyes and hemodynamic signals, Neurophotonics 1 (2014) 015003, http://dx.doi.org/10.1117/1.NPh.1.1.015003.
[16] Allen Institute for Brain Science, Allen Mouse Brain Atlas, Allen Mouse Brain Atlas Internet, (2015). http://mouse.brain-map.org.
[17] S. Bélanger, B.O.F. de Souza, P. Pouliot, C. Casanova, F. Lesage, Neurovascular coupling in the deep brain using confocal fiber-optic endomicroscopy, in: Neurovascular Coupling Methods, Springer, New York, 2014, pp. 77–95, http://dx.doi.org/10.1007/978-1-4939-0724-3_5 (accessed 15.12.14).
[18] O. Garaschuk, R.-I. Milos, A. Konnerth, Targeted bulk-loading of fluorescent indicators for two-photon brain imaging in vivo, Nat. Protoc. 1 (2006) 380–386, http://dx.doi.org/10.1038/nprot.2006.58.
[19] B. Münch, P. Trtik, F. Marone, M. Stampanoni, Stripe and ring artifact removal with combined wavelet—Fourier filtering, Opt. Express 17 (2009) 8567, http://dx.doi.org/10.1364/OE.17.008567.
[20] E. Guevara, N. Sadekova, H. Girouard, F. Lesage, Optical imaging of resting-state functional connectivity in a novel arterial stiffness model, Biomed. Opt. Express 4 (2013) 2332, http://dx.doi.org/10.1364/BOE.4.002332.
[21] J.A. Turley, M. Nilsson, F.R. Walker, S.J. Johnson, A comparison of signal processing techniques for Intrinsic Optical Signal imaging in mice, IEEE (1982) 6281–6284, http://dx.doi.org/10.1109/EMBC.2015.7319828.
[22] B.R. White, A.Q. Bauer, A.Z. Snyder, B.L. Schlaggar, J.-M. Lee, J.P. Culver, Imaging of functional connectivity in the mouse brain, PLoS One 6 (2011) e16322, http://dx.doi.org/10.1371/journal.pone.0016322.

Neuromethods 88

Springer Protocols

Mingrui Zhao
Hongtao Ma
Theodore H. Schwartz
Editors

Neurovascular Coupling Methods

Humana Press

Chapter 5

Neurovascular Coupling in the Deep Brain Using Confocal Fiber-Optic Endomicroscopy

Samuel Bélanger, Bruno Oliveira Ferreira de Souza, Philippe Pouliot, Christian Casanova, and Frédéric Lesage

Abstract

Developing fast functional imaging approaches of subcortical structures is essential to make progress in our understanding of brain function and diseases. Positron emission tomography and functional magnetic resonance imaging have been used to improve our understanding of brain function and integration of neuronal activity between deeper structures and the superficial cortex but limitations remain associated with signal interpretation. This work describes the design and utilization of confocal microendoscopy techniques to image brain structures involved in visual processing, either deep or on the surface of the cortex. Also, multiple examples using different experimental approaches are described.

Key words Confocal microendoscopy, Calcium imaging

1 Background and Historical Overview

The investigation of neurovascular coupling remains at the forefront of current brain research due to its role in fundamental brain mechanisms and pathologies but also to link these mechanisms with macroscopic imaging observations. Multiple studies have explored the role of cell types and their topology in different cortical layers [1–3]. Separately, advances in our knowledge of brain vasculature [4, 5] and its function have also been achieved [6–8]. The aim of research on neurovascular coupling is to link these two areas with the goal of characterizing the system as a whole [9–13]. A better understanding of this coupling and how it is reflected in clinical imaging may help understand and diagnose diseases such as strokes (CVA) [14, 15], Alzheimer (AD) [16, 17], and attention deficits [18], to name a few. However, in these pathologies or even with aging, some of the key degenerative mechanisms are not only affecting the cortex but also subcortical areas. Therefore, an understanding of brain function in subcortical

Mingrui Zhao et al. (eds.), *Neurovascular Coupling Methods*, Neuromethods, vol. 88,
DOI 10.1007/978-1-4939-0724-3_5,

areas and their connection to the cortex is of interest. Imaging remains the tool of choice for these investigations.

Imaging tools used to study brain function can be divided into two distinct categories related to the spatial scale of the acquired information: macroscopic and microscopic techniques. Macroscopic devices have been used to measure the relation between different functional areas of the brain [19] or even to map functional organization of a particular cortical area [20, 21]. Hemodynamic methods, such as functional magnetic resonance imaging (fMRI) and diffuse optical and intrinsic signal imaging (ISI), use macroscopic scale hemodynamic fluctuations to infer neuronal activity. While their spatial resolution is not high enough to measure single cell activity, they have proven very useful to quantify local activity on large spatial scales and to map brain function indirectly [22]. However limitations remain and questions persist about the origin of the measured signals. Recent work suggests a role for astrocytes in blood flow control [23, 24], as well as in neuronal communication [25–28]. Macroscopic imaging is inadequate to uncover this potential role since distinguishing neurons from glia in the generated data from hemodynamic modalities is not possible.

At the microscopic scale, some of these questions can be addressed. Depending on the method used, the recording spatial extent can encompass from a single to a few hundred cells. By imaging cell ensembles, neuronal networks were investigated including the relationship between different cell types [29] or between layers of the cortex [1, 30–32]. Such high-resolution imaging using two-photon (2P) [33] or confocal microscopy [34] is mostly performed with the use of fluorescent dyes. Both techniques offer subcellular resolution and the possibility to acquire on a multidimensional area containing a few neurons. Different fluorescent indicators can be used depending on the application. Vascular architecture can be imaged by injecting a dye in the circulatory system [35–37]; when combined with specialized scanning techniques it can further be used to measure blood flow [38–40]. Oxygen consumption can also be measured with phosphorescent quenching probes [5]. To increase specificity, compounds targeting specific types of cells have been used to identify a single cell or multiple neurons in an area (with multicellular bolus loading (MCBL) injections) [41, 42]. In this case, fluorescence signal yields either anatomical data (e.g., in the case of SR-101 and astrocytes labelling [43]) or cell activity through its intensity variations (e.g., Oregon Green Bapta-1 (OGB-1) and calcium imaging [44, 45]).

Kerr et al. [46] demonstrated the ability of 2P microscopy with a calcium indicator (OGB-1) to map the spatial organization of the rat barrel cortex and to identify specific neural networks. By analyzing the occurrence of spiking activity for each neuron related to stimulation of whiskers, they were able to establish a spatial map of

the deflection sensitivity tuning in this cortical area. Using a pairwise correlation of neuronal temporal response, networks were identified and analyzed in order to establish the columnar organization in layers 2/3 of the rat barrel cortex. Calcium imaging of astrocytes and their function represent another area of intense activity to investigate their role in neurovascular coupling [11, 13, 23, 24]. Specific astrocyte stains have been developed [43], making it possible to outline their role in the neurovascular coupling and in selected clinical applications like AD [47–49].

Further potential of microscopic imaging was demonstrated in another study by Wilson et al. [50] who added an optogenetic [51, 52] component to the 2P microscope in order to activate directly the targeted cells during imaging sessions and to measure the effect of these activations on local networks in the visual cortex. There, it was shown that two different classes of inhibitory cells, parvalbumin (PV) and somatostatin (SOM) expressing neurons, have distinct functions and also belong to different network types. The responses of target cells to directional stimulation were modulated by PV neurons as their influence was proportional to the cell response. On the other hand, SOM inhibitory cells reduced the response equally for all directions (subtraction). This finding led the authors to conclude that SOMs might be useful to sharpen the selectivity of target cells while PVs control the gain on excitatory neurons.

The possibility to use 2P or confocal microscopy to measure oxygen delivery spatially in blood vessels and brain tissue was demonstrated in a recent work by Sakadzic et al. and Yaseen et al. [5, 53]. Using a gated illumination source and a photon counting detector, they were able to measure the spatially varying phosphorescence decay of an oxygen quenching probe to evaluate the local oxygen pressure in vessels (pO_2). With the 2P microscope, Sakadzic et al. were also able to follow this measurement both in vessels and tissue at different depths.

All studies above used microscopy to image the surface of the cortex and reached a maximum depth of a few hundred microns. These limitations are due to the optical properties of tissue (scattering and absorption) combined with the intrinsic design of the optics used in these instruments. Yet, many questions remain unexplored in subcortical areas: functional organization [54, 55], relationship with afferent and efferent connections [56, 57], and the central role these regions may have in brain diseases. While it is possible to work with tissue slices to answer some of these questions, one of the major concerns with ex vivo slices is the absence of cell–vasculature interaction. Transferring slice results in vivo is not trivial. The importance of this interaction is also underlined by new evidence leading to the idea that some of these subcortical regions may have a major influences on blood flow control [58]. Hamel et al. have identified different nuclei that are involved in a

vasoactive pathway [58, 59]. This forms the rationale for this chapter: the development of an imaging system that enables to record single cell activity deep in the brain and over a large area.

1.1 Confocal Microendoscopy

Confocal microendoscopy is based on the classic confocal technique. The main idea behind the confocal microscope is to eliminate most of the light originating from structures placed over and under the focal plane under the microscope objective. This is achieved by placing a pinhole (a hole with a diameter of a few tenths of microns) between an imaging lens and the detector (i.e., a photomultiplier tube (PMT)) [60–62] (*see* Fig. 1a). The thickness of the optical section (depth of view) in the sample being imaged is then directly proportional to the diameter of the pinhole used.

Two-dimensional images are created by moving the laser spot on the sample and by sampling the output of the detector at a given frequency. The position of the laser spot is determined by the angle of the laser beam into the objective (Fig. 1c), controlled by galvanometric mirrors (or another scanning device) and an optical telescope between the objective and the laser source. The telescope has two main functions: first, it is used to realign the laser beam with the desired angle towards the objective; second, it enables adjusting the size of the beam in order to set the focal spot

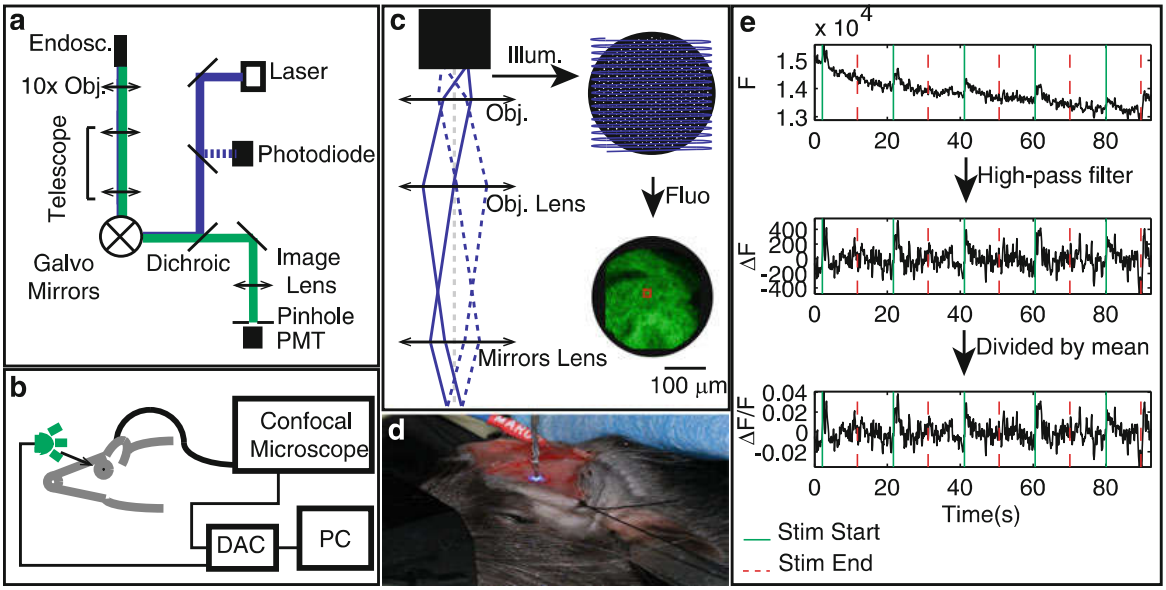

Fig. 1 (**a**) Schematic of the confocal microscope. Light comes from the laser source at 473 nm. A PMT is used to read fluorescent light coming back from the endoscope. Galvo mirrors are used to scan through each fiber of the bundle. (**b**) Example of a typical experimental setup. (**c**) Telescope part of the optical pathway presented in (**a**). The scanning pattern on the optic fiber bundle is shown with the fluorescence return. (**d**) Installation of the fiber on the head of the animal for validation (without cannulation). (**e**) Filtering process of the signal red from pixels (F) to recover fluorescence variations ($\Delta F/F$)

diameter. Fluorescence coming back from the sample that will reach the pinhole will come out of the objective lens with the same angle as the excitation beam. A dichroic mirror is placed in the pathway to split the two wavelengths (excitation at 488 nm and emission at 535 nm for OGB-1). From there, the emission light will go through the pinhole and the detector.

To image deep structures of the brain, simple modifications can be done to the confocal microscope: Essentially, by translating the optical plane using a miniature optic fiber bundle (e.g., Sumitomo IGN-035/6 or Mitsubishi Cable Industries Silica Image Guide), the latter can be used as a microendoscope with imaging performed at the distal end. With a classic confocal design, this can be done by placing the tip of the image guide right at the focal plane of the objective [62, 63]. Since the image guide is flexible, its tip can be moved anywhere within its length. By positioning a cannula from the top of the skull down to the desired recording area, the microendoscope can be inserted in the cannula to form images. Injecting the desired fluorescent dye on site and then sliding the endoscope into the cannula, neuronal activity can be recorded (Fig. 1d, e).

2 Equipment, Materials, and Setup

Table 1 provides the list of reagents, materials, and equipment required to realize a typical confocal microendoscopy experiment. Other fluorescent dyes can be used than OGB-1; nevertheless, it is important to make sure that excitation and emission wavelengths are compatible with the filters installed on the confocal microscope. Anesthetic choice may have a strong influence on neuronal responses [64]. According to the region being imaged and the type of stimulation used here, isoflurane was chosen for the experiments presented below. It may not be the best choice in all circumstances.

3 Procedures

All experiments below were performed on rats (adult Long Evans, 250–350 g). All procedures were performed in accordance with the directives of the Canadian Council for the Protection of Animals and the Ethics review board of the Université de Montréal.

Prior to the surgery, the exact position of the targeted area in the brain and the best path to reach the brain structure had to be determined. In planning the cannula implantation surgery, it was important to avoid brain structures that are functionally related to the target to ensure minimum damage to the function that was being investigated. In this regard, it might be better in some cases

Table 1
List of reagents, materials, and equipment required to realize a typical confocal microendoscopy experiment

Material (reagents)
Anesthetic (isoflurane)
Anti-inflammatory (dexamethasone sodium phosphate and carprofen)
Local anesthetic (xylocaine and epinephrine)
Skin disinfectant (iodine solution)
Ethanol (70 %)
Dental cement
Oregon Green Bapta-1 AM (Invitrogen)
Pluronic (Sigma Aldrich)
DMSO (Sigma Aldrich)
Calcium-free standard pipette solution (150 mM NaCl, 2.5 mM KCl, and 10 mM Hepes)
ACSF (124 mM NaCl, 36 mM $NaHCO_3$, 3 mM KCl, 2.5 mM $MgSO_4$, 1.25 mM KH_2PO_4, 1.8 g/L $C_6H_{12}O_6$, 3.4 mM $CaCl_2$)
Atropine 1 % (eyedrops)
Equipment
Standard surgery tools
Micro drill
Cannula (PlasticOne)
Cannula holder for stereotaxic device (Kopf)
Precision Pump (WPI, Ultra-Micro pump 3 and Micro 4 controler)
Syringe for small volume (Hamilton, 10 µL, Model 1701 RN SYR and Neuros Adapter Kit)
Priming kit to fill syringe (Hamilton, Priming Kit)
Image guide (Sumitomo, IGN-035/06 or Mitsubishi, Silicia Image Guide)
Setup
Confocal microscope (custom built to be used with an endoscope)
Stereotaxic system with stereotaxic arm and electrode holder (Kopf)
Visual stimulation system (controllable LED and video projector used with Vpixx software)

to insert the cannula towards the desired area with an angle to avoid other relevant structures. In the results below, the target was the superior colliculus (SC), situated at –5 mm from bregma in the sagittal axis, ±1 mm on the lateral axis (depending on whether stimulation was ipsilateral or contralateral), and 3 mm deep. For implantation, a straight 90° angle was chosen since visual areas

are more lateral than the SC and projections from them to the SC are minimal.

Finally, all surgery tools and cannula, as any other component put in direct contact with the animal, were sterilized with alcohol before use.

3.1 Animal Preparation

One hour before anesthesia, the rat was administered dexamethasone (4 mg/kg, IM) and carprofen (Rimadyl, 5 mg/kg, SC) in order to reduce inflammation and to facilitate an efficient recovery. Anesthesia induction was done in a small chamber, ventilated with a mixture of isoflurane (5 %) and oxygen (500 mL/min), for a period of 10 min. After testing reflexes on one hindpaw, the animal was installed on a stereotaxic frame as quickly as possible and equipped with a respiratory mask supplied with the same isoflurane mixture (set to 3 % during surgery). With the animal installed and head fixed on the stereotaxic frame, vital signs monitoring was initiated and maintained according to normal rat physiology: heart rate (320–420 beat per minute), respiratory rate (40–60 breaths/min), and oxygen saturation (over 95 %). Adjustments to anesthesia mixture were done accordingly. Before starting the surgery protocol, a xylocaine and epinephrine mix was injected locally in the surgical area (xylocaine 0.2 % with epinephrine at 0.001 mg/mL, 0.3 mL SC).

As a first step, the head of the rat was shaved and disinfected to avoid any contamination. Then, skin and muscles over the area of interest were removed in order to have an access for cannula implantation. Tissue cutting or removal was minimized in order to limit bleeding and inflammation. With the position well identified on the cranium, a small hole was drilled using the micro-drill (less than 1 mm of diameter) to expose the dura mater.

3.2 Installation of a Cannula

The cannula was cut to the desired length (3 mm for SC) and sterilized before the surgery. It was then slowly put in place using stereotaxic guidance, making sure that it was lowered according to the selected parameters (position of the target and angle of the path towards it). The cannula was then fixed in place by the application of dental cement. Muscles and tissues were put back in place and skin was sutured to close the wound. After this procedure, the animal was transferred to its cage and given 1–2 weeks of rest. During this period, daily monitoring of the recovery was done to make sure that the animal did not suffer from any infections. Also, a topical ointment (polysporin) was applied over the scar and a daily dose of anti-inflammatory was given (carprofen, 5 mg/kg, over a 3 days period)

3.3 Dye Injection

On the day of the experiment, animals were anesthetized again and put back into the stereotaxic device, following the same procedure as in Sect. 3.1. Once positioned, the cap from the cannula

was removed. If necessary, the area around the cannula was carefully washed with artificial cerebrospinal fluid (ACSF) in order to remove anything that could eventually obstruct it. If any liquid was seen inside the cannula, ACSF was also used to delicately wash it out.

Dye was prepared ahead of time. The detailed method for the dye preparation (Oregon Green Bapta-1 AM in this case) can be found in the literature [65–67]. A solution of OGB-1, diluted in a 20 % pluronic acid in DMSO, was mixed with a calcium-free HEPES preparation in order to get a 1 mM final concentration. For every injection site, 1 μL of this OGB-1 preparation was needed, according to the protocol used here. Since the dose of dye had to be injected slowly (0.1 μL/min, over a 10 min period), a pump (WPI, Ultra-Micro pump 3 and Micro 4 controller) was used with a precision syringe. This setup was used with either a pulled glass micropipette (50 μm opening) or with a small gauge needle (Hamilton, Neuro-syringe kit with needle gauge 33) with no significant difference in results. The solution was loaded in the injecting needle using a priming kit.

The injection system was then mounted on a stereotaxic arm over the cannula and the needle was aligned with it. It was very important to set the angle on the stereotaxic arm to fit that of the cannula in order to avoid any pressure on the needle during the lowering since it could cause damage to the injection tip or displace the cannula within tissue. Then, the tip of the needle (or micropipette) was lowered a few microns (100–300 μm) past the end cannula in the target area. During this step, any bleeding was monitored. Blood clots at the bottom of the cannula would compromise the ability to get a good image. After the whole 1 μL had been delivered, a rest period of 10 min was necessary to let the pressure in the injector come back at its normal level and avoid any loss of dye during retraction of the needle. Even after this period, removing the needle was done in small steps of a hundred microns, with pauses of 1 min in-between each step. At the end of this process, the animal was put in complete darkness for a whole hour to let OGB-1 diffuse inside the cells.

3.4 Installation of the Image Guide

The optic fiber bundle was installed on a stereotaxic holder (WPI). All manipulations of the image guide had to be done with great care to avoid any scratching or chipping of the tip. In order to have the most stable signal possible, the laser had to be turned on at least 5 min before imaging. The bundle was then lowered down the cannula, until it reached the region to be imaged. During this step, the position of the image guide tip was monitored through the fluorescence images. To avoid any bleaching, the power of the laser was adjusted as required during this step.

3.5 Visual Stimulation and Experimental Protocol

A final step prior to starting the experiment was to put one drop of atropine in the contralateral eye of the rat. This was used to dilate the pupil of the animal to maximize the response of the retina to light. From this moment to the end of the experiment, it was important to keep the room in the dark to insure activity measurements originated from stimulation only.

After a 10–15 min rest period, the visual stimulation protocol was initiated. With a controllable LED system, trains of light pulses (10 ms pulses at 5 Hz during 5 s) were directed towards the eye, interlaced with rest periods of 25 s. Stimulation wavelengths were either green (535 nm) or amber (590 nm). All signals from the confocal microscope and from the stimulation system were synchronized and recorded on a computer using a custom Labview interface (National Instruments; code available upon request). Post-processing analysis was done using homemade Matlab software (Mathworks).

4 Analysis

The confocal microendoscope software was designed to save all the signals needed to reconstruct frame by frame the acquisition and also to be able to synchronize the data with stimulation. Both reconstruction and analysis were done in post-processing using the following signals:

- The position of the two galvanometric mirrors
- The measured laser output power
- Stimulation status (active or rest)
- The photomultiplier tube (PMT) measured output

The acquisition rate of the system had to be high enough in order to have a fluorescence reading for each individual fiber of the endoscope on every frame. For this, the system used resonant galvanometric scanners with a fixed frame rate of 15 fps. Frame dimensions varied from 100×100 to 400×400 pixels, depending on the number of individual fiber in the fiber guide used as a microendoscope. However, the resolution of each pixel was fixed since individual fibers were always 4 μm of diameter and no additional GRIN lens was used in these experiments. Using a 10,000 elements bundle, and in order to get the desired 15 Hz frame rate, the input sampling rate of the different signals used to rebuild images was set to 1.2 MHz.

As a first step to reconstruct the fluorescence signal, the PMT output was corrected for laser power variations that might occur. These fluctuations could be misinterpreted as neuronal activity if not rectified and the PMT signal was divided by the time-varying averaged laser output signal. The PMT signal was then reshaped

into a three-dimensional matrix (X, Y, and time) using mirror positions recorded synchronously with the data. Each single frame was then assembled to form a 3D matrix representing the evolution in time of fluorescence within a 2D slice. Then, a high-pass filter was applied along the time direction on each pixel to remove photobleaching artifacts making the signal decay exponentially over time. Since higher laser powers lead to higher photobleaching, it is best to adjust illumination to minimize this effect. Finally, to get the measure of interest, i.e., calcium-induced fluorescence variations caused by neuronal activity ($\Delta F/F$), the intensity measured on each frame is divided by its average over the full acquisition, pixel per pixel.

5 Typical Results

5.1 Validation of Neuronal Activity Measures

When used with OGB-1, the confocal microendoscope will measure fluorescence signals indicating fluctuating calcium levels in cells under the tip of the endoscope. Comparing stimulation and rest periods, it is possible to quantify the activity induced by a specific stimulus.

In a first experiment, the system was used to detect neuronal activity in the visual cortex of an adult rat. The stimulation protocol used was a train of green flashes going on for a period of 5 s at a frequency of 5 Hz, every 30 s (Fig. 2b). The experiment was divided into three different trials (Fig. 2c): (1) stimulation on contralateral eye, (2) stimulation on ipsilateral eye, (3) stimulation on contralateral eye.

As shown in Fig. 2a, the scanned area presented significant fluorescence indicating large neuronal density which diminished contrast between somas and neuropils. Still, individual neurons can be observed as brighter spots on the 2D image. A region of interest was chosen encompassing one such neuron (red box in Fig. 2a). When computing the mean signal of this ROI averaged over stimulation and resting periods for the three trials (Fig. 2d), the ROI displayed a 5 % increase of fluorescence during stimulations on the contralateral eye as expected.

5.2 Neuronal Activity in the Superior Colliculus of the Rat

As described in the methodology section, the installation of a cannula was mandatory in order to image deep in the brain. Figure 3a, b shows the stereotaxic coordinates for this session determined with the use of a brain atlas. In this example, the position was chosen to avoid the visual areas of the rat (V2 and V1). Once installed, the cannula provided direct access to the brain structure under study (Fig. 3b). Validation of positioning could be performed ex vivo with histology following the experiment (Fig. 3c). The area where the interior part of the cannula was installed into the brain was marked with the red arrow. The yellow arrow showed the SC

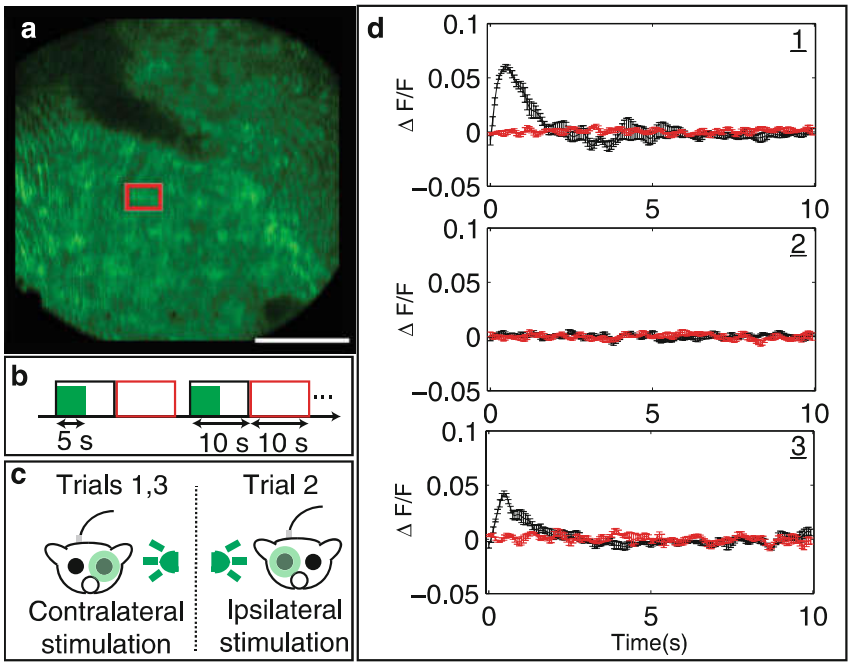

Fig. 2 (**a**) Image from the optic fiber bundle. Scale bar: 100 μm. *Red box* is the region from where the signal in D came from. (**b**) Experimental protocol: 5 s stimulation (light flashes of 10 ms, at 5 Hz), followed by a 25 s pause period. Black and red signals in D represent the mean of $\Delta F/F$ signal taken during the period showed by the *boxes* in **b**. (**c**) First and third trials were made with contralateral stimulation of the eye, second trial was on ipsilateral side. (**d**) Presentation of $\Delta F/F$ signals for the different trials for the stimulation period (*black*) and the poststimulation period (*red*)

(stained with Chicago Blue). Dangling tissue was seen in the path of the cannula due to aspiration by the cannula removal prior to histology.

A typical image of fluorescence coming back from the SC is shown in Fig. 3d. The brighter areas on the image correspond to cells (neurons or glia) and neuronal activity was recovered as described in Sect. 4. A typical example of neuronal activity is provided in Fig. 3e displaying $\Delta F/F$ for the red box area of Fig. 3d.

5.3 Hemodynamic Signals

The hemodynamic response could also be recorded with the confocal microendoscope in this configuration. Since the filter placed just before the detector was a bandpass between 515 and 560 nm, hemodynamic fluctuations through slow signal changes were observed as a modulator of measured fluorescence. Furthermore, based on the spectrum of both oxygenated hemoglobin (HbO) and reduced hemoglobin (HbR) (Fig. 4a), it could be expected that signal changes modulated by hemodynamics should reflect mostly cerebral blood volume with a smaller dependence on HbO/HbR concentration variations.

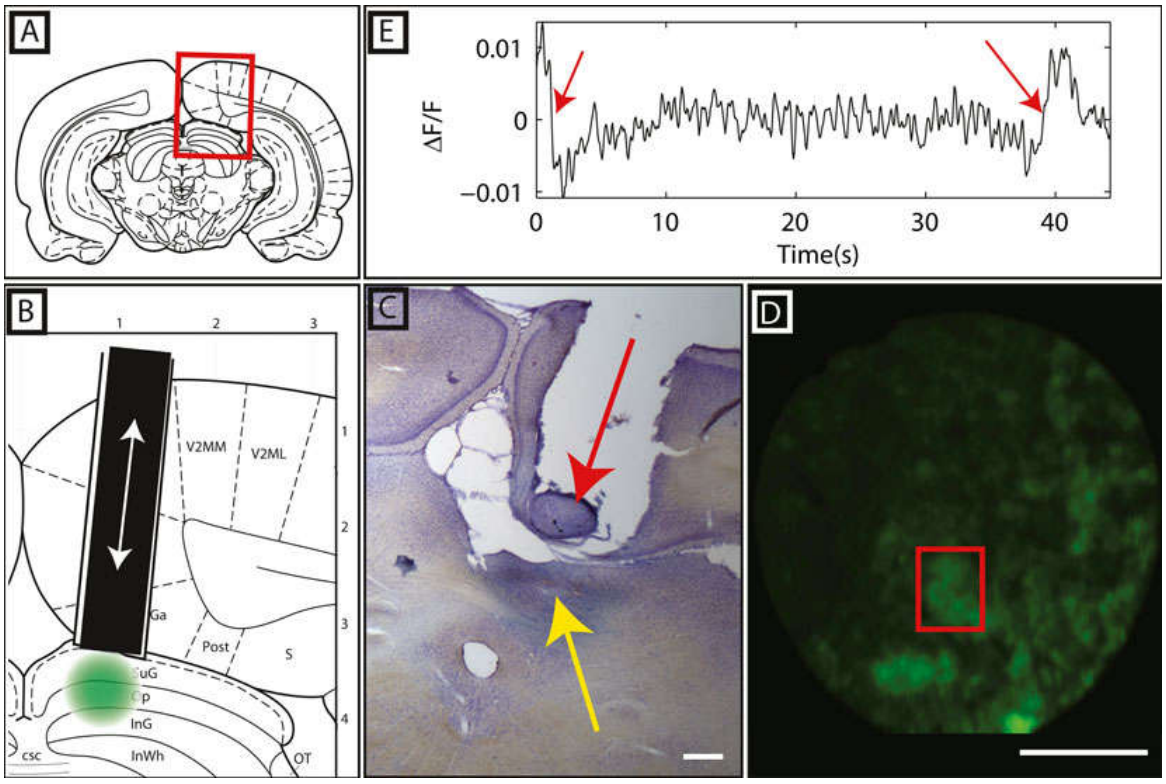

Fig. 3 (**a**) Stereotaxic coordinates from a rat brain atlas [68] (close-up in **b**, with the injection site in *green* and the endoscope represented by the *black rectangle*). (**c**) Histological slice showing the position of the cannula in the brain (*red arrow*). The *yellow arrow* shows the position of the superior colliculus that was stained with Chicago Blue at the end of the experiment. (**d**) Image of the fluorescence from the endoscope. In red, neuron from which the signal showed in (**e**) was taken. Scale bar: 100 μm. (**e**) $\Delta F/F$ signal. *Red arrows* target neuronal activity (10 % increase in fluorescence signal)

The hemodynamic response is much slower than neuronal activity and the peak response is usually found 4–10 s after the stimulus. Using the same stimulation protocol as Sect. 5.1, changes in fluorescence using ROIs located in a cortical area and in blood vessels were investigated. Figure 4b showed that when taking an average over multiple stimulation and rest cycles (30 s cycles over a 10 min experiment for a total of 20 blocks), a small variation in the signal over the blood vessel could be observed (1.5 %, 4–6 s after the end of the stimulation).

In Fig. 4c, a frame by frame sequence showed the difference in the signal for each pixel of the endoscope, showing a stronger decrease for the pixels corresponding to the blood vessel area. It was noted however that signal-to-noise ratio (SNR) over vessels would always be lower because a large amount of the emitted fluorescence was absorbed by the blood.

5.4 Continuous Stimulation

Continuous stimulation paradigms, using a periodic stimulation at a constant frequency, could also be used to investigate neural cell selectivity with calcium imaging. Fourier analysis could then be

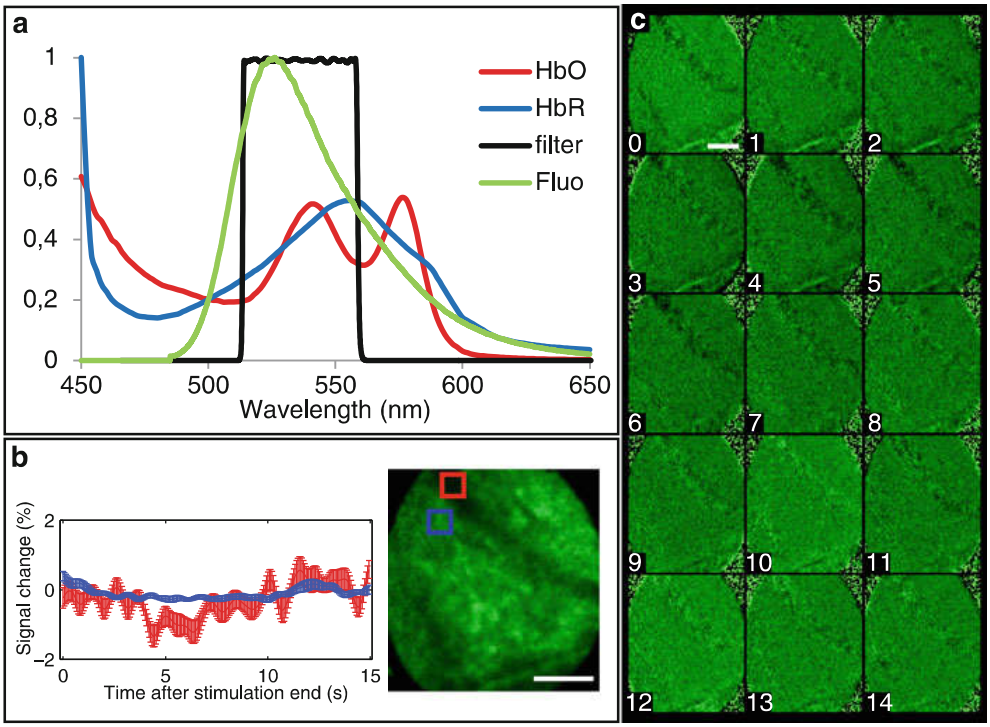

Fig. 4 (**a**) Superposition of the HbO/HbR absorption curves, fluorescence emission for OGB-1 and filter transmission curve. Most of the fluorescence light corresponds to an isobestic area of HbO/HbR. To be noted that the excitation wavelength used here is at 473 nm, which is not an isobestic point. (**b**) Fluorescence signals change over a cortical area (*blue*) and a blood vessel (*red*), in the 15 s after stimulation. Vessel signal shows hemodynamic response. (**c**) Frame by frame representation of the fluorescence variations (between −2 and 2 %). All scale bars are 100 μm

performed to gather organizational maps by looking at the phase of the calcium signal at the stimulation frequency. In Fig. 5, a retinotopic mapping experiment was presented while imaging with the confocal microendoscope. The rat was placed in front of the screen with a bar moving at a frequency of 0.2 Hz (5 s period to move through the screen). For each position of the bar on the screen, a phase was computed (between $-\pi$ and π) (Fig. 5a). Repeating this along two opposite directions of the screen, it was then possible to find the position on the screen associated with the neurons being imaged (called receptor field) (Fig. 5b–d).

6 Troubleshooting

6.1 Fluorescence Intensity Fades Quickly

As explained in Sect. 4, photobleaching is a phenomenon that has to be minimized as much as possible. This phenomenon is caused by the photochemical destruction of the dye molecules and is not reversible once the molecule has changed conformation. When an area is bleached, the only practical way to get signal from this area again is to inject the dye once again. The two principal causes for

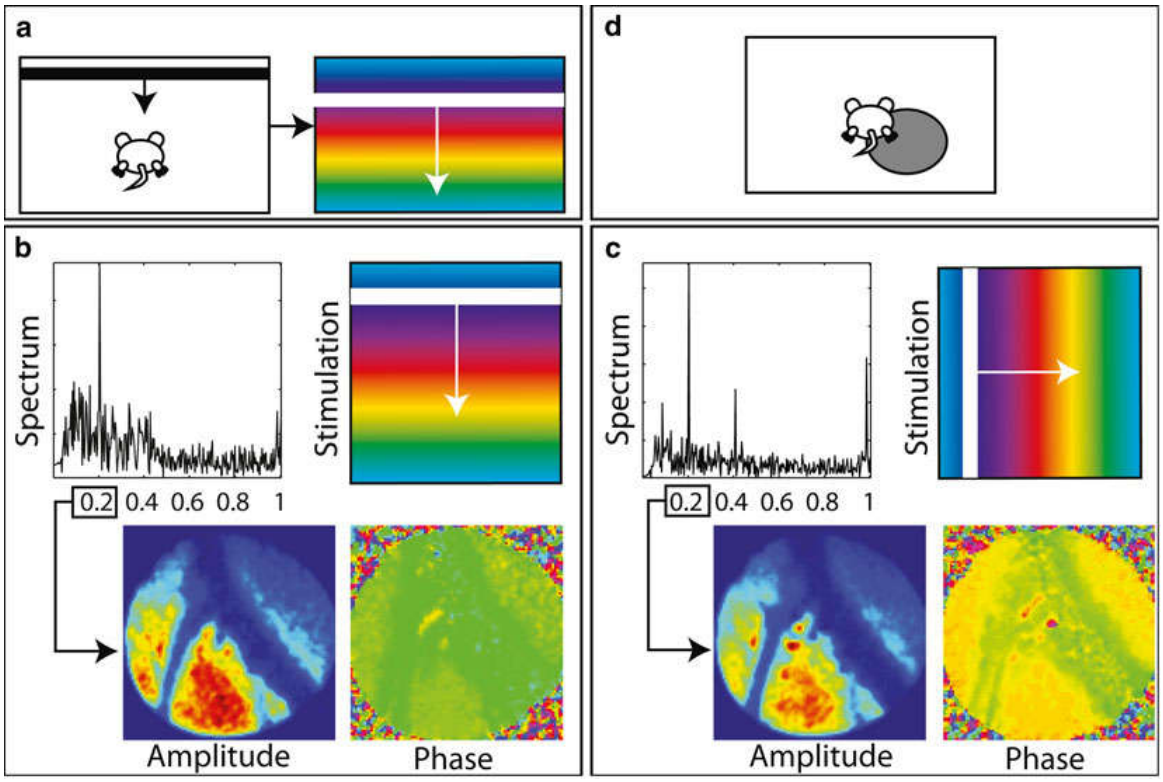

Fig. 5 (**a**) Representation of the experimental setup. The rat is placed on a stereotaxic device, with a screen in front. The bar (usually white on a black background) moves in one direction at a constant frequency. In Fourier analysis, the phase at the stimulation frequency corresponds to a specific position on the screen, for which a color is associated. (**b**) Results for a stimulation going from the top of the screen to the bottom (0.2 Hz). The spectrum is calculated from the mean of an ROI taken over cortical area. A strong response is observed at the 0.2 Hz stimulation frequency. Both amplitude and phase map are presented. From the phase map, it can be seen that most of the neurons imaged are associated with an area in the $-\pi/2$ (bottom quarter of the screen). (**c**) Same presentation as in (**b**), but for a left to right stimulation. The phase map shows that the area related to this cortical region is situated in the 2/3 of the screen ($-2\pi/3$). (**d**) From these two experiments, the receptor field linked to this cortical area is represented by a *gray circle* on the screen

photobleaching are high laser power and poor injections. Laser power: Since the destruction process of the fluorescent dye is proportional to the light level received, it is important to monitor and minimize laser power. Injection: If the amount of dye absorbed by the tissue is too low, it has been observed that the exponential decay of fluorescence level is more rapid.

Possible explanations for bad injections are:

- Error in the preparation of the dye
- Error in the injection pump's settings
- Clotted needle or micropipette
- Needle or micropipette tip not deep enough past the end of the cannula

6.2 Noise Level

Fluctuations of fluorescence during neuronal activation vary from 2 % to around 10 %, depending on stimulation parameters and on the region of the brain being imaged. According to this range, a SNR limit to efficiently measure activity can be estimated to be less than 1 %. Noise sources in a confocal microscope setup are many, but here is a list of the most common points to verify when noise level is too high.

6.2.1 Laser Power

Laser power has to be as low as possible to avoid photobleaching (which will reduce fluorescence level and, consequently, lower the SNR). However, if the power is set too low, the low levels of fluorescence coming back to the PMT will require higher PMT gains. Associated Poisson noise (shot noise) will then limit SNR, typical of low light level application.

6.2.2 Light Interference

Structured noise (always on the same pixels of each frame) that seems to increase (or even saturate) PMT readings is typical of light interference coming from outside the optical pathway. A practical way to identify this is to measure black noise (run the microscope with laser off) and to find the unwanted source of light (most of the time, from a joint around the microscope enclosure). Once found, a way to block this source has to be put in place before doing an experiment.

6.2.3 Cleaning Optics

Noise may also originate from optics that needs to be cleaned. Dry air can be used to remove dust from some optical component. Otherwise, one should follow usual procedures to clean lenses (soft cloth and methanol) and check with lens manufacturers to make sure that the procedure is coating safe.

6.3 Blurry Image

After the installation of the endoscope inside the cannula, the image may appear blurry or out of focus. In this situation, the ability to distinguish neurons from each other is greatly reduced. Also, the resulting $\Delta F/F$ signal might be of lower intensity, making it closer to the noise level.

6.3.1 Position of Tip from Objective

The first thing to check is the position of the tip of the endoscope on the microscope side. The face of the image guide has to be as close as possible to the focal plane of the objective in order to be inside the optical slice of the confocal microscope. A good way to adjust this position is a micrometric stage that moves the endoscope tip towards the optical axis direction.

6.3.2 Cleaning Fiber Bundle

After the few days recovery period following the cannula installation, clots or thick liquid might be located at the bottom. The cannula itself may be cleaned by gently pumping in and out some ACSF. However, some substances stick to the end of the endoscope over time. In this case, a gentle wash with a soft cloth and

some ACSF is recommended to remove any particles that could block light. After the experiment, methanol can also be used to clean efficiently. Finally, in the case where the tip of the endoscope is damaged, a fine repolishing should be performed.

6.4 No Neuronal Signal

During the recording session, it may happen that no fluctuations of fluorescence are observable from the brain. Variations in the response quality from experiment to experiment are normal. But in the case where this problem is recurrent, here is a list of what should be investigated.

6.4.1 PMT Saturated

PMT gain can be adjusted to optimize SNR during acquisition. Nevertheless, too high a gain can lead to saturation of the fluorescence signal in which case it will not be possible to measure signal increases. Gain should be set in order to make sure that the highest level of fluorescence at rest is at least 20 % under the maximum of the dynamic range of the PMT. Otherwise, any strong neuronal activation in this area would saturate the output of the device and lead to wrong analysis.

6.4.2 Position in the Brain

Subcortical structures are not always easy to target due to their small size and hidden location. Any error in the installation of the cannula could lead to testing the wrong brain region. A possible method to make sure that the installation procedure is not the cause of the absence of neuronal recording activity is to do a histological study postmortem. Some dyes will not resist to the histology protocol and it may thus be necessary to inject a small amount of a secondary dye to stain the area under the cannula before the end of the experiment.

6.4.3 Damaged Cortex

The resting period after cannula installation surgery is necessary to help reduce inflammation and to provide time for the cortex to heal. However, if the cannula is not fixed properly on the head of the animal, it might move (even slightly) during this period, causing swelling and generating inflammation. The animal may also have a tendency to scratch itself in the area of the surgery since the healing process of the skin can be irritating. There are two ways to control these issues: First, the dental cement base can be solidified by adding some anchor points on the skull (e.g., small screws). Second, a head cone can be installed to protect the head from any scratching.

7 Conclusion

Exploring the neurovascular coupling of deep-seated brain areas remains challenging, but new techniques that will enable unprecedented explorations of these brain structures are emerging. Confocal microendoscopy is a relatively new technique that gives

the ability to image neuronal activity in deep areas of the brain. This tool provides new opportunities to better investigate brain mechanisms and the role of these structures in information integration. Further improvements may even lead to the possibility to distinguish between different cell types and to activate (or to inhibit) targeted cells with the use of optogenetics.

References

1. Olsen SR, Bortone DS, Adesnik H, Scanziani M (2012) Gain control by layer six in cortical circuits of vision. Nature 483(7387):47–52
2. Ghose GM, Ohzawa I, Freeman RD, DeAngelis GC (1999) Functional micro-organization of primary visual cortex: receptive field analysis of nearby neurons. J Neurosci 19(10):4046–4064
3. Nelson SB, Le Vay S (1985) Topographic organization of the optic radiation of the cat. J Comp Neurol 240(3):322–330
4. Hirsch S, Reichold J, Schneider M, Székely G, Weber B (2012) Topology and hemodynamics of the cortical cerebrovascular system. J Cereb Blood Flow Metab 32(6):952–67. http://www.ncbi.nlm.nih.gov/pubmed/22472613. Accessed 1 Jun 2012
5. Sakadžić S, Roussakis E, Yaseen MA, Mandeville ET, Srinivasan VJ, Arai K et al (2010) Two-photon high-resolution measurement of partial pressure of oxygen in cerebral vasculature and tissue. Nat Methods 7(9):755–759
6. Chen BR, Bouchard MB, McCaslin AFH, Burgess SA, Hillman EMC (2011) High-speed vascular dynamics of the hemodynamic response. Neuroimage 54(2):1021–1030
7. Srinivasan VJ, Sakadzić S, Gorczynska I, Ruvinskaya S, Wu W, Fujimoto JG et al (2010) Quantitative cerebral blood flow with optical coherence tomography. Opt Express 18(3): 2477–2494
8. Devor A, Hillman EMC, Tian P, Waeber C, Teng IC, Ruvinskaya L et al (2008) Stimulus-induced changes in blood flow and 2-deoxyglucose uptake dissociate in ipsilateral somatosensory cortex. J Neurosci 28(53): 14347–14357
9. Koehler RC, Roman RJ, Harder DR (2009) Astrocytes and the regulation of cerebral blood flow. Trends Neurosci 32(3):160–169
10. Cauli B, Hamel E (2010) Revisiting the role of neurons in neurovascular coupling. Front Neuroenergetics 2:9. http://www.ncbi.nlm.nih.gov/pmc/articles/PMC2899521/. Accessed 10 Sep 2012
11. Carmignoto G, Gómez-Gonzalo M (2010) The contribution of astrocyte signalling to neurovascular coupling. Brain Res Rev 63(1–2):138–148
12. Devonshire IM, Papadakis NG, Port M, Berwick J, Kennerley AJ, Mayhew JEW et al (2012) Neurovascular coupling is brain region-dependent. Neuroimage 59(3):1997–2006
13. Petzold GC, Murthy VN (2011) Role of astrocytes in neurovascular coupling. Neuron 71(5):782–797
14. Blicher JU, Stagg CJ, O'Shea J, Østergaard L, MacIntosh BJ, Johansen-Berg H, et al (2012) Visualization of altered neurovascular coupling in chronic stroke patients using multimodal functional MRI. J Cereb Blood Flow Metab 32(11):2044–54. http://www.nature.com/jcbfm/journal/vaop/ncurrent/full/jcbfm2012105a.html. Accessed 21 Sep 2012
15. Lin WH, Hao Q, Rosengarten B, Leung WH, Wong KS (2011) Impaired neurovascular coupling in ischaemic stroke patients with large or small vessel disease. Eur J Neurol 18(5): 731–736
16. Girouard H, Iadecola C (2006) Neurovascular coupling in the normal brain and in hypertension, stroke, and Alzheimer disease. J Appl Physiol 100(1):328–335
17. Lin AJ, Konecky SD, Rice TB, Green KN, Choi B, Durkin AJ, et al (2012) Towards spatial frequency domain optical imaging of neurovascular coupling in a mouse model of Alzheimer's disease. Proc SPIE 8207:82074U
18. Da Silva N, Szobot CM, Anselmi CE, Jackowski AP, Chi SM, Hoexter MQ et al (2011) Attention deficit/hyperactivity disorder. Clin Nucl Med 36(8):656–660
19. White BR, Bauer AQ, Snyder AZ, Schlaggar BL, Lee J-M, Culver JP (2011) Imaging of functional connectivity in the mouse brain. PLoS One 6(1):e16322
20. Ayling OGS, Harrison TC, Boyd JD, Goroshkov A, Murphy TH (2009) Automated light-based mapping of motor cortex by photoactivation of channelrhodopsin-2 transgenic mice. Nat Methods 6(3):219–224
21. Vanni MP, Provost J, Casanova C, Lesage F (2010) Bimodal modulation and continuous

stimulation in optical imaging to map direction selectivity. Neuroimage 49(2):1416–1431
22. Chemla S, Chavane F (2010) A biophysical cortical column model to study the multi-component origin of the VSDI signal. Neuroimage 53(2):420–438
23. Attwell D, Buchan AM, Charpak S, Lauritzen M, MacVicar BA, Newman EA (2010) Glial and neuronal control of brain blood flow. Nature 468(7321):232–243
24. Haydon PG, Carmignoto G (2006) Astrocyte control of synaptic transmission and neurovascular coupling. Physiol Rev 86(3):1009–1031
25. Henneberger C, Papouin T, Oliet SHR, Rusakov DA (2010) Long-term potentiation depends on release of d-serine from astrocytes. Nature 463(7278):232–236
26. Lee S, Yoon B-E, Berglund K, Oh S-J, Park H, Shin H-S et al (2010) Channel-mediated tonic GABA release from glia. Science 330(6005): 790–796
27. Agulhon C, Fiacco TA, McCarthy KD (2010) Hippocampal short- and long-term plasticity are not modulated by astrocyte Ca2+ signaling. Science 327(5970):1250–1254
28. Shigetomi E, Bowser DN, Sofroniew MV, Khakh BS (2008) Two forms of astrocyte calcium excitability have distinct effects on NMDA receptor-mediated slow inward currents in pyramidal neurons. J Neurosci 28(26): 6659–6663
29. Adesnik H, Bruns W, Taniguchi H, Huang ZJ, Scanziani M (2012) A neural circuit for spatial summation in visual cortex. Nature 490(7419): 226–231
30. Lee S-H, Kwan AC, Zhang S, Phoumthipphavong V, Flannery JG, Masmanidis SC, et al (2012) Activation of specific interneurons improves V1 feature selectivity and visual perception. Nature 488(7411): 379–83. http://www.nature.com/nature/journal/vaop/ncurrent/full/nature11312.html?WT.ec_id=NATURE-20120809. Accessed 9 Aug 2012
31. Kätzel D, Zemelman BV, Buetfering C, Wölfel M, Miesenböck G (2010) The columnar and laminar organization of inhibitory connections to neocortical excitatory cells. Nat Neurosci 14(1):100–107
32. Nauhaus I, Nielsen KJ, Disney AA, Callaway EM (2012) Orthogonal micro-organization of orientation and spatial frequency in primate primary visual cortex. Nat Neurosci 15(12):1683–1690. http://www.nature.com/neuro/journal/vaop/ncurrent/full/nn.3255.html. Accessed 13 Nov 2012
33. Denk W, Delaney KR, Gelperin A, Kleinfeld D, Strowbridge BW, Tank DW et al (1994) Anatomical and functional imaging of neurons using 2-photon laser scanning microscopy. J Neurosci Methods 54(2):151–162
34. Pawley JB (ed) (2006) Handbook of biological confocal microscopy. Springer, Boston. http://www.springerlink.com/content/978-0-387-25921-5/#section=746528&page=1&locus=0. Accessed 24 Aug 2011
35. Zhang Z, Davies K, Prostak J, Fenstermacher J, Chopp M (1999) Quantitation of microvascular plasma perfusion and neuronal microtubule-associated protein in ischemic mouse brain by laser-scanning confocal microscopy. J Cereb Blood Flow Metab 19(1): 68–78
36. Villringer A, Them A, Lindauer U, Einhäupl K, Dirnagl U (1994) Capillary perfusion of the rat brain cortex. An in vivo confocal microscopy study. Circ Res 75(1):55–62
37. Serduc R, Vérant P, Vial J-C, Farion R, Rocas L, Rémy C et al (2006) In vivo two-photon microscopy study of short-term effects of microbeam irradiation on normal mouse brain microvasculature. Int J Radiat Oncol Biol Phys 64(5):1519–1527
38. Schaffer CB, Friedman B, Nishimura N, Schroeder LF, Tsai PS, Ebner FF et al (2006) Two-photon imaging of cortical surface microvessels reveals a robust redistribution in blood flow after vascular occlusion. PLoS Biol 4(2):e22
39. Shih AY, Driscoll JD, Drew PJ, Nishimura N, Schaffer CB, Kleinfeld D (2012) Two-photon microscopy as a tool to study blood flow and neurovascular coupling in the rodent brain. J Cereb Blood Flow Metab 32(7):1277–1309
40. Chaigneau E, Oheim M, Audinat E, Charpak S (2003) Two-photon imaging of capillary blood flow in olfactory bulb glomeruli. Proc Natl Acad Sci U S A 100(22):13081–13086
41. Göbel W, Helmchen F (2007) In vivo calcium imaging of neural network function. Physiology (Bethesda) 22(6):358–365
42. Lütcke H, Helmchen F (2011) Two-photon imaging and analysis of neural network dynamics. Rep Prog Phys 74(8):086602
43. Nimmerjahn A, Kirchhoff F, Kerr JN, Helmchen F (2004) Sulforhodamine 101 as a specific marker of astroglia in the neocortex in vivo. Nat Methods 1(1):31–37
44. Thomas D, Tovey SC, Collins TJ, Bootman MD, Berridge MJ, Lipp P (2000) A comparison of fluorescent Ca2+ indicator properties and their use in measuring elementary and

global Ca2+ signals. Cell Calcium 28(4): 213–223

45. Rochefort NL, Jia H, Konnerth A (2008) Calcium imaging in the living brain: prospects for molecular medicine. Trends Mol Med 14(9):389–399
46. Kerr JND, de Kock CPJ, Greenberg DS, Bruno RM, Sakmann B, Helmchen F (2007) Spatial organization of neuronal population responses in layer 2/3 of rat barrel cortex. J Neurosci 27(48):13316–13328
47. Tian G-F, Takano T, Lin JH-C, Wang X, Bekar L, Nedergaard M (2006) Imaging of cortical astrocytes using 2-photon laser scanning microscopy in the intact mouse brain. Adv Drug Deliv Rev 58(7):773–787
48. Takano T, Han X, Deane R, Zlokovic B, Nedergaard M (2007) Two-photon imaging of astrocytic Ca2+ signaling and the microvasculature in experimental mice models of Alzheimer's disease. Ann N Y Acad Sci 1097: 40–50
49. Riera J, Hatanaka R, Uchida T, Ozaki T, Kawashima R (2011) Quantifying the uncertainty of spontaneous Ca2+ oscillations in astrocytes: particulars of Alzheimer's disease. Biophys J 101(3):554–564
50. Wilson NR, Runyan CA, Wang FL, Sur M (2012) Division and subtraction by distinct cortical inhibitory networks in vivo. Nature 488(7411):343–8. http://www.nature.com/nature/journal/vaop/ncurrent/full/nature11347.html?WT.ec_id=NATURE-20120809. Accessed 9 Aug 2012
51. Boyden ES, Zhang F, Bamberg E, Nagel G, Deisseroth K (2005) Millisecond-timescale, genetically targeted optical control of neural activity. Nat Neurosci 8(9):1263–1268
52. Han X, Boyden ES (2007) Multiple-color optical activation, silencing, and desynchronization of neural activity, with single-spike temporal resolution. PLoS One 2(3):e299
53. Yaseen MA, Srinivasan VJ, Sakadzić S, Wu W, Ruvinskaya S, Vinogradov SA et al (2009) Optical monitoring of oxygen tension in cortical microvessels with confocal microscopy. Opt Express 17(25):22341–22350
54. Huppé-Gourgues F, Bickford ME, Boire D, Ptito M, Casanova C (2006) Distribution, morphology, and synaptic targets of corticothalamic terminals in the cat lateral posterior-pulvinar complex that originate from the posteromedial lateral suprasylvian cortex. J Comp Neurol 497(6):847–863
55. Casanova C (2004) The visual functions of the pulvinar. The visual neurosciences. MIT, Cambridge, pp 592–608
56. Guillery RW, Sherman SM (2002) Thalamic relay functions and their role in corticocortical communication: generalizations from the visual system. Neuron 33(2):163–175
57. Sherman SM, Guillery RW (2011) Distinct functions for direct and transthalamic corticocortical connections. J Neurophysiol 106(3):1068–77. http://jn.physiology.org/content/early/2011/06/10/jn.00429.2011.abstract. Accessed 8 Aug 2011
58. Hamel E (2006) Perivascular nerves and the regulation of cerebrovascular tone. J Appl Physiol 100(3):1059–1064
59. Cauli B, Tong X-K, Rancillac A, Serluca N, Lambolez B, Rossier J et al (2004) Cortical GABA interneurons in neurovascular coupling: relays for subcortical vasoactive pathways. J Neurosci 24(41):8940–8949
60. Nichols AJ, Evans CL (2011) Video-rate scanning confocal microscopy and microendoscopy. J Vis Exp (56). http://www.jove.com/video/3252/video-rate-scanning-confocal-microscopy-and-microendoscopy. Accessed 5 Oct 2012.
61. Pierce M, Yu D, Richards-Kortum R (2011) High-resolution fiber-optic microendoscopy for in situ cellular imaging. J Vis Exp (47). http://www.jove.com/details.php?id=2306. Accessed 9 Aug 2011
62. Vincent P, Maskos U, Charvet I, Bourgeais L, Stoppini L, Leresche N et al (2006) Live imaging of neural structure and function by fibred fluorescence microscopy. EMBO Rep 7(11): 1154–1161
63. Flusberg BA, Cocker ED, Piyawattanametha W, Jung JC, Cheung ELM, Schnitzer MJ (2005) Fiber-optic fluorescence imaging. Nat Methods 2(12):941–950
64. Franceschini MA, Radhakrishnan H, Thakur K, Wu W, Ruvinskaya S, Carp S et al (2010) The effect of different anesthetics on neurovascular coupling. Neuroimage 51(4):1367–1377
65. Garaschuk O, Milos R-I, Konnerth A (2006) Targeted bulk-loading of fluorescent indicators for two-photon brain imaging in vivo. Nat Protoc 1(1):380–386
66. Stosiek C, Garaschuk O, Holthoff K, Konnerth A (2003) In vivo two-photon calcium imaging of neuronal networks. Proc Natl Acad Sci U S A 100(12):7319–7324
67. Sullivan MR, Nimmerjahn A, Sarkisov DV, Helmchen F, Wang SS-H (2005) In vivo calcium imaging of circuit activity in cerebellar cortex. J Neurophysiol 94(2):1636–1644
68. Paxinos G, Watson C (2006) The rat brain in stereotaxic coordinates. Academic Press, Elsevier, London